NASA Technical Memorandum 104606, Vol. 7

Technical Report Series on Global Modeling and Data Assimilation

Max J. Suarez, Editor

Volume 7

Proceedings of the Workshop on the GEOS-1 Five-Year Assimilation

Siegfried D. Schubert and Richard B. Rood

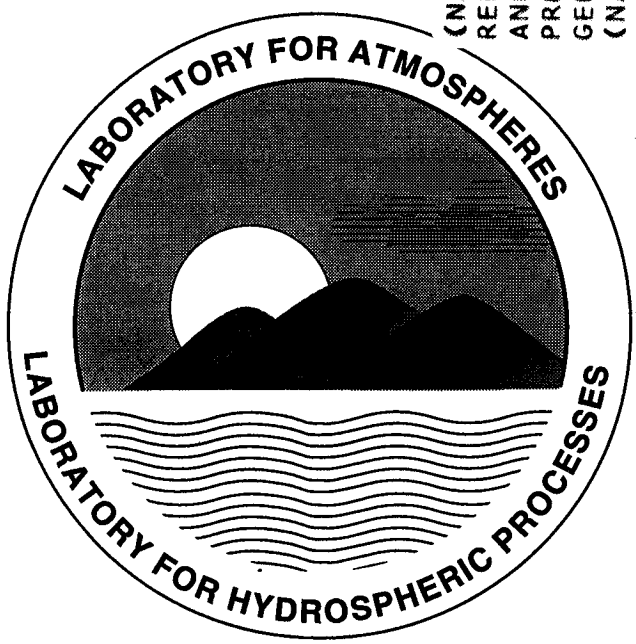

September 1995

DATA ASSIMILATION OFFICE

NASA Technical Memorandum 104606, Vol. 7

Technical Report Series on Global Modeling and Data Assimilation

Max J. Suarez, Editor
Goddard Space Flight Center
Greenbelt, Maryland

Volume 7

Proceedings of the Workshop on the GEOS-1 Five-Year Assimilation

Siegfried Schubert
Richard Rood
Goddard Space Flight Center
Greenbelt, Maryland

National Aeronautics and
Space Administration

Goddard Space Flight Center
Greenbelt, Maryland
1995

This publication is available from the NASA Center for AeroSpace Information,
800 Elkridge Landing Road, Linthicum Heights, MD 21090-2934, (301) 621-0390.

Abstract

A three–day workshop on results from the Data Assimilation Office (DAO) five–year assimilation was held March 6–8, 1995 at Goddard Space Flight Center. The primary objective of the workshop was to provide timely feedback from the data users concerning the strengths and weaknesses of version 1 of the Goddard Earth Observing System (GEOS–1) assimilated products. A second objective was to assess user satisfaction with the current methods of data access and retrieval.

There were a total of 49 presentations, with about half (23) of the presentations coming from scientists outside of Goddard. The total attendance was about 120. The first two days were devoted to applications of the data: these included studies of the tropical circulation, geodynamics applications, constituent transport, momentum and energy diagnostics, precipitation and diabatic heating, hydrological modeling and moisture transport, cloud forcing and validation, various aspects of intraseasonal, seasonal and interannual variability, ocean wind stress applications, and validation of surface fluxes. The last day included talks about several related efforts at the National Meteorological Center (NMC), the National Center for Atmospheric Research (NCAR), the Center for Ocean–Land–Atmosphere Studies (COLA), the United States Navy, and the European Center for Medium Range-Weather Forecasts (ECMWF). This was followed by talks from several members of the DAO on current and future development efforts. The workshop concluded with a general discussion on data quality, data access experiences and suggestions for future development of the GEOS system.

This report includes most of the extended abstracts from the workshop, and attempts to summarize the major findings as well as the planned development activities designed to address the deficiencies in the GEOS–1 system.

Contents

* No extended abstract submitted.

1 Introduction

The DAO has as its primary mission the development of a global assimilation system suitable for ingesting EOS and other satellite and in situ observations to produce dynamically, physically, and chemically consistent, gridded high level data products for studying the Earth System. Such a synthesis of the various observations, which are characterized by widely differing error characteristics, and irregular temporal and spatial coverage, is deemed vital to enhance the utility of the EOS satellite observations. In addition to synthesizing the available observations, data assimilation provides numerous value added products; these include estimates of quantities or processes not readily observable (e.g. vertical motion, surface fluxes and latent heating), and objectively determined estimates of the errors of the final synthesized data products. In this regard, the mission of the DAO differs from that of operational numerical weather prediction centers. The primary concern is not increased forecast skill, but instead, it is the usefulness of the products for climate applications which drives the development effort. This rather general requirement makes it difficult to assess the quality of the assimilation by just a few objective measures (e.g. forecast skill). The large range of potential applications of the data thus makes it imperative that the DAO obtain feedback on the quality and usefulness of the data products from a wide as possible spectrum of users.

In recognition of the need for timely user feedback, version 1 of the GEOS system was fixed or "frozen" in March 1993, and a commitment was made to generate a five–year assimilation (March 1985–February 1990) suitable for climate applications. This experiment has now been extended through 1993, and current plans are to complete the period 1979–1994 by the end of 1995. The idea of a reanalysis of historical observations with a fixed data assimilation system was first suggested a number of years ago (Bengston and Shukla 1988) as a way of improving the utility of current meteorological observations for climate studies by eliminating the spurious climate signals often found in operational NWP analyses. In addition to the DAO effort, there are a number of other reanalyses currently underway at NMC (Kalnay and Jenne 1991), ECMWF, and the United States Navy. While some limited intercomparisons between these products have already been made (and presented at the workshop), the next year should bring forth an abundance of studies addressing the quality of the various products.

An important concern expressed early on by potential users of the DAO products was that adequate documentation of the GEOS system and data products be provided. In the past year various technical reports have been prepared documenting the GEOS–DAS, and most of these were available (at least in draft form) at the time of the workshop. The GCM is described in Takacs et al. (1994), Suarez and Takacs (1995), and Molod et al. (1995). The former also provides a complete listing and description of all the diagnostic quantities available from the data assimilation system. The analysis system is described in Pfaendtner et al. (1995). Some early results and a user guide to all the datasets available from the

five–year assimilation are provided in Schubert et al. (1995). All documents are available on–line or in hard copy form. Further information about data access may be obtained by sending e–mail to data@dao.gsfc.nasa.gov.

In view of the tight development schedule of the DAO, it was deemed vital that a workshop be held to specifically address the quality of the first version of the GEOS system. The workshop was held March 6–8, 1995 at Goddard Space Flight Center. The objectives were to assess the strengths and weaknesses of the GEOS–1 assimilated products, and to assess user satisfaction with the current methods of data access and retrieval.

There were a total of 49 presentations, with about half (23) of the presentations coming from scientists outside of Goddard. The total attendance was about 120. The first two days were devoted to applications of the data: these included studies of the tropical circulation, geodynamics applications, constituent transport, momentum and energy diagnostics, precipitation and diabatic heating, hydrological modeling and moisture transport, cloud forcing and validation, various aspects of intraseasonal, seasonal and interannual variability, ocean wind stress applications, and validation of surface fluxes. The last day included talks about several related efforts at the National Meteorological Center (NMC), the National Center for Atmospheric Research (NCAR), the Center for Ocean–Land–Atmosphere Studies (COLA), the United States Navy, and the European Center for Medium Range–Weather Forecasts (ECMWF). This was followed by talks from several members of the DAO on current and future development efforts. The workshop concluded with a general discussion on data quality, data access experiences and suggestions for future development of the GEOS system.

This report includes most of the extended abstracts from the workshop, and attempts to summarize the major findings as well as the planned development activities designed to address the deficiencies in the GEOS–1 system. Section 2 contains the extended abstracts organized by session as follows: 1) circulation statistics and transport (chair: L. Takacs), 2) precipitation, clouds, and radiation (chair: M. Suarez), 3) phenomenology and diagnostics (chair: M.-L. Wu), 4) surface characteristics (chair: A. Molod), 5) related projects and collaboration (chair: D. Lamich), and 6) current and future development (chair: C.-K. Park). The summary is given in section 3, and the Appendix gives a brief overview of the GEOS–1 system.

2 Results

2.1 Circulation Statistics and Transport

Evolution of Large Scale Circulation during TOGA-COARE: Model Intercomparison and Basic Features

K. - M. Lau, P. J. Sheu , S. Schubert, D. Ledvina and H. Weng

NASA/Goddard Space Flight Center
Laboratory for Atmospheres
Greenbelt, MD 20771

An intercomparison study of the evolution of large scale circulation features during TOGA-COARE has been carried out using products from three 4-dimensional assimilation systems: the National Meteorological Center (NMC), the Navy Fleet Numerical Oceanography Center (FNOC) and the NASA Goddard Space Flight Center (GSFC), GEOS-1. Our basic conclusion is that the preliminary assimilation product, albeit somewhat crude, can provide important information concerning the evolution of the large scale atmospheric circulation and probable causes for the westerly wind burst (WWB) over the warm pool of the tropical western Pacific during TOGA-COARE.

Figure 1 shows the evolution of the 5-day mean zonal wind (upper panel) from sounding observations at Kavieng: this is compared with the three assimilated wind products in Figure 2. All three assimilated products show very similar wind profiles which compare favorably with the observations. The two westerly wind bursts are clearly evident in the assimilated results, though the second event appears to be somewhat weaker than observed. In contrast, the precipitation estimates (lower panels) vary considerably. The GPI estimate shows substantially stronger rainfall rates compared with the radar estimates. Similarly, the three assimilations show substantially different rain rates, with the GEOS values generally weaker than the NMC and NOGAPS values.

Based on the comparative model diagnostics, the following picture of large scale evolution and multi-scale interaction during TOGA-COARE emerges:

> The propagation of the Madden and Julian Oscillation (MJO) from the equatorial Indian Ocean region into the western Pacific foreshadows the establishment of WWB events over the COARE region. The Maritime Continent appears to play a critical role in modulating the characteristics of the propagation signals.
>
> The maintenance of the WWB during TOGA-COARE is related to the establishment of a large scale east-west pressure dipole between the Maritime Continent and the equatorial central Pacific. This pressure dipole can be identified in part with the ascending (low pressure) and descending branch (high pressure) of the MJO and in part with the fluctuations of the austral summer monsoon.
>
> Accompanying the development of WWB over the Intensive Flux Array (IFA) and crucial to its maintenance is a robust meridional circulation, with strong cross-equatorial flow and rising motion near the entrance region of the WWB and sinking motion in the extratropical northern hemisphere.

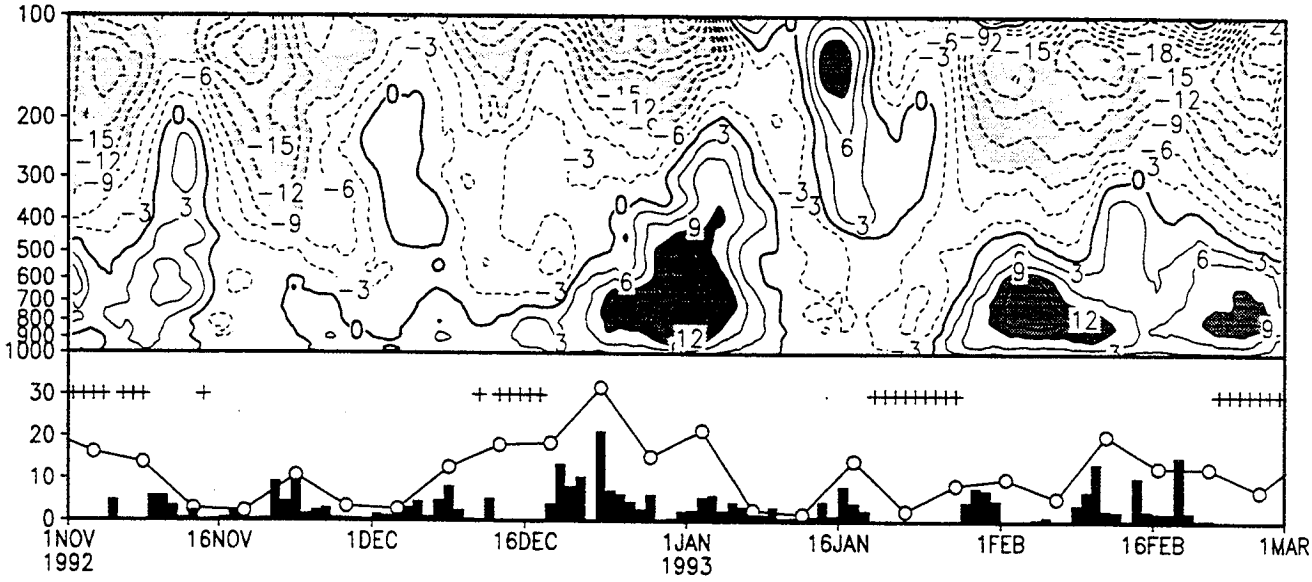

Figure 1: Time-pressure cross-section of 5-day mean zonal wind at Kavieng (m/s). Lower panel shows GPI pentad-precipitation (connected open circles) and daily radar estimates (histogram). Heavy (light) shading indicates westerlies (easterlies) with magnitude exceeding 9 m/s. Missing data in the radar record are shown as closed circles. Unit of rainfall is mm/day.

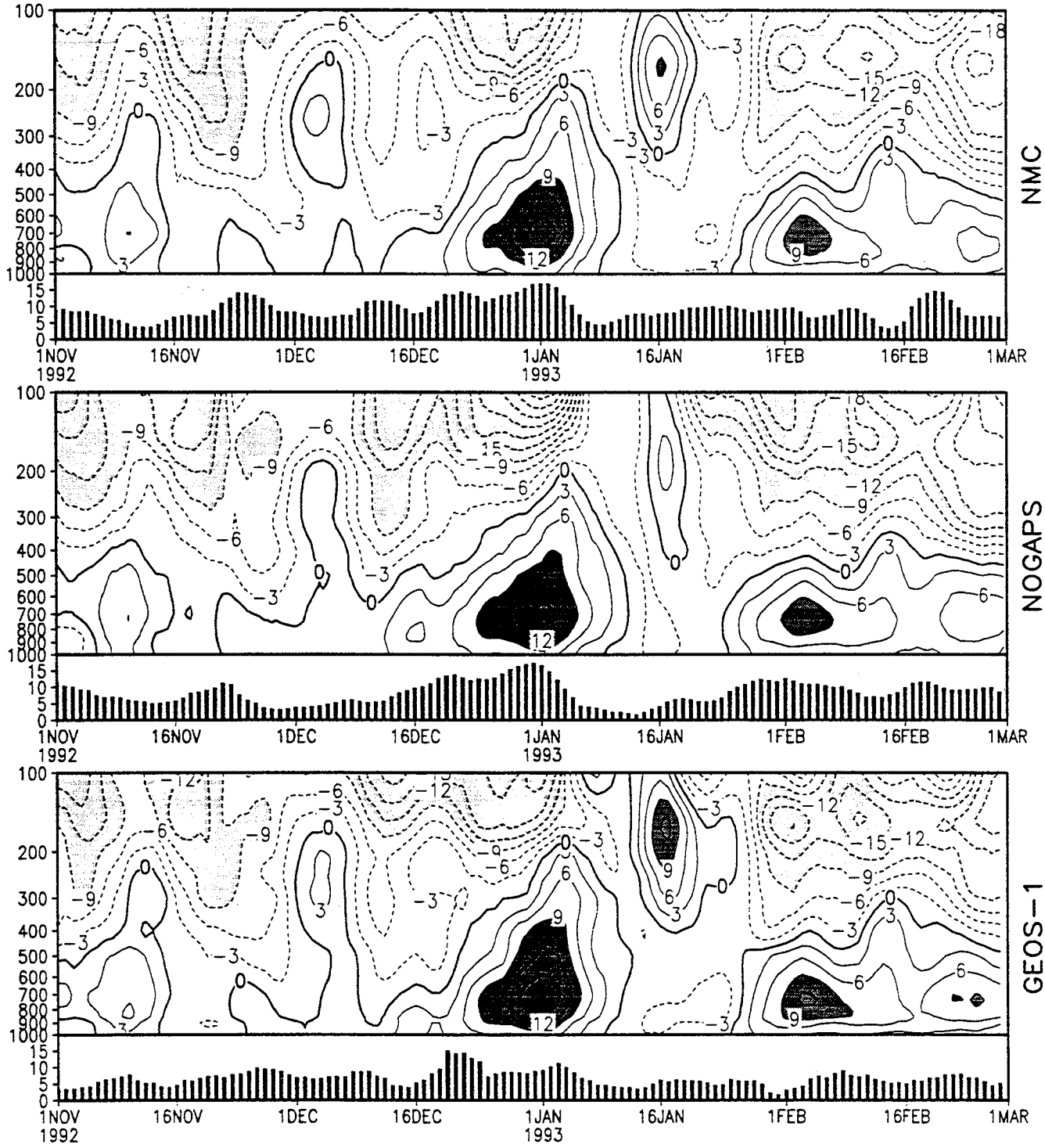

Figure 2: Same as Fig. 1, except for the grid box (0°-5°S, 150°-160°E) for NMC (top), NOGAPS (middle) and GEOS-1 (bottom).

Monitoring Global Geodynamics using the Goddard EOS Data Assimilation System

B. F. Chao
D. J. Steinberg
Geodynamics Branch, NASA Goddard Space Flight Center, Greenbelt, MD 20771

The wind structure and mass distribution of the atmosphere both vary on a wide variety of temporal and spatial scales. Globally, two distinct dynamic consequences of these variations are felt by the planet as a whole despite the small overall mass ratio between atmosphere and solid Earth: (1) The motion and the associated mass redistribution modify the atmospheric angular momentum (AAM). The AAM variation in turn causes the solid Earth's rotation to vary under the conservation of total angular momentum of the combined atmosphere-solid Earth system. The most striking example is in the Earth rotational speed often noted as changes in the length-of-day, virtually all of which on time scales from a few days to several years can be accounted for by the variations of AAM [for a review, see *Dickey*, 1993]. Recent studies [e.g., *Chao*, 1993] have also demonstrated a dominant role of AAM in exciting changes in the orientation of the Earth rotational axis, known as the polar motion. (2) The mass redistribution modifies the Earth's external gravitational field according to Newton's gravitational law. This perturbs the orbits of satellite, from which the low-degree gravitational harmonics can be best detected [e.g., *Chao and Au, 1991; Nerem et al.*, 1993].

These effects have been observed in the precise measurements of the Earth's rotation and its gravitational field variations made by modern space geodetic techniques. Among the new techniques are laser ranging to artificial satellites and the moon, very-long-baseline interferometry to remote cosmic radio sources, and most recently, precise positioning by the multi-satellite Global Positioning System.

Studying the above relationships involves comparisons of geodetically-measured quantities of Earth rotation and gravitational parameters, on one hand, with corresponding quantities calculated from meteorological analyses, i.e. AAM and spherical harmonics of atmospheric mass distribution, on the other hand. The appropriate meteorological variables for these purposes are now available routinely on a sub-daily basis from four major operational weather centers: the U.S. National Meteorological Center (NMC, since 1976), the European Centre for Medium-Range Weather Forecasts (ECMWF; since 1980), the United Kingdom Meteorological Office (since 1981), and the Japan Meteorological Agency (since 1984). A special data center for AAM quantities [*Salstein et al.*, 1993] has been operating at NMC since 1989 under the auspices of the International Earth Rotation Service (IERS), an agency organized jointly by the International Union of Geodesy and Geophysics and the International Astronomical Union. Parallel efforts are underway elsewhere, including the routine computation of the atmospheric gravitational effects with ECMWF data at the NASA Goddard Space Flight Center [*Chao and Au*, 1991].

This heritage will continue and be expanded to the Goddard Earth Observing System-1, or GEOS-1, developed at the Data Assimilation Office (DAO) and currently being used to perform an analysis (or re-analysis) of historical data [*Schubert et al,* 1993]. The GEOS-1 system was run at a horizontal resolution of 2 degree (latitude) by 2.5 degree (longitude) and 20 levels in the

vertical, given on the non-dimensional "sigma" coordinate, from the surface to about the 20 hPa (or mb) level. Output for the re-analysis is produced four times daily (0000, 0600, 1200, 1800 UT) for upper air quantities, while several single level and vertically-integrated quantities are available 8 times daily. The output routine is, however, quite general and can be easily modified to allow output at any desired sampling interval.

The meteorological quantities of concern for our present application are the (2-D) global surface pressure and the (3-D) wind velocity field. The computations involve area integrations of the surface pressure and volume integrations of the wind velocity fields given, for each variable, appropriate geographical weighting functions, or "kernels" often in the form of spherical harmonic functions [e.g., *Chao*, 1994]. The amount of data input to the computation is about a quarter of a million values per time step of 6 hours.

Specifically, we compute the following parameters: AAM zonal and meridional components due to winds and pressure, and gravitational effect in terms of all the harmonic Stokes coefficients from degrees 0 to 4 and additional zonal harmonics (order 0 only) up to degree 20. There are 45 independent parameters by count; but for the pressure-based parameters, we compute separately for land-only, ocean under IB (Inverted Barometer), and ocean under non-IB, using the 2 degree by 2.5 degree land-ocean mask employed by GEOS-1.

An equally important and practical step that we are taking is to incorporate these integration computations as a module within the process of GEOS-1, so that the 128 geodynamic parameters become part of the standard output of GEOS-1. The extra computational and archival burden on GEOS-1 is relatively simple, but it completely alleviates the need for subsequent input/output and processing. Plans for extending the time series back to 1979 and to the present are also underway.

References

Chao, B. F., and A. Y. Au, Temporal variation of Earth's zonal gravitational field caused by atmospheric mass redistribution: 1980-1988, *J. Geophys. Res., 96*, 6569 6575, 1991.

Chao, B. F., Excitation of Earth's polar motion by atmospheric angular momentum variations, 1980-1990, *Geophys. Res. Lett., 20*, 253-256, 1993.

Chao, B. F., The Geoid and Earth Rotation, in *Geophysical Interpretations of Geoid*, ed. by P. Vanicek and N. Christou, CRC Press, 1994.

Dickey, J. O., Atmospheric excitation of the Earth's rotation: Progress and prospects via space geodesy, in *Contributions of Space Geodesy to Geodynamics: Earth Dynamics*, 55-70, ed. D. E. Smith and D. L. Turcott, AGU, Washington, D. C., 1993.

Nerem, R. S., B. F. Chao, A. Y. Au, J. C. Chan, S. M. Klosko, N. K. Pavlis, and R. G. Williamson, Temporal variations of the Earth's gravitational field from satellite laser ranging to LAGEOS, *Geophys. Res. Lett., 20*, 595-598, 1993.

Salstein, D. A., D. M. Kann, A. J. Miller, and R. D. Rosen, The sub-bureau for atmospheric angular momentum of the International Earth Rotation Service: A meteorological data center with geodetic applications, *Bull. Amer. Meteor. Soc., 74*, 67-80, 1993.

Schubert, S. D., J. Pfaendtner and R. Rood, An assimilated data set for Earth Science applications, *Bull. Am Met. Soc., 74*, 2331-2342, 1993.

Global momentum and energy diagnostics from the GEOS-1 assimilation

David A. Salstein and Richard D. Rosen
Atmospheric and Environmental Research, Inc.
840 Memorial Drive, Cambridge, Massachusetts 02139

1. Introduction

Based on output from the Goddard Earth Observing System Data Assimilation System, we have examined five years of global and hemispheric statistics related to atmospheric angular momentum and energy. The global momentum values are calculated from the wind and surface pressure fields and are related to geodetic measurements of Earth orientation values. Components of the energy cycle that we evaluated include zonal mean and eddy kinetic and available potential energies, conversions between different energy forms, and the generation of potential energy by diabatic heating processes. These large-scale diagnostics help us evaluate the quality of the fields from the data assimilation, and they are useful also in studies relevant to climate and geophysical signals.

2. Angular momentum diagnostics

Using five years of NASA GEOS-1 analyses, 1 March 1985 - 28 February 1990, we have evaluated each of the components of the three-dimensional atmospheric angular omentum vector (Salstein et al. 1993). These quantites include wind-based motion terms and surface pressure-based mass terms. Their variations are related to the small but measurable motions of Earth, through the exchanges of angular momentum occurring between planetary components; contributions to these terms by the ocean are known to be relatively small. Those variations about Earth's axis are related to changes in the length of the day (l.o.d.) and are due primarily to the motion term. A plot of the relative momentum term shows good agreement with an l.o.d. series for the same period, produced by the technique of Very Long Baseline Interferometry. A coherence analysis for subseasonal time scales reveals significant agreement between momentum and l.o.d. terms at all frequencies greater than about 10-12 days. When the mass term is added to the motion term for atmospheric momentum, the level of coherence at all time scales longer than 8 days increases, and significant coherence now becomes established down to periods as short as 8-9 days. A separate analysis comparing the momentum from the GEOS-1 DAS system to that from the NMC reanalyses for the same period reveals significant coherence on all scales greater than about 3 days, a shorter limit than was typically obtained between pairs of the older operational angular momentum series. Thus we conclude that the reanalysis series are in closer agreement than operational series have been in the past for this quantity.

When comparing the GEOS-1 DAS momentum series to the NMC operational series, we note a decrease in fluctuations at the highest frequencies. Their energy density spectra are about one-half an order of magnitude different in power on scales shorter than 4 days. However, the difference in smoothness at the highest frequencies might be due in part to the post-processing involved in archiving wind fields.

Regarding the strength of the seasonal cycle in angular momentum, we note the importance of stratospheric levels on these scales. The stratosphere has a particularly strong influence at semi-annual frequencies, and amplitudes of the semi-annual signal increase with the inclusion of higher stratospheric layers. For example, including layers up to 100 and 20 millibars produce semi-annual momentum amplitudes of 0.116 and 0.144 respectively; the l.o.d. value is 0.173. [All values are given in equivalent l.o.d. units of milliseconds]. Including values to 10 millibars, with the help of the NMC reanalysis, increases the value to 0.149, and even higher stratospheric levels are likely to bring the momentum budget into better balance (Rosen and Salstein 1991).

We assess elements of interannual variability during the five-year period by subtracting the long-term seasonal values from each of the seasons at each of 46 equal-area belts from the south to north pole. Higher values during the 1987 El Nino and lower values during the 1988 La Nina are evident, and these signals are determined largely by contributions in the subtropics to middle latitudes. We also note evidence of poleward propagation of interannual momentum anomalies, with precursors to the subtropical signals existing in tropical latitudes (Dickey et al. 1992, Black et al. 1995).

The availability of subdaily data, particularly for the equatorial wind components, is important for diagnosing the atmosphere's contribution to polar motion. These equatorial quantities involve the zonal wavenumber-1 parts of the horizontal wind field, and, as such, are sensitive to diurnal fluctuations related to atmospheric tides and are modulated by the seasonal cycle (Bell 1994). In this formulation, values at 00 and 12 UTC form an envelope for the equatorial momentum component centered on the 0 - 180 degree axis, and 06 and 18 UTC values form a similar envelope for the 90 E - 90 W-based quantity. We note that the GEOS-1 DAS wind values appear to successfully capture the subdaily behavior in these tidally-related quantities.

3. Energy diagnostics

To diagnose aspects of the energetics of the atmosphere in each hemisphere, we have calculated monthly values of energy levels, conversions, and generations in a classical framework (Peixoto and Oort 1992). In particular, we have calculated time series of the potential and kinetic energy values, for both zonal mean and eddy forms, the conversions between mean and eddy forms of potential and kinetic energies, and the generation of zonal mean and eddy energies.

Potential and kinetic energies follow very strong seasonal cycles within each of the five years, typically out of phase between northern and southern hemispheres, but stronger in the northern hemisphere. Interannual variability of these energy terms are calculated by removing a mean seasonal cycle, calculated from the five years. Interannual anomalies in zonal mean potential and kinetic energies display a strong transition from the 1987 El Nino to the 1988 La Nina periods in both hemispheres, with stronger values during 1987. For the potential and kinetic energy terms, this interannual transition likely results from a reduction in mean winds and temperature gradient terms respectively. Although energy conversion terms do have contrasting seasonal signatures, they contain no clear interannual signals during this period.

Zonal mean available potential energy is generated when diabatic heating effects increase the meridional temperature gradient. Hence, a positive correlation between the heating and temperature fields will result in positive energy generation. We have calculated the time series of the generation of zonal mean available potential energy, for the total, as well as for each of the four separately-determined model-produced heating fields: sensible, latent, longwave radiational, and shortwave radiational heating. Monthly fields for the five-year period reveal a generally steady seasonal pattern whose total is driven primarily by the positive latent heating contribution in both hemispheres. Generation due to longwave processes is negative due to the inverse relationship between that (negative) heating process and temperature. Shortwave and sensible heating cause positive energy generation, though with typically smaller magnitudes than that for latent heating; they seem largely to balance the negative generation from the longwave radiational component.

We examine the latent heating anomalies in two months in which the minimum and maximum interannual anomalies in the generation of zonal available potential energy by latent heating occur: January 1987 and January 1989, respectively. The zonal mean heating cross sections of latent heating anomalies for these two months are different,

particularly in the northern middle latitudes. Though the maximum in latent heating on a long-term basis occurs in the deep tropics due to deep convection, in these middle latitudes a secondary maximum in latent heating typically occurs in connection with shallower processes. Stronger values of heating over middle latitudes, which are cooler than lower latitudes, would act to decrease the meridional temperature gradient and, hence, reduce zonal potential energy generation. The 1987 latent heating anomaly in the middle latitudes is stronger than normal by up to 40 percent, and the 1989 anomaly is negative by almost the same amount. Further consideration of relevant data sets will be required to understand the details responsible for the type of large-scale behavior revealed by these time-series anomalies.

References

Black, R.X., D.A Salstein, and R.D. Rosen, 1995: Interannual modes of variability in atmospheric angular momentum. Manuscript in preparation.

Bell, M.J., 1994: Oscillations in the equatorial components of the atmosphere's angular momentum and torques on the earth's bulge. Q. J. R. Meteorol. Soc., 120, 195-213.

Dickey, J.O., S.L. Marcus, and R. Hide, 1992: Global propagation of interannual fluctuations in atmospheric angular momentum. Nature, f357, 484-488.

Rosen, R.D., and D.A. Salstein, 1991: Comment on "A seasonal budget of the Earth's axial angular momentum" by Naito and Kikuchi. Geophys. Res. Lett., 18, 1925-1926.

Peixoto, J.P., and A.H. Oort, 1992: Physics of Climate. American Institute of Physics, 520 pp.

Salstein, D.A., D.M. Kann, A.J. Miller and R.D. Rosen, 1993: The Sub-bureau for Atmospheric Angular Momentum of the International Earth Rotation Service: A meteorological data center with geodetic applications. Bull. Amer. Meteorol. Soc., 74, 67-80.

F-11 and Rn-222 calculations using a 3-d CTM and assimilated data

Mr. Dale Allen and Dr. Robert Hudson -- University of Maryland
Dr. Richard Rood and Dr. Anne Thompson -- NASA-GSFC

INTRODUCTION

The three-dimensional constituent continuity equation is solved for F-11 and Rn-222 using GEOS1-DAS input fields. F-11 is a long lived tracer that is emitted predominantly in the northern hemisphere at locations where industrial use of electricity is large. It is destroyed by photolysis in the stratosphere. Rn-222 is a short-lived tracer that is emitted over land. Its only loss mechanism is radioactive decay.

Five questions will be addressed. 1) Are synoptic events cap tured? 2) Is interhemispheric exchange realistic? 3) Is ventilation of the planetary boundary layer (PBL) realistic? 4) Is the correct amount of mass transported to the upper troposphere by convection? 5) Does data assimilation provide additional information that is not available from a general circulation model.

THE CALCULATION

The mixing ratio change due to advection, turbulent mixing, convective mixing, and chemical processes are solved for.

The mixing ratio change due to advection is solved using a flux-form semi-Lagrangian algorithm. The standard version of this algorithm uses a monotonic piece-wise parabolic method (PPM) in the horizontal and a semi-monotonic PPM in the vertical.

The horizontal winds needed to calculate the horizontal advection are obtained from the GEOS1-DAS. The instantaneous winds at 0, 6, 12, and 18UT are used. The vertical velocity is calculated kinematically and matches the GEOS1-GCM vertical velocity.

Convective mixing is parameterized using six hour time-averaged convective cloud mass flux and detrainment information from the Relaxed Arakawa Schubert (RAS) algorithm that is used in GEOS1-DAS. A one-dimensional continuity equation is solved for each model column in order to determine the entrainment and subsidence in the column. The constituent mass change in each layer is obtained by adding the mass change due to subsidence and detrainment to the mass in each layer not involved in convection.

Two calculations were performed. The first calculation was

initialized at 00UT 26 April 1985 and run through 31 December 1988. Rn-222 was initially set to zero. F-11 was initially set to 207 pptv south of 20S, 222 pptv north of 20N, and allowed to vary linearly with latitude between 20S and 20N. The initial condition did not vary with longitude. The mixing ratio fell off linearly with pressure above 100 hPa. An additional Rn-222 calculation was initialized 00UT 1 January 1991 and run through 31 December 1992.

Turbulent mixing is parameterized by assuming a well (partially) mixed PBL for the 1985-1988 (1991-1992) calculation. The depth of the PBL is interpolated from the GEOS1-DAS PBL depth that is available every three hours.

Emission of Rn-222 is set to 1.16 atoms cm^{-2} over land and to zero over water. The emission is reduced by a factor of three when the temperature in the surface layer falls below 273 K. A loss frequency of 2.1×10^{-6} s^{-1} is specified giving Rn-222 a lifetime of 3.8 days.

The emission of F-11 is based on electrical consumption. The global production varies with time, but the production sites are held fixed during the calculation. The loss frequency for F-11 is obtained from the Goddard two-dimensional model.

The F-11 calculation will be compared with 1987-1988 F-11 data at ALE/GAGE sites in Ireland, Oregon, Barbados, and Samoa.

The Rn-222 calculation will be compared with surface layer data at Bermuda, Cincinnati, and Socorro; a climatological continental summertime profile; measurements taken aboard a ship in the Pacific during 1986; and aircraft measurements taken in the eastern Pacific.

RESULTS

The calculated and observed F-11 fields are strikingly similar in Ireland. The timing and magnitude of pollution events are well simulated. In addition the seasonal change in the variability from the monthly mean is well simulated. Transport of F-11 by synoptic events to Ireland is well modeled.

Individual events are only occasionally captured at Oregon. The seasonal cycle of variability is fairly well modeled.

The summertime variability of F-11 at Barbados and Samoa is underestimated. The increased variability at these locations during the summer is believed to be due to the summertime incursion of air from the opposite hemisphere. Interhemispheric exchange of F-11 is not well modeled in this calculation.

The annual cycle of Rn-222 in the boundary layer at Cincinnati is well modeled during the afternoon. Concentrations are largest during the winter and increase slightyly from March through December. Model concentrations during the morning are much too low during non-winter months.

The calculated afternoon summertime profile at Cincinnati and Socorro are compared to a climatological afternoon profile. The Cincinnati profile is within a standard deviation of the

average profile throughout the lower and middle troposphere. The model profile is higher than the observed profile in the upper troposphere, however only two summertime measurements extend above 8 kms. The Socorro profile is nearly constant with height in the lower troposphere due to the depth of the PBL. Mid-tropospheric concentrations at both locations are lower than the climatological profile.

The abrupt increase in Rn-222 concentrations at Bermuda due to frontal passage is well modeled. Increases of a factor of five or more are not unusual. The good agreement provides evidence that ventilation of the east coast of the United States PBl is realistic. A more sophisticated algorithm for filtering out contamination by local Rn-222 production is needed. The annual cycle is also well modeled. Continental air reaches Bermuda much more frequently during during the winter than summer.

Calculated and measured Rn-222 are also compared for a 1986 ship cruise. The time series are highly correlated during June and July when the ship was well off the coast. The agreement is much worse during May when the ship passed near the coast of Alaska. The 1986 cruise data is also compared to 1987 model output. The poor agreement demonstrates that interannual variability is important.

Finally, Rn-222 measured in the upper troposphere during the summers of 1983 and 1984 are compared to model output from 1986. Model concentrations are lower than observed concentrations south of 35N but are consistent with the observations at latitudes north of 35N.

SUMMARY

Northern hemisphere synoptic events are well captured. Interhemispheric exchange is not well modeled. Upper troposphere concentrations of Rn-222 are not inconsistent with variable and scarce observations. Mid-tropospheric concentrations of Rn-222 appear low. Finally, data assimilation provides additional information that a GCM cannot provide. Individual events can be studied and dynamical variability can be eliminated.

TRANSPORT INVESTIGATIONS USING THE GEOS-1 CONVECTIVE FLUXES

Kenneth E. Pickering[1], Wei-Kuo Tao[2], Yansen Wang[3], John R. Scala[3], Anne M. Thompson[2], Donna P. McNamara[4], Shian-Jiann Lin[5], Andrea M. Molod[5], and Richard B. Rood[2]

[1] Joint Center for Earth System Science, University of Maryland, College Park, Maryland
[2] NASA Goddard Space Flight Center, Greenbelt, Maryland
[3] Science, Systems, and Applications, Inc., Lanham, Maryland
[4] Applied Research Corporation, Landover, Maryland
[5] General Sciences Corporation, Laurel, Maryland

A critical component of all 3-D global tropospheric chemical transport models is the representation of vertical transport through convective clouds. Because convection takes place on spatial scales smaller than the size of a grid cell of a global model, the transport associated with this process must be parameterized. Chemical transport in 3-D global models is driven by meteorological fields produced by data assimilation systems or by free running general circulation models. In this report we evaluate the GEOS-1 global data assimilation system convective cloud mass fluxes using vertical fluxes from a cloud-resolving model (the 2-D Goddard Cumulus Ensemble (GCE) Model, Tao et al. (1991, 1993)). First, a case study of a particular squall line event (the well-studied 10-11 June 1985 PRESTORM episode) is chosen as representative of summertime mid-latitude continental convection. In both the GEOS-1 and GCE models, estimates of vertical flux are made to approximate the amount of venting of the boundary layer. Vertical profiles of cloud mass flux from the two models are also compared. Second, we compare tracer transport results using output from GEOS-1 (winds and cloud mass fluxes) with those using GCE winds. Third, from monthly-averaged satellite cloud observations and GCE model simulations of the 10-11 June 1985 event and other episodes, we have estimated a convective mass flux for all of June 1985 in the central US. This is compared to the GEOS-1 convective mass flux over the same period and region.

Penetrative convection originating in the boundary layer is parameterized in GEOS-1 using the relaxed Arakawa-Schubert (RAS) scheme [Moorthi and Suarez, 1992]. The assimilated data sets contain six-hour average values of cloud mass flux and cloud detrainment. The GCE model is nonhydrostatic and variables include horizontal and vertical velocities, potential temperature, and mixing ratios of water vapor, cloud water, rain, cloud ice, snow, and hail/graupel. Solar and infrared radiative transfer processes are included.

We use the major squall line type mesoscale convective system that occurred over Kansas and Oklahoma on June 10-11, 1985, during the Preliminary Regional Experiment for Stormscale Operational and Research Meteorology Program - Central Phase (PRE-STORM) for our case study. We have examined the cloud mass flux estimates produced by the GEOS-1 assimilation for the peak intensity period of the squall line. These values are averages for the six-hour period centered on 0000 UT June 11 for the model level,

sigma = 0.874. This level approximately corresponds to the top of the boundary layer over the Oklahoma/Kansas region. The GEOS-1 cloud parameterization places the greatest cloud mass flux associated with this weather system over Nebraska. This location is about 2 model grid cells north of where the strongest convective activity was noted on radar and satellite imagery. This position error likely results either from errors in the temperature, moisture or wind fields entering the assimilation system or from the cumulus parameterization itself. The magnitude of the peak cloud mass flux is about 0.09 kg m^{-2} s^{-1} over a small area. A region of greater than or equal to 0.06 kg m^{-2} s^{-1} covers a region with dimensions of approximately 450 km in the north-south direction and 200 - 300 km in the east-west direction. These dimensions are similar to those of the observed squall line.

A simulation of the entire life cycle of the most intense region of the June 10-11 squall line using the 2-D GCE model has been described in detail by Tao et al. [1993] and Pickering et al. [1992a]. The model produced a cloud that is in good agreement with radar data (cloud height and vertical velocity). The 2-D wind fields from the cloud model were used to transport tracers from each of eight layers. The amount of tracer that is lifted above the top of the second layer during the 6.5 hour simulation in a 274 km wide sector centered on the main convective region of the squall line corresponds to 10.9% h^{-1}. Using this statistic along with the air density we can estimate the amount of cloud mass flux over the same time period as in the assimilation (6 hours). We compute a value of 0.054 kg m^{-2} s^{-1} which compares favorably with the cloud mass flux of 0.06 kg m^{-2} s^{-1} computed in the GEOS-1 assimilation for a similar size area.

Figure 1 shows a comparison of the profiles of cloud mass flux produced by GEOS-1 and by the GCE model for the 10-11 June squall line. The GEOS-1 profile is an average over four grid cells (centered at 40° and 42° N and 97.5° and 100° W) that comprise the cloud mass flux maximum. While the magnitudes of the two profiles are quite similar, there are some differences in the profile shape. The GCE profile shows values increasing with altitude in the lower troposphere, indicating that the cloud system was entraining air throughout the lower levels. In contrast, the GEOS-1 profile is nearly constant with altitude in the lower and middle troposphere, and cloud detrainment (also produced by the RAS parameterization) is quite small (typically, 0.001 - 0.006 kg m^{-2} s^{-1}) in this altitude range. These results suggest that the RAS parameterization is causing most of the cloud air to be entrained at the bottom of the cloud. The GCE flux is larger than the GEOS-1 flux at the upper levels, suggesting that the cloud produced in the assimilation did not penetrate as high as that generated in the cloud-resolving model.

We have used carbon monoxide (CO) for tracer transport calculations using the GCE wind fields and the GEOS-1 winds and cloud mass fluxes. The GEOS-1 data are used in the 3-D Goddard Chemical Transport Model. Both transport codes were initialized with measured CO mixing ratios. The GCE data produce a large CO anvil with maximum CO exceeding 120 ppbv; the GEOS-1 output produce a slighly larger anvil with similar CO mixing ratios. The major difference is that downward transport in the GCE simulation is much stronger than in the simulation with the global model. This result is due to the lack of downdraft parameterization in GEOS-1.

We have also compared the performance of the data assimilation system in

estimating cloud mass flux over the period of a month (June 1985) over the central United States. We extracted the upward cloud mass flux from the assimilation output every 6 hours during the entire month of June 1985 and computed a total value for the month for each grid cell at the 0.874 sigma level. We use the statistical/dynamical technique developed by Pickering et al. [1992b] to make an observationally-based estimate of upward cloud mass flux for the region. This technique uses monthly mean gridded statistics for deep convective cloud cover taken from the International Satellite Cloud Climatology Project (ISCCP; Rossow and Schiffer, 1991) for June 1985 and upper and lower limit convective transport statistics from GCE model simulations of prototype convective events (including the June 10-11, 1985 PRE-STORM squall line). Summing over all the grid cells we obtain upper and lower limit estimates of the total cloud mass flux of 3.20×10^{16} and 5.17×10^{16} kg month^{-1}, respectively for the region. The GEOS-1 regional estimate (5.77×10^{16} kg month^{-1}) is just slightly greater than the upper limit estimate from the statistical/dynamical technique. The assimilation product is expected to be slightly greater than that based on the statistical/dynamical approach because the convective parameterization in the GEOS-1 model considers convective clouds of all sizes but the ISCCP data used in the statistical/dynamical approach is only for deep convective clouds.

We have demonstrated that the RAS parameterization of convective clouds in the GEOS-1 data assimilation produces reasonable values of cloud mass flux in a case study of a major summertime midlatitude continental squall line and on a regional monthly-total basis.

References

Moorthi, S. and M. J. Suarez, Relaxed Arakawa-Schubert: A parameterization of moist convection for general circulation models, Mon. Weather Rev., 120, 978-1002, 1992.

Pickering, K. E., A. M. Thompson, J. R. Scala, W.-K. Tao, R. R. Dickerson, and J. Simpson, Free tropospheric ozone production following entrainment of urban plumes into deep convection, J. Geophys. Res., 97, 17,985-18,000, 1992a.

Pickering, K. E., J. R. Scala, A. M. Thompson, W.-K. Tao, and J. Simpson, A regional estimate of convective transport of CO from biomass burning, Geophys. Res. Lett., 19, 289-291, 1992b.

Rossow, W. B. and R. A. Schiffer, International Satellite Cloud Climatology Project (ISCCP) cloud data products, Bull. Amer. Met. Soc., 72, 2-20, 1991.

Tao, W.-K., J. Simpson, and S.-T. Soong, Numerical simulation of a subtropical squall line over Taiwan Strait, Mon. Weather Rev., 119, 2699-2723, 1991.

Tao, W.-K., J. Simpson, C.-H. Sui, S. Lang, J. Scala, B. Ferrier, M.-D. Chou, and K. Pickering, Heating, moisture, and water budgets in the convective and stratiform regions of tropical and midlatitude squall lines: Their sensitivity to longwave radiation, J. Atmos. Sci., 50, 673-690, 1993.

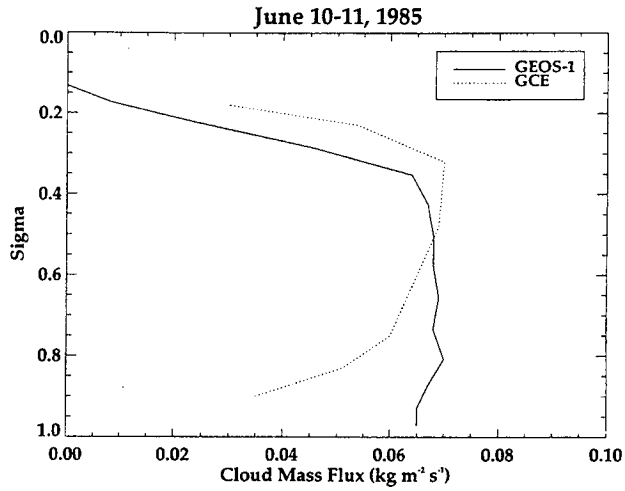

Figure 1. Profiles of cloud mass flux for June 10-11, 1985 squall line computed by the GEOS-1 assimilation and by the GCE model.

The Use of GEOS-1 Data for the ASHOE/MAESA Mission

P. Newman, L. Lait, M. Schoeberl, M. Seablom, L. Coy, D. Lamich, R. Rood, R. Stimpfle, K. Roland Chan

GEOS-1 data was extensively used during the Airborne Southern Hemisphere Ozone Experiment (ASHOE) and the Measurements for Assessing the Effects of Stratospheric Aircraft (MAESA) mission. ASHOE/MAESA used the high altitude NASA ER-2 aircraft from New Zealand, California, and Hawaii. The goals of ASHOE/MAESA were to: 1) investigate ozone losses in the southern hemisphere, 2) investigate the relationship of these losses to polar, mid-latitude, and tropical processes, and 3) provide information on stratospheric photochemistry and dynamics for assessing the potential impact of a future fleet of stratospheric aircraft.

The ASHOE/MAESA mission was scheduled in four parts. The first part took place in March-April 1994, and consisted of a flight from Moffett Field, California to 60N; followed by a flight to Hawaii; 2 flights from Hawaii to the equator; a flight to Fiji and then onto Christchurch, New Zealand; and finally 3 flights to 68S near Antarctica from Christchurch. This first flight series was timed to sample the stratospheric conditions near the equator, and the stratospheric conditions over Antarctica prior to the appearance of polar stratospheric clouds (PSCs). The second deployment took place in May-June 1994, and consisted of 4 flights down to Antarctica and back and 1 flight to the southern subtropics. This second part was timed to the first appearace of PSCs in the Antarctic stratosphere. The third deployment took place in August 1994, and consisted of 4 flights down to Antarctica and back and 1 flight to the southern subtropics.
This third part was timed to the coldest period in the Antarctic stratosphere. The final flight series took place in October 1994 and was timed to the disappearance of PSCs and the period of largest ozone losses in the Antarctic stratosphere.

The GEOS-1 data were extensively used in the ASHOE/MAESA mission for both forecasting and for analysis of aircraft data. These data were utilized to both plan the details of ER-2 flights, and to analyze the aircraft data after each flight. The need for high quality meteorological analyses and forecasts is required for 3 reasons. The first reason is that the chemical makeup of air parcels inside the polar vortex is substantially different than mid-latitude stratospheric air. Measurements of N2O, various CFCs and HCFCs, H2O, CO2, O3, NOy, and CH4 show distinctly different characteristics between polar and mid-latitude air masses. Second, the temperature of the air is critical to the formation of PSCs. Type I PSCs are found to form near the nitric acid trihydrate vapor saturations, hence the air temperature is crucial to understanding whether PSCs. Further, when temperatures fall below water ice saturation temperatures, these ice particles are large enough to settle out of the stratosphere. Since both water and nitric acid are carried out of the stratosphere by the settling of these particles, cold temperatures can have an extreme effect on the stratospheric chemistry. Finally, an accurate knowledge of an air parcels history is crucial to understanding the observations of the highly reactive gases such as ClO, NO, OH, and HO2. Trajectories calculated via the coarse grained meteorological fields are of prime importance for interpreting these ER-2 observations.

In this presentation, various analyses will be compared to aircraft observations. Winds, and temperatures from the GEOS-1 data will be compared to the ER-2 aircraft observations. Estimates of analysis errors will be discussed and compared to both NMC and UKMO UARS analyses. A case study of the use of GEOS-1 data will be employed to reveal the evolution of the the Antarctic polar vortex during the period of May 28 to June 3, 1994. This case demonstrates the general good agreement between the trajectory calculations from the GEOS-1 data, and the observations of the constituents.

Table I displays the RMS deviation of the GEOS-1 data and the ER-2 Meteorolgical Measurements System observations (Chan et al.,) for all 37 flights of the ASHOE/MAESA mission. The GEOS-1 data were comparable to both the NMC and the UKMO observations for the entire mission. Figure 1 illustrates the comparison between

observations from MMS and the GEOS–1 data for June 1, 1994. Note the 1 K cold bias of the GEOS–1 data. The region covered by this flight has virtually no radiosonde coverage, and is primarily covered by NESDIS satellite retrievals derived from the TOVS. instruments (HIRS, MSU, and SSU). The MMS observations reflect the proliferation of small scale structure that is unresolved by the conventional observation network. MMS wind observations additionally showed structure of this nature with many small scale features that are not resolved by conventional observations. Particularly poor wind comparisons occured on most of the tropical flights from Hawaii and the Hawaii to Fiji ferry flights.

Table I

	Temp.	*U–wind*	*V–wind*
NMC	2.1	5.6	4.6
UKMO	2.0	4.9	4.9
GEOS–1	2.4	6.0	5.2

Table I. RMS deviations of analyses and winds for all of the ASHOE/MAESA flights. The deviations were only calculated for pressures below 100 mb.

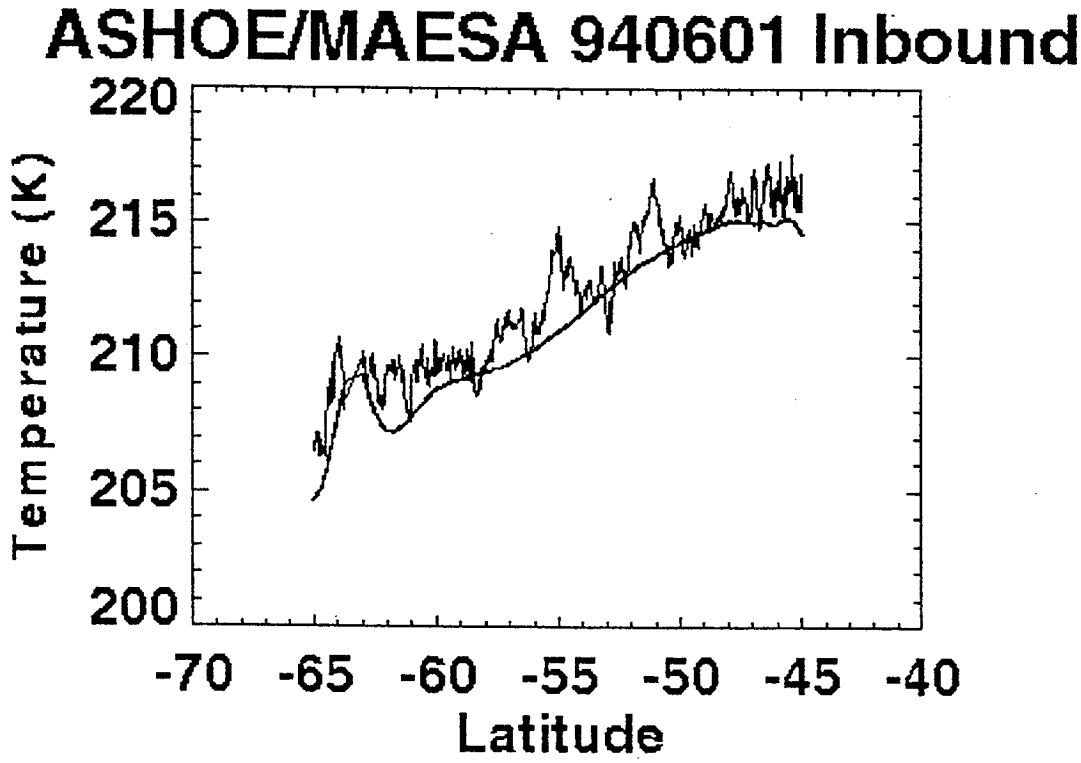

Figure 1. GEOS–1 temperatures for 940602 at 00Z versus latitude, and MMS temperatures versus latitude for the ASHOE/MAESA flight of 940601. The observations span the time from 2300 UT on 940601 to 0230 UT on 940602. The GEOS–1 temperatures are biased 1K cooler than the MMS data with a 0.9 K standard deviation of the difference.

Trajectories are utilized to trace the history of air parcels in the stratosphere. This is particularly important in the polar vortex. As the air cools below about 195 K, PSCs form. and heterogeneous chemical reactions of CLONO2 and HCl occur on the PSC surfaces, releasing chlorine from these relatively benign species into Cl2 which can photolyze in the presence of sunlight, form ClO, and catalytically destroy ozone. On the ASHOE/MAESA flight of 940601, enhanced levels of ClO were observed poleward of approximately 62S. These enhanced levels of ClO indicated that the air had probably been exposed to PSCs within a short period prior to the sampling. Back trajectories using the GEOS-1 data indicate that temperatures were cold enough to form PSCs, consistent with the theory and previous results.

The enhanced ClO observed on 940601 was followed by the sampling of isolated piece of enhanced ClO air by the ER-2 near New Zealand on the flight of 940603. This enhanced ClO air was sampled well away from the polar vortex at relatively low altitudes. Potential vorticity analyses on the 385K isentropic surface indicate that this air encountered cold temperatures inside the polar vortex on about 28 June 1994, extended in a tongue of air that was sampled on June 1 by the ER-2, and continued to move northward towards New Zealand where it was sampled a second time on 3 June. Back trajectories from GEOS-1, UKMO, and NMC winds confirmed this behavior. Kinematic studies using forward trajectories suggest that the vortex at these low altitudes during early June does not present a strong barrier to transport.

A Three Dimensional Simulation of the Ozone Annual Cycle Using winds from a Data Assimilation System

Anne R. Douglass*, Clark J. Weaver*, Richard B. Rood+,
Lawrence Coy*

NASA/Goddard Space Flight Center, Greenbelt, MD

The wind fields from the NASA/Goddard stratospheric data assimilation procedure are used in a 3 dimensional chemistry and transport model to produce an ozone simulation for the year Sept. 11, 1991 - Sept. 10, 1992. Photochemical production and loss are taken from the Goddard 2 dimensional model. The calculated ozone is compared with observations from the Total Ozone Mapping Spectrometer (TOMS) on board Nimbus 7 and the Microwave Limb Sounder (MLS) on the Upper Atmospheric Research Satellite (UARS). The simulated ozone fields reproduce many of the features in the observations. Even at the end of this integration, the synoptic features in the modeled total ozone are very similar to TOMS observations, indicating that the model maintains realistic values for the horizontal and vertical gradients, at least in the lower stratosphere. From this good comparison between model and observations on time scales ranging from days to months, we infer that the transport driven by the assimilated wind fields closely approximates the actual atmospheric transport. Therefore, the assimilated winds are useful for applications which may be sensitive to the lower stratospheric transport.

*Code 916
+Code 910.3

2.2 Precipitation, Clouds, and Radiation

Comparison of GEOS-1 data with analysis and short-range forecast data from ECMWF and other estimates of the truth.

Klaus Arpe and Martin Stendel
Max-Planck-Institut for Meteorology
Bundesstr.55, D-20146 Hamburg, Germany

Operational analyses are often not suitable for detection of climate variability because of numerous changes in the analysis/forecasting schemes. These changes may lead to variations of some sensitive variables which are larger than the signal of climate variability itself. Therefore several meteorological centres have started to create analyses with a frozen scheme. These schemes are then applied to historical data (at ECMWF backwards to 1979) and should be so advanced that they need not be changed for a while in the future. One of the most important variable for climatological studies is the precipitation and unfortunately it is also a most difficult quantity to analyse or simulate. A key question is therefore, how reliable are the precipitation estimates created with the analysis scheme. A comparison of different analysis schemes can help to identify sensitive areas and in areas with a good observational data coverage one can compare the estimated precipitation with observations. Both schemes do not analyse the precipitation but it is gained from the atmospheric forecast model which at ECMWF is providing the first guess field or is in the GEOS-1 scheme used for adjusting the observed data. Such precipitation data are closely related to the divergent wind and therefore also a comparison of wind observations with wind analysis may help to gain or lose confidence in the analysis data.

The re-analysis at ECMWF has just started and there are no common time periods from the two analysis centres yet available except from an early trial experiment at ECMWF for two months (January 1986 and July 1985) which agree with the GEOS-I period. These two month will be the main basis for the comparison. We will start the study with some basic quantities.

The mean sea level pressure (MSLP) is probably one of the best known quantities and therefore we start the comparison of the two analysis with this quantity. The monthly means from both analysis centres are very similar in most respect. So we will concentrate on the few points where both analysis differ. Firstly there are differences in the extrapolation below ground which could make differences of up to 5 hPa over very high or hot ground.

More important are systematic differences over the northern Pacific, the ECMWF analysis for January 1986 provide in the area 135°-180°W/30°-40°N about 2hPa higher monthly mean MSLP and this difference continues vertically almost unchanged through the atmosphere, i.e. 20dam difference at 500hPa and 40dam at 50hPa. When looking into the diurnal cycle one finds that this difference results from the 12GMT analysis. The ECMWF analysis provides 2 hPa higher MSLP at 12 GMT than at the other 3 analysis times while the GEOS-1 analysis has hardly any diurnal cycle in this area. One possible source for differences is a different treatment of the tides. In MSLP the strongest component of the tides is the semi-diurnal tide, which can be made visible by plotting 06 minus 12 GMT analysis and similar combinations. Both analysis scheme are very similar in reproducing the semi-diurnal tide which is very clear in the tropics equator-wards of 45°. The difference between both analysis in the northern Pacific seems not to be part of this tide. Also the fact that the diurnal cycle in this area is hardly present during July 1985 speaks against the possibility of an involvement of the tides. We do not believe that this 12GMT maximum over the northern Pacific in the ECMWF analysis is real but do not yet know

the cause of it.

A further large difference in the MSLP can be found in the southern hemisphere especially during July 1985. This difference has a strong zonal mean component with lower ECMWF values between 40° to 50°S and higher values between 50° and 60°S (up to 3hPa and 6hPa respectively over the Pacific). Also this difference has a strong equivalent barotropic component and is reflected also by differences of the zonal mean wind. The pattern of this difference in the zonal mean wind (GEOS-1 has up to 4m/s stronger mean winds in the upper troposphere at 55°S) reminds strongly on the patterns found in plots of the systematic error of many models, also of the ECMWF model, but taking the sign of the difference into account, it is clear that the GEOS-1 model must have a much stronger systematic error than the ECMWF model and that this error is carried over into the analysis in the southern hemisphere.

Differences of the zonal mean temperature between both analyses reveal that the ECMWF analysis provides cooler tropopauses of 1 to 3K, especially in the tropics. Investigating those few tropical radiosonde stations which have reported at least 29 times in a month of consideration and comparing the two analysis at these sites with the observations, reveals that the ECMWF analysis has drawn closely to the observations while the GEOS-1 analysis provides monthly mean 100 hPa temperatures which are 2 to 3K warmer than the observations in both months and at 00 and 12GMT.

A further quantity we looked at is the Hadley circulation, which turned out to be much weaker in the GEOS-1 analysis than in the ECMWF analysis during January 1986. Again we compared the few tropical radiosonde observations with the analyses at their sites. The monthly mean v-component of the wind was reproduced faithfully by the ECMWF analysis scheme while the GEOS-1 data differed mostly by 2 to 4 m/s from the observations (often this means a 50% weaker v-wind). A part of this might be due to our way of calculation, which was done on a T42 grid and for that we had to perform an extra interpolation step with the GEOS-1 data but we believe that this is less important.

As a main quantity of interest we investigated the precipitation, where we expected larger differences. ECMWF provides not only precipitation values every 6 hours (means during the 6hour forecast for the first guess) but also twice a day forecasts for 24 hours. This allows an investigation of the spin-up of the model. A strong spin-up is an indication of inconsistencies between analysis data and model formulations. Therefore one is inclined to use the data with more care where there is a strong spin-up. The ECMWF precipitation data show a spin-up from the 6hour forecasts to the 12-24 hour means with often more precipitation of 10 mm/month in the longer range forecasts in the mid-latitudes of both hemispheres and in both months of consideration and occasionally over tropical oceans. This increase of precipitation can often mean an increase of 25%. Unfortunately we do not have this information for the GEOS-1 scheme. Comparisons with climatological estimates and analysis data of precipitation suggest that the 12-24 hour forecast means by ECMWF provide a better estimate of the truth than the 6hour forecasts.

A comparison of GEOS-1 with ECMWF precipitation and comparisons with climatological estimates or monthly mean analyses give the following results:
*GEOS-1 has a weaker ITCZ than ECMWF, probably the ECMWF values are more realistic (see also the comparison of the Hadley circulation).
*GEOS-1 precipitation values are too low along the northern Rockies and along the US south coast during January 1986.

*GEOS-1 precipitation values are too large over S.E. USA and too low over western USA in July 1985.
*Over India during July 1985 the gap of precipitation between the western Ghats and the bay of Bengal is missing in the GEOS-1 analysis. (July 1987 was however well simulated in this respect)
*There is too much precipitation over continental Europe in July85 and too little over the Mediterranean during January in the GEOS-1 data.
*Over Africa the ITCZ is further north in the ECMWF analysis compared to GEOS-1. The ITCZ in the ECMWF analysis has there a more zonal pattern. It is not clear which of the two analyses is more correct.

By looking into the fields of the other years we find that some of the findings here for January 1986 and July 1986 are probably generally true but we could not substantiate it as we did not have all the data for comparison available.

This preliminary comparison cannot be taken as a final judgement on the quality of either of the two analysis schemes but may guide for further investigations which will hopefully lead to improvements of one or the other analysis scheme.

In this study we have picked on some points of weaknesses of the analysis scheme which does not reflect our appreciation of the value of the data for climate research. We are convinced that the data can be used successfully especially when one is interested more in the variability of quantities than in their absolute values and if one takes the deficiencies of the analysis data into account when interpreting them.

We are in debt of Per Kållberg, Sakari Uppala and Rex Gibson for providing us with the preliminary ECMWF reanalysis data and for discussions on possible causes for differences between the analyses.

Comparisons of Global Precipitation Estimates from the Satellite-Gauge-Model Technique and the GEOS-1 Assimilation

George J. Huffman*
NASA/GSFC Laboratory for Atmospheres and Science Systems and Applications, Inc.

Robert F. Adler
NASA/GSFC Laboratory for Atmospheres

1. SGM Introduction

The Satellite-gauge-model (SGM) technique is being developed as a robust global scheme to combine independent observations and estimates of precipitation into a suite of data products that can used for validating models, computing regional and global precipitation, and detecting long-term trends (Huffman et al., 1995). We seek to remove biases from individual estimate and then combine estimates with method depending on sources. The biases are assumed least for gauges, then SSM/I, IR, and model.

The SGM starts with independent precipitation estimates from a variety of sources. In this presentation we use

- low-orbit microwave (SSM/I analyzed with the Goddard Scattering algorithm – GSCAT2);
- geo-IR (merged histograms from Climate Analysis Center, CAC, analyzed with the GOES Precipitation Index – GPI);
- gauge analyses (smoothed versions of analyses from CAC of gauge data collected in real time as part of the Climate Assessment and Monitoring System – CAMS); and
- four-dimension data assimilation estimates (monthly accumulation from the Data Assimilation Office's Goddard EOS assimilation system – GEOS-1).

Where the geo-IR data exist, the GPI estimates are adjusted by the microwave estimates using the Adjusted GPI (Adler et al., 1995). A multi-satellite precipitation product is formed of AGPI, where available, and GSCAT2 microwave estimates elsewhere. The large-scale (3x3 grid box) average of the multi-satellite is adjusted to agree with the large-scale average of the gauges (where available), then the adjusted satellite and gauge fields are linearly combined using the local inverse error variance of each field as weights. This satellite-gauge (SG) product is used for comparison in this talk. As a final step, remaining holes in the SG product are filled with GEOS-1 accumulations to produce the satellite-gauge-model (SGM).

Errors are estimated for each of the underlying fields assuming that the random error dominates the total error field. The nominal error depends on the particular field and fluctuations depend on sampling.

2. Comparisons of SG and GEOS-1

At the time of the talk 26 months of SG fields were available (July 1987 to September 1989, except December 1987), allowing a limited comparison of interseasonal and interannual variation, as well as a 2-year average (Figure 1). The fields are "matched" in space and time, so that corresponding grid boxes have exactly the same sampling in time.

* *Author Address:* Dr. George J. Huffman/SSAI, NASA/GSFC Code 912, Greenbelt, MD 20771. huffman@agnes.gsfc.nasa.gov

Grid boxes with less than 6 samples are replaced with cross-hatching. Most of the globe away from the poles has complete coverage.

The global-scale patterns of SG and GEOS-1 are qualitatively similar (existence of the ITCZ, subtropical dry zones, and mid-latitude storm tracks). On the other hand, there are significant differences. In some cases this can be explained by characteristics in GSCAT2, such as the relative dryness of the SG in the South Pacific and South Atlantic subtropical highs, as well as the Southern Ocean. In other cases more work needs to be done, including explaining the relative strengths of the western and eastern ends of the ITCZ in the Pacific, and the relative strengths of the midlatitude storm tracks compared to the ITCZ for each of the techniques.

Over the whole 2-year period the SGM global-total precipitation (which essentially matches the SG global-total) is consistently lower (by about 8%) than the GEOS-1. The land contributions to the GEOS-1 have a larger seasonal fluctuation than the SG, while in both the ocean contributions are nearly constant with time.

A comparison of the June/July/August and December/January/February shows relatively good agreement between SG and GEOS-1 on the sign of the seasonal difference, but large fluctuations in the magnitude of the change. In part, this reflects differences in the relative strengths of the features in question, including segments of the ITCZ and the storm tracks.

The most detailed comparisons attempted, interannual comparisons of June/July/August and of November/December/January/February gave the least consistent results, as we might expect. Features directly associated with the El Niño of 1987 appear in both the SG and GEOS-1, such as enhanced precipitation over New Guinea and a deficit to the east. As well, both show the drought in the summer of 1988 over much of North America. However, objective measures are hard to apply due to shifts in sign as well as magnitude.

To summarize, the SGM technique is starting to provide a new approach to determining the accuracy of the GEOS-1 precipitation estimates. Although both approaches are still under study, the comparison allows us to critically examine each, and to have improved confidence where they are in agreement.

3. Experiences Acquiring GEOS-1 Data

To date, our work with the GEOS-1 has been narrowly focused on monthly precipitation. After some experimentation with the full 240-field data sets, we found it much more convenient to pull across the monthly average fields. It is necessary to re-grid the GEOS-1 fields to our standard grid, but otherwise we can use the precipitation fields "as is." In the future we might take advantage of the division between convective and large-scale precipitation.

4. References

Adler, R.F., G.J. Huffman, and P.R. Keehn, 1994: Global rain estimates from microwave-adjusted geosynchronous IR data. *Remote Sensing Rev.*, **11**, 125-152.

Huffman, G.J. R.F. Adler, B. Rudolf, U. Schneider, P.R. Keehn, 1995: Global precipitation estimates based on a technique for combining satellite-based estimates, raingauge analysis, and NWP model precipitation information. *J. Climate*, **11**, in press.

Figure 1 Caption (see next page) Two-year averages (July 1987 to June 1989, minus December 1987) of Satellite-Gauge and GEOS-1 data (top and bottom, respectively) in mm/mo. Averages are computed on time/space-matched data, and boxes with less than 6 samples are filled with cross-hatching.

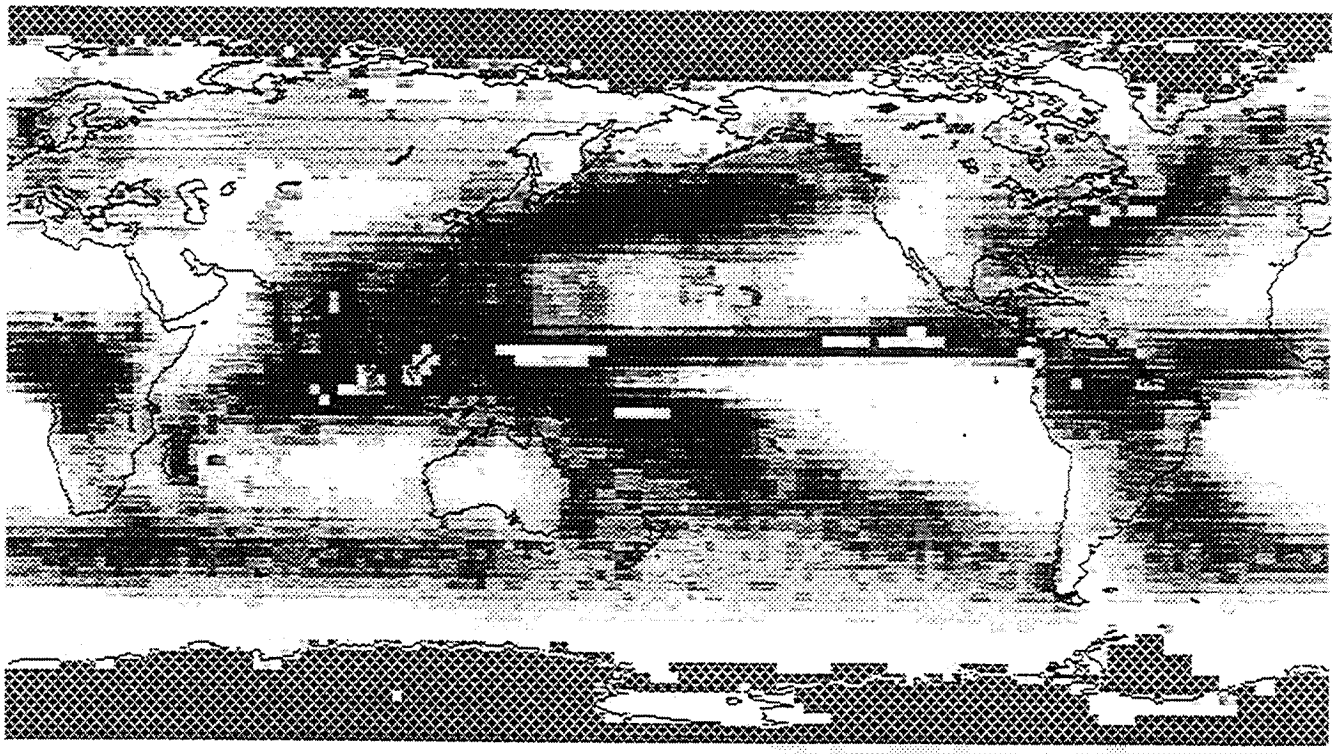

Matched SG 8707–8906 (mm/mo)

0 100 200 300 400 500+

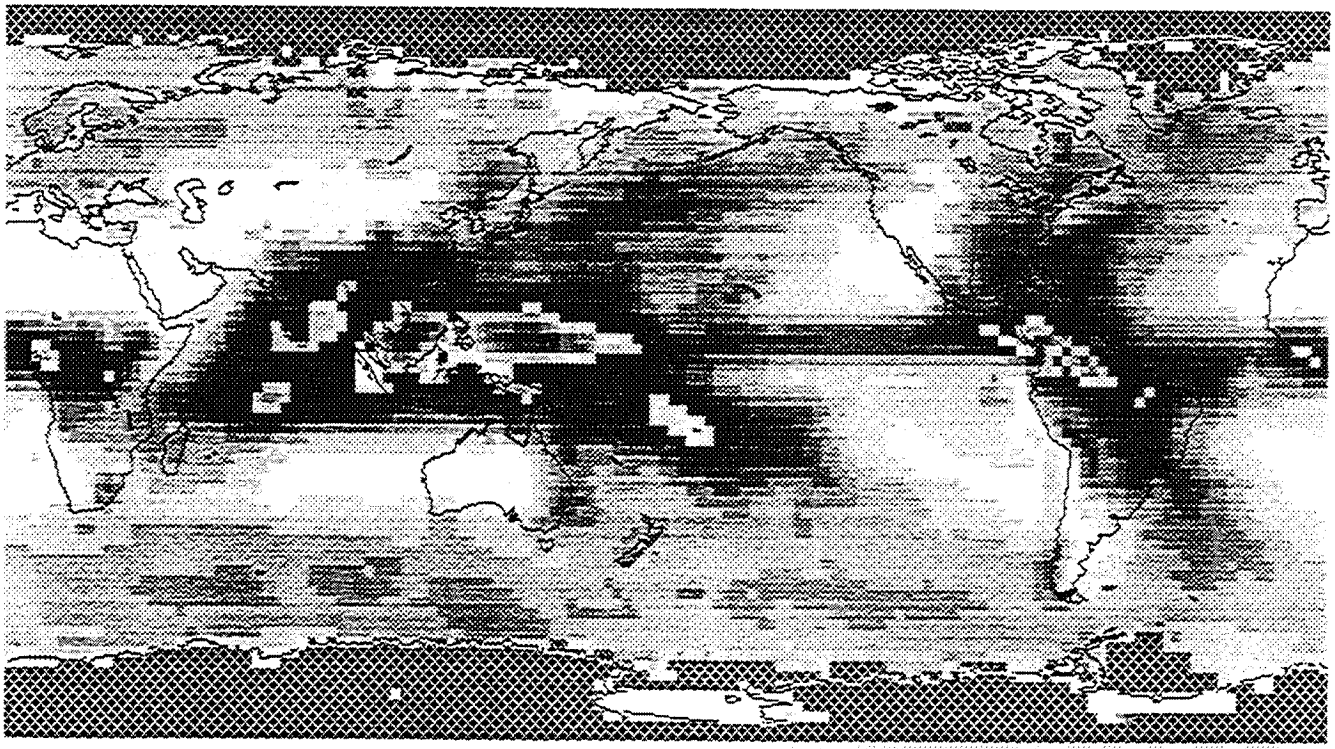

Matched GEOS-1 8707–8906 (mm/mo)

0 100 200 300 400 500+

Analysis of GEOS-1 Rainfall Data for Hydrological Modeling

Eric F. Wood and Theodore Stephens, Water Resources Program, Princeton University, Princeton, NJ 08544 (efwood@pucc.princeton.edu)
Randal Koster, NASA/GSFC, Greenbelt, MD

(Presented at the Workshop on Results from the GEOS-1 Five Year Assimilation, Goddard Space Flight Center, Greenbelt, MD March 6-7, 1995.)

Introduction

Using meteorological data products from 4DDA models in climate analyses is very appealing because the assimilated data sets are consistent and global in coverage. 4DDA precipitation products are particularly attractive given the importance of precipitation time series data in land-atmospheric modeling and the difficulty in obtaining such data globally at fine temporal resolutions (hourly or daily) from other sources.

As an example of the potential use of 4DDA hydrologic fields, the ISLSCP global soil moisture initiative plans to use rainfall (and other surface meteorology) to drive surface hydrological models to estimate surface soil moisture. Such a strategy has significant risks if the quality of the 4DDA rainfall fields are poor. This concern arises from the parameterization of the water balance equation for the land surface. In its lumped form, the water balance equation for a control volume is

$$dS = P - E_i - E_s - T_v - Q \tag{1}$$

where dS is the change in soil moisture, P is precipitation, E_i is interception loss, E_s is evaporation from the soil surface, T_v is vegetal transpiration, and Q is runoff (both surface and drainage). This lumped equation says little about the inherent spatial and temporal scales operating in nature, which must be built into the specific parameterizations of the flux terms. Spatial variation in P, for example, can have significant effects on surface fluxes (see Liang, 1994). The parameterization of bare soil surface evaporation and transpiration is related to soil texture, which varies spatially, and to the surface meteorology - especially temperature and humidity.

To evaluate fully the appropriateness of using 4DDA surface meteorology to drive surface hydrological models, the 4DDA products must be tested at temporal resolutions that are relevant to the response times of the surface hydrology. This implies a temporal resolution of between 1 hour and 1 day. Globally, the average cycling time for atmospheric water is on the order of 6 days, and the day-to-day variation in atmospheric evaporative demand can be significant; thus, looking at the 4DDA derived products at the monthly time scale may be insufficient.

For a full evaluation of 4DDA surface meteorology and rain rates, one would

want to substitute the 4DDA fields into a distributed water and energy balance model and make comparisons of the model's outputs to the surface hydrology estimated (and validated) through ground-based observations. As a first step, we have focused here on precipitation over the United States (in general) and over the Missouri River in particular. We present below both a comparison of observed and 4DDA-generated storm and interstorm statistical characteristics and a discussion of the impact of applying 4DDA fields to a hydrologic model.

Statistical Model Analysis.

Hawk and Eagleson (1992) analyzed hourly rainfall gauge data over the United States to estimate the parameters of a stochastic rainfall generation model that treats rainfall arrival times as a Poisson process. The model's parameters include average storm duration and intensity, average interstorm (dry period) duration and the correlation between storm intensity and duration. The derived seasonal values for these parameters at the rain gauge sites were used to construct contour maps such as that in Figure 1a, which shows the average storm duration for July across the United States.

We performed an analogous analysis of the GEOS-1 3-hour precipitation time series data, which we extracted from the data archives for each grid cell around the globe. The analysis produced global maps, on a seasonal basis, of average storm intensity, average storm duration, average time between storms, average number of storm events per month, and certain other parameters specific to the Poisson model. Figure 1b presents the average storm duration for July over North America estimated from the GEOS-1 data. A comparison with Figure 1a indicates that, though the monthly precipitation volumes contained in the two data sets may compare favorably, the GEOS-1 data has significant deficiencies at higher temporal resolutions (e.g., daily). The storms produced in the GEOS-1 assimilation last far too long.

Figures 2a and 2b present the average July storm intensities calculated from the gauge and GEOS-1 data, respectively. The average intensities in the GEOS-1 model are low by a factor of 10 or so, which is consistent with the model's excessive storm durations, since the model's precipitation volumes are relatively accurate. For surface hydrology, the low intensities would imply that the partitioning of rainfall into infiltration and runoff, which depends on the rainfall rate, would be seriously in error.

One can speculate on the reasons for the excessively long storm durations and low intensities. One logical explanation lies in the interpretation of GEOS-1 grid cell rainfall and the associated fundamental inconsistency in the GEOS-1 and gauge data sets. Unlike the gauge data, which provide rainfall information at a point, the GEOS-1 data provide the areally-averaged rainfall rate P within a full grid cell. If this rainfall is interpreted as only falling within an areal fraction f of the cell, then the true local rainfall rate in the wetted fraction is P/f; i.e., the intensity where the rain actually falls is greater than that suggested by the areal average. In nature, precipitation over an area the size of a typical

GCM grid cell is indeed rarely uniform, and the fractional storm coverage over such an area may range from 5% - 15% (Gong et al., 1994). An f of 0.1 would increase local intensities tenfold. Likewise, inferred local storm durations would decrease, since a seemingly long storm in the GEOS-1 data could actually consist of several storms of shorter duration in different parts of the cell. (See Figure 3.)

To allow a fairer comparison of the GEOS-1 and gauge data statistics, we tried to convert the areally-averaged precipitations in the GEOS-1 data into equivalent time series of point precipitation rates. We first assumed that the conditional probability of rainfall at a point in the cell, given that rainfall occurs somewhere in the cell, is equal to a prescribed fractional storm coverage f. We then 'filtered' the GEOS-1 rainfall data by zeroing the rainfall over a fraction 1-f of the time intervals (chosen randomly) and increasing it by a factor of 1/f over the remaining time intervals. This procedure maintains the monthly total GEOS rainfall depth for the grid cell.

The GEOS-1 July rainfall data was filtered using an f of 0.1; this fraction reflects the convective nature of July rainfall and would need to be larger for, say, January precipitation. The resulting derived storm duration and intensity maps are shown in Figures 4a and 4b. In general, the statistics obtained with the filtered data are in much better agreement with the gauge-derived statistics. Additional analyses are required to determine the best spatial and seasonal filtering parameters and perhaps better ways to establish storm duration when filtering the data.

Hydrologic Modeling.

In a separate analysis, the (unfiltered) GEOS-1 rainfall time series data were used to drive a distributed hydrological model over the Missouri River basin. The hydrological model (Liang et al., 1994), which is referred to in the literature as the two-layer variable infiltration capacity (VIC-2L) model, was run at a 1 degree spatial resolution and without its standard energy balance formulation; for the present application the model used a monthly-varying, climatological potential evapotranspiration to allow us to focus on the GEOS-1 precipitation alone rather than on the full suite of GEOS-1 surface meteorology. The corresponding analysis with the full energy balance formulation remains to be done.

Figure 5 shows a plan of the Missouri basin with three sites identified for our hydrological model studies. The Missouri basin is particularly interesting for this analysis; it is of significant size (approximately 1.5 million sq. km.), and it has a very strong west-to-east rainfall gradient, with the Rocky Mountains in the west, a very arid climate in the center and more humid conditions in the south-east. The three sites shown in the figure span this climatic gradient.

The hydrological model had already successfully simulated the surface hydrology at these sites using station observations from 1948 through 1987; we are now interested in the changes induced when GEOS-1 data are used instead. Because the GEOS-1 rainfall data are available only from 1986 to 1990, there

are only two years (1986 and 1987) that overlap. These two years of GEOS-1 precipitation data were appended to the station data for the years 1948 through 1985 to create a modified 1948 through 1987 rainfall time series, and this modified time series was applied to the hydrological model using a daily time step. Thus, to examine the effect of applying GEOS-1 data to a hydrological model, we examine the final two years (1986-1987) of this second simulation.

Figure 6 compares the monthly mean runoffs generated in the final two years of each simulation. In general, at all three sites, the seasonal cycle of the runoff produced with the GEOS-1 data is similar to that produced with the station data. The Site 3 simulations show the closest agreement because the station and GEOS-1 rainfall time series compare well. In fact, for these test cases, the differences in the runoff produced with the station and GEOS-1 data appear to be related to differences in the time-integrated volumes of the imposed rainfall rather than to differences in their short-term temporal characteristics.

These preliminary results are encouraging but incomplete. Further comparisons for the other water balance terms, particularly soil moisture, are needed. In addition, the hydrological model needs to be forced with both the GEOS-1 rainfall data and GEOS-1 surface meteorology.

Summary

The results of the preliminary studies described above lead us to make the following observations.

1. The storm statistics from the GEOS-1 model seem at first glance to be poor, with underestimated storm intensities ("drizzle") and overestimated storm durations. Accounting for fractional coverage of storms, however, brings the GEOS-1 product more in line with observations. The proper interpretation of fractional coverage needs to be further investigated.

2. When 4DDA precipitation output is applied to a hydrological model, the resulting runoff has a reasonable seasonal cycle but tends to be overestimated due to the overestimated precipitation volumes in the particular regions studied. It is unclear whether this overestimation would be worse if fractional storm coverage were assumed, since rainfall intensities would be higher but soils would tend to be drier.

3. Other potential problems in applying the GEOS-1 output to hydrological models include the interpretation of 4DDA values of near-surface humidity, temperature and so forth. A hydrological modeler may be required to assume a subgrid distribution for these variables as well.

Acknowledgements. The research reported herein was supported in part by NASA contract NAS5-31719, entitled "Global Hydrologic Processes and Climate" as part of the Earth Observing System.

References

Gong, G., D. Entekhabi, and G. Salvucci, Regional and seasonal estimates of fractional storm coverage based on station precipitation observations, J. Climate, 7(12), 1495-1505, December 1994.

Hawk, K.L., and Eagleson, P.S., Climatology of station storm rainfall in the continental United States: parameters of the Bartlett-Lewis and Poisson rectangular pulses models, Tech. Rep. 336, Ralph M. Parsons Lab., Dept. Civil Eng., M.I.T., Cambridge, MA, 1992.

Liang, Xu, A two layer variable infiltration capacity land surface representation for general circulation models, Water Resources Series Technical Report No. 140, Department of Civil Engineering, University of Washington, Seattle, May 1994, 208 pp.

Liang, X., D. P. Lettenmaier, E. F. Wood, and S. Burges, A simple hydrologically based model of land surface water and energy fluxes for general circulation models, J. Geophys. Res. 99(D7), 14415-14428, July 20, 1994.

Figure Captions

1. Average storm duration (in hours) for July across the United States, as derived from (a) rainfall gauge data (Hawk and Eagleson, 1992), and (b) GEOS-1 products.
2. Average storm intensity (in 10^{-2} mm/hour) for July across the United States, as derived from (a) rainfall gauge data (Hawk and Eagleson, 1992), and (b) GEOS-1 products.
3. Illustration of subgrid precipitation processes within a grid cell.
4. (a) Average storm duration (in hours) and (b) average storm intensity (in 10^{-2} mm/hour) for July across the United States, as derived from "filtered" GEOS-1 products (see text). The intensity map is smoothed for clarity.
5. Sites analyzed with hydrological model and GEOS-1 data.
6. Monthly mean precipitation forcing for the hydrological model and the resulting monthly mean runoff rates, using gage data (solid lines) and GEOS-1 precipitation products (dashed lines).

1(a)

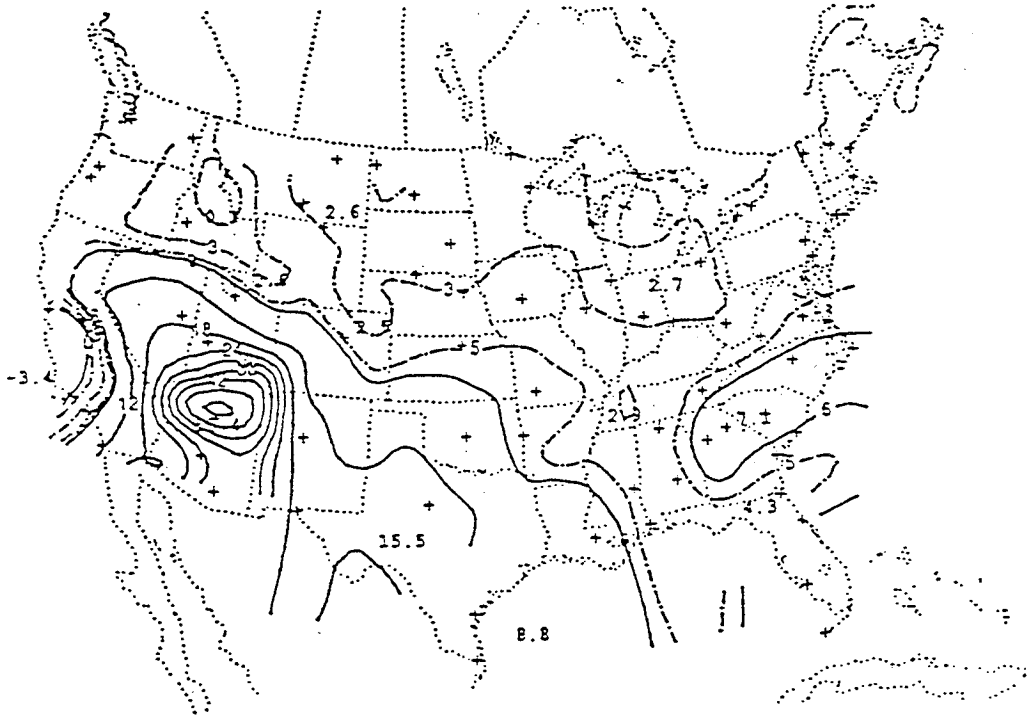
2.6
2.7
15.5
8.8

1(b)

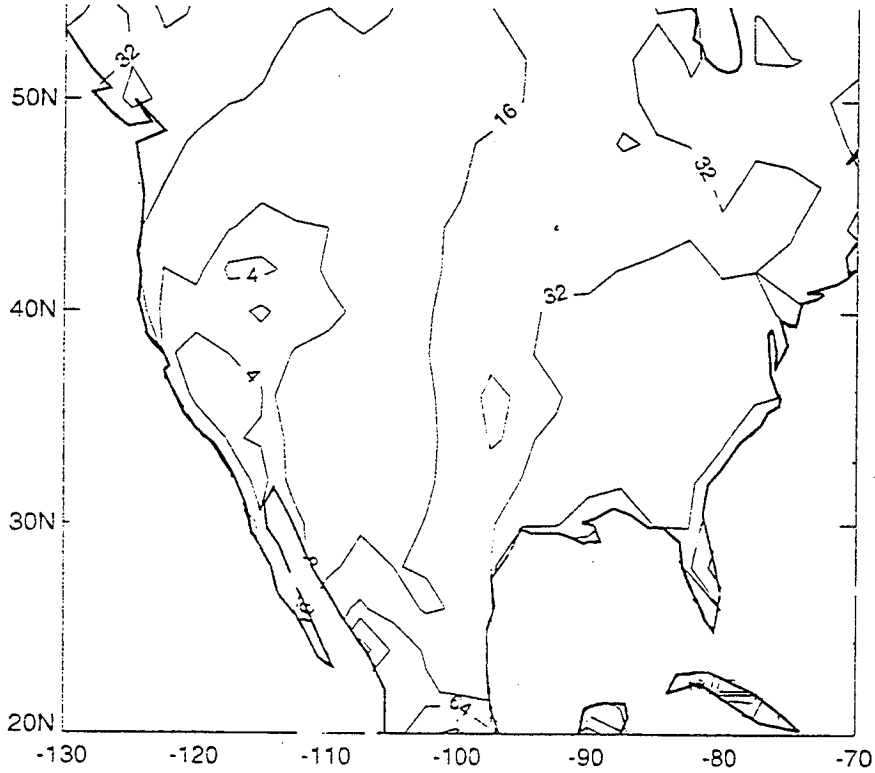
50N
40N
30N
20N
-130
-120
-110
-100
-90
-80
-70
32
16
32
4
32
4
4

2(a)

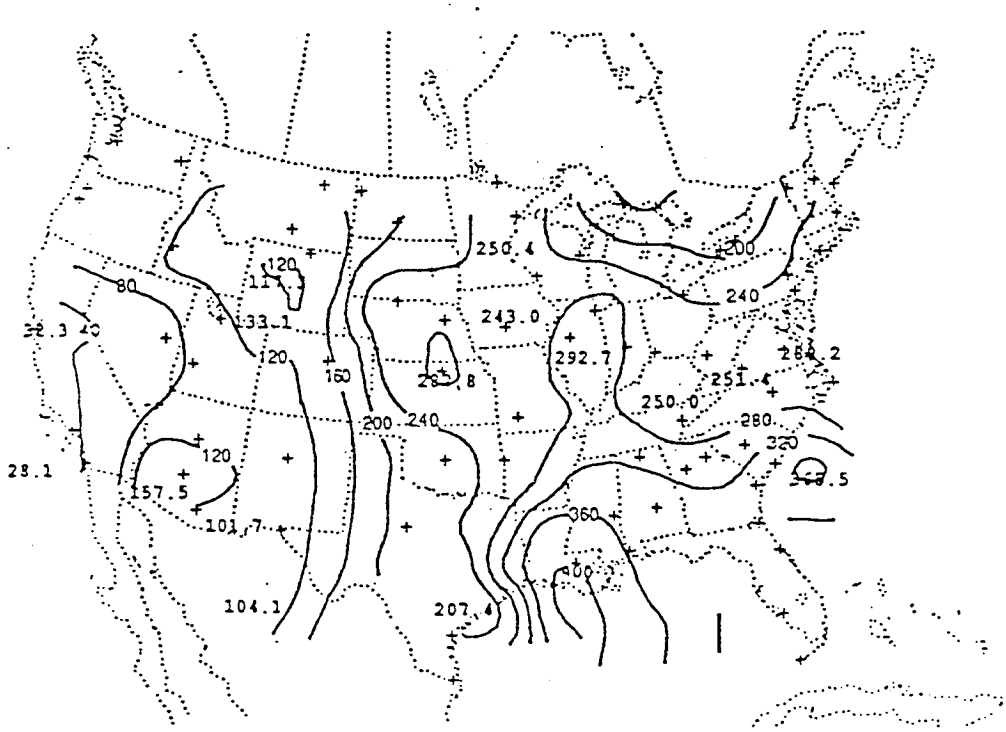
250.4
200
240
243.0
292.7
251.4
250.0
280
320
360
80
120
160
200
240
28.1
157.5
101.7
104.1
207.4

2(b)

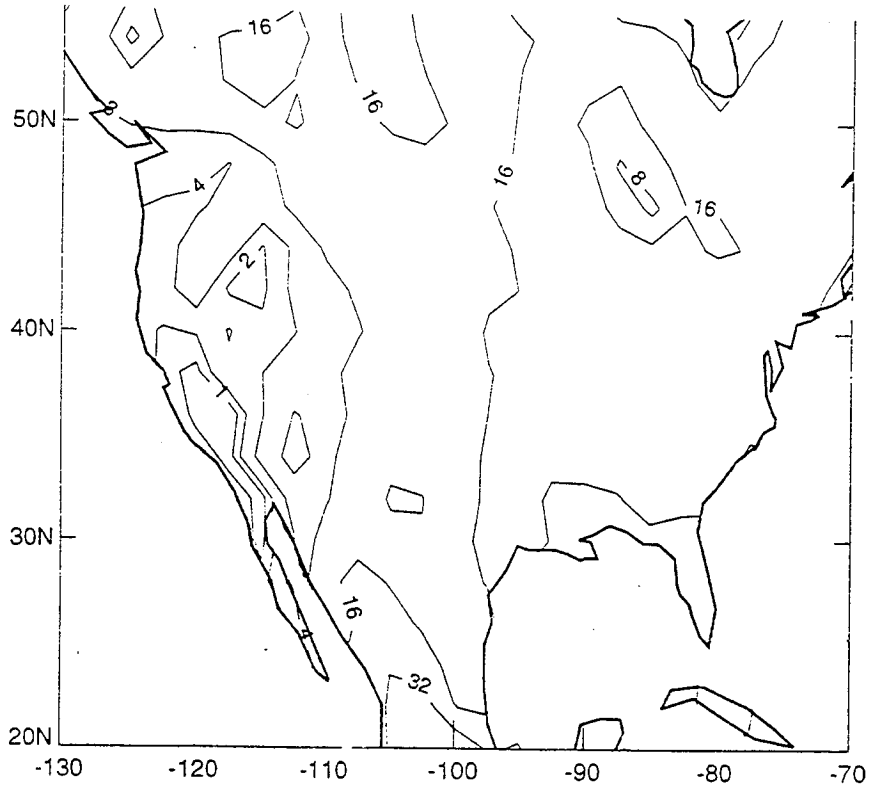
16
8
4
2
1
32
50N
40N
30N
20N
-130
-120
-110
-100
-90
-80
-70

FRACTIONAL WETTING CONSIDERATIONS

A precipitation regime characterized by high intensity, short duration storms...

...may seem to be characterized by low intensity, prolonged storms when the precipitation is averaged over a large area.

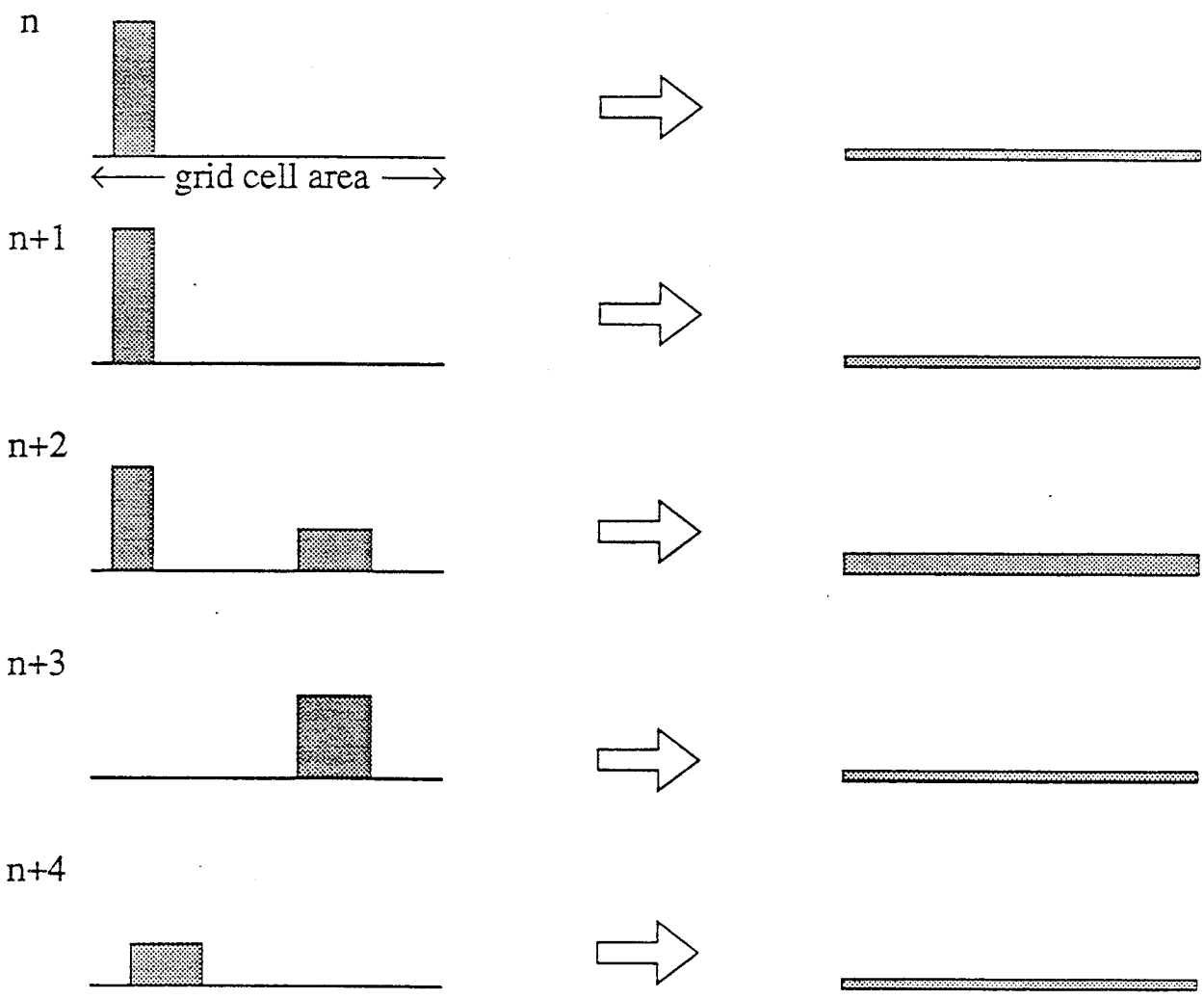

Figure 3

4(a)

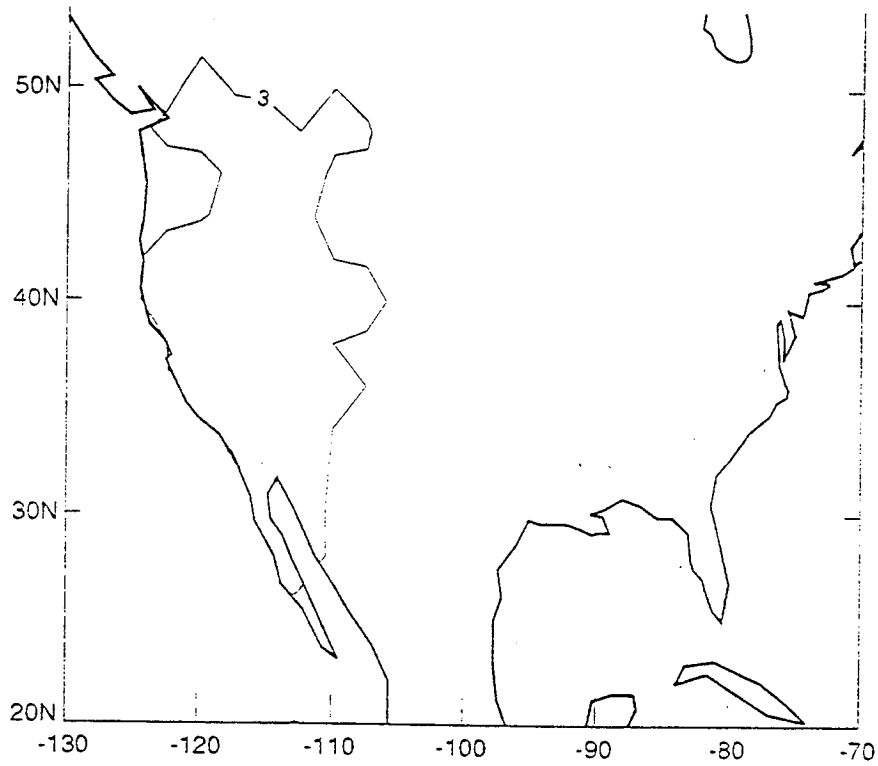
50N
40N
30N
20N
3
-130
-120
-110
-100
-90
-80
-70

4(b)

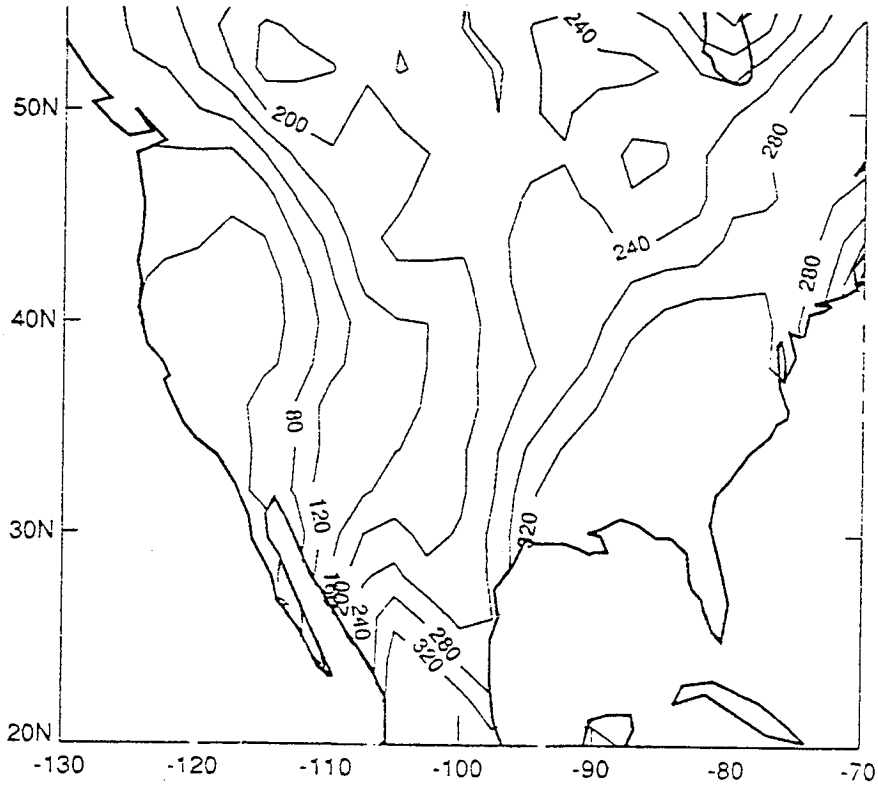
50N
40N
30N
20N
200
240
280
240
280
80
120
160
240
280
320
-130
-120
-110
-100
-90
-80
-70

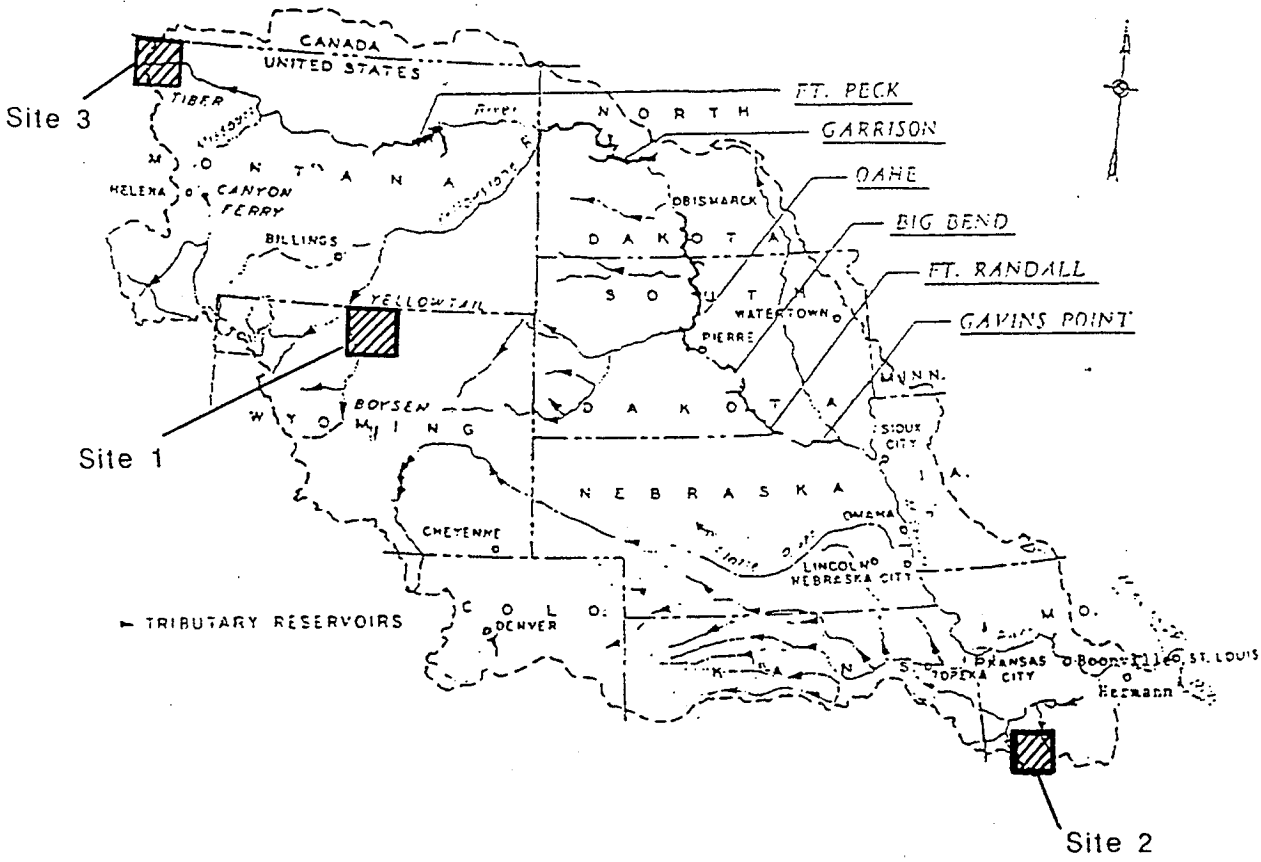
Site 3
CANADA
UNITED STATES
TIBER
FT. PECK
GARRISON
OAHE
BIG BEND
FT. RANDALL
GAVINS POINT
HELENA
CANYON FERRY
BILLINGS
YELLOWTAIL
BISMARCK
PIERRE
WATERTOWN
SIOUX CITY
BOYSEN
Site 1
CHEYENNE
OMAHA
LINCOLN
NEBRASKA CITY
DENVER
KANSAS CITY
ST. LOUIS
Hermann
TRIBUTARY RESERVOIRS
Site 2

Figure 5

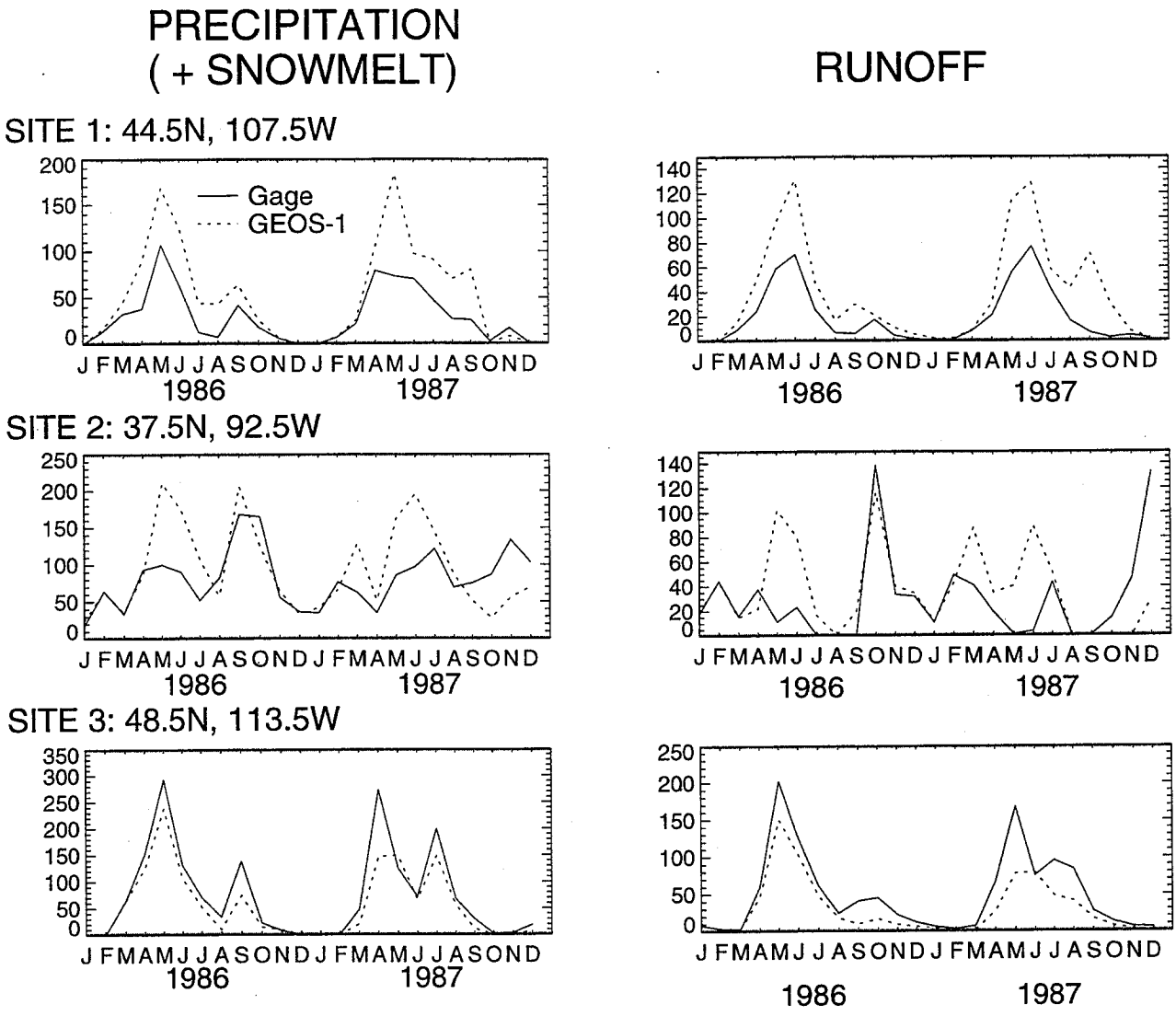
PRECIPITATION
(+ SNOWMELT)
RUNOFF
SITE 1: 44.5N, 107.5W
Gage
GEOS-1
SITE 2: 37.5N, 92.5W
SITE 3: 48.5N, 113.5W
J F M A M J J A S O N D J F M A M J J A S O N D
1986
1987

Figure 6

Studies of the Radiation Budget at the Top of the Atmosphere and Surface Energy Budget from the 5-Year Assimilation with the Goddard Earth Observing System

Man Li C. Wu
K.- M. Lau, P. Beaudoin, and W. Smith

NASA/Goddard Space Flight Center
Laboratory for Atmospheres
Greenbelt, MD 20771

Summary:

I. Climate Diagnostics:

* Version 1 of both the GEOS-DAS and the GEOS-GCM compare favorably with the ERBE data.

* The GEOS-DAS is able to circumvent some of the model deficiencies, therefore it produces very reasonable spatial distribution of clouds in the tropics and produces very reasonable clear sky OLR.

The results indicate that the radiation parameters of the GEOS-DAS are affected by three aspects of the model: dynamics, cloud parameterization, and radiation parameterization. Cases exist illustrating:

* The model underestimates low level coastal stratoform clouds, highlighting a need for improvement in cloud and PBL parameterization.

* 1) Weak cloud structures and even weaker cloud radiative effect in high latitudes, 2) strong cloud structures and cloud radiative effect in the tropics, and 3) large differences among radiation parameters, clouds, and rainfall, all illustrating a need to improve cloud and radiation parameterization.

* In addition to the problem mentioned above, the ratio between the shortwave cloud radiative forcing at the surface and at the top of the atmosphere is less than 1.

  Observations indicate the ratio should be around 1.5. Further studies and improvement in the cloud model and radiation parameterization are needed in order to resolve this problem.

II. Assess the usefulness of the GEOS-DAS products:

* The GEOS-DAS data proves useful for carrying out studies related to the variation of SST and surface fluxes.

* The migration of the warmest SST (higher than 302K) from south to north or vice versa in the western Pacific is largely due to solar zenith angle change accompanied by the seasonal change.

* The dSST/dt variation in the equatorial region does not follow the variation of net atmospheric surface energy balance. In this region both atmosphere and ocean dynamics play important roles.

Cases exist illustrating:

* In the eastern Pacific, SST seems to be controlled largely by ocean dynamics.

* In the western Pacific, the short-wave absorption at the surface is readily reducible by the presence of clouds, which are associated with large scale circulation such as the Hadley and Walker circulation. In other words, over the warm pool, in addition to the radiative forcing, the atmospheric dynamics and ocean dynamics all play important roles in controlling the SST.

* In the central Pacific, the clouds are also associated with large scale circulation, the changes in SST are affected by the atmospheric and oceanic dynamics.

  The relationship between He and SST is better than that in the warm pool.

Comparison of Pre-CERES, Satellite-Based Calculations of the Atmospheric Longwave Radiation Budget with GEOS-1

Thomas P. Charlock (NASA LaRC, t.p.charlock@larc.nasa.gov) and Fred G. Rose (Lockheed Engineering and Sciences Co., f.g.rose@larc.nasa.gov)

Extended abstract for Workshop on Results from the GEOS-1 Five Year Assimilation (NASA GSFC, Greenbelt, Maryland, March 6-8, 1995)

We have used the Goddard Earth Observing System (GEOS-1; Schubert et al., 1995) simulation of longwave (LW) fluxes, temperatures, and humidities for December 1988 in a series of exercises preparatory to the NASA Langley Clouds and the Earth's Radiant Energy System (CERES) satellite program of EOS. CERES (Wielicki and Barkstrom, 1991) will observe top-of-the-atmosphere (TOA) fluxes with ERBE-like instruments and retrieve cloud properties with imagers (VIRS on TRMM and MODIS on EOS). CERES will also combine TOA fluxes, cloud properties, atmospheric soundings, and radiative transfer calculations to estimate the vertical profiles of LW and shortwave fluxes within the atmosphere (Charlock et al., 1994a).

In the upper left panel of Fig. 1, we show the difference of total-sky (with clouds if present) OLR from GEOS-1 and ERBE (Barkstrom et al., 1989). In most midlatitude regions, the GEOS-1 cloud forcing to OLR is too small, while in some tropical regions, the GEOS-1 cloud forcing to OLR is too large. In the upper right of Fig. 1, we have used satellite-based ISCCP clouds (Rossow et al., 1991), the GEOS-1 temperature and humidity profiles, and the Wang, Shi and Kiehl (1991) LW code to re-simulate GEOS-1 OLR; the results are quite similar to the lower right, wherein this calculation is repeated with ECMWF temperatures and humidities. Both calculations of OLR with ISCCP satellite clouds (right panels in Fig. 1) show the signals of the dependence of cloud area on the viewing angles of the ISCCP geostationary satellites, but the satellite clouds give a better OLR than do the GEOS-1 model clouds (upper left of Fig. 1).

The GEOS-1 simulation of clear-sky OLR (lower left of Fig. 1) is quite good. We simulated the clear-sky OLR for December 1988 with 3 other sounding profiles: (1) ECMWF temperature and humidity, (2) TOVS temperature and humidity with ISCCP clear sky composite land temperature, and (3) ECMWF temperature and METSAT (Randel and Vonder Haar, 1994) precipitable water (SSM/I, TOVS, and NMC) distributed with height according to ECMWF. All of the soundings yielded clear-sky OLR fields that were close to ERBE for the global average, and all greatly exceeded ERBE over parts of the Sahara. Except for the Sahara region, the difference of clear sky OLR from the 4 soundings and ERBE varied from region to region. Each of the 4 soundings produced clear sky OLR in some regions that we closer to ERBE than were the others (not shown).

The LW heating rate of GEOS-1 (upper left of Fig. 2) is compared with our re-simulation using ISCCP clouds (no overlap) and the Wang et al. code (upper right of Fig. 2) and differenced (lower left of Fig. 2). Our 20-layer calculation uses a near-surface formulation that is quite different from GEOS-1, and the

differences in the LW heating rates below 800-hPa are based heavily on our near-surface formulation. The GEOS-1 clouds have produced a dramatically different LW budget within the free troposphere, however (lower left). In the lower right, we repeat the calculation but use *randomly overlapped* ISCCP clouds; the differences are still very large; to capture the difference of ISCCP cloud and GEOS-1 clouds, we have been forced to use a scale that barely shows the substantial effect of overlapping clouds. The difference in the GEOS-1 and ISCCP cloud forcing is quite large and cannot be readily explained by factors such as cloud overlap, which is uncertain in the satellite observations (Charlock et al., 1994b). To capture the main features of the difference of the total-sky LW heating rates as determined with GEOS-1 clouds and ISCCP clouds (lower panels of Fig. 2), a scale of -1.5 to 1.5 deg/day is needed. To capture the differences in the clear sky LW heating rates based on the 4 global soundings in the previous paragraph, a smaller scale of -0.8 to 0.8 deg/day suffices (not shown). The GEOS-1 humidity in the upper troposphere is larger than in the ECMWF analysis; this also induces a higher upper tropospheric cooling rate in GEOS-1, when compared with calculations based on ECMWF.

We acknowledge the assistance of Man-Li Wu, Paul Beaudin, and Jean Rosenberg at NASA GSFC and Timothy Alberta at Lockheed in Hampton, Virginia.

References

Barkstrom, B., E. Harrison, G. L. Smith, R. Green, J. Kibler, R. Cess, and the ERBE Science, 1989: Earth Radiation Budget Experiment (ERBE) archival and April 1985 results. Bull. Amer. Meteor. Soc., Vol. 70, 1254-1262.

Charlock, T., F. Rose, T. Alberta, G. L. Smith, D. Rutan, N. Manalo-Smith, T. D. Bess, and P. Minnis, 1994a: Retrievals of the surface and atmospheric radiation budget: Tuning parameters with radiative transfer to balance pixel-scale ERBE data. 8th Conf. on Atmospheric Radiation., AMS, 23-28 January 1994, Nasheville, TN., pp. 435-437.

Charlock, T., F. Rose, T. Alberta, G. L. Smith, D. Rutan, N. Manalo-Smith, P. Minnis, and B. Wielicki, 1994b: Cloud profiling radar requirements: Perspective from retrievals of the surface and atmospheric radiation budget and studies of atmospheric energetics. Workshop on Utility and Feasibility of a Cloud Profiling Radar, IGPO Publication Series No. 10, WMO/TD-No. 593, pp. B10-B21.

Randel, D., and T. Vonder Haar, 1994: Personal communication from STC-METSAT Inc., NASA sponsored project (randel@phobos.cira.colostate.edu).

Rossow, W., L. Garder, P. Lu, and A. Walker, 1991: International Satellite Cloud Climatology Project (ISCCP) Documentation of Cloud Data. In WMO/TD-No.266 (Revised). World Meteorological Organization, Geneva, 76 pp.

Schubert, S., C.-K. Park, C.-Y. Wu, W. Higgins, Y. Kondratyeva, A. Molod, L. Takacs, M. Seablom, R. Rood, 1995: A multi-year assimilation with the GEOS-1 system: Overview and results. In Technical Report Series on Global Modeling and Data Assimilation. M. Suarez, Ed., NASA Technical Memorandum 104606.

Wang, W.-C., G.-Y. Shi, and J. T. Kiehl, 1991: Incorporation of the thermal radiative effect of CH4, N2O, CF2Cl2, and CFCl3 into the National Center for Atmospheric Research Community Climate Model. J. Geophys. Res., Vol. 96, 9097-9103.

Wielicki, B., and B. Barkstrom, 1991: Clouds and the Earth's Radiant Energy System (CERES): An Earth Observing System Experiment. Second Symposium on Global Change Studies, New Orleans, LA, Jan. 14-18, 1991, pp. 11-16.

GEOS1 - ERBE
FULL SKY OLR
DECEMBER 1988

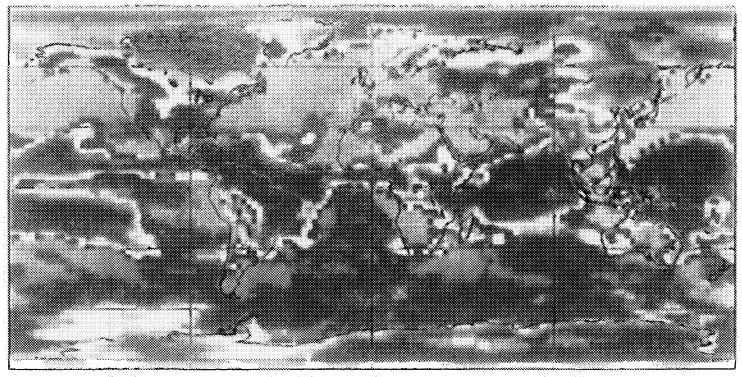

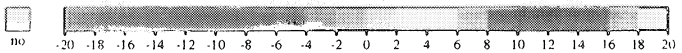

WATTS/METER^2
DOMAIN AVG = 4.41

WANG - ERBE
FULL SKY OLR
DECEMBER 1988 GEOS1 Temperature & Water Vapor; ISCCP CLOUDS

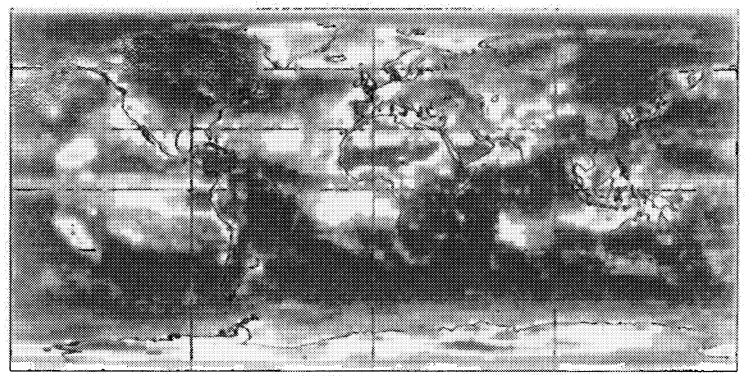

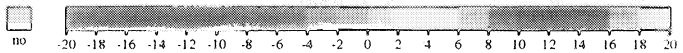

WATTS/METER^2
DOMAIN AVG = -3.04

GEOS1 - ERBE
CLEAR SKY OLR
DECEMBER 1988

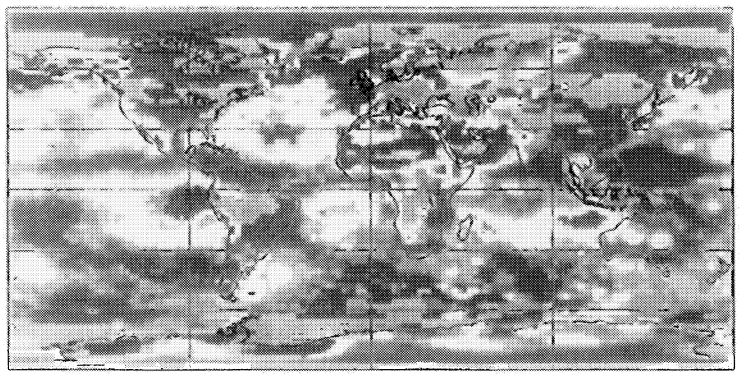

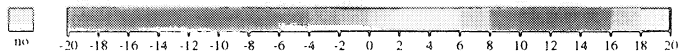

WATTS/METER^2
DOMAIN AVG = -1.05

WANG - ERBE
FULL SKY OLR
DECEMBER 1988 ECMWF WATER VAPOR

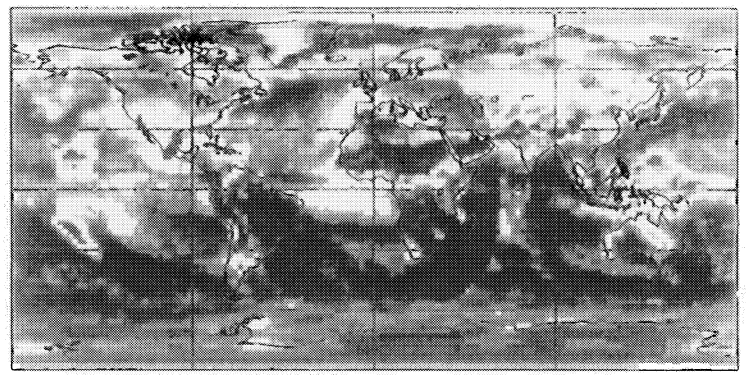

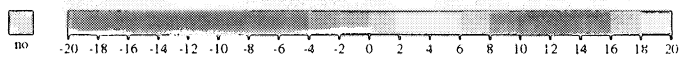

WATTS/METER^2
DOMAIN AVG = -1.01

Fig. 1

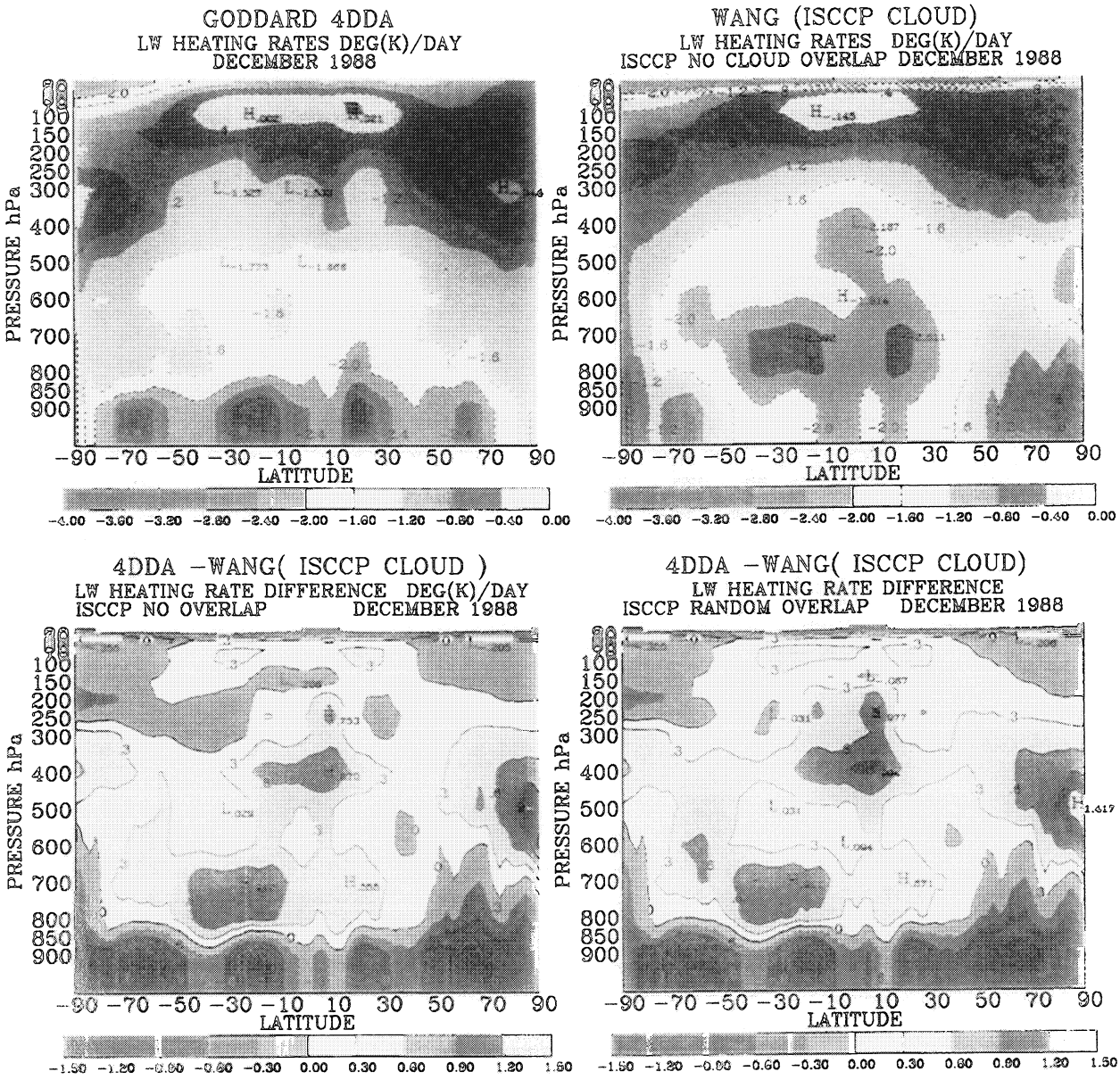

Fig. 2

Cloud Radiative Forcing: GEOS-1 Assimilation Versus ERBE Observation

Minghang Chen and J. Ray Bates

Data Assimilation Office, NASA/Goddard Space Flight Center

The cloud radiative forcing and seasonal cloud radiative forcing derived from the GEOS-1 five-year assimilation produced by the Data Assimilation Office at NASA/Goddard Space Flight Center are compared to those from the observation of the Earth Radiation Budget Experiment (ERBE) for the same time period. The comparison is focused on both five-year means and interannual variations.

The clear-sky longwave flux and albedo assimilated by GEOS-1 are in good agreement with the ERBE observations. The assimilation system is capable of reproducing basic features of the observed longwave and shortwave cloud forcing. However, the assimilation system overestimates longwave cloud forcing over the deep convection centers along the intertropical convergence zone, especially for July. For shortwave cloud forcing, the overestimate is even more severe. The main reason for the overestimate is the large constant cloud extinction coefficient prescribed for deep convective clouds. The problem becomes worse for July when there are more deep convective clouds. At mid-latitudes of both hemispheres, especially along the winter storm tracks, the assimilated longwave and shortwave cloud forcing are significantly weaker than the ERBE cloud forcing. This is due to the significant underestimate of cloud amount at mid-latitudes, which is caused by the cloud prediction scheme used in the system. The assimilated seasonal cloud forcing shows a similar problem: overestimate at low latitudes and underestimate at mid-latitudes.

The assimilated longwave and shortwave cloud forcing have greater interannual variations in the tropics than the ERBE cloud forcing. At mid-latitudes, the assimilated longwave cloud forcing has less interannual variations while the assimilated shortwave cloud forcing have compatible variations with the observation. The large cloud forcing anomaly in the central equatorial Pacific associated with the 1986/1987 El Niño is well assimilated by GEOS-1.

Comparison of the Diabatic Fields in the GEOS DAS with those in the Atmosphere

R. R. Joseph, Dr. M. A. Geller

(ITPA, State University of New York, Stony Brook, NY 11794)

Diabatic processes are crucial in controlling the atmospheric circulation. Generally, they are obtained as a consequence of different assumptions in various models involving subgrid-scale parameterizations. We have attempted to evaluate the diabatic fields in terms of rainfall and clouds in the GEOS DAS by comparing them with observations. The observational data sets used for this were the rain gauge measurements for the FGGE year (for which the GEOS 1.0 was run with the IAU procedure), ERBE S4 data set and the ISCCP C1 and C2 data sets of the summer and winter seasons of 1985 and 86.

Some of our significant findings are as follows:

1. Both ISCCP and ERBE comparisons with the assimilation model indicate that more high clouds are predicted in the model for the tropics. A lesser amount of middle and low clouds are predicted for the mid-latitudes by the model.

2. The Radiation Budget (RB) comparisons indicate that the small scale variability of the radiation budget parameters are underpredicted in the extratropics as indicated in Figure(1). The thicker line is the model result.

3. In general, the correlation of the cloud amounts and RB terms between the model and observations are poor in the tropics and better in the extratropics. The correlation of cloud amounts seem to be worse than those of rainfall and most RB terms.

4. Longwave clear sky comparisons indicate that the assimilation model is drier than the real atmosphere in the JJA season.

5. The subtropical deserts are less reflective in the model than in the real data. This can be seen from clear sky albedo comparisons.

6. The diurnal variability of the radiation budget terms were compared between observations and the model. The phase of the first harmonic in the short wave radiation budget terms of the model lagged behind that in the real atmosphere by about one and a half hours. Figure(2) indicates a comparison of the OLR after the phase lag was accounted for. We still find an additional phase lag in the model over land which could be because the soil moisture takes time to respond to heating.

7. There was a greater agreement in the amplitudes of the first diurnal harmonic of all the radiation budget parameters in January than in July.

8. Temporal averaging of rainfall drastically improves correlation between the rain gauge data and the model while spatial averaging does not.

9. The monthly averaged spatial distributions look similar but the model produces rainfall by frequent light drizzle while in reality most of the rain gauge locations have larger rainfall on a fewer number of days.

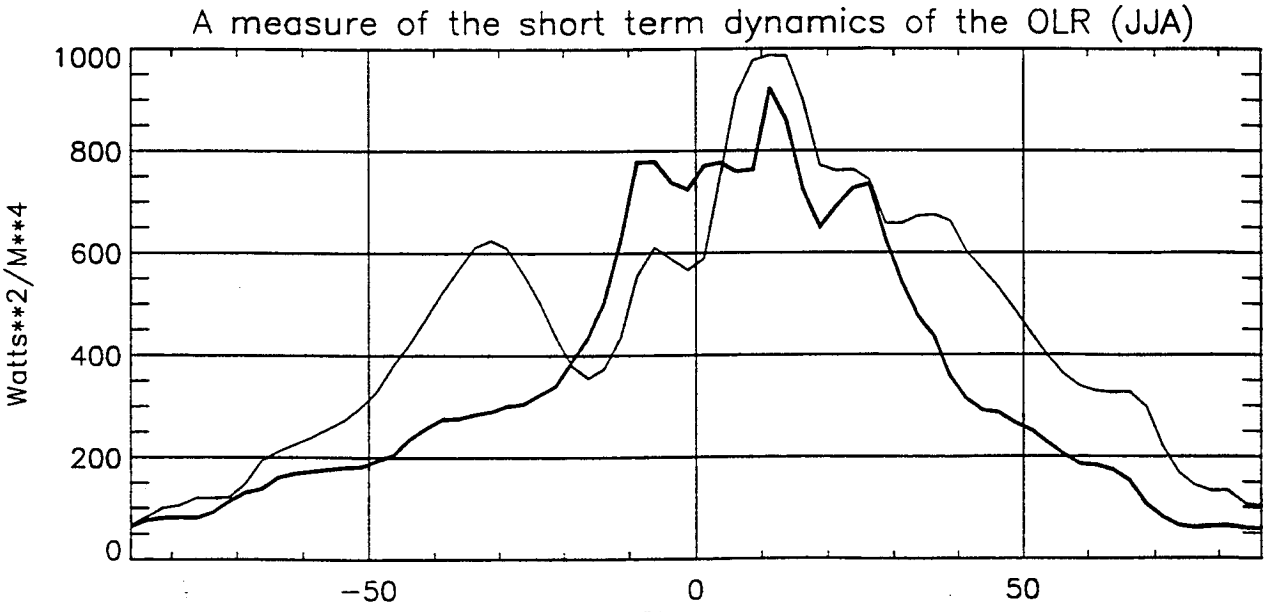

Figure 1.

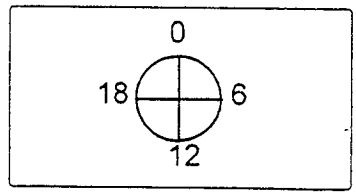

Diurnal Amplitude and Phase of Total LW from ERBE Data (Jan, 1986)

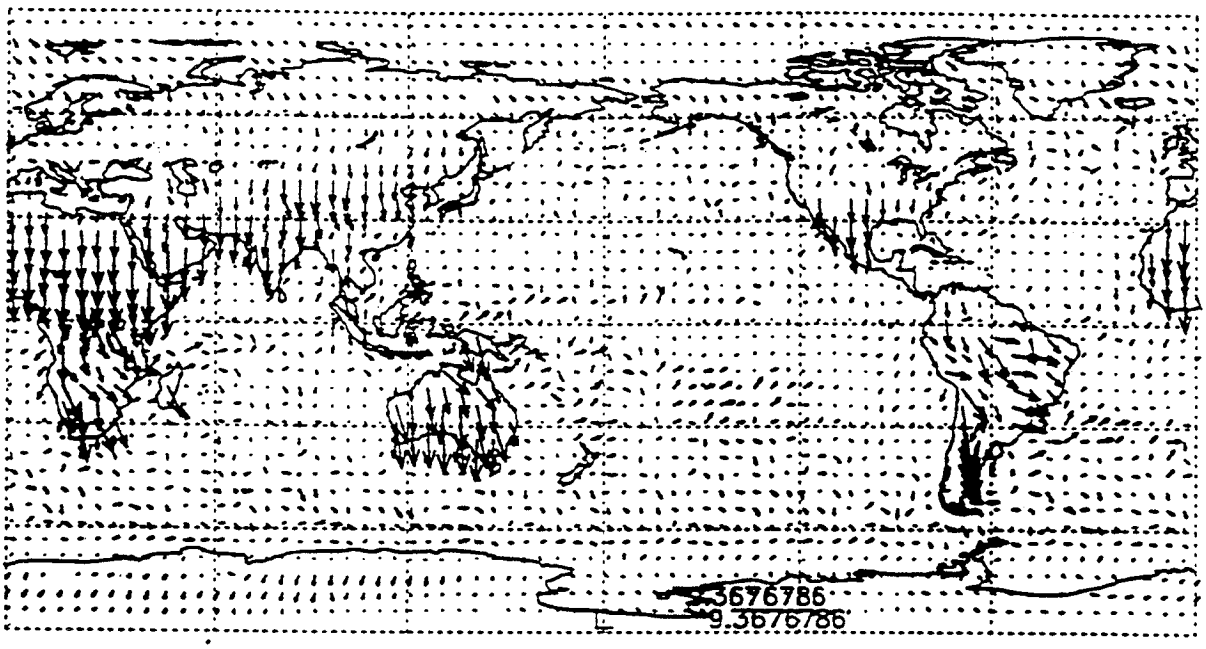

Diurnal Amplitude and Phase of Total LW from Model Data (Jan, 1986)

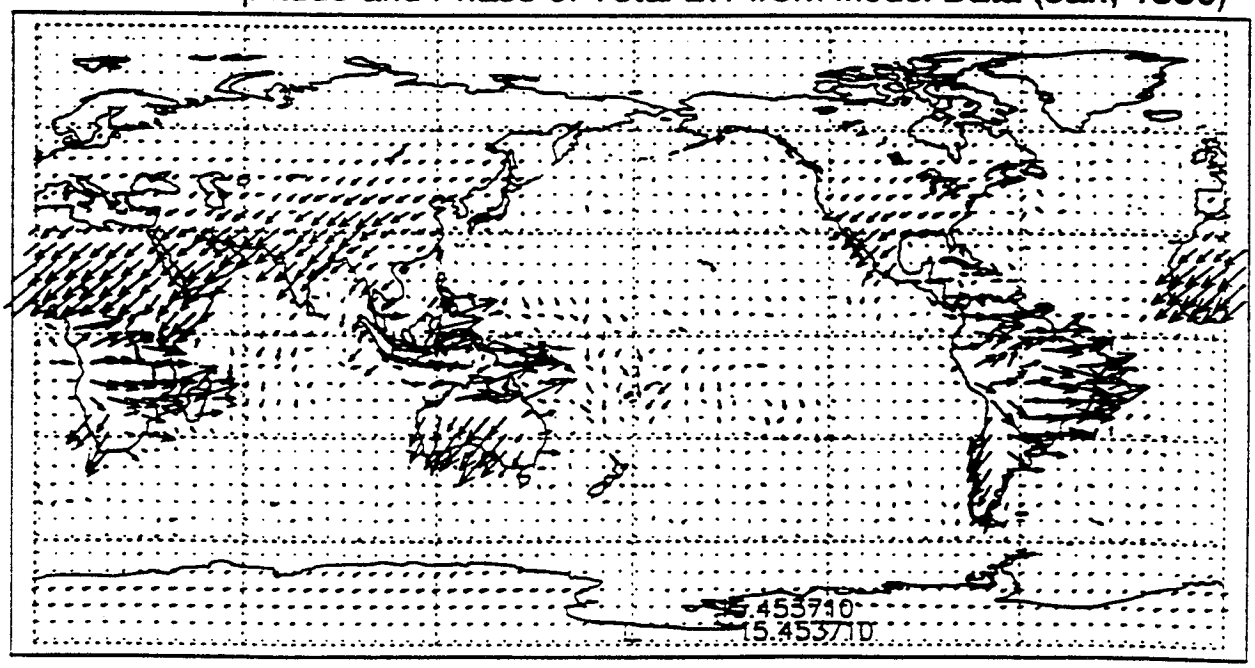

Figure 2.

Diabatic Heating in the NASA DAO Re-Analysis:

Interactions with Dynamics

David M. Straus
Dan Paolino

Center for Ocean-Land-Atmosphere Studies
Calverton MD 20705

1. Introduction. The interactions of observations with the numerical model's forecast in data assimilation can be categorized very broadly in terms of regimes. In the *tropical regime*, atmospheric data is scarce although the boundary forcing (SST) so important in determining seasonal tropical anomalies is well known. Here the details of the model's cumulus parameterization scheme may have a large impact on the vertical distribution of heating, which itself impacts the tropical / midlatitude interactions. In *data rich regions* (such as over North America), the details of the circulation are well defined by the observations, while the heating (at least in winter) is predominantly large scale and not highly dependent upon the cumulus scheme. Over the *Northern Hemisphere oceanic storm tracks*, most of the observations are satellite derived layer temperatures. Yet the geostrophic circulation should be fairly well defined by model advection of the down-stream continental observations. The divergent circulation is more dependent upon the numerical model, and the diabatic heating largely determined by the divergence field strongly feeds back onto the circulation. It is this last regime which is the subject of this paper, which examines the diabatic heating, transient vertical heat transport and the transient kinetic energy during northern winter.

2. Data. The total diabatic heating was obtained on pressure levels for the winters of 1985/86 through 1988/89 from the DAO archives. The transient vertical heat transport (given by the temporal covariance between vertical pressure velocity and temperature) and the transient kinetic energy were obtained for the same winter from the DAO archives, and compared to the corresponding data from the ECMWF operational analyses.

3. Heating. The diabatic heating at 1000 hPa shows strong maxima (over 10 °K/day) in narrow bands hugging the coasts in both the Atlantic and Pacific basins. These maxima are particularly strong over the Sea of Japan, the Sea of Okhotsk and the Bering Sea in the Pacific and off the Greenland coast in the Atlantic. At 850 hPa we also see intense cooling associated with orography, whose origin is in the turbulence heating term of the DAO model. At 850 hPa and 700 hPa a very broad maximum of just over 2 °K/day is seen in the Pacific over the storm track region, representing the excess of large scale heating over radiative cooling. Over the Atlantic this maximum is only half as large (1 °K/day) and is more narrowly confined. Here the storm track heating is nearly completely compensated by radiative cooling.

Detailed examination of the twice-daily heating shows that this field is extremely intermittent, with values at a typical oceanic location reaching well over 10 °K/day at widely scattered times, presumably as strong systems propagate. This suggests that the *variance* (or *rms*) of heating would show a much stronger signature of the storm tracks, and we find this to be the case.

4. Transient Vertical Heat Transport. This quantity is both a measure of the transient divergent circulation and a critical link in the energy cycle. It is worth pointing out that the vertical motion needed for this field is not analyzed, but comes directly from the model forecast. Longitude-height sections of this quantity averaged over 10° degree latitude bands show broad maxima of upward transport in both storm track regions. These maxima occur at the 850 hPa level in the DAO analyses, but are deeper (extending to 700 hPa) in the operational ECMWF analyses. While the maximum values in both analyses are roughly the same over the Pacific, the DAO heat transport is only about 60% of that in the ECMWF analyses over the Atlantic.

5. Transient Kinetic Energy. In order to see if the relative weakness of the DAO transient vertical heat transport (compared to ECMWF) in the Atlantic is seen in other measures of transients, we examined the total and band-pass (periods of 1-8 days) transient kinetic energy at 300 hPa. The difference field (DAO minus ECMWF) for the total is shown in the Figure on the next page. While the DAO transients are more vigorous in the far eastern Pacific, they are weaker in a broad region of the North Atlantic, over the downstream region of the Atlantic storm track. In fact there is a hint of an equatorward shift in the DAO storm track compared to that analyzed by ECMWF. Much of the difference seen in the figure comes from the band-pass transient kinetic energy.

6. Discussion. The diagnostics examined are fairly consistent with each other in regard to the relative depiction of the Atlantic storm track region in the DAO and operational ECMWF analyses. That both the DAO transient vertical heat transport and kinetic energy are weaker in the Atlantic suggest that the baroclinic development, propagation and the barotropic decay processes of the storm track are different in the two analyses. If we view the mean diabatic heating as a diagnostic of the actual storms as they propagate, the small values in the Atlantic compared to the Pacific are also suggestive.

Clearly these diagnostics need to be extended, both in terms of examining other reanalyses (NMC, ECMWF) and a more complete depiction of the mid-latitude baroclinic energy cycle.

WINTER Trans KE minus ECTOGA 300 hPa

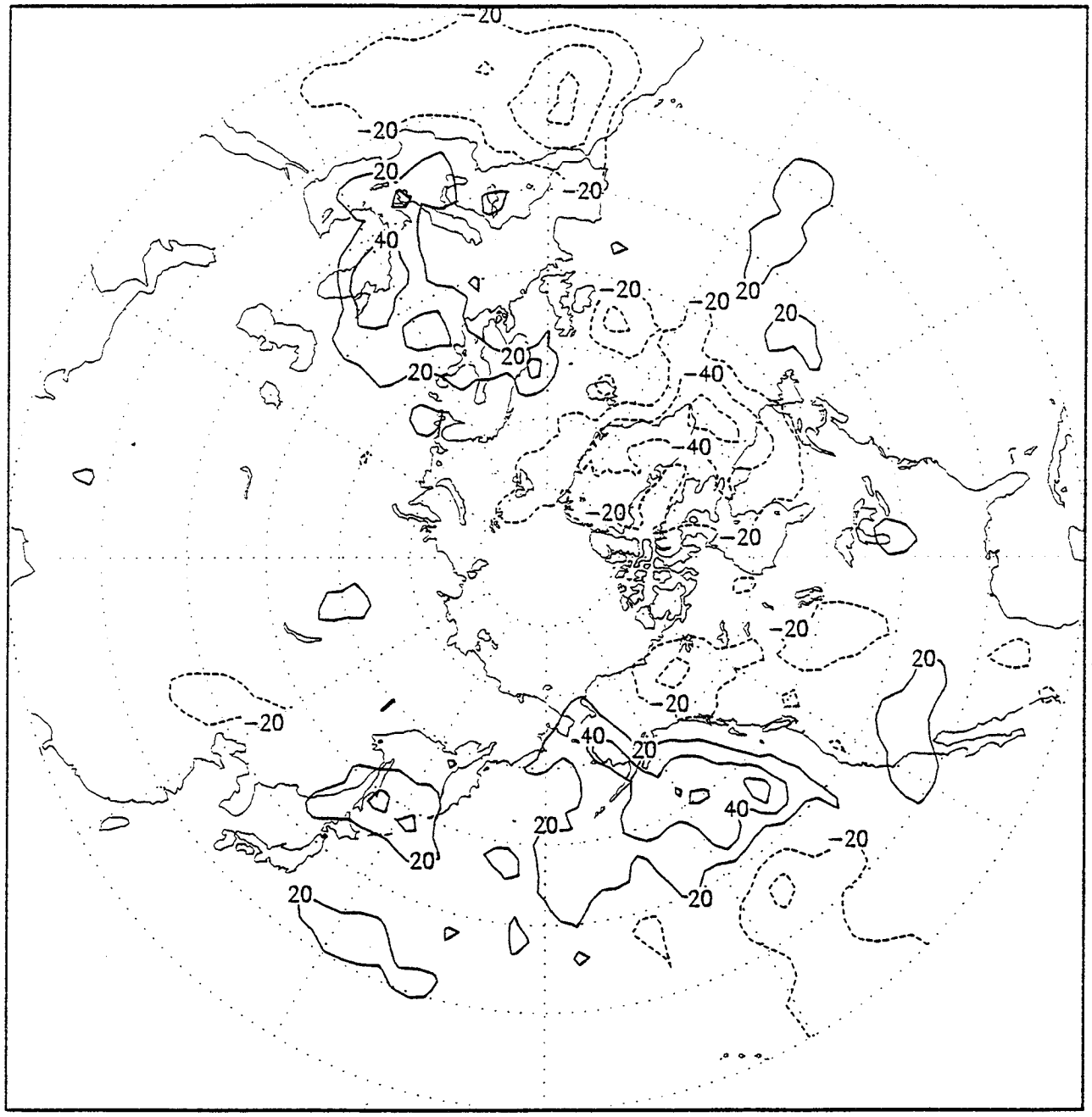

3 winters 1986/87 - 1988/89

GrADS: COLA/IGES

DIVERGENT CIRCULATIONS AND DEEP CONVECTIVE PROCESSES IN THE GEOS-1 ASSIMILATED FIELDS AS COMPARED TO REMOTELY SENSED DATA

[1]Franklin Robertson, [1]William Lapenta, [1]Diane Samuelson,
[2]Jayanthi Srikishen, [2]Eugene McCaul

[1]NASA/ Marshall Space Flight Center ES42
[2]Universities Space Research Association
977 Explorer Boulevard
Huntsville, AL 35806

1. Introduction

The quality of the divergent wind as depicted in reanalyses from GEOS, or any other assimilation system, is of considerable interest for two primary reasons. First, divergent circulations are intimately related to all diabatic processes such as radiation, convection, and surface energy exchange. Any inferences of climate variability or climate change based on diagnostics from the assimilation would be sensitive to the quality of the dynamical response to these various forcing mechanisms. A second and related point is that accurate wind data, and especially the divergent component, are poorly sampled by the current observing system. Thus, "analyzed" divergent circulations are significantly affected by the physics of the assimilation system.

We are interested in assessing the quality of the divergent flow and its relationship to moist physical processes (convective mass flux, cloudiness, and radiative fluxes). Recent advances in several of the NASA / NOAA Pathfinder data sets and other observational records can be brought to bear on this problem.

2. Depicting 3-Dimensional Divergent Circulations

To provide some overall perspective of the nature of the divergent flow in the GEOS 1 assimilation we have adopted the formalism of Keyser *et. al.* (1989) wherein the velocity potential recovered from the omega field is used to define a streamfunction in the x and y-planes. The u and v wind components are irrotational and are linked to omega components in each plane which have no cancellation. A decomposition of this sort is quite useful for isolating local contributions to the Hadley circulation and to East-West overturning. We have examined the five year mean 200 mb divergent flow components and found substantial similarity to patterns found earlier by Krishnamurti (1971) and Krishnamurti *et. al.* (1973). Prominent zones of meridional flow delineate the centers of convection and their annual migration associated with the planetary monsoons over Asia / Maritime Continent, the Tropical Americas, and Central Africa.. Two large east-west

circulation cells are found on either side of, and linked to, upward motion over Southeast Asia in July. The entire north Pacific is dominated at 200 mb by eastward divergent flow with a maximum near 170° E, 15° N. Strong westward flow is found oriented along 60° E extending from 45° N to 15° S.

To a great degree the circulations are dominated by a single vertical mode with divergence / convergence maximized at low and high levels. However, in the eastern tropical Pacific and Atlantic, significant maxima in vertical motion occur at low levels (near 850 mb). These structures are consistent with forcing by low-level pressure gradients that are confined largely to the PBL, and maintained by meridional sea-surface temperature gradients (Lindzen and Nigam, 1987).

3. Preliminary Comparisons to Satellite Data Sets

Validating the analyzed flow fields is quite problematical in view of limited direct measurements over the global domain. Satellite derived estimates precipitation, cloudiness and radiation parameters-- particularly those being prepared in conjunction with the NASA / NOAA Pathfinder effort will be needed. Our initial comparisons have focused on both IR and microwave-based estimates precipitation. The general patterns of tropical precipitation and annual migration are well captured in the analysis. However the details of local maxima within the three major tropical convective centers lack agreement with the observations. It should be noted however that significant differences in detail also exist between the IR and microwave precipitation fields.

SSM/I scattering signatures from convectively produced ice are a strong indicator of vertical convective / mesoscale mass flux between the freezing level and cloud top. We have only examined several months and compared them to GEOS fields. Figure 1 shows a comparison between an SSM/I ice scattering index (arbitrary units) and the 300-500 mb mean vertical motion for December 1992, a month within TOGA-COARE. Since this ice is graupel and snow (not cloud ice crystals) it is associated with vertical motion penetrating the freezing level. Within strongly convective regions the patterns would be expected to correlate strongly with omega on a monthly time scale. This figure emphasizes how agreement between the ice index and vertical motion degrades at regional and smaller scales.

4. Summary and Future Plans

We hope to carry these analyses to greater detail and to characterize the accuracy of the divergent flow and its consistency with various diabatic forcing components. It would probably be beneficial for several research groups to collaborate on this given the interactions between disparate processes such as land surface forcing and parameterized cloud microphysics.

Some of our work currently involves using analyzed fields to drive large-scale water vapor and prognostic condensate equations to understand better the processes controlling upper-tropospheric water balance. Ultimately, this work would be extended to examine the model cloudiness and the role of convective ice detrainment versus baroclinic overturning as a means of maintaining observed upper-level cloudiness. We would be interested in helping to test and diagnose incorporation of these type microphysics parameterizations within GEOS.

5. Data Accessibility

We have obtained most of our current data from the GSFC DAAC by ftp of monthly mean and some time series data. One month of global daily time series data during TOGA-COARE was graciously provided by David Ledvina. We have generally found the data set acquisition to be relatively pain free. The on-line documentation of the DAO homepage has been a big help. The occurrence of missing omega values at some pressure levels above the surface was unexpected. It also seems that cloud mass flux diagnostics include dry convection. If this is true, it would have been more useful to have moist and dry convective mass flux separated.

6. References

Keyser, D., B. D. Schmidt and D. G. Duffy, 1989: A technique for representing three-dimensional vertical circulations in baroclinic disturbances. *Mon. Wea. Rev.*, **117**, 2463-2494.

Krishnamurti, T. N., 1971: Tropical east-west circulations during the northern summer. *J. Atmos. Sci.*, **28**, 1342-1347.

Krishnamurti, T. N., M. Kanamitsu, W. J. Koss, and J. D. Lee, 1973: Tropical east-west circulations during northern winter. *J. Atmos. Sci.*, **30**, 780-787.

Lindzen, R. S. and S. Nigam, 1987: On the role of sea-surface temperature gradients in forcing low level winds and convergence in the tropics. *J. Atmos. Sci.*, **44**, 2440-2448.

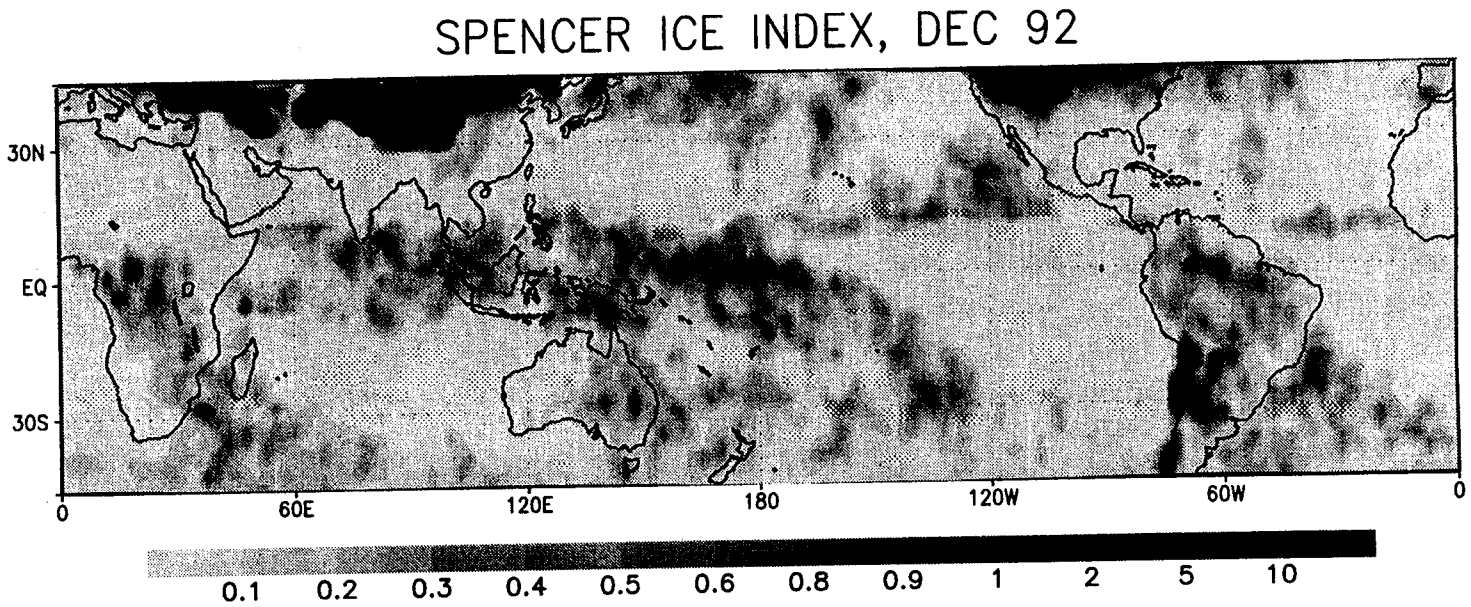

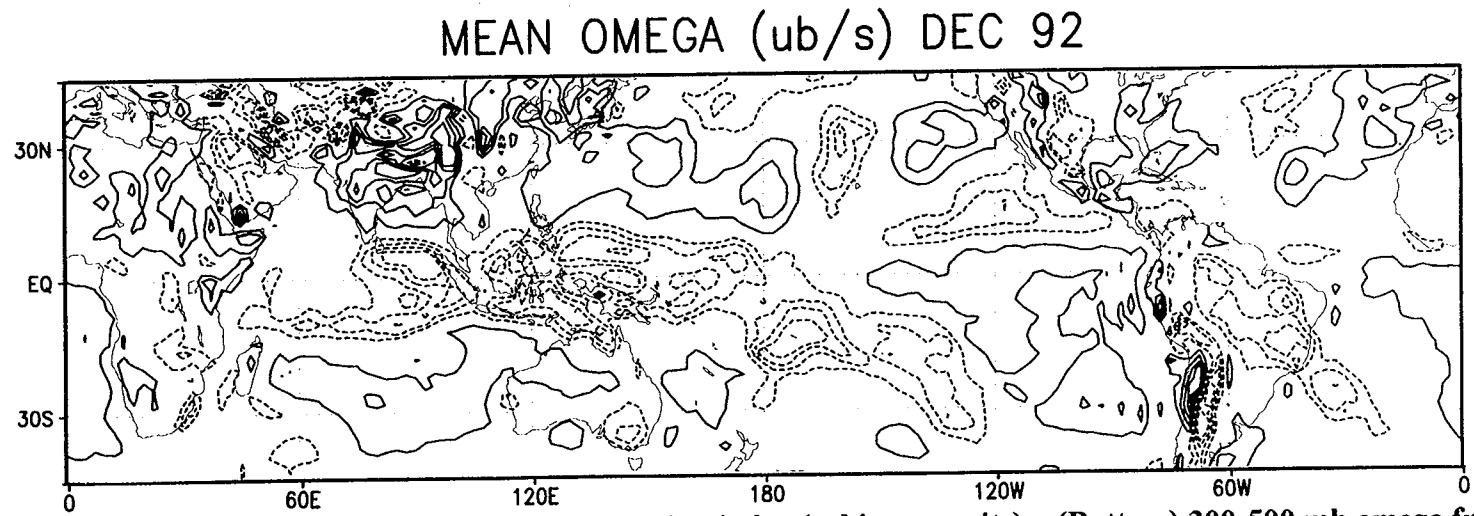

Figure 1. (Top) SSM/I precipitating ice scattering index (arbitrary units). (Bottom) 300-500 mb omega from GEOS assimilation. Zero line is not plotted and contours are .25 microbars / sec.

The Impact of the GEOS-1 GCM on the GEOS-1 Data Assimilation System

Andrea Molod
Lawrence Takacs and H. M. Helfand
Laboratory for Atmospheres Data Assimilation Office
Goddard Space Flight Center Greenbelt, Maryland 20771

The Goddard Earth Observing System (GEOS) General Circulation Model (GCM) is part of the GEOS Data Assimilation System (DAS), which is being developed at the Goddard Data Assimilation Office for the production of climate data sets. This study examines Version 1 of the GEOS GCM by evaluating the quality of the fields which relate most closely to the GCM physical parameterizations, and examines the impact of the GCM climate errors on the climate of the DAS assimilated fields.

The climate characteristics are evaluated using independent satellite and ground-based data for comparison. The GEOS-1 GCM shows reasonably good agreement with available observations, in terms of general global distribution and seasonal cycles. The major biases or systematic errors are a tendency towards a dry tropical atmosphere and an inadequate cloud radiative impact in the extratropics. Other systematic errors are a generally wet subtropical atmosphere, slightly excess precipitation over the continents, and excess cloud radiative effects over the tropics. There is also an underestimation of surface sensible and latent heat fluxes over the area of maximum flux.

The GEOS-1 DAS, in general, has been shown to exhibit a reasonably good agreement with available data, in terms of general global distribution and seasonal cycles, and shows improvements over the GEOS-1 GCM climate. There are four distinct ways that the GCM impacts the DAS which have been identified by this study. The first, and perhaps the most promising in terms of our ability to produce useful climate data sets for model diagnosed fields, is the GCM bias that has little or no deleterious impact on the DAS fields because it is corrected by the input data during the assimilation. Examples of this type of impact are the surface fluxes of latent heat, sensible heat and momentum. Figure 1 shows the evaporation difference between the GCM and COADS and between the DAS and COADS, and the closer agreement of the DAS to the verification can be seen. Although the verification for these fields is not from direct observations, the close resemblance of the DAS fields to the independent verification demonstrates the ability of the OI and IAU to reproduce currently acceptable estimates of the near surface fluxes.

The second type of impact of the GCM on the DAS is a model bias in an assimilated field which cannot be completely corrected by the OI because the input data is not the absolute determinant of the analysed field. This is seen in the DAS moisture field, which is closer to the observations than the GCM, but still exhibits the GCM dry bias in the tropics.

A third type of impact of the GCM on the DAS is due to a basic parameterization inaccuracy that is not corrected even when provided with the DAS more accurate input. An example of this is the GCM and DAS similar underestimate of extratropical cloud forcing. If the GCM parameterization does not produce non-precipitating grid scale clouds, the improvement to the atmospheric temperature and humidity profiles by the OI will not correct this parameterization bias.

Finally, the fourth and last type of impact of the GCM bias on the DAS, and perhaps the most urgent to address, is due to a spurious feedback between the GCM and the OI that causes the DAS fields to exhibit an error not seen in the GCM simulation. An example of this type of feedback is seen in the DAS tropical cloud forcing (figure 2) and net

radiation fields. The GCM dry tropical moisture bias, which is related to the parameterization of excessive tropical convection, neccessitates a systematic OI correction, and the positive analysis increment of moisture, in turn, causes the GCM to respond by generating convection and clouds. This constant generation of cloud cover causes the DAS tropical cloud forcing to be excessive.

The identification in this study of the key GCM parameterization-related errors which impact the DAS, along with some directions for improvement of these errors which have been effective in other GCMs, makes the outlook for the ability of a DAS to produce realistic estimates of model-derived diagnostic fields promising.

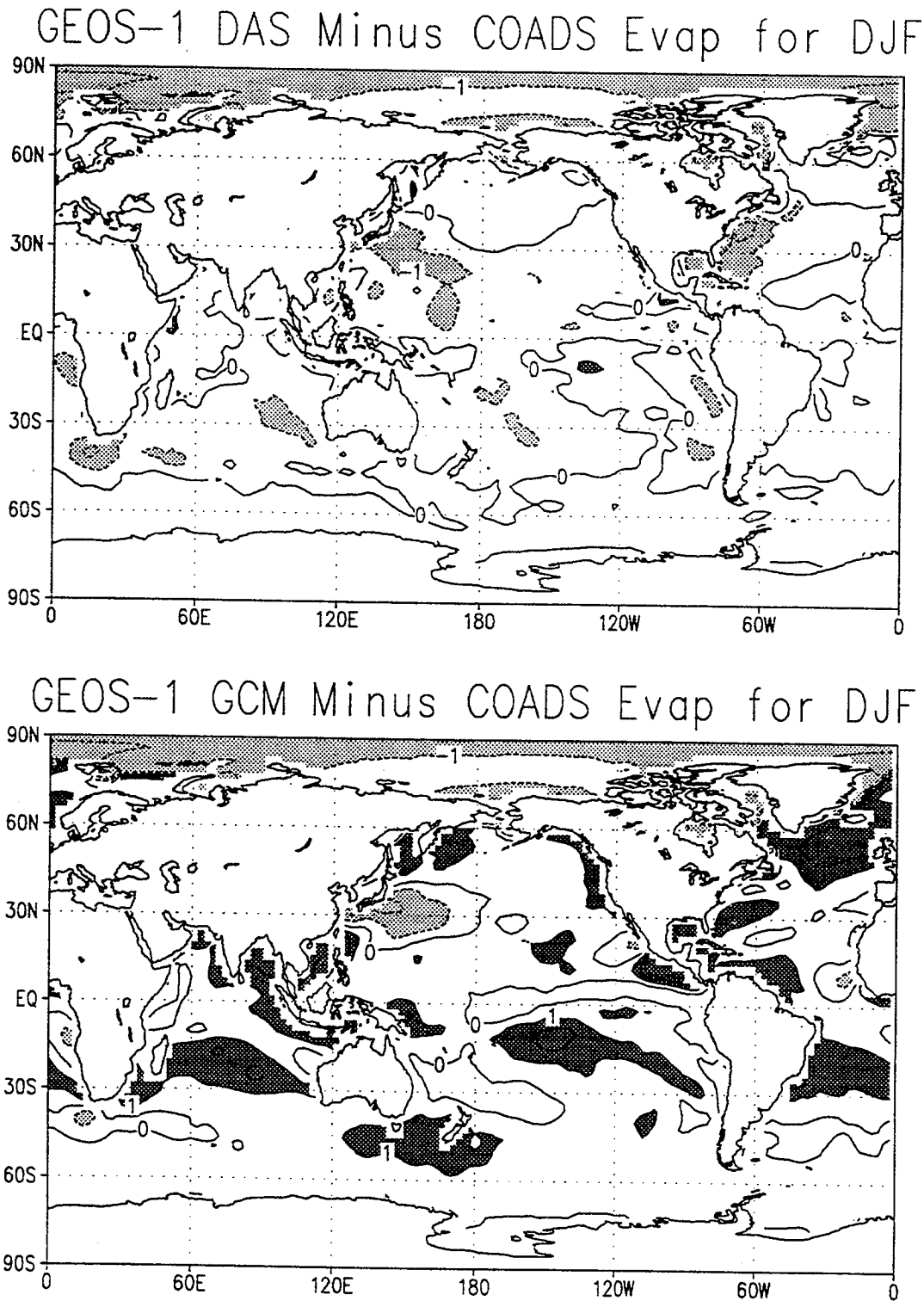

Figure 1: 5-Year Averaged DJF GCM Minus COADS Evaporation Difference and DAS Minus COADS Evaporation Difference in *mm/day*. The contour interval is 1 *mm/day*, and the shading is for differences greater than 1 *mm/day*, dark for positive, light for negative.

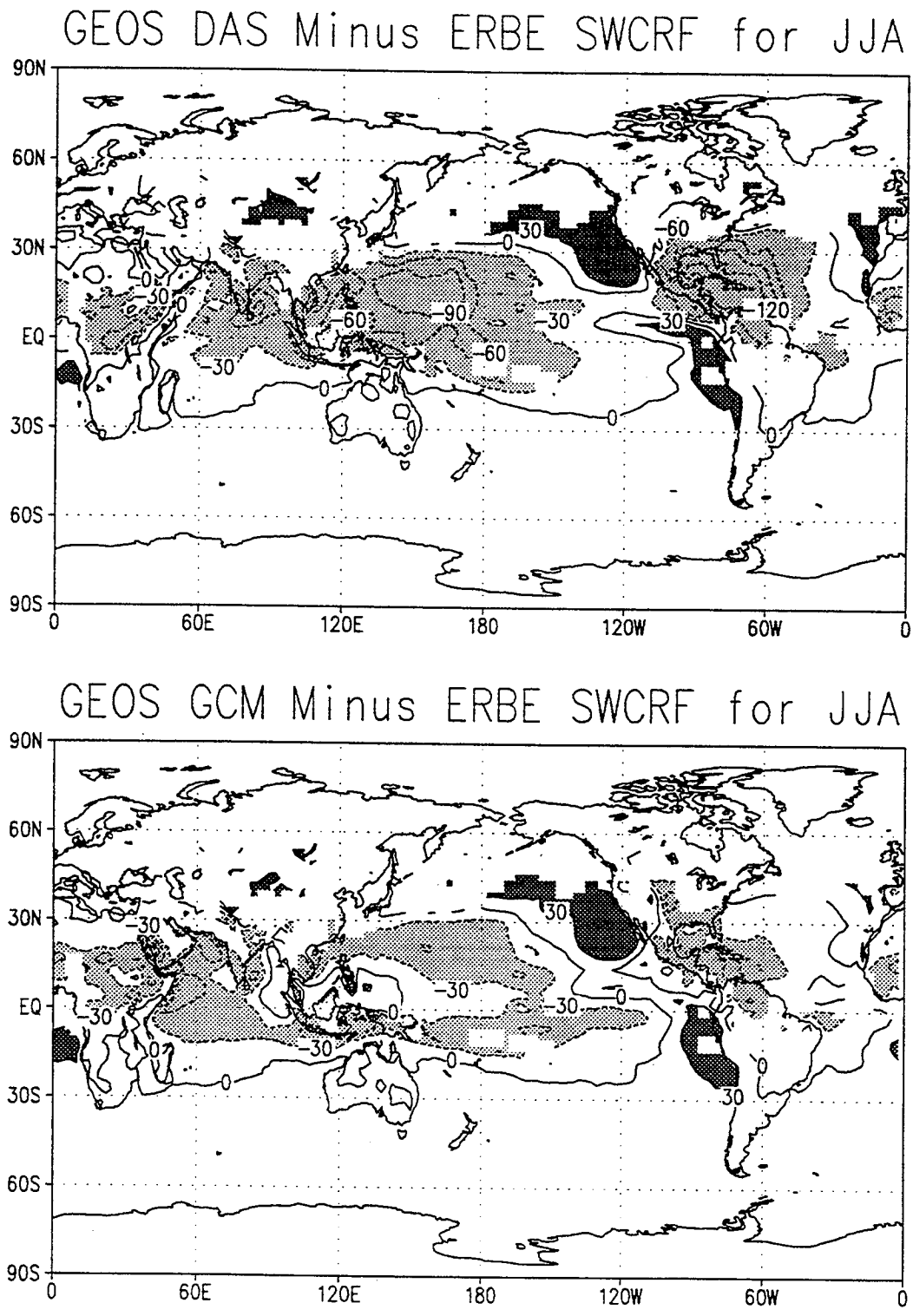

Figure 2: 5-Year averaged JJA GEOS-1 GCM Minus ERBE and GEOS-1 DAS minus ERBE difference in Shortwave Cloud Radiative Forcing at the top of the atmosphere in W/m^2. The contour interval is 30 W/m^2 and the shading is for differences greater than 30 W/m^2, with the darker shading for positive values and lighter shading for negative values.

Shortwave Radiation Absorption in Clear and Cloudy Atmospheres

Albert Arking
Johns Hopkins University
Baltimore, Maryland 21218

Introduction

Recent papers have reported large inconsistencies between observations of solar radiative fluxes in the atmosphere and numerical calculations with radiative transfer models (Cess et al 1995; Ramanathan et al 1995; Pilewskie and Valero 1995). The inconsistency is with respect to the difference between the average radiative flux under all cloud conditions and an estimate of what the average flux would be under "clear sky" conditions. Measurements of solar flux were made at the top of the atmosphere, from satellite sensors, and at instrumented surface sites. They were also made from coordinated aircraft flying above and below clouds. The studies indicate that the cloud radiative effect—i.e., the difference between all-sky and clear-sky fluxes—is much higher at the surface, or below the cloud layers, than at the top of the atmosphere, or above the cloud layers. Expressed numerically, they find that the observed ratio of the cloud radiative effect at the surface to that at the top of the atmosphere is ~1.5, compared to the calculated value of ~1.0. These results imply that clouds cause substantially more absorption of solar radiation by the atmosphere, and less by the surface, than one would calculate with numerical models.

To provide some insight into the problem, we examine the output data of the Goddard Earth Observing System / Data Assimilation System (GEOS/DAS) described by Schubert et al (1993). We compare the model's calculated radiative fluxes with satellite observations at the top of the atmosphere, and determine the effect of clouds on the partitioning of solar energy between the atmosphere and surface. The comparisons are made for monthly mean values over a 5-year period, Mar 1985 through Feb 1990. The satellite data used in the comparison include monthly mean radiation energy budget parameters at the top of the atmosphere from the Earth Radiation Budget Experiment (ERBE), described by Barkstrom et al (1989), and cloud parameters from the International Satellite Cloud Climatology Project (ISCCP), described by Rossow and Schiffer (1991).

Global Averages

The global mean total column absorption of solar radiation (net downward solar flux at the top of the atmosphere), and its partition into atmospheric and surface components, for the GEOS/DAS dataset is shown in the upper part of Table 1. The columns show the average for all sky conditions, the average for clear sky conditions. and the *cloud radiative effect* (CRE), which is the difference between *all-sky* and *clear-sky* fluxes. The total column values are compared with ERBE observations, and averaged over the globe, they agree quite well.

With reference to Table 1, of the 246.6 W m^{-2} of solar energy absorbed by the earth-atmosphere system (Q^T) the fraction 0.227 (P) is absorbed by the atmosphere, and the remaining fraction of 0.773 is absorbed by the surface. Under clear-sky conditions, the total solar energy absorbed increases by 48.2 W m^{-2}, with almost all of it (except for 3.7 W m^{-2}) going into the surface. As a result, the fraction absorbed by the atmosphere is reduced to 0.203 (P_{clr}). Thus, clouds cause less energy to be absorbed by the surface, with only a very small change in atmospheric absorption. The reason why clouds have such a small effect on atmospheric absorption is that cloud particles are weakly absorbing, their primary effect being to redirect and scatter the solar radiation.

Table 1 also shows the ratio of the CRE at the surface to that for the total column, R. The expression for R is shown, conventionally, as the ratio of the CRE at the surface ($Q^S - Q^S_{clr}$) to that at the top of the

Table 1. Solar radiation budget in W m^{-2} based on 5 years (Mar85–Feb90) of output data from the GEOS data assimilation system, shown for the globe and for the tropical Pacific (25S–25N, 150E–270E). Top-of-the-atmosphere fluxes from ERBE are shown for comparison.

Global: Incoming solar flux 345.1 (ERBE: 341.9)

	All-sky	Clear-sky	CRE
Total Column absorption	246.6 (Q^T)	294.8 (Q^T_{clr})	−48.2 ($Q^T - Q^T_{clr}$)
(ERBE:	241.1	288.8	−47.7)
Absorbed by Surface	190.6 (Q^S)	235.1 (Q^S_{clr})	−44.5 ($Q^S - Q^S_{clr}$)
Absorbed by Atmosphere	56.0	59.7	−3.7
Ratio Surface/Total Column	0.773	0.797	0.923 (R)
Ratio Atmosphere/Total Column	0.227 (P)	0.203 (P_{clr})	0.077

$$R = \frac{Q^S - Q^S_{clr}}{Q^T - Q^T_{clr}} = (1 - P_{clr}) + \frac{Q^T}{Q^T_{clr} - Q^T} \cdot (P - P_{clr})$$

$$0.92 = 0.80 + 5.12 \cdot 0.024$$

Tropical Pacific: Incoming solar flux 409.8 (ERBE: 401.5)

	All-sky	Clear-sky	CRE
Total Column absorption	295.3 (Q^T)	367.9 (Q^T_{clr})	−72.6 ($Q^T - Q^T_{clr}$)
(ERBE:	306.1	345.7	−39.6)
Absorbed by Surface	225.7 (Q^S)	293.7 (Q^S_{clr})	−68.0 ($Q^S - Q^S_{clr}$)
Absorbed by Atmosphere	69.6	74.2	−4.6
Ratio Surface/Total Column	0.764	0.798	0.937 (R)
Ratio Atmosphere/Total Column	0.236 (P)	0.202 (P_{clr})	0.063

$$R = \frac{Q^S - Q^S_{clr}}{Q^T - Q^T_{clr}} = (1 - P_{clr}) + \frac{Q^T}{Q^T_{clr} - Q^T} \cdot (P - P_{clr})$$

$$0.94 = 0.80 + 4.07 \cdot 0.034$$

ERBE for Q^T, Q^T_{clr} & GEOS for P, P_{clr}: $0.80 + 7.73 \cdot 0.034 = 1.06$

atmosphere ($Q^T - Q^T_{clr}$), and in terms of the top-of-the-atmosphere fluxes (Q^T and Q^T_{clr}) and the partitioning coefficients (P and P_{clr}). As shown, the global mean ratio R in GEOS/DAS is 0.92. Being less than 1 implies that the atmospheric CRE has the same sign as the surface CRE—viz., clouds reduce, albeit slightly, the energy absorbed by the atmosphere.

Since the values of Q^T and the difference $Q^T - Q^T_{clr}$ are fairly well established (Arking 1991), the key factor for raising R is $P - P_{clr}$, the difference in the partitioning coefficients. To make R = 1.5, it would be necessary to increase $P - P_{clr}$ by more than a factor of 5—from 0.024 to 0.137 (line shown in lower right graph of Fig. 1). This large increase in $P - P_{clr}$ does not necessarily correspond to a 5-fold increase in absorption by cloud particles. Most of the difference $P - P_{clr}$ is due to: (1) increased absorption by atmospheric gases in the clear layers, as a result of the increased path length due to diffuse scattering by the cloud layer, and (2) increased absorption inside the cloud layer, as a result of multiple scattering within a saturated environment. Thus, P would generally be larger than P_{clr} even if cloud particle absorption were 0. Chou et al (1995) estimate that the specific absorption by cloud particles would have to increase by a factor of ~40 to raise R to ~1.5.

The global distribution of R and the partitioning coefficients P and P_{clr}, and their difference, are shown in Fig. 1 as functions of the mean soar zenith angle. To bring the number of plotted points down to a manageable number, the points—each representing the monthly average in a 2° latitude by 2.5° longitude box— are randomly selected so that within each latitude band and for each month the number of selected boxes is proportional to area and the mean incoming solar flux. Also, for the ratios to be meaningful, we excluded points where the CRE at the top of the atmosphere was >-1 W m^{-2}. The vertical scatter in R indicates a broad distribution that is practically independent of mean solar zenith angle, but within a range where its value rarely exceeds 1.5 (occurring for only ~1% of the points). Where the values of R are negative (occurrence <2%), the CRE at the surface is positive, meaning that the effect of the clouds is to *increase* the net downward flux at the surface. These cases need to be explored further. The 10th, 50th, and 90th percentiles of R are 0.74, 0.945, and 1.11, respectively.

The high values of P and P_{clr} that occur at mean cosine zenith angles less than ~0.4 are associated with points that have high surface albedo. In those cases a higher proportion of the net incoming solar energy is absorbed by the atmosphere, but with little or no effect on the difference $P - P_{clr}$.

Tropical Pacific

While the global mean top-of-the-atmosphere fluxes are in good agreement with ERBE observations, the geographical (and seasonal) distribution is not. The lower part of Table 1 shows the mean values over the tropical Pacific (25°S–25°N, 150°E–270°E). Here the disagreement is quite large: the all-sky flux is too low, and the clear-sky flux too high, relative to the observations. The result is that the magnitude of the CRE at the top of the atmosphere is 33 W m^{-2} larger than indicated by ERBE.

The biases in top-of-the-atmosphere clear-sky fluxes have little impact on R. As shown in the lower portion of Table 1, substituting the ERBE values for Q^T and Q^T_{clr}, but maintaining the partitioning coefficients of the model (P and P_{clr}), only raises R in the tropical Pacific from 0.94 to 1.06.

To diagnose the cause of the CRE discrepancy, the outgoing SW and LW fluxes at the top of the atmosphere from GEOS/DAS are compared with ERBE observations in Fig. 2. The comparisons reveal that the clear-sky fluxes are reasonably consistent, with GEOS/DAS showing a small bias of -2 W m^{-2} in the clear-sky outgoing SW flux. The large biases occur in the all-sky fluxes: GEOS/DAS has biases of 27.5 W m^{-2} in outgoing SW and -11.7 W m^{-2} in outgoing LW. Clearly, the cloud effects in GEOS/DAS are much stronger than in ERBE for both SW and LW radiation. It is not due to cloud amount, however. A comparison of cloud fractions, also in Fig. 2, reveals only a small bias—in fact, its sign is opposite to what is needed to explain the CRE bias.

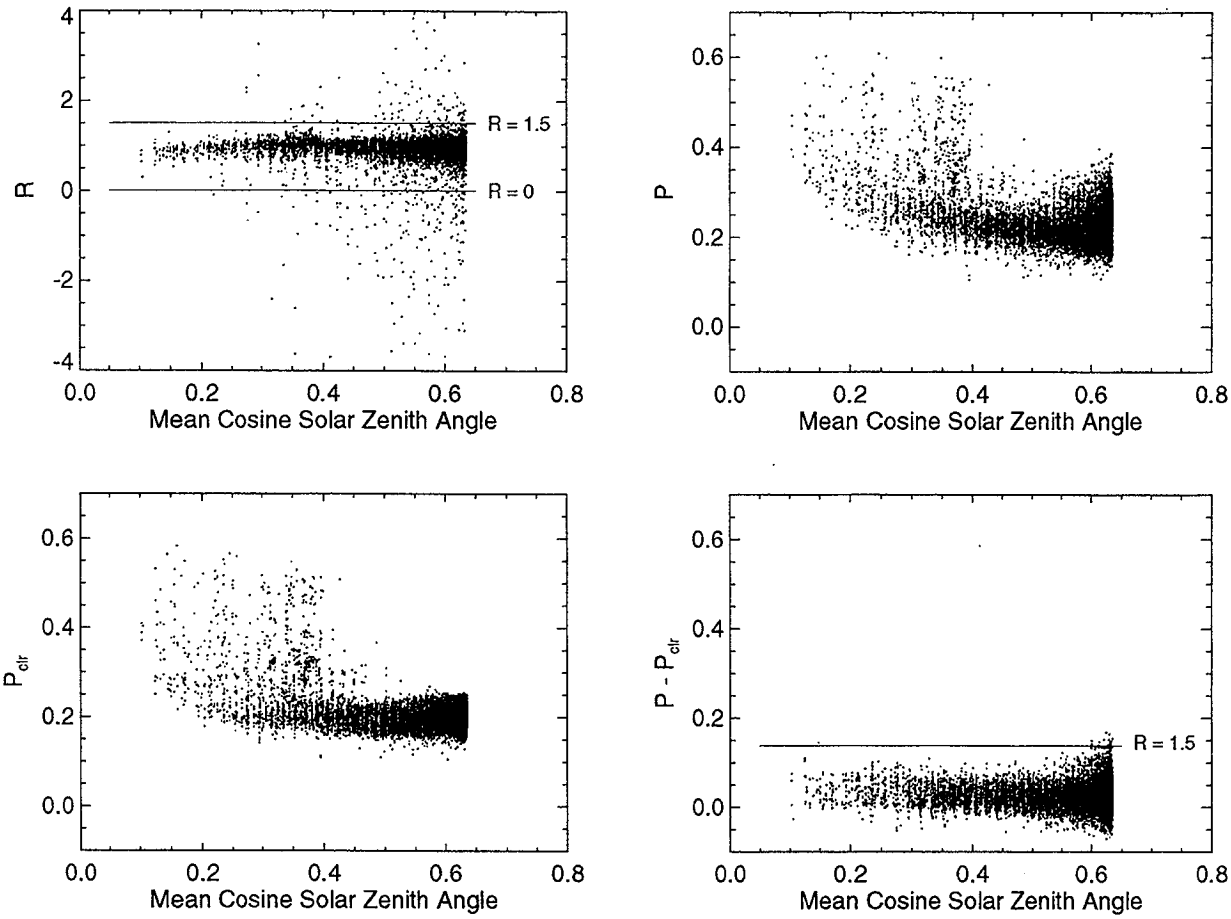

Figure 1. Global distribution of the ratio of the cloud radiative effect at the surface to that at the top of the atmosphere (R) and the solar energy partitioning terms (P and P_{clr}) and their difference (P – P_{clr}). Each point represents a monthly mean value for a 2° latitude by 2.5° longitude box. The points are randomly selected so that within each latitude band and for each month the number of selected boxes is proportional to area and the mean incoming solar flux. There are 10,000 points in each graph.

The results in Fig. 2 suggest that it is the cloud optical properties, rather than fractional cloud cover, which could explain the large bias in CRE. This is demonstrated by scatter plots of planetary albedo versus cloud fraction in Fig. 3. The albedo in GEOS/DAS is too high, and it increases with cloud fraction. At low cloud fractions, the GEOS/DAS albedo exceeds ERBE by ~0.05, and at high cloud fractions, by ~0.15. Since the bias appears with respect to both SW and LW flux, these results suggest that the clouds in GEOS/DAS are optically too thick in the tropical Pacific.

Conclusions

On the ratio of the cloud radiative effect (CRE) at the surface to that at the top of the atmosphere (R), the global mean in the GEOS/DAS dataset is 0.92, much less than the 1.5 reported in some recent studies. The critical parameter affecting R is the difference in the fraction of the net incoming flux absorbed by the atmosphere between all-sky and clear-sky conditions, which is too small by a factor ~5.

The global distribution of monthly mean R at individual grid points ranges from 0.74 to 1.11 (10th and 90th percentiles, respectively), and for only 1% of the points does R exceed 1.5.

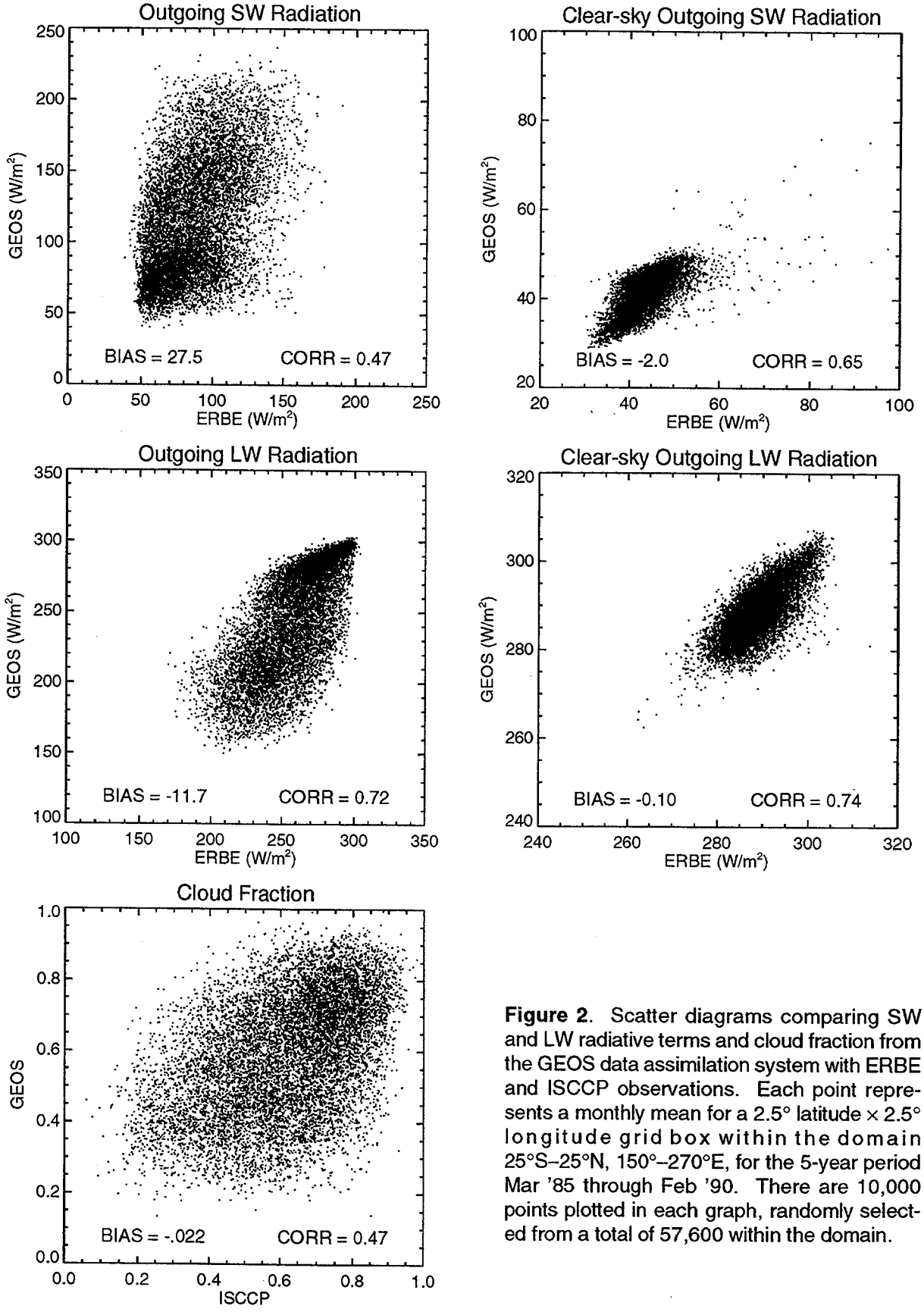

Figure 2. Scatter diagrams comparing SW and LW radiative terms and cloud fraction from the GEOS data assimilation system with ERBE and ISCCP observations. Each point represents a monthly mean for a 2.5° latitude × 2.5° longitude grid box within the domain 25°S–25°N, 150°–270°E, for the 5-year period Mar '85 through Feb '90. There are 10,000 points plotted in each graph, randomly selected from a total of 57,600 within the domain.

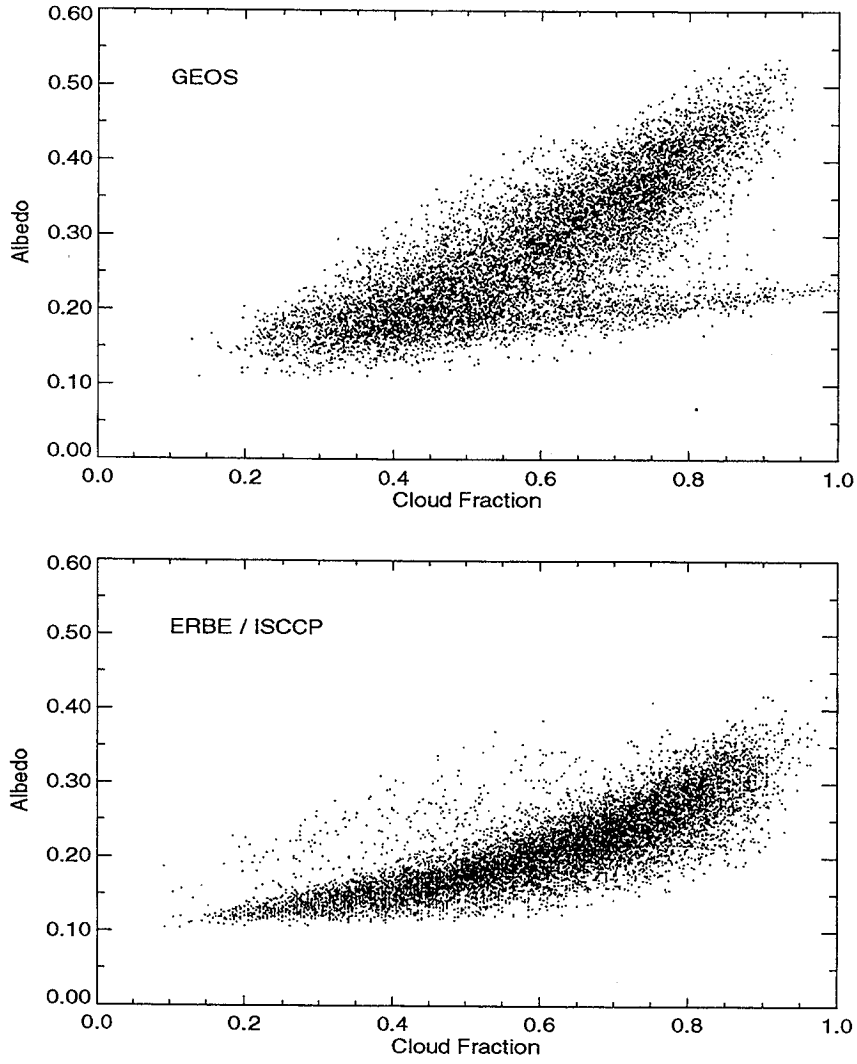

Figure 3. Relationship between planetary albedo and cloud fraction in the tropical Pacific. Each point represents a monthly mean for a 2.5° latitude × 2.5° longitude grid box within the domain 25°S–25°N, 150°–270°E, for the 5-year period Mar '85 through Feb '90. The points in the upper graph come from the GEOS data assimilation model, and in the lower graph, from ERBE and ISCCP observations. There are 10,000 points plotted in each graph, randomly selected from a total of 57,600 within the domain.

The global average net incoming solar flux at the top of the atmosphere for all-sky and clear-sky conditions, and hence the CRE, compare well with ERBE. But that masks a problem with the geographic distribution. Over the tropical Pacific (25°S–25°N, 150°E–270°E), the all-sky flux is too low, and the clear-sky flux too high, relative to the observations. As a result, the CRE at the top of the atmosphere is too high by about 30 W m^{-2}.

Comparing all-sky and clear-sky fluxes with ERBE, and fractional cloud cover with ISCCP, we conclude that the bias in the tropical Pacific is due to cloud optical properties, rather than cloud fraction. The planetary albedo, as a function of cloud fraction, is too high by an amount ranging from ~0.05 at low cloud fractions to ~0.15 at high cloud fractions.

References

Arking, A., 1991: The radiative effects of clouds and their impact on climate. *Bull. Amer. Meteor. Soc.*, **72**, 795–813.

Barkstrom, B., E. Harrison, G. Smith, R. Green, J. Kibler, R. Cess, and the ERBE Science Team, 1989: Earth radiation budget experiment (ERBE) archival and April 1985 results. *Bull. Amer. Meteor. Soc.*, **70**, 1254–1262.

Cess, R. D., M. H. Zhang, P. Minnis, L. Corsetti, E. G. Dutton, B. W. Forgan, D. P. Garber, W. L. Gates, J. J. Hack, E. F. Harrison, X. Jing, J. T. Kiehl, C. N. Long, J.-J. Morcrette, G. L. Potter, V. Ramanathan, B. Subasilar, C. H. Whitlock, D. F. Young, and Y. Zhou, 1995: Absorption of solar radiation by clouds: observations versus models. *Science*, **267**, 496–499.

Chou, M.-D., A. Arking, J. Otterman, and W. L. Ridgway, 1995: The effect of clouds on atmospheric absorption of solar radiation. *Geophys. Res. Lett.*, in press.

Pilewskie, and F. P. J. Valero, 1995: Direct observations of excess solar absorption by clouds. *Science*, **267**, 1626–1629.

Ramanathan, V., B. Subasilar, G. J. Zhang, W. Conant, R. D. Cess, J. T. Kiehl, H. Grassl, and L. Shi, 1995: Warm pool heat budget and shortwave cloud forcing: a missing physics? *Science*, **267**, 499–503.

Rossow, W. B., and R. A. Schiffer, 1991: ISCCP cloud data products. *Bull. Amer. Meteor. Soc.*, **72**, 2–20.

Schubert, S. D., R. B. Rood, and J. Pfaendtner, 1993: An assimilated dataset for earth science applications. *Bull. Amer. Meteor. Soc.*, **73**, 2331–2342.

Upper Tropospheric Humidity in the 5-Year GEOS Assimilation

David Starr
NASA Goddard Space Flight Center
Greenbelt, MD 20771

Brad Diehl and Andrew Lare
Applied Research Corporation

Brian Soden
NOAA GFDL

1. INTRODUCTION

Upper tropospheric water vapor (UTWV) is an important component of the global climate system (Starr and Melfi, 1991). UTWV directly affects the top-of-atmosphere radiative heat budget and significantly regulates the vertical distribution of radiative heating in the atmospheric column. This is a particularly important process over the vast subtropical oceans where the primary source of UTWV is vertical transport by deep convection in the tropics with subsequent incorporation into the large-scale upper tropospheric circulation. The importance of UTWV in determining the vertical distribution of infrared heating in the subtropics results from strong thermal contrast between the warm surface (and boundary layer) and the cold upper troposphere and the tendency to dry conditions in the middle troposphere with suppressed cloudiness. Satellite observations (6.7 μm channel) show highly-structured UTWV fields in the subtropics in concert with the patterns of large-scale dynamical processes, such as the subtropical jet stream. Patterns of heating (or cooling) in the upper troposphere can have a significant impact on dynamical development depending on the correlation with existing temperatures. In situations with a dry middle troposphere, the radiative impact of UTWV extends to the boundary layer and therefore also to atmosphere-surface heat exchange. Upper tropospheric cirrus cloudiness is also highly correlated with upper tropospheric relative humidity (UTH) and exerts an even greater radiative impact than that directly due to UTWV.

There has been a lively debate in recent years about the mechanisms controlling the UTWV budget in tropical and subtropical regions and their response to CO_2-induced global warming (mitigating versus amplifying effects). However, the climatology of UTWV has been poorly known due to severe limitations in conventional rawinsonde observing systems, including sparse coverage and poor sensor performance at cold temperatures (few reliable humidity observations at colder than -40°C). Fu et al. (1992) also argue that tropical-extratropical dynamical interactions are an essential component of such considerations indicating the potential importance of dynamical-radiative-UTH-cirrus interactions in subtropical regions. General circulation models have long had difficulty in producing realistic temperatures in the subtropical upper troposphere while the UTH fields are largely unvalidated. Various theories have been proposed to explain the temperature discrepancy but none has, as yet, been proven.

The results presented here are an outgrowth of a project to examine the climatology of tropical-extratropical cirrus cloud bands (Kuhnel, 1989) and upper tropospheric processes in a 10-year simulation of the global climate system for the period 1978-1988 that was conducted with the Goddard Laboratory for Atmospheres (GLA) General Circulation Model (Kim and Sud, 1993) as part of the Atmospheric Model Intercomparison Project (AMIP). While our original purpose was to establish the realism or deficiency in the synoptic climatology of large-scale upper tropospheric cloud systems and processes in a GCM simulation in comparison to observations, we have also correspondingly analyzed UTH and other fields. The plan was to use the GEOS 5-year data set (Schubert et al., 1994) for the period 1985-1989 to define the actual dynamic and thermodynamic (including moisture) state of the atmosphere since this is a self-consistent observationally-based analysis using a fixed analysis system. *However, our analysis of the GEOS data revealed major discrepancies in the analyzed UTH which are reported here.* Rawinsonde and satellite are also utilized in the present analysis.

2. DATA AND METHODOLOGY

The analysis region includes much of the tropical and northern hemisphere Pacific Ocean basin (10°S-45°N and 100°E-100°W). This domain was selected because of prevalence and regional and interannual variability of large-scale tropical-extratropical cirrus cloud bands (Kuhnel, 1989) and so-called "moisture bursts" (McGuirk et al., 1987) in this region and because of possible downwind implications for the weather and climate of North America. Our analyses have been mainly focused on upper tropospheric levels (500 mb and above).

The GLA GCM data set was generated on a 4° x 5° grid and was accessed via the sigma-level history files where the 6-hourly fields were averaged to daily values. The simulation was forced with time-dependent sea surface temperature fields corresponding to the observed fields during the 1979-1988 time period. Corresponding fields of relative humidity with respect to a pure plane surface of ice (RHI) were calculated on sigma levels from the daily-averaged fields of temperature, water vapor specific humidity and pressure using the Goff-Gratch standard formula. The RHI fields were then linearly interpolated to standard pressure levels, such as 300 mb that will be shown here, while temperature and specific humidity were interpolated linearly with respect to logarithm of pressure (LLP).

The GEOS data set is the standard-level time-series data set generated on a 2° x 2.5° grid using the available observations from 1985-1989. In this case, the vertical interpolation of temperature and specific humidity to standard levels was accomplished using LLP as part of the GEOS processing. The 6-hourly fields were averaged to produce a daily analysis and the corresponding RHI field was then calculated. The reason for examining UTH in terms of RHI is that RHI is a more physically meaningful moisture parameter in terms of cloudiness at cold temperatures (typically about -40°C at 300 mb) and gives an expanded scale in comparison to the more commonly used relative humidity with respect to liquid (RH) or specific humidity.

A 13-year (1979-1991) data set of UTH derived using observations from the 6.7 μm HIRS channel on NOAA operational polar orbiting satellites is also utilized in the present analysis. The HIRS/UTH data set was generated on a 2.5° x 2.5° grid and consists of daily average values based on all UTH pixel retrievals within each grid area. The retrievals were made using the methodology of Soden and Bretherton (1993). Cloudy pixels were excluded from the analysis resulting in a probable dry bias for climate applications. The retrieved UTH corresponds to an average relative humidity within the layer extending roughly from 500 mb to 200 mb. Comparisons to various types of rawinsonde humidity observations, in situ aircraft observations, and water vapor observations using Raman lidar indicate that the HIRS/UTH is a useful characterization of integrated upper tropospheric relative humidity (Soden et al., 1994). Conversion to UTHI (with respect to ice) was made here using the corresponding daily GEOS temperature fields interpolated (LLP) to 350 mb.

The rawinsonde (RAOB) humidity data set was obtained from the GEOS archives (data from 1985-1989 that were input to the assimilation). Unfortunately, the temperature data were stored separately from the humidity data and were not readily available. *We recommend that, in the future, the observed temperature be stored with the observed humidity.* The archived values of RH at standard pressure levels were converted to RHI using the temperatures for the corresponding grid and time from the assimilation. This was done in two steps: 1) calculation of the originally transmitted dew point depression using the inverse of the approximate formula actually applied in GEOS and then calculation of RHI using Goff-Gratch. We also discovered that, in processing the input data for GEOS, the standard reporting code of a 30°C dew point depression that is operationally used to denote RH less than 20% or so (Garand et al., 1992) had been handled as if it were literal data which caused some misrepresentation at low humidity, i.e., a 30°C dew point depression translates to a humidity of about 10% at -40°C. Thus, RHI values of about 6-8% are fairly common, but few, if any, values below 6% or between 8% and 20% are found in this RAOB archive. There is no good way to compensate for this problem since the actual RH observations were never reported. Upper air reporting practices for humidity have recently been changed in the United States and this problem (using 30°C dew point depression as a code) may have already been resolved for future data sets.

3. RESULTS

Shown in Figure 1 are the mean annual RHI at the 300 mb level from the GEOS assimilation along with the difference fields between the GEOS RHI analysis and the HIRS UTHI climatology and the GLA GCM simulation, respectively; and between the GLA GCM and the HIRS UTHI. *It is immediately obvious that the GEOS RHI at 300 mb is substantially larger than in either of the other data sets. This is not attributable to differences in temperature as the 300-mb specific humidity is systematically about twice as large in the GEOS data* (not shown). It should be noted that the GLA GCM and HIRS fields differ by less than 10% over most of the region of interest here with the GCM being wetter in the subtropics but drier in midlatitude and equatorial regions, especially over the "warm pool" region of the tropical western Pacific Ocean and the maritime continent, where the differences in RHI reach nearly 30%. Notable features in the GEOS analysis include the very moist upper troposphere (RHI exceeding 90%) over the "warm pool" region of the tropical western Pacific Ocean and the maritime continent and over the eastern Pacific Ocean north of 30°N. Annual mean RHI exceeds 100% in the latter region. These large-scale moist features are also found in the other analyses though the

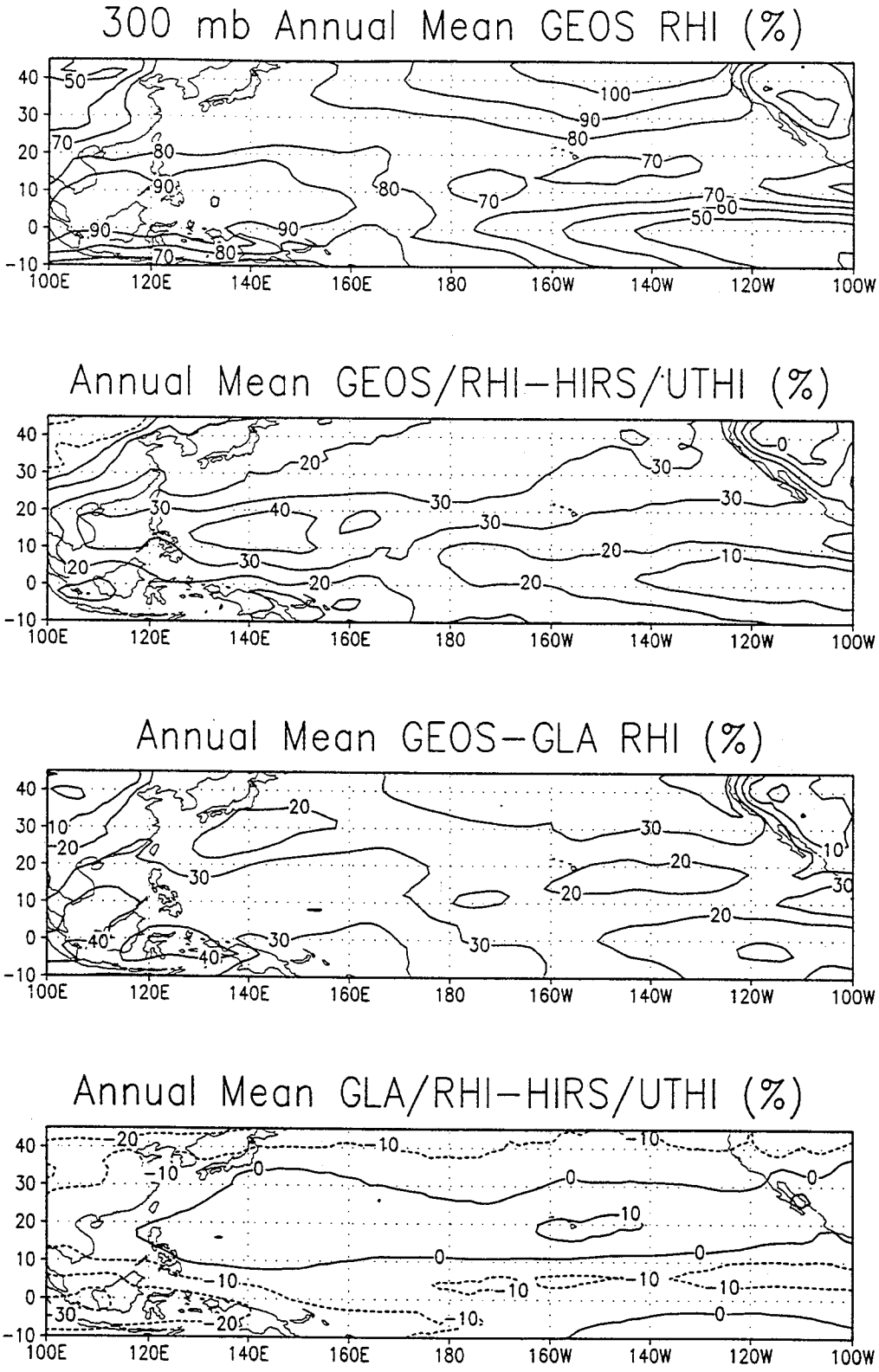

Figure 1: Mean annual relative humidity with respect to ice (RHI) at the 300 mb pressure level from the GEOS 5-year (1985-1989) assimilation (top) and various difference fields of mean annual RHI at 300 mb where HIRS/UTHI is upper tropospheric humidity (ice) derived from a 13-year (1979-1991) satellite data set and GLA RHI is from a 10-year (1979-1988) simulation with the GLA GCM.

magnitude is appreciably less. In fact, the relative patterns in the GEOS and GLA GCM RHI fields at 300 mb are quite similar over the ocean as is evident from the rough similarity in the pattern of the GEOS-HIRS and GLA-HIRS difference analyses. The other very notable feature of the GEOS analysis is that the continents are clearly identifiable with a strong gradient to much drier conditions approximately coincident with the continental boundary, especially along the west coast of the United States, a data rich region. This feature is not found in either of the other two data sets (not shown but evident here in the preservation of the coastal gradient in the difference analyses involving GEOS). Thus, the 300-mb RHI field in the GEOS analysis is much too moist over the Pacific Ocean but snaps back to more realistic values over the land masses of Asia and especially North America. This is somewhat surprising in that RAOB humidity data are not generally available during the cool season at the 300 mb level due to the cold temperatures (less than -40°C). The drier conditions analyzed over the western United States could reflect the impact of data at lower levels, i.e., RAOB humidity data are generally available at the 400 mb and lower levels in all seasons. *The widespread moist bias found in the GEOS moisture fields at 300 mb was not evident in the 500 mb level.*

We have found that the relative frequency distribution (histogram) of RHI is a very useful tool to characterize spatial and temporal variability in climatic regime and to compare these data sets. For example, differences between histograms for tropical, subtropical and extratropical locations at various longitudes clearly indicate geographical and seasonal differences in large-scale circulation and weather systems. To illustrate, a comparison of histograms of RHI at 300 mb based on 1200 UTC rawinsondes launched at Wake Island (1201 soundings over 5 years) are shown in Figure 2 along with the difference between the Wake Is. histogram and those for the corresponding grid point in the GLA and GEOS data sets. The 30°C dew point depression problem in the RAOB data is immediately apparent with many values in the first bin (0-10%) but none in the second (10-20%). The Wake Is. soundings reveal a dry climate at 300 mb with 75% of the observations corresponding to RHI less than 49% (quartiles annotated on plot) and 45% of the observations with RHI less than 20%. In comparison, the GLA GCM simulation exhibits a tendency for more frequent values in the middle and upper end of the RHI scale while the GEOS data show a very marked moist bias (note the scale change to accommodate RHI values exceeding 140% on this panel). For contrast, the histograms for winter season at 150°W and 38°N are shown in Figure 3 for the GLA and GEOS data as well as the difference. While both distributions are relatively flat, many more extremely moist values (and fewer very dry values) occur in the GEOS data. For example, nearly 45% of all the GEOS RHI values exceed 100% while only about 12% are supersaturated with respect to ice in the GLA simulation at this location. Both distribution exhibit maximum values exceeding 160%.

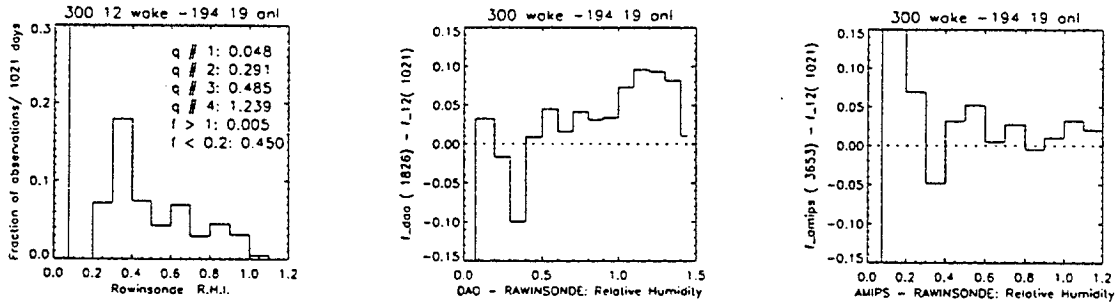

Figure 2: Frequency distribution of 300 mb relative humidity with respect to ice at Wake Is. from the 5-years of rawinsondes and difference with GEOS assimilation and the GLA GCM simulation (see text).

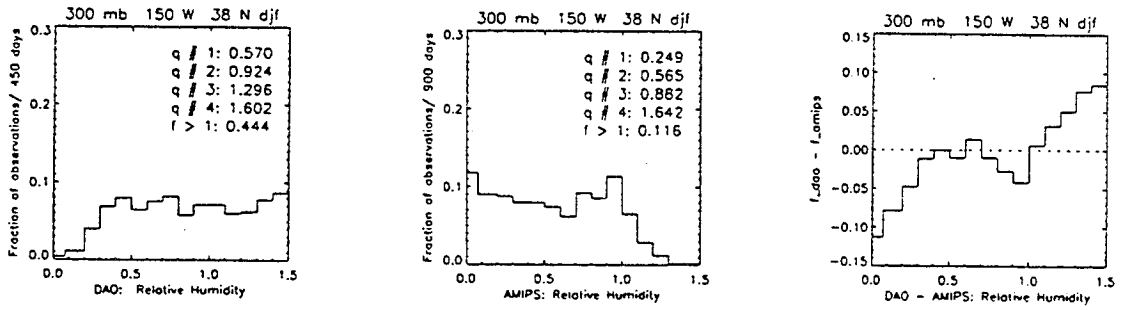

Figure 3: Frequency distributions of relative humidity with respect to ice at 300 mb from the 5-year GEOS assimilation and the 10-year GLA GCM simulation at 38°N and 150°W and the difference (see text).

4. DISCUSSION

Upper tropospheric relative humidity has been found to be much too large at the 300 mb level over the Pacific Ocean in the GEOS assimilated data set. We estimate that the analyzed specific humidity is systematically about twice as large as the actual moisture values at this level. This problem is not very evident at the 500 mb level. *As a result, great caution must be used in calculating vertical profiles of radiative heating based upon the analyzed fields (or using the GEOS calculated radiative profiles).* In particular, the radiative heating of the upper troposphere is likely to be significantly in error. In addition, it is likely that the net radiative flux at the top of the atmosphere and at the top of the boundary layer will also be adversely affected.

Two factors potentially contributing to the gross moisture enhancement in the GEOS upper tropospheric analysis over the Pacific Basin are the use of relative humidity with respect to liquid (RH) instead of the more physically realistic RHI for the diagnosis of stratiform cloudiness and the lack of a fractional cloudiness parameterization. At -40°C, the ratio of RHI to RH is about 1.4. Thus, the former factor could explain nearly half of the moist bias. The latter factor would allow cirrus cloud formation at values of RHI greater than some threshold value (e.g., 70% as implemented in various GCMs) coupled with a downward ice water transport scheme to account for the non-negligible particle fall speeds typically found in cirrus clouds (~0.5 m s^{-1} for the ice mass) and result in drying of the upper troposphere. However, the dry conditions analyzed over the major continental regions would seem to indicate that the problem may be more complex.

It has also been suggested (this workshop) that tropical convection is too active in the GEOS assimilation which could result in too much vertical transport of water into the tropical upper troposphere with subsequent transport into the subtropics and extratropics. Even if the tropical convection is overly active, however, the existence of the extremely moist region north of 30°N over the eastern Pacific Ocean may indicate that this explanation is inadequate.

Future activities will include consideration of levels above 300 mb and comparison of the GEOS upper tropospheric cloudiness fields with our analyses of these fields from the GLA GCM 10-year simulation.

REFERENCES

Fu, R., A.D. Del Genio, W.B. Rossow and W.T. Liu, 1992: Cirrus cloud thermostat for tropical sea surface temperatures tested using satellite data. *Nature*, **358**, 394-397.

Garand, L., C. Grassotti, J. Halle and G.L. Klein, 1992: On differences in radiosonde humidity-reporting practices and their implications for numerical weather prediction and remote sensing. *Bull. Amer. Meteoro. Soc.*, **73**, 1417-1433.

Kim, J.-H., and Y.C. Sud, 1993: Circulation and rainfall climatology of a 10-year (1979-1988) integration with the Goddard Laboratory for Atmospheres general circulation model. NASA Tech. Memo. 104591, NASA, Washington, D.C., 236 pp.

Kuhnel, I., 1989: Tropical-extratropical cloudband climatology based on satellite data. *Inter. J. Climato.*, **9**, 441-463.

McGuirk, J.P., A.H. Thompson and N.R. Smith, 1987: Moisture bursts over the tropical Pacific Ocean. *Mon. Wea. Rev.*, **115**, 787-798.

Schubert, S.D., R.B. Rood and J. Phaendtner, 1993: An assimilated dataset for earth science applications. *Bull. Amer. Meteor. Soc.*, **74**, 2331-2342.

Soden, B.J., and F.P. Bretherton, 1993: Upper tropospheric relative humidity from GOES 6.7 μm channel: Method and climatology for July 1987. *J. Geophys. Res.*, **98**, 16669-16688.

Soden, B.J., S.A. Ackerman, D.O'C. Starr, S.H. Melfi and R.A. Ferrare, 1994: Comparison of Upper Tropospheric Water Vapor from GOES, Raman Lidar, and CLASS Measurements During FIRE Cirrus-II. *J. Geophys. Res.*, 99, 21005-21016.

Starr, D.O'C., and S.H. Melfi, 1991: The Role of Water Vapor in Climate: A Strategic Research Plan for the GEWEX Water Vapor Project (GVaP). NASA CP-3120, NASA, Washington, D.C., 50 pp. (available from DS)

ACKNOWLEDGMENTS

We gratefully acknowledge the following individuals for their invaluable assistance: Dan Ziskin supported our efforts to access the GEOS data through the GSFC DAAC, Dave Ledvina helped us acquire the RAOB humidity data, Greg Walker provided the GLA GCM data set, and David Makofski provided access to data handling hardware (TRMM) that expedited our task. This work is a component of the EOS-IDS Hydrologic Processes and Climate Project of Dr. W. K.-M. Lau supported through the NASA Mission to Planet Earth under Dr. Ghassem Asrar.

EVALUATION OF UPPER-TROPOSPHERIC MOISTURE IN THE GEOS ASSIMILATION USING TOVS RADIANCE OBSERVATIONS

Eric P Salathé, Jr and Dennis Chesters
Climate and Radiation Branch
NASA Goddard Space Flight Center

1. Introduction

Predictions of the net climate response to anthropogenic carbon dioxide are highly dependent upon how water vapor processes are modeled at different layers in the atmosphere. The influence of sea surface temperature on moisture is fairly direct in the lower troposphere where moisture evaporates from the surface and is distributed through the boundary layer by shallow convection. However, the Earth's radiation balance is also sensitive to the relatively small amounts of water vapor in upper troposphere (Arking, 1990; Shine and Sinha, 1991). In the subtropics, large-scale descent suppresses deep local convection, isolating the upper troposphere from the sea surface immediately below, and the vertical transport of moisture is downward (Piexoto and Oort, 1993). Thus, the mechanisms controlling upper-tropospheric moisture are not confined to a single vertical column, but involve planetary scale circulations and horizontal transport over great distances. Consequently, many researchers have recently probed the way GCMs depict upper-tropospheric hydrology and particularly its response to climate forcing (Sud and Molod, 1988; Lindzen, 1990; Del Genio et al., 1991). Given the sensitivity of the climate to upper-tropospheric water, it is essential that GCM upper-tropospheric hydrology be tested and improved by comparison with observations. Since the radiosonde measurements of moisture above 500mb are scarce and of poor quality, the upper-tropospheric moisture generated in a data assimilation GCM are far more dependent upon the modeled hydrology than on the assimilated observations. Thus deficiencies in the GCM parameterizations may lead to large errors in the moisture field.

In this paper, the TOVS radiance observations in the 6 to 7 μm water vapor band are used to evaluate the upper tropospheric moisture analyses generated by the recent 5-year run of Goddard EOS (GEOS) data assimilation system. Comparisons are made directly between the observed brightness temperature and brightness temperatures computed from the model moisture and temperature fields. In earlier studies, we have used the TOVS data to evaluate the upper tropospheric moisture in the ECMWF analyses (Salathé and Chesters, 1995) and a 10-year run of the GLA GCM (Salathé et al, 1995). The ECMWF analyses accurately capture the spatial patterns of upper tropospheric moisture, but not the strong regional moisture contrast that is indicated by satellite observations. The GLA GCM shows some success generating the observed moisture climatology. It does not yield as accurate a spatial distribution of moisture, as the ECMWF analyses, but can generate much stronger gradients between moist and dry regions.

2. Data

TOVS radiance data are archived by NOAA as idealized nadir-viewing clear-sky brightness temperatures after applying corrections to the raw observations for satellite view angle and cloud contamination. (see Chesters and Sharma, 1992 and Salathé and Chesters, 1995). The brightness temperatures presented here are a linear combination of the TOVS 6.7 and 7.2 μm channels used to enhance the sensitivity to the upper-most levels of the water vapor profile. The peak sensitivity of the composite brightness temperature is at 300 mb; thus, it serves as a better indicator of upper-tropospheric moisture and more rigorous test of model predictions than the 6.7 mm channel alone. The composite brightness temperature used here will be referred to simply as the TOVS brightness temperature. To create daily images, the data along the satellite sub-orbital swaths were placed on a polar stereographic grid using the NOAA objective analysis, and then interpolated to a 5°x5° rectangular grid from 40S to 40N. In gridding the archived TOVS brightness temperatures, some daily images were unrecoverable or were discarded due to a lack of observations over more than 25% of the globe; approximately 6% of the data are missing or unacceptable (see Chesters and Sharma (1992) for details). Monthly and seasonal averages are obtained from the remaining quality-controlled images.

To compute brightness temperatures corresponding to the TOVS observations, we performed radiative transfer calculations on the daily data using a narrow band molecular absorption model . Given the uncertainties in the radiative transfer calculations, the mean difference between computed and observed brightness temperatures cannot be

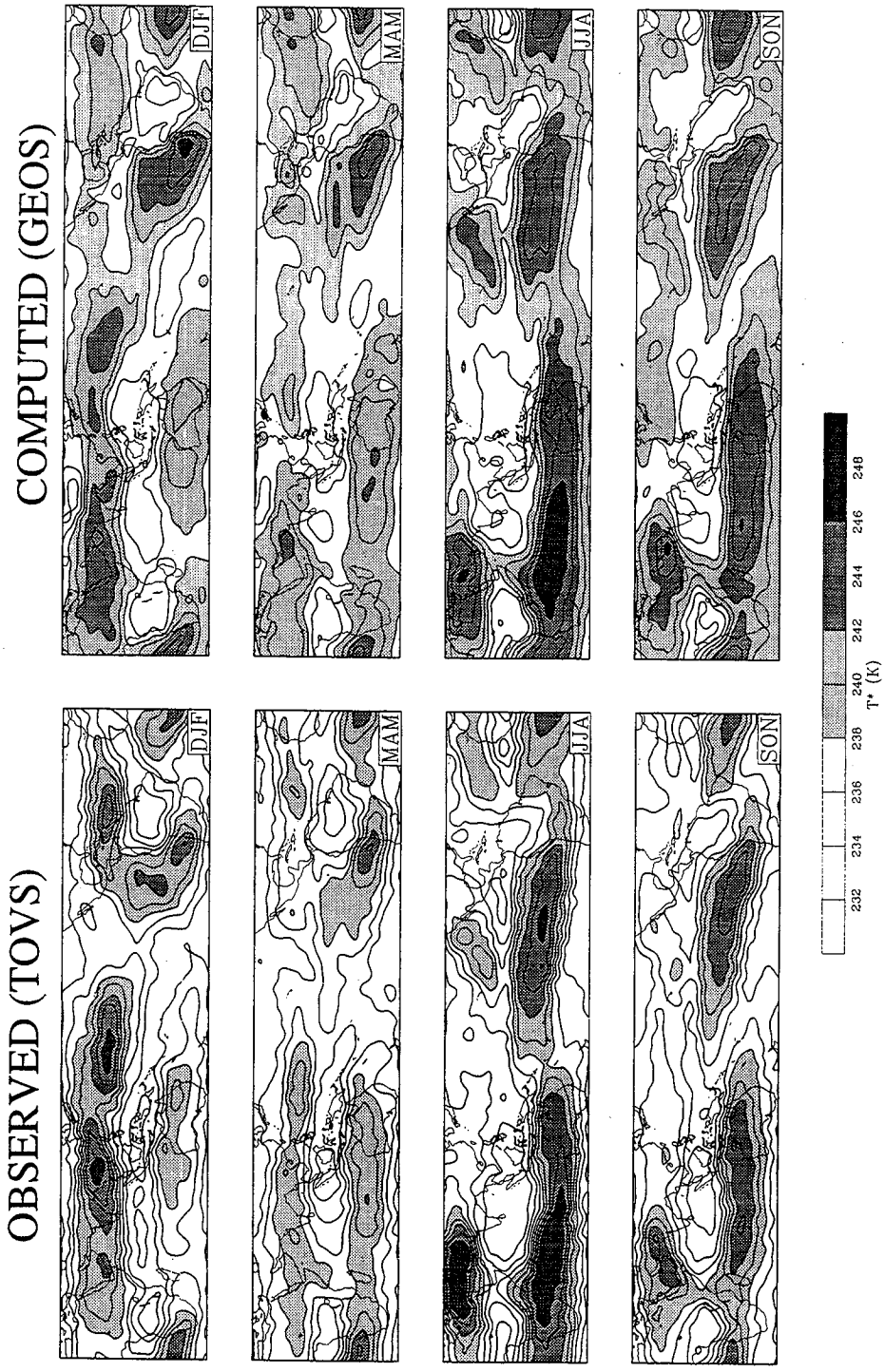

Fig. 1. Observed and Computed Brightness Temperatures. Dark areas are high brightness Temperature values where the upper troposphere is very dry.

interpreted as a bias in the modeled moisture. However, the comparison of computed and observed brightness temperatures is, however, a reliable means for testing the temporal and spatial variability of the modeled moisture.

The GEOS analyses are from the GEOS-1 5-year (1985-1989) data assimilation run. Brightness temperatures are computed using the temperature and moisture profiles on the 2°x2.5° horizontal and 18-level GEOS grid. The brightness temperatures are then interpolated to the 5°x5° TOVS grid for comparisons.

3. Results

Figure 1 shows the 5-year seasonal means of observed brightness temperature, which may be compared to the computed brightness temperature fields in Fig 2. Dark shaded areas indicate regions of high brightness temperature where the upper troposphere is very dry. The GEOS brightness temperatures are on average 2.2K higher than observed, but this bias reflects uncertainties in the radiative transfer, and does not imply the model is too dry. The analyses capture the overall placement of the seasonal moisture patterns quite well. The success in data void regions (e.g. the eastern Pacific) indicates that the model generates reasonable moisture patterns unaided by assimilated moisture data. However, the simulated moisture field is rather diffuse compared to the observed field; the gradient between very moist and very dry regions is much weaker in the simulated moisture than the observations indicate.. This character of the simulated moisture field is similar to results from the ECMWF analyses (Salathé and Chesters 1995, Soden and Bretherton, 1994). The spatial correlation of the monthly-mean brightness temperature patterns from the observations, the GEOS analyses, and the ECMWF analyses (Fig 2.) show that for most of 1989, there is little difference in how well the two analyses match the observations.

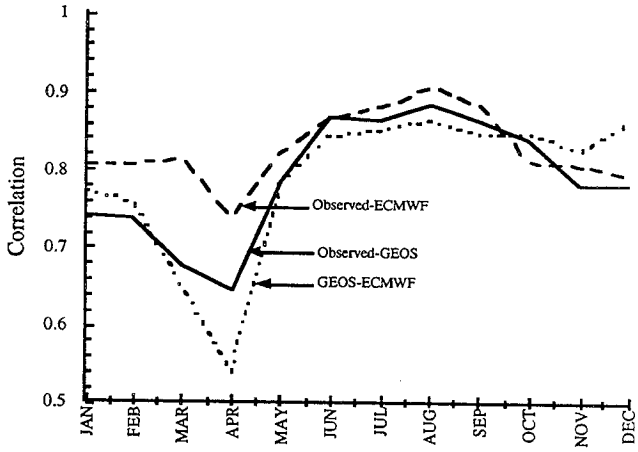

Fig 2. Correlation of observed and computed brightness temperature patterns in 1989.

References

Arking, A., 1990: Feedback processes and climate response. Climate Impact of Solar Variability, NASA Conf. Publ. 3086, K. H. Shatten and A. Arking (Eds.), NASA, Washington DC., p219-226.

Del Genio, A. D., A. A. Lacis, and R. A. Ruedy, 1991: Moist convection and water vapor feedback on climate. *Nature*, **351**, 382-385.

Chesters, D. and O. Sharma, 1992: An Atlas of Upper Tropospheric Radiances Observed in the 6 to 7 Micrometer Water Vapor Band Using TOVS Data from the NOAA Weather Satellites During 1979-1991. *NASA Technical Memo 104563,* Goddard Space Flight Center, Greenbelt, MD., 183pp.

Lindzen, R.S., 1990: Some coolness concerning global warming. *Bull. Amer. Meteor. Soc.*, **71**, 288-299.

Peixoto, J. P. and A. H. Oort, 1992: Physics of Climate. American Institute of Physics, 520pp.

Salathé, E. P. and D. Chesters, 1995: Seasonal and regional variability of moisture in the upper troposphere, as inferred from TOVS satellite observations and ECMWF model analyses. *J. Climate,* **8,** 120-132.

Salathé, E. P., D. Chesters, and Y. C. Sud 1995: Evaluation of the upper-tropospheric moisture in a general circulation model using TOVS satellite observations. *J. Climate,* submitted.

Shine, K. P. and A. Sinha, 1991: Sensitivity of the Earth's climate to height-dependent changes in the water vapour mixing ratio. *Nature,* **354**, 382-384.

Soden, B. J. and F. P. Bretherton, 1994: Evaluation of water vapor distribution in general circulation models using satellite observations. *J. Geophys. Res.*, **99**, 1187-1210.

Sud, Y. and Molod, 1988: The roles of dry convection, cloud-radiation feedback processes and the influence of recent improvements in the parameterization of convection in the GLA GCM. *Mon. Wea. Rev.*, **116**, 2366-2387.

2.3 Phenomenology and Diagnostics

POTENTIAL VORTICITY-BASED DIAGNOSES OF SEASONAL AND INTRASEASONAL VARIABILITY IN AN ASSIMILATED DATASET

Robert X. Black
Georgia Institute of Technology, Atlanta, GA.
Randall M. Dole
NOAA, ERL/Climate Diagnostics Center, Boulder, CO.
Jeffrey S. Whitaker
CIRES, University of Colorado/NOAA, Boulder, CO.

1. Introduction

The primary objective of our research is to employ the GEOS-1 DAS to study the dynamics of seasonal climate and intraseasonal transient eddy variability within a potential vorticity framework. Our scientific approach focuses on the contributions of various physical processes to budgets of potential vorticity and eddy potential enstrophy. An important aspect of this approach is a detailed assessment of the uncertainties in individual budget components. A second goal is to use the analysis increments of the DAS to study the dynamical characteristics of short-term systematic error development. We summarize the primary methods of our project and present preliminary analyses related to the 1988 heat/wave drought.

2. Methods

Potential vorticity (PV) budgets are constructed for the seasonal-mean flow. Because frictional and diabatic sources of PV can be directly diagnosed from the assimilated data, more complete budgets can be constructed than using conventional observational data. Direct and indirect measures of PV fluxes are used to deduce errors in the PV budget due to systematic errors in the diabatic heating and frictional dissipation rates parameterized by the DAS. Potential enstrophy and PV analyses are also performed for intraseasonal transient eddies. Our scope includes phenomena ranging from synoptic-scale eddies to low frequency anomalies. We are very interested in deducing the role of diabatic heating in producing and maintaining intraseasonal eddy activity, particularly cyclones and heat wave/droughts. Uncertainties in individual budget terms are estimated by comparing key assimilated quantities to similar fields derived from NOAA NMC reanalyses. These fields include diabatic heating, frictional dissipation, and potential enstrophy. Analysis increments are used to characterize short-term forecast error in the GEOS-1 DAS. The dynamical impact of short-term systematic error development is examined using a PV approach.

3. Results

Our initial research has focused on characteristics of the diabatic heating fields derived from the GEOS-1 assimilated data. Two projects have been initiated, the first comparing diabatic heating fields obtained from GEOS-1 and NMC reanalyses, and the second comparing GEOS-1 analyses with observational data and diagnostic analyses of the major U.S. heat wave/drought of 1988 (Lyon and Dole, 1995, henceforth LD).

In the first project, GEOS-1 and NMC analyses of total diabatic heating are compared for the 1985-86 winter season. Although the diabatic heating fields from the two analyses (not shown) are broadly similar, there are also several significant differences. Some of the larger differences include a tendency for GEOS-1 analyses to have stronger heating over Indonesia and the South Pacific ITCZ, and weaker heating in the eastern Pacific ITCZ region and in the North Pacific and North Atlantic storm tracks. Cross sections (not shown) also display substantial differences in the vertical distributions of heating, including a tendency for heating in the Northern Hemisphere storm tracks to be shallower in the GEOS-1 than in the NMC analyses. These differences provide a lower bound on the uncertainty on diabatic heating distributions and, hence, on the uncertainty in corresponding potential vorticity sources.

In the second project, we have examined aspects of the 1988 heat wave/drought evolution obtained from GEOS-1 analyses, and compared these with observational data derived from the Global Climate Perspectives System (GCPS) dataset (a quality-controlled subset of Global Historical Climate Network station data available at the Climate Diagnostics Center). Preliminary results are illustrated in Fig. 1.

Fig. 1a shows, for a 4° by 5° box centered over the north-central U.S., time series of monthly-mean temperature anomalies from March to August 1988 obtained from GEOS-1 and GCPS, where anomalies are defined relative to the respective (GEOS-1 or GCPS) climate means for the period 1985-1992. Though the GCPS data show positive temperature anomalies throughout the period, GEOS-1 analyses indicate negative anomalies for March and April. Following this time, GEOS-1 anomalies are also positive and, in fact, become larger than those derived from the station data in July and August. Time series of precipitation anomalies (Fig. 1b) show that the GEOS-1 and GCPS anomalies are remarkably similar throughout the Spring; thereafter, GEOS-1 tends to have larger negative precipitation anomalies than GCPS, particularly in July. Corresponding GEOS-1 evaporation anomalies are quite small through June, but become large and negative in July and August. Comparisons with evapotranspiration anomalies derived from residuals in the atmospheric moisture budget over roughly the same region (LD) show a fairly similar evolution, with the exception of July, during which time the negative evaporation anomalies in GEOS-1 are substantially larger than those derived from the residual calculations.

The evolution of evaporation anomalies in GEOS-1 provides support for LD's conclusion that surface evapotranspiration anomalies were unlikely to have played a significant role in the early stages of the 1988 heat wave/drought, but may have done so at later stages. Fig. 1c extends LD's work by using the GEOS-1 data to examine the evolution of surface anomalies of net downward short wave radiation fluxes, and net upward fluxes of long wave radiation, sensible and latent heat. Throughout the period, anomalies in downward short wave fluxes are positive, likely due to reduced cloud cover. These are approximately, but not entirely, compensated by positive anomalies in upward long wave fluxes, partly due to reduced cloud cover and, at later stages, to anomalously warm surface temperatures. Consistent with the evaporation anomalies described above, upward latent heat flux anomalies are quite small through June, and then become large and negative later in the summer. The latent heat flux anomalies are approximately balanced by positive anomalies in upward sensible heat fluxes. The August anomalies in latent heat fluxes are very similar in magnitude to those obtained in LD, who estimated a corresponding anomalous boundary layer heating to be about 1° C day^{-1}. The GEOS-1 results therefore support LD in indicating that anomalous local boundary conditions likely played a significant role in the later stages of the 1988 heat wave/drought, but also add to LD's results by providing quantitative estimates of additional terms in the surface heat budget.

Although the broad features of the 1988 drought are captured by the GEOS-1 analyses, there are also interesting discrepancies from observations. For example, GEOS-1 is relatively warmer and drier in July, and the corresponding reduction in upward latent heat fluxes during this period is significantly larger than indicated by the moisture budget results of LD. We speculate that these differences are connected to the absence of a land-surface model in the present analysis scheme, so that changes in evapotranspiration and albedo that occur during the drought are not adequately captured in the present model.

To the extent that there is consistency with observable quantities, the GEOS-1 assimilation dataset provides a very exciting opportunity to improve our understanding of processes occurring in major weather and climate events, such as the 1988 heat wave/drought. To the extent that there are differences, the results are also valuable in suggesting possible directions for improving the current data assimilation system.

Acknowledgments. We gratefully acknowledge the help of Andy Loughe and Kriste Paine of CIRES for their help in acquiring the GEOS-1 and GCPS data and for performing analyses on this project. Support for this work is provided through interagency agreement NASA Order No. S-41363-F and a grant from the Earth System Modeling and Analysis Program of NASA's Mission to Planet Earth (grant number pending).

Reference. Lyon, B., and R. M. Dole, 1995: A diagnostic comparison of the 1980 and 1988 U.S. summer heat wave/droughts. *J. Climate,* **8,** in press.

Figure legend (see next page). Monthly mean anomalies for March to July 1988 in (a) surface temperatures from GEOS-1 and GCPS (units = °C); (b) precipitation (P) from GEOS-1 and GCPS, and evaporation (E) and evaporation - precipitation (E - P) from GEOS-1 (units mm day^{-1}); and (c) Net downward shortwave radiation, net upward long wave radiation, sensible and latent heat fluxes at the surface from GEOS-1 (units W m^{-2}). Line patterns for all terms are shown on the figure.

1988 ANOMALIES FROM 1985-92 CLIMATOLOGY

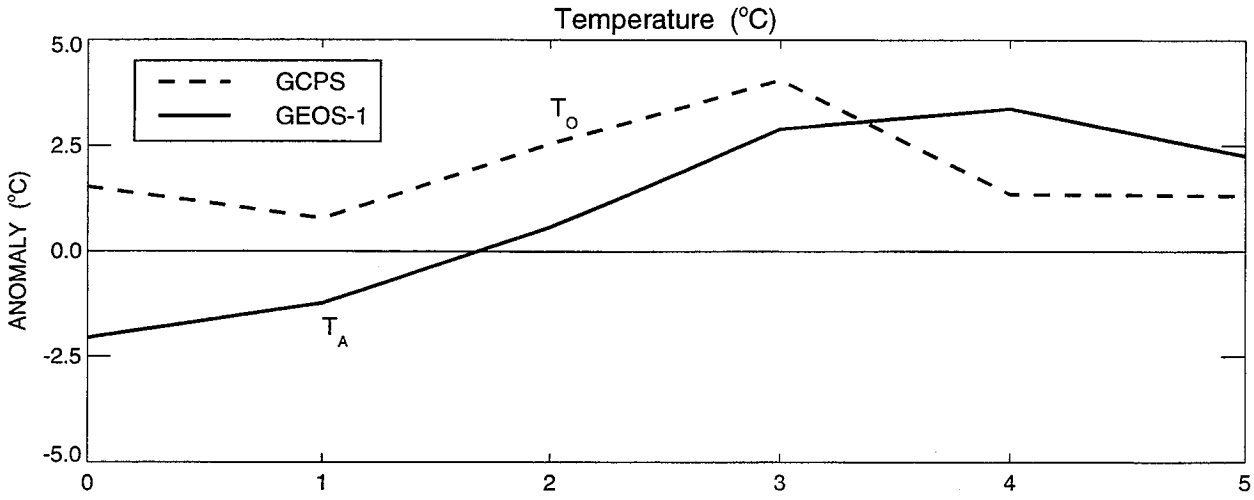

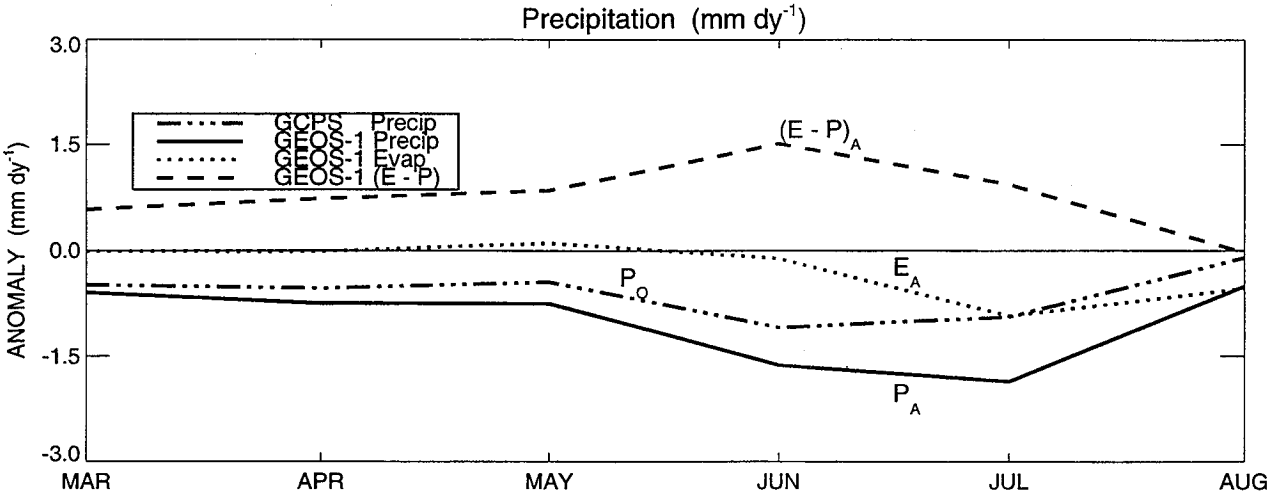

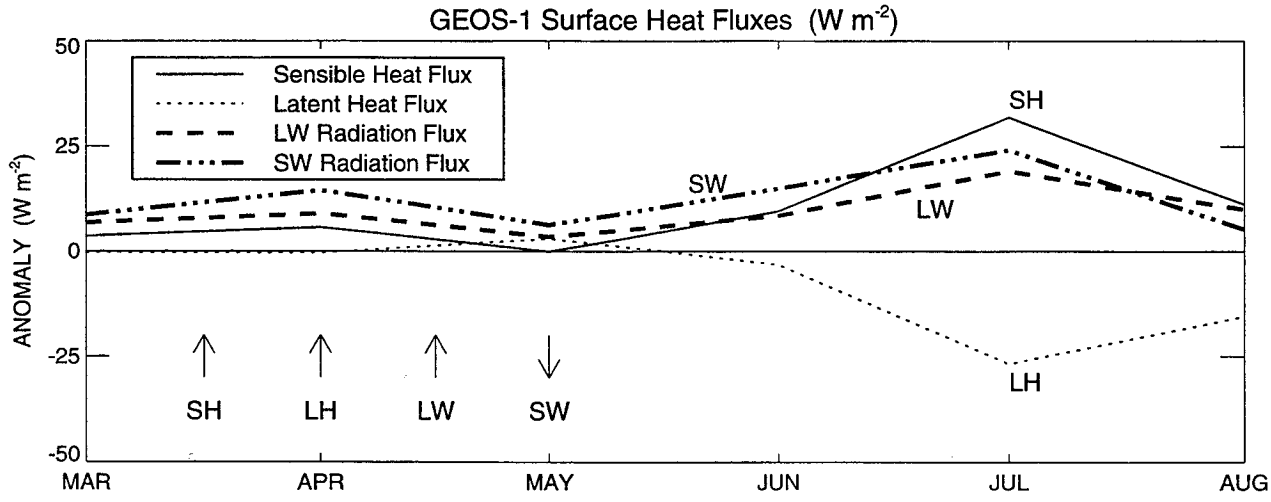

Variability of the Global Precipitable Water with a time Scale of 90-150 Day

Tsing-Chang Chen*, James Pfaendtner+,
Jau-Ming Chen* and Christopher K. Wikle*

* Atmospheric Science Program, Department of Geological and Atmospheric Sciences, Iowa State University, Ames, IA.
+ National Meteorological Center/NOAA, Camp Springs, MD

Many studies have been conducted to examine the global-scale variability of atmospheric water vapor at different time scales; the interannual (e.g. Salstein and Rosen 1983), annual (Chen et al. 1995a) and intraseasonal (e.g. Chen et al. 1995b) time scales. The present study extends the previous work outlined in Chen et al. (1995a,b) with the 1985-1991 moisture data generated by the Global Data Assimilation System (GDAS) of the Goddard Laboratory for Atmospheres (GLA) (Schubert et al. 1993), National Meteorological Center (NMC) (Kanamitsu et al. 1991), and European Centre for Medium Range Weather Forecasting (ECMWF). An intraseasonal signal of global precipitable water, <W> becomes discernible in the time series (not shown) after the annual- and semiannual-cycle components are removed by a simple harmonic analysis. Spectral analysis (e.g., Madden and Julian, 1971) was used to identify the frequency band containing the intraseasonal signal in the residual <W> time series. A distinct spectral peak with a period of 120 days is evident in the <W> power spectrum for each time series (Fig. 1). Since the assimilated moisture data are clearly sensitive to the GDAS, and the amplitude of the 90-150 day <W> signal is much smaller than the annual-cycle component of <W>, we need to verify the existence of this 90-120 day signal of <W> in the "true" hydrological field of the atmosphere. This verification should be pursued with the data containing no GDAS bias. We used two different data sets which satisfied this criteria: (a) the precipitable water observed by the Special Sensor Microwave/Imager (SSM/I) which is flown on the DMSP (Defense Meteorological Satellite Program) satellite and (b) the monthly moisture observations from radiosondes over the continental U.S. The SSM/I precipitable water data at our disposal only covers a four-year period (1988-91), but it is sufficient to demonstrate the existence of the 90-150 day signal in the global precipitable water. A major deficiency of the SSM/I precipitable water is that these data only cover oceanic areas. Thus, for an adequate comparison we reanalyzed the precipitable water obtained from the three GDAS data sets over the oceans. To aid in spatial comparison over land, the radiosonde observations of moisture data over the U.S. were used.

Shown in Fig. 2 are the SSM/I and GDAS residual 5-day-mean [W] (area-mean precipitable water over oceans) time series (dashed line) after removing the annual- and semiannual-cycle components. A pronounced spectral peak between periods of 90-150 days (not shown) stands out in all of the power spectra of these time series, similar to those of the <W> spectra shown in Fig. 1. The correlation coefficient between two time series offers a statistical indication as to the normalized coherency between temporal variations of the two series. If the $[\tilde{W}]$

(the 90-150 day filtered [W]) over the oceans contributes the major part of $\langle\tilde{W}\rangle$ (the 90-150 day filtered <W>) over the globe, we would expect that the correlation coefficient between the $[\tilde{W}]$ and $\langle\tilde{W}\rangle$ time series, σ_{OG}, should be close to unity. This speculation is confirmed by computation: $\sigma_{OG}(GLA)$, $\sigma_{OG}(NMC)$ and $\sigma_{OG}(ECMWF)$ are 84%, 74% and 92%, respectively. Now let us use the SSM/I precipitable water to verify the 90-150 day $[\tilde{W}]$ signal in the GDAS data. The correlation coefficients between $[\tilde{W}]$ time series from the SSM/I data set and $[\tilde{W}]$ from the GDAS data sets, $\sigma_{OS}(GLA)$, $\sigma_{OS}(NMC)$ and $\sigma_{OS}(ECMWF)$, are 70%, 7% and 38%, respectively. Clearly, *the* $[\tilde{W}](GLA)$ *time series most closely matches the 90-150 day signal in the SSM/I precipitable water time series.*

The simple statistical analyses presented above show non-uniform contributions from land and ocean areas to the 90-150 day $\langle\tilde{W}\rangle$ signal. In order to understand this differentiation better, and to explore the spatial agreement between $\tilde{W}(SSM/I)$ and $\tilde{W}$ from the GDAS data sets, composite charts of $\tilde{W}$ at the *maximum* and *minimum* phases of the $[\tilde{W}]$ time series (i.e., for which $|[\tilde{W}]| \geq 0.8$ standard deviations) were constructed. Because the spatial structures of the $\tilde{W}$ composite charts during these two phases are essentially *opposite* in sign but equal in magnitude, only the composite $\tilde{W}$ charts for the $[\tilde{W}]$ maximum phase are shown in Fig. 3 to avoid redundancy. For $\tilde{W}(SSM/I)$, the major contribution is from *three* regions north of 15°S: the ITCZ from the East-African coast to New Guinea, the Pacific ITCZ and the Pacific storm track. *The GLA composite most closely resembles the* $\tilde{W}(SSM/I)$ *chart.* This explains why $\sigma_{OS}(GLA)$ (=70%) is highest among the three GDAS data sets. The contrast between composite charts of $\tilde{W}(NMC)$ and $\tilde{W}(ECMWF)$ reveals that the major $\tilde{W}$ content of the former GDAS data resides over land and that of the latter GDAS data primarily over oceans. This contrast makes clear why $\sigma_{OG}(NMC)$ is smaller and $\sigma_{OG}(ECMWF)$ is larger.

Because the radiosonde data collected over the continental U.S. is relatively dense and of high quality, we used this data as a verification of the 90-150 day $\tilde{W}$ signal over land. The continental U.S. monthly mixing ratios from an upper air archive at the National Center for Atmospheric Research were gridded (approximately 200 x 200 km) with a simple Cressman-type objective analysis scheme (1959). After removing the annual- and semiannual-cycle component from the gridded mixing ratios averaged over the domain (30°-50°N, 70°-125°W), a pronounced spectral peak (not shown) is evident in the frequency band from 3-5 months (i.e., 90-150 days). Using the $\{\tilde{W}\}$ (area-mean $\tilde{W}$ over the U. S. continent time series (not shown) as an index, maximum and minimum phases (i.e., where $|\{\tilde{W}\}| \geq 0.8$ standard deviation) are selected separately for composite. Composite charts of these two $\{\tilde{W}\}$ phases (not shown) are essentially *opposite* in sign but similar in magnitude. A major positive center of $\{\tilde{W}\}(station)$ is located over the southeastern U.S. Contrasting the $\tilde{W}$ distributions of the three GDAS data sets over the continental U.S., *the spatial structure of* $\tilde{W}(GLA)$ *most closely resembles that of* $\tilde{W}(station)$. Based upon the spatial structure of $\tilde{W}$ composite charts during maximum $\{\tilde{W}\}$ phases, the 3-5 month (90-150 day) signal of the US precipitable water is portrayed most accurately by the GLA GDAS data.

The finding of the 90-150 day signal in the global precipitable water is significant for two reasons:

(a) Water vapor is important not only to the radiative heat budget, but also to the transport

of latent energy which can be released in the form of diabatic heating. Thus, the 90-150 day intraseasonal signal of the global precipitable water may be closely linked to the short-term variability of the climate system.

(b) Since the assimilated moisture data are sensitive to the GDAS and the amplitude of this 90-150 day signal of the global precipitable water is much smaller than the amplitude of the annual-cycle component, the existence of this intraseasonal signal constitutes a useful means to test the sensitivity of the GDAS data to portray the intraseasonal variability in the atmospheric branch of the global hydrological cycle.

Acknowledgement

This study is supported by the NSF Grant ATM9416954 and the NASA grant NAG5-355. We would like to thank Dr. Siegfried D. Schubert for his comments on this study and to Mr. David Ladvina for preparation of the SSM/I data.

References

Chen, T.-C., M.-C. Yen, J. Pfaendtner and Y. C. Sud, Annual variation of the global precipitable water and its maintenance: Observation and climate simulation. *Tellus* 47A (in press), 1995a.

Chen, T.-C., J.-M. Chen and J. Pfaendtner, Low-Frequency variations in the atmospheric branch of the global hydrological cycle. *J. Climate*.**8**, 92-107, 1995b.

Cressman, G., An operational objective analysis system. *Mon. Wea. Rev.*, **87**, 367-374, 1959.

Kanamitsu, M., J. C. Alpert, K. A. Campana, P. M. Caplan, D. G. Deaven, M. Tredell, B. Katz, H.-L. Pan, J. Sela, and G. H. White, Recent changes implemented into the global forecast system at NMC. *Weather and Forecasting*, 6, 365-376, 1991.

Madden, R. A., and P. R. Julian, Description of a 40-50 day oscillation in the zonal wind in the tropical Pacific. *J. Atmos. Sci.*, **28**, 702-708, 1971.

Murakami, M., Large-scale aspects of deep convective activity over the GATE area. *Mon. Wea. Rev.*, **107**, 997-1013, 1979.

Salstein, D. A., R. D. Rosen, and J. P. Peixoto, Modes of variability in annual hemispheric water vapor and transport fields. *J. Atmos. Sci.*.**40**, 788-803, 1983.

Schubert, S. D., R. B. Rood, and J. Pfaendtner, An assimilated data set for earth science applications. *Bull. Amer. Met. Soc.*, 74, 2331-2342, 1993.

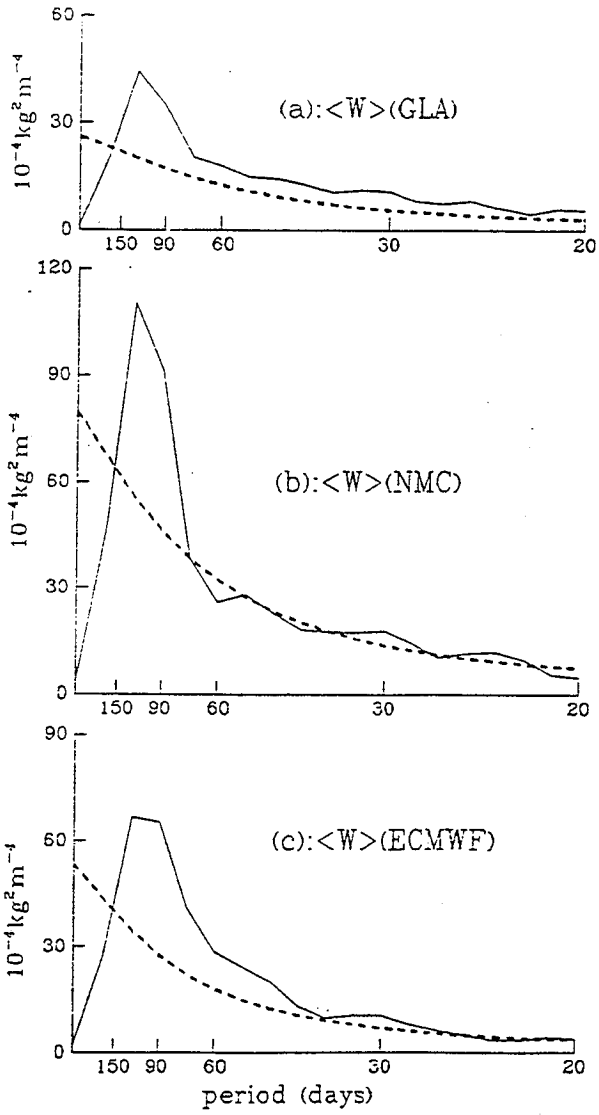

Fig. 1 Power spectra of the residual time series of the 5-day-mean globally-averaged precipitable water anomalies shown in Fig. 1. The dashed lines superimposed on the <W> power spectra represent a confidence level of 99%.

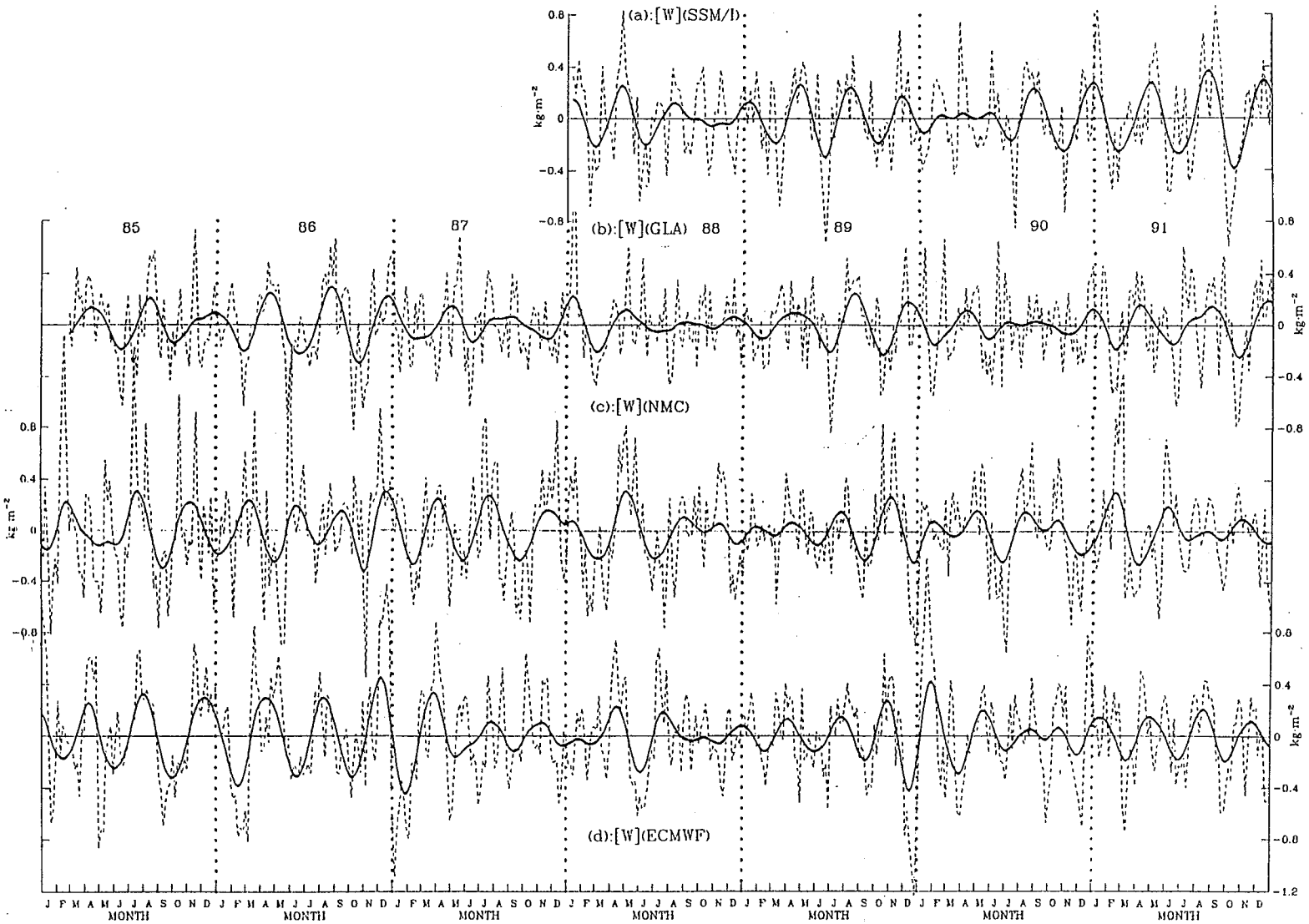

Fig. 2 Time series of the 5-day-mean precipitable water anomalies (dashed line) averaged over global oceans after removing the annual- and semiannual-cycle components; and the 90-150 day bandpass filtered precipitable water anomalies averaged over the global oceans (thick-solid line) with (a) the SSM/I data and GDAS data of (b) GLA, (c) NMC and (d) ECMWF.

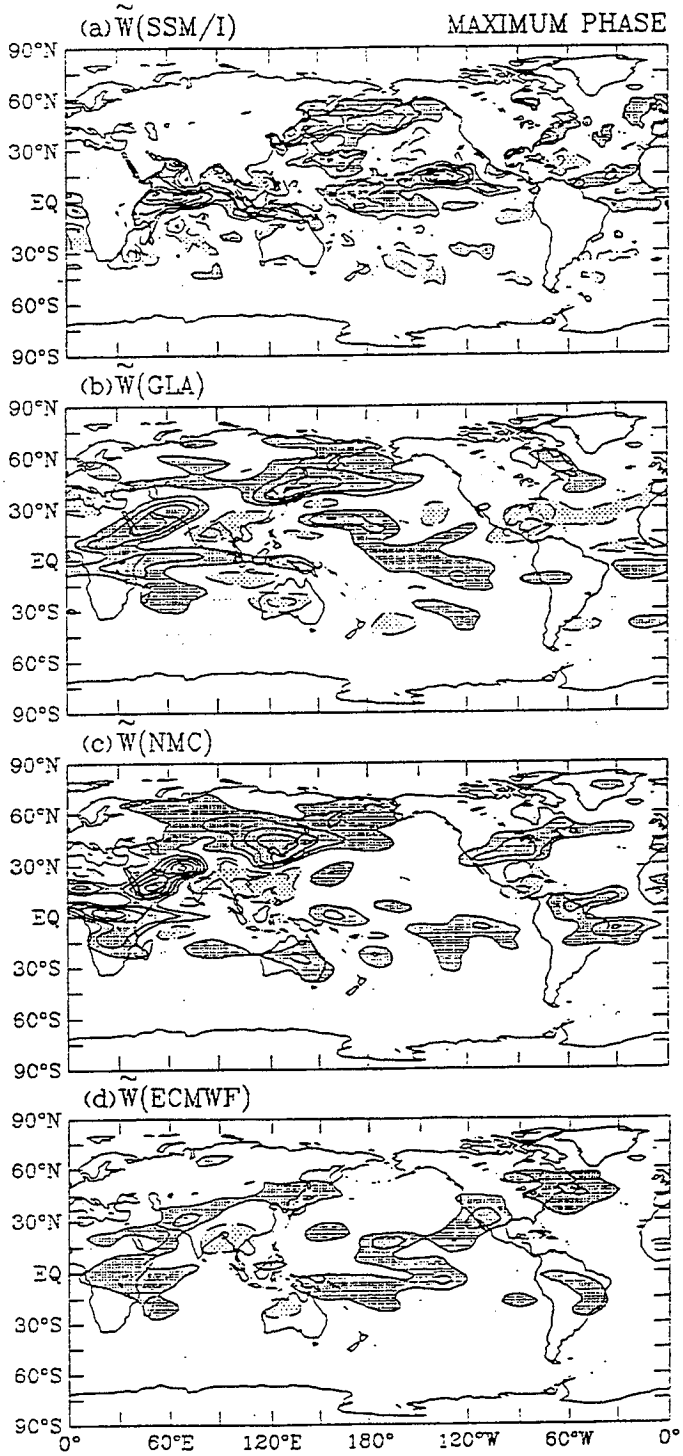

Fig. 3 Composite charts of the 90-150 day bandpass filtered precipitable water, $\tilde{W}$, for the maximum phases when $<\tilde{W}>$ is larger than 0.8 standard deviation of the $<\tilde{W}>$ time series with (a) SSM/I data, and the GDAS data of (b) GLA, (c) NMC and (d) ECMWF. The contour interval is 0.5 kg m^{-2}. Values of $\tilde{W}$ are heavily (lightly) stippled when $\tilde{W} \geq 0.5$ ($\leq$ - 0.5) kg m^{-2}.

Large-Scale Atmospheric Moisture Transport as Evaluated in the NMC/NCAR and the NASA/DAO Reanalyses

Kingtse C. Mo and R. Wayne Higgins
Climate Analysis Center
NMC/NWS/NOAA, Washington D. C. 20233

and

S. D. Schubert
DAO/Goddard Space Flight Center
NASA Greenbelt Md

Large-scale aspects of the atmospheric moisture transport and the overall moisture budget are studied using data from the NMC/NCAR reanalysis. Our objective is to critically evaluate the usefulness of the reanalysis products for studies of the global hydrologic cycle. The study period is from January 1985 to December 1989. Monthly mean water vapor transport, evaporation, and precipitation are compared to the NASA/DAO reanalysis for the same period and with satellite estimates and station observations.

Comparisons of the moisture flux fields form the NMC/NCAR and NASA/DAO reanalyses show general agreement in most respects, but there are regional differences. Discrepancies in tropical moisture transport are largely due to uncertainties in the divergent winds. The DAO reanalysis shows a weaker Hadley circulation and weaker cross equatorial flow.

Fig.1 plots the annual mean evaporation averaged over 5 years for NMC and DAO. The global patterns of evaporation from the two reanalyses are similar , but the NMC values are higher over the oceans and lower over the land masses. The comparison between the latent heat climatology from Oberhuber and forecasts from two centers indicates that the NMC values are close to the observations over oceans. In the eastern Pacific, the DAO has less total precipitable water and less rainfall. While the large-scale features of precipitation from the reanalyses agree with each other and with the GPI, there are regional differences. Both analyses show questionable features in the moisture flux divergence fields over North and South America which are for the most part terrain related.

Interannual variability related to the 1987-1989 ENSO cycle is well captured by both reanalyses. On intraseasonal time scales the NMC reanalysis has difficulty capturing the signal associated with the 30-60 day oscillation, but both reanalysis capture the dynamical signal in the moisture flux divergence.

An examination of the overall moisture budget for rectangular regions over North and South America in both reanalyses reveals large differences in the moisture flux divergence. The largest uncertainties are directly related to differences in the topographically bound low-level jets. Fig.2 shows the July mean vertically integrated meridional moisture flux averaged over 5 years for the NMC and DAO. Both analyses capture the pattern of the low level jet but the magnitude differs. The NMC LLJ is much stronger than that from the DAO.

Fig.1 (a) :Annual mean evaporation averaged over five years of the NMC 0-6 h forecasts. Contour interval 1 mm/day.(b) Same as (a), but from the DAO.

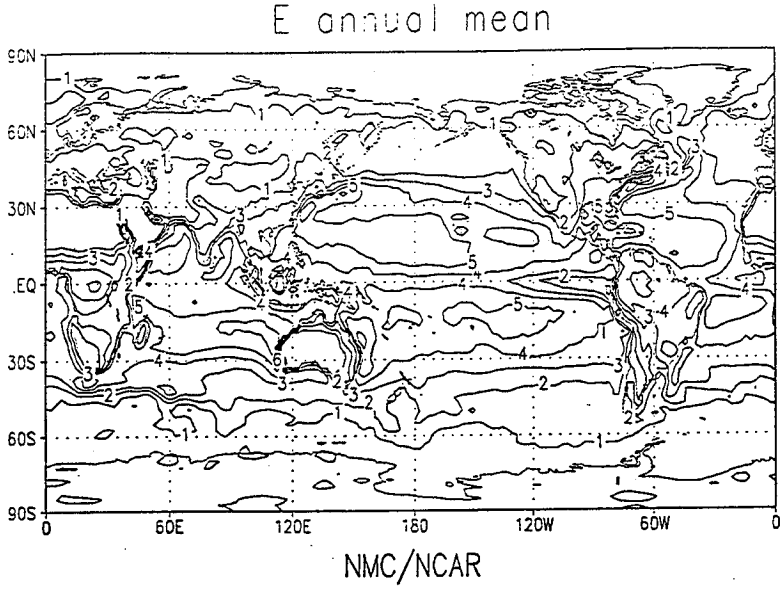

C-2

Fig.1 (b)

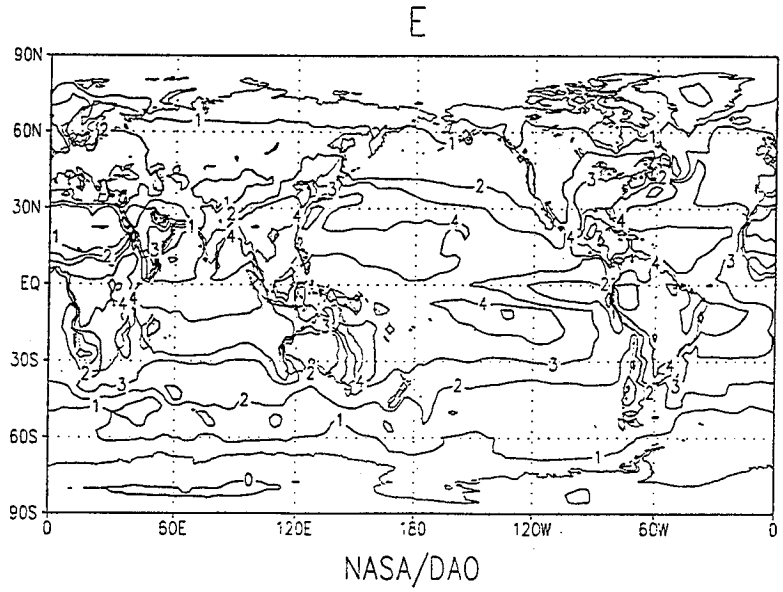

Fig.2: Vertically integrated meridional moisture transport averaged over five years of the (a) NMC analysis and (b) DAO analysis for July. Contour interval 400 g/(cm*s)

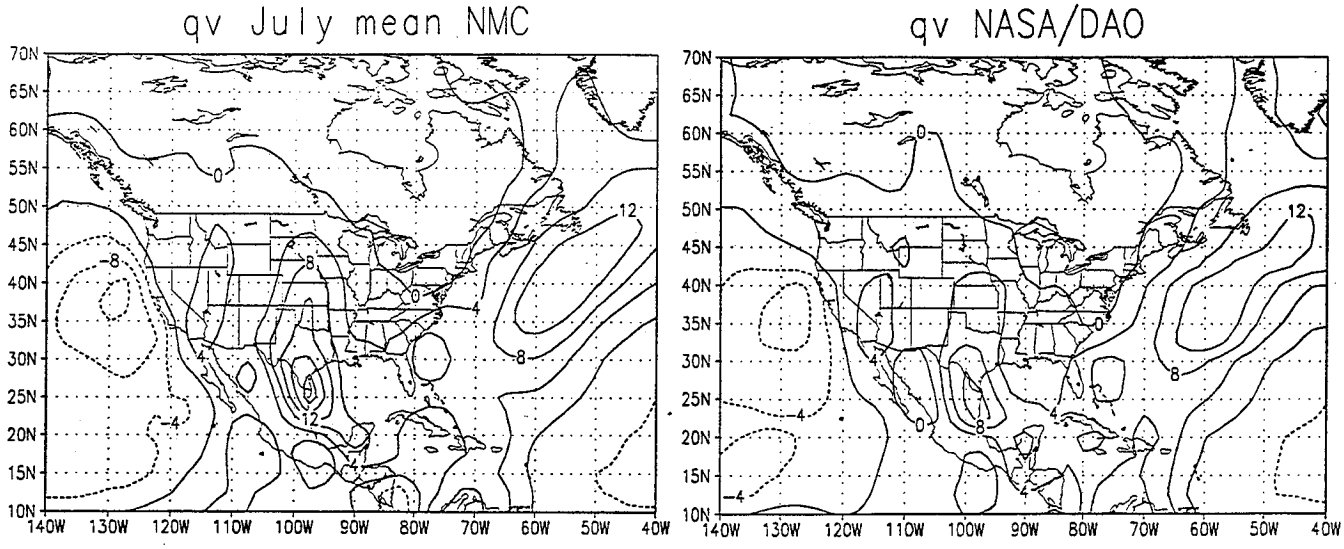

A DIAGNOSIS OF MID-LATITUDE BLOCKING ANTICYCLONES

Anthony R. Lupo

Department of Earth and Atmospheric Sciences
Purdue University
West Lafayette, Indiana, USA 47907 - 1397
e-mail: tlupo@meteor.atms.purdue.edu

1. INTRODUCTION

Many studies have shown the importance of large-scale forcing, such as long-wave baroclinic processes or topography, in the formation and maintenance of blocking anticyclones. Tung and Lindzen (1979) attempt to explain blocking as caused by the resonant amplification of planetary-scale waves, and McWilliams (1980) demonstrates that blocking anticyclones have characteristics consistent with those of solitary waves. Frederiksen (1982) considers the problem of blocking as instabilities which grow within three-dimensional flows. All of these studies show plausible mechanisms for block formation; however, they fail to address such questions as why blocks are observed to form and decay on time scales more consistent with synoptic scale phenomena, or why blocks are observed to fluctuate in intensity during their lifetime.

In this paper, the life-cycles of four individual blocking anticyclone events are examined. Using the Zwack-Okossi equation as the diagnostic framework, the horizontal (500 hPa) and vertical distribution of various atmospheric forcing mechanisms are studied in some detail. While this methodology bears some resemblance to other similar studies (e.g. Tsou and Smith, 1990; Tracton, 1990; Alberta et al., 1991), this is the only study that examines more than one case and examines each over its entire life-cycle. Additionally, these four blocking anticyclones were chosen to encompass a wide range of characteristics, such as, region and season of occurrence, duration, and intensity. These cases were also chosen so as to represent both high (mode 2) and low (mode 1) amplitude planetary-scale flow regimes.

2. DATA

The data used in this study were 2.0^{o} x 2.5^{o} lat/lon gridded analyses for 14 mandatory pressure levels at 6-h intervals, and were provided by NASA/Goddard Laboratory for Atmospheres (see Schubert et al., 1993). These fields included upper air parameters, which were then interpolated linear in ln[p] to 50 mb isobaric intervals, and a variety of surface parameters. The data are directly available from GLA via a computer account established with NASA. The data are stored using the UniTree central file manager and are easily accessible using file transfer protocol ("ftp"). The data files are easily read using C language, and a copy of the code can be provided by the author at the e-mail address shown above.

3. DIAGNOSTIC METHODOLOGY

The diagnosis was accomplished using the Zwack-Okossi (Z-O) equation (Zwack and Okossi, 1986) in its complete form (Lupo et al., 1992; Lupo and Smith, 1995b). The Z-O equation is a generalization of the Petterssen-Sutcliffe equation, and is a geostrophic vorticity tendency equation derived by coupling the vorticity tendency equation and the thermodynamic equations through the hydrostatic thickness tendency equation (Lupo et al., 1992). The result is an equation that allows the diagnosis of geostrophic vorticity tendency at any pressure level (in this study, 500 hPa) as forced by vertically-integrated dynamic and thermal forcing mechanisms. The vorticity tendencies were then relaxed to produce height tendencies, which were then filtered using a fourth-order, two-dimensional Shapiro (1970) filter to remove small scale noise without significantly degrading synoptic-scale and larger scale information. A more thorough expose of the Z-O methodology can be found contained within the references mentioned in this section.

4. SYNOPTIC DISCUSSION

The characteristics of the four blocking anticyclones chosen for this study are shown below in Table 1 and Figure 1. These blocking anticyclones were chosen from the set of all blocking anticyclones that occurred within a three-year period between the dates of 01 July 1985 and 30 June 1988. The characteristics of this set of blocking events are examined in more detail in Lupo and Smith (1995a).

The characteristics of the four events shown here are derived using the methodologies and criterion described in that study, with the exception of flow regime which used the methodology described by Hansen (1986). The life-cycle of an individual event (Case 1) is described in detail by Lupo and Smith (1995b).

Table 1. Some characteristics of the four blocking events chosen for this study.

Case	*Onset*	*End*	*Region*	*Season*	*Mode*
1	*30 Oct 85*	*5 Nov 85*	*ATL*	*Fall*	*1*
2	*13 Nov 85*	*27 Nov 85*	*ATL*	*Fall*	*2*
3	*19 Nov 85*	*27 Nov 85*	*PAC*	*Fall*	*2*
4	*15 Jul 85*	*20 Jul 85*	*ATL*	*Summer*	*2*

5. DISCUSSION

The development period of each case was examined using the Tsou and Smith (1990) block formation mechanism as a guide. All four cases were preceded by a developing surface cyclone and amplifying short wave ridge embedded within a large-scale trough and upstream from a quasi-stationary large-scale ridge. Each surface cyclone developed due to baroclinic instability, and a jet streak either developed or amplified on the western (eastern) flank of the large-scale ridge. The developing jet streak in each case changed from possessing cyclonic curvature to anticyclonic curvature. The strengthened anticyclonic vorticity advection (AVA) field then acted as the primary block formation mechanism in all four cases. Adiabatic warming due to lower tropospheric subsidence and vorticity tilting also contributed to the development of case 1. In the remaining cases, temperature advection was as important as adiabatic warming for development.

During the maintenance period of case 1, all atmospheric forcing processes, as well as the Z-O height tendencies, were weak. The same was true for the first half of the maintenance period of case 4. However, for the second half of this case, and for cases 2 and 3, the atmospheric forcing and Z-O height tendencies were not weak. During this time, these three cases interacted with successive surface cyclones in a similar fashion to that described in the development period. It was also noted that case 1 tended to have a single, lower tropospheric vertical motion maximum throughout its life cycle, while the other cases tended to have a double downward motion maximum (around 300 hPa and 850 hPa). The double maximum noted for the mode 2 cases coincided with stronger upper tropospheric cold air advection fields in the vicinity of the block center. It was also noted that, in general, the forcing associated with cold season and mode 2 blocking events tended to be stronger than that of warm season and mode 1 blocking events.

During the decay period of cases 1 and 4, the

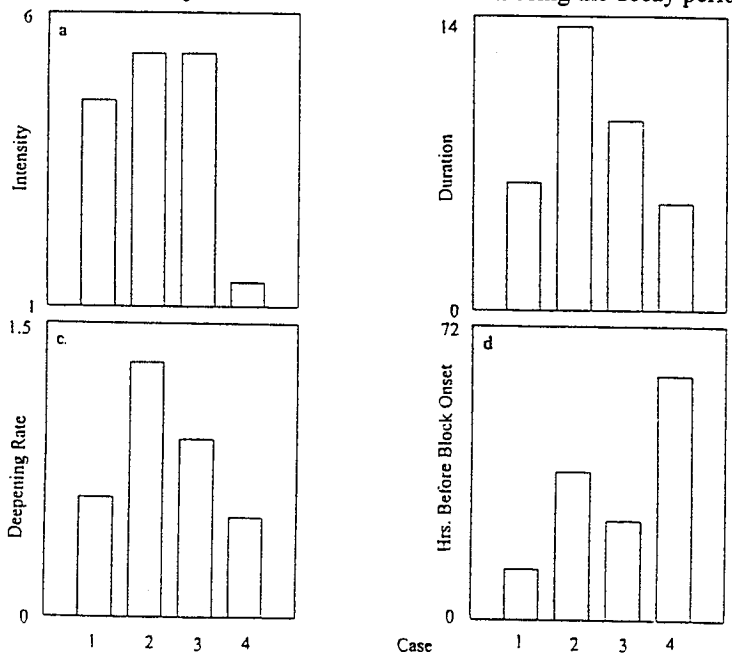

Figure 1. a) Block Intensity (as defined in Lupo and Smith 1995a), b) duration of each event (days), c) deepening rate of each precursor cyclone (Bergerons), and d) hours before block onset the 24-h period of most rapid cyclogenesis commenced.

maximum height rise regions were located south-southeast of the block center. For case 1, the block center and western flank of the block were located in a region of height falls associated with an advancing upper air trough. For case 4, the atmospheric forcing became weak and the total forcing field was less coherent than for case 1. In each case, forcing mechanisms contributing to height rises became weak. The dominant mechanism forcing height falls in both cases was temperature (warm air) advection.

6. SUMMARY AND CONCLUSIONS

The entire life-cycle of four blocking anticyclones having varied characteristics have been examined over their entire life-cycle using the Z-O equation as the diagnostic framework and the Tsou and Smith (1990) block formation model as a guide. This paper, like many others, demonstrates the importance of mid-latitude transients in block formation and maintenance.

In this diagnosis, it was found that AVA was the largest and most consistent contributor to block formation and maintenance. Temperature advection was a more consistent contributor to block formation and maintenance during high amplitude large-scale flow regimes. Adiabatic warming and vorticity tilting also contributed consistently to 500 hPa height rises. During the maintenance period of case 1, the forcing processes represented by each term in the Z-O equation tended to be weak. Decay occurred when the forcing processes contributing to height falls overcame those contributing to height rises. In these two cases, upper tropospheric warm air advection was the most prominent mechanism contributing to height falls.

Blocking events in mode 2 flow regimes exhibited a double maximum in downward motion compared to a single maximum found in the mode 1 event. This difference is at least partially attributable to the stronger upper tropospheric cold air advection fields associated with the former events. Finally, the atmospheric forcing tended to be stronger in cold-season blocking events and in high amplitude large-scale flow regimes.

7. REFERENCES

Alberta, T.L., Colucci, S.J., and Davenport, J.C., 1991. Rapid 500 mb cyclogenesis and anti-cyclogenesis. *Mon. Wea. Rev. 119*, 1186 - 1204.

Frederiksen, J.S., 1982. A unified 3-D instability theory of the onset of blocking and cyclogenesis. *Mon. Wea. Rev. 110*, 969 - 982.

Hansen, A.R., 1986. Observational characteristics of atmospheric planetary waves with bimodal amplitude distributions. *Adv. Geophys. 29,* 101 - 134.

Lupo, A.R., Smith, P.J., and Zwack, P., 1992. A diagnosis of the explosive development of two extratropical cyclones. *Mon. Wea. Rev. 120, 1490 - 1523.*

_____, and _____, 1995a. Climatological features of blocking anticyclones in the Northern Hemisphere. *Tellus 47A no. 4 (Aug. issue), in press.*

_____, and _____, 1995b. Planetary and synoptic-scale interactions during the life cycle of a mid-latitude blocking anticyclone over the North Atlantic. *Tellus Special Issue: The life cycles of extratropical cyclones symposium, in press.*

McWilliams, J.C., 1980. An application of equivalent modons to atmospheric blocking. *Dyn. Atmos. Oc. 5*, 43 - 66.

Schubert, S.D., Rood, R.D., and Pfaentner, J., 1993. An assimilated dataset for Earth science applications. *Bull. Amer. Met. Soc. 74*, 2331 - 2342.

Shapiro, R., 1970. Smoothing, filtering, and boundary effects. *Rev. Geophys., 8*, 359 - 387.

Tracton, M.S., 1990. Predictability and its relationship to scale interaction processes in blocking. *Mon. Wea. Rev. 118,* 1666 - 1695.

Tsou, C.-H., and Smith, P.J., 1990. The role of synoptic/planetary-scale interactions during the development of a blocking anticyclone. *Tellus 42 A*, 174 - 193.

Tung, K.K., and Lindzen, R.S., 1979. A theory of the stationary long waves, part I: A simple theory of blocking. *Mon. Wea. Rev. 107*, 714 - 734.

Zwack, P. and Okossi, B., 1986. A new method for solving the quasi-geostrophic omega equation by incorporating surface pressure tendency data. *Mon. Wea. Rev. 114*, 655 - 666.

Interannual and Subseasonal Variations of the Summer Monsoon During the ENSO Cycle

Chung-Kyu Park and Siegfried D. Schubert
Data Assimilation Office Code 910.3
Goddard Space Flight Center/NASA
Greenbelt, MD 20771

The prediction of monsoon rainfall is a challenging task in the modeling community because of the complexities associated with the thermal and mechanical effects of high mountain terrain and the land/sea contrast interacting with the seasonal cycle. While the monsoon evolution is largely phase-locked with the seasonal cycle, the interannual variations of the intensity and arrival of the monsoon are yet to be understood. The Data Assimilation Office (DAO) in the Goddard Space Flight Center/NASA has recently produced a multi-year global analysis employing a fixed assimilation system. The Goddard Earth Observing System (GEOS) analysis dataset is used to study the contrasting dynamical and thermodynamical characteristics of the Indian summer monsoon and the possible connection between the El Nino-Southern Oscillation (ENSO) and the abnormal drought/flood conditions in the Asian summer monsoon region during the 87/88 ENSO cycle.

A comparison between the GEOS reanlyses and the ECMWF operational analyses indicates that they have almost identical zonal mean u-wind variations in the subtropics and middle latitudes, while some differences are found in the tropics. In the meantime, these analyses clearly show systematic differences in the zonal mean v-wind which represents the intensity of the Hadely circulation. The GEOS analyses show consistently weaker northern hemispheric winter Hadely cell and stronger southern hemispheric winter cell, which seem to reflect strong model characteristics in the tropics. The zonal mean v-wind anomalies from their own seasonal cycles indicate that the interannual variability such as the 1987/88 contrast related to the ENSO is not obvious in the operational analyses due to the dominant variability introduced by frequent model changes. While the operational analysis data have been widely used for climate studies, the most difficult problem we often encounter is how to deal with the variability introduced by continuous model changes which is inseparable from climate signals. The model changes in the operational analyses appear to significantly modify the variability in the interannual time-scales.

A comparison between GEOS precipitation and NOAA OLR in Figure 1 indicates a fair agreement in the Indian monsoon rainfall variations, including a dramatic contrast between

87 drought and 88 flood in this region. However, the GEOS analyses seem to clearly overestimate the Indian monsoon rainfall during the 1989 summer comparing to the NOAA OLR. It is under investigation what causes the spurious rainfall over the Indian monsoon region during that period.

The years 1986/87 were characterized by a major El Nino event; this was followed by a strong La Nina in 1988 characterized by cold SST anomalies in the tropical eastern Pacific. The 88-87 SST difference for MJJA clearly shows a dramatic contrast between these two years with prominent anomnalies both in the tropics and subtropics. An apparent coupling between ENSO and the monsoons manifested itself during these years by a drought in 1987 and flood in 1988 over the Indian summer monsoon region. It is interesting to note, however, that there was no significant SST difference over the Indian Ocean, while the precipitation shows the most pronounced difference in the Indian summer monsoon region. Figure 2 shows the 88-87 difference of the zonal mean height and the zonal mean u-wind averaged during May-August. The enhanced easterlies at around $20°N$, associated with the zonal mean heating anomalies, appear to have a significant impact in the Indian summer monsoon region. The results indicate the redistribution of zonal mean heating associated with ocean surface conditions during the ENSO cycle has a significant impact on the global and monsoon circulations and that the ENSO/monsoon coupling is primarily through the redistribution of zonal men differential heating in the entire tropics rather than the local boundary forcing over the Indian monsoon region.

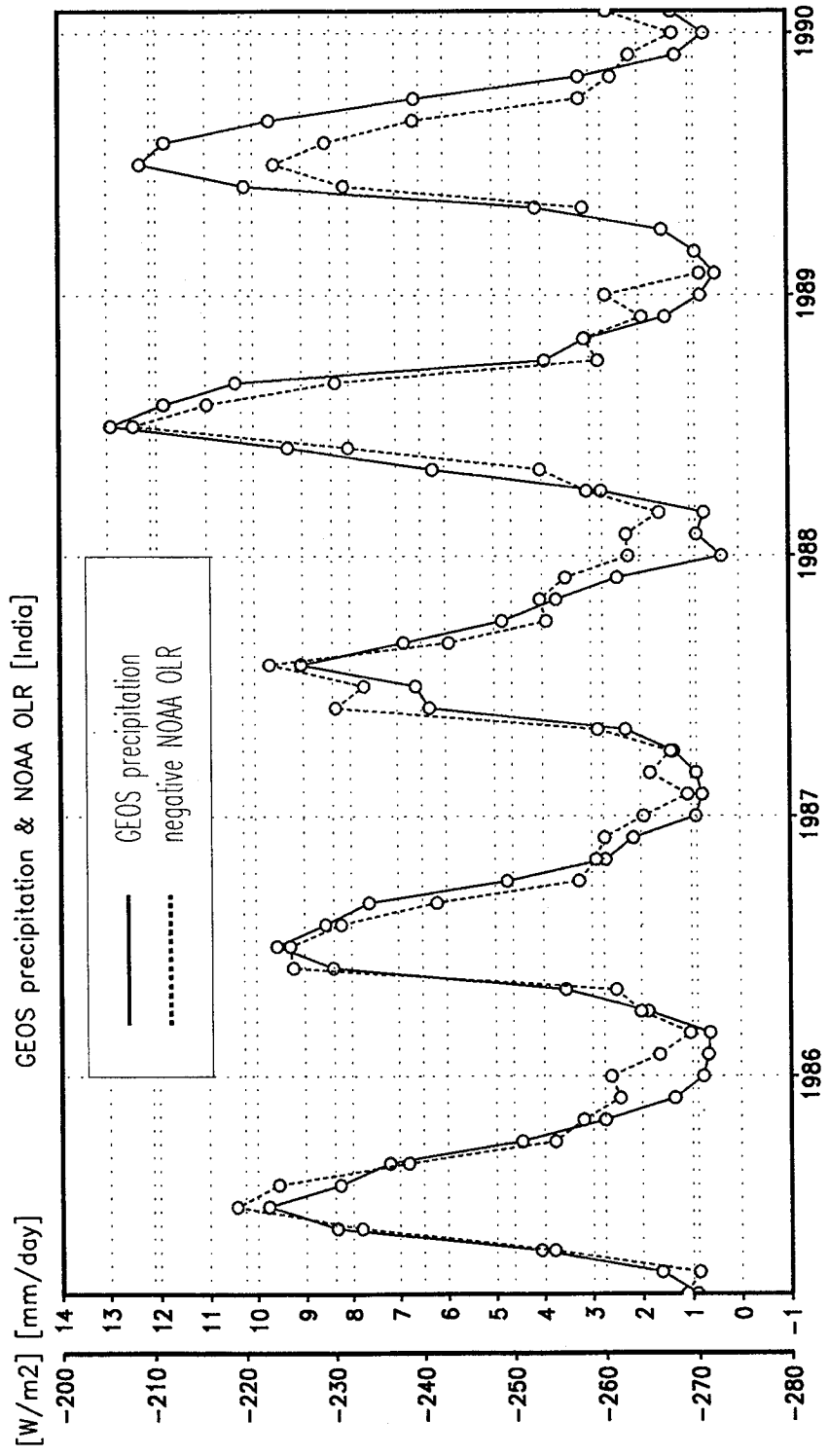

Figure 1: Time-series of the GEOS precipitation and the negative NOAA OLR averaged over the Indian summer monsoon region [$10°N$-$30°N$,$60°E$-$100°E$].

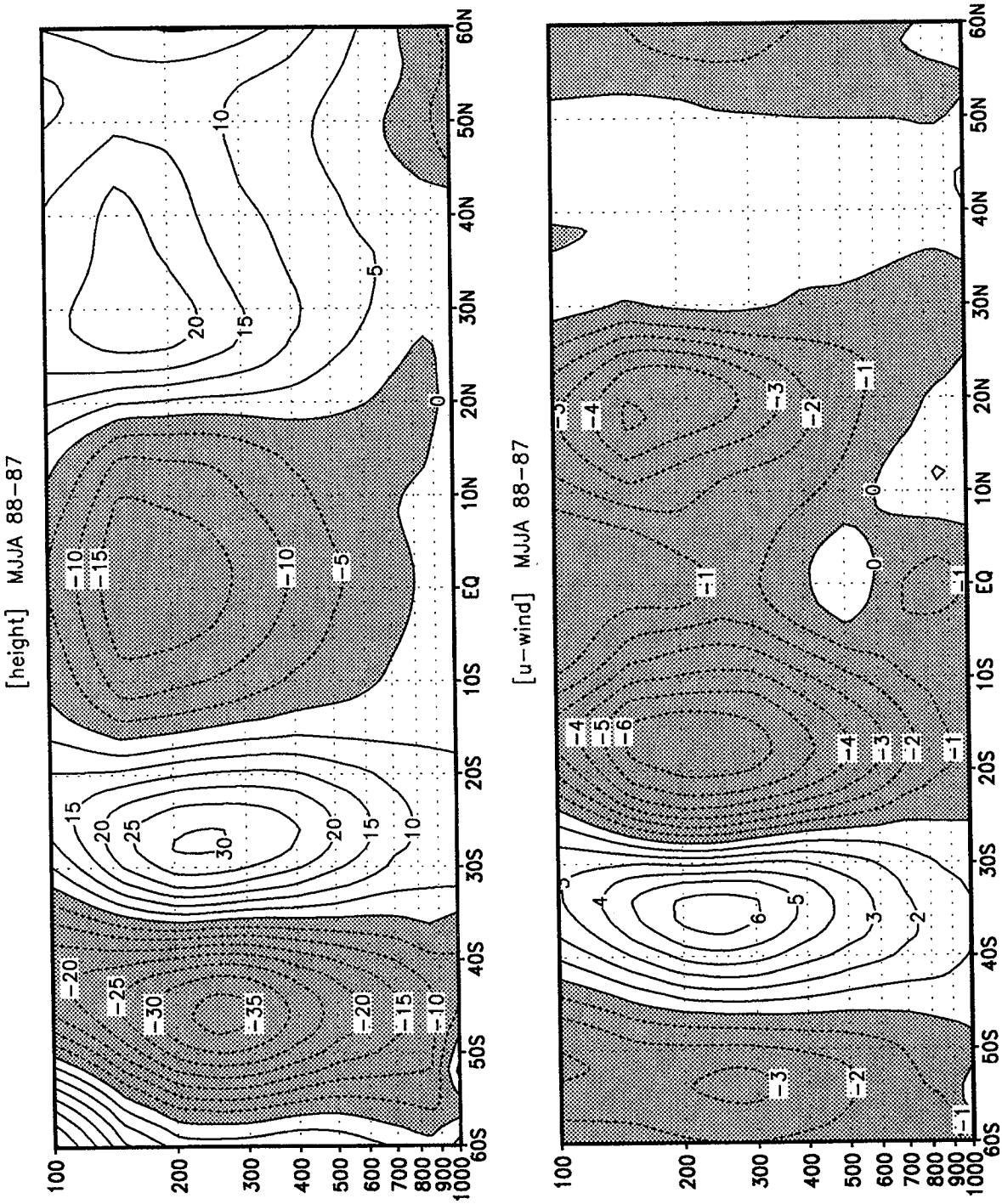

Figure 2: The latitude-pressure sections of (a) the zonal mean height anomalies and (b) the zonal mean u-wind anomalies for May-June-July-August mean difference between 1987 and 1988 [88-87]. Contour intervals are 5 m for the height anomalies and 1 m/sec for the u-wind anomalies. Negative regions are shaded.

Characteristics of the Simulated and Assimilated Great Plains Low-Level Jet

H. M. Helfand, S. D. Schubert and C.-Y. Wu
Data Assimilation Office, Laboratory for Atmospheres
NASA/Goddard Space Flight Center, Greenbelt, Maryland

The value of a skillful atmospheric data assimilation system is that it can use the atmospheric data that is available to infer additional information for which there is no data directly available. Determination of the vertical structure of the atmospheric boundary layer (ABL) is a case in point. Conventional atmospheric soundings are generally made available at mandatory levels (1000 mb, 850 mb, 700 mb, etc.), missing virtually the entire structure of the ABL. There is little evidence, in these conventional data sets, of the nocturnal low-level jet, so prevalent over the Great Plains of the United States and over other regions of the globe.

Helfand and Schubert (1995) have recently demonstrated the success of the GEOS-1 GCM, and its parameterization for the physics of the ABL, in realistically simulating the Great Plains low-level jet (GPLLJ) and its climatology. This suggests that the GEOS-1 Data Assimilation System, which uses the same physical parameterization of the ABL, will also be able to accurately reproduce the structure of the GPLLJ, even in the absence of direct data for the jet.

Comparisons have been made between a simulation and an assimilation for May and June of 1989. There is a striking similarity between the simulated and assimilated mean low-level flow pattern over the North American continent and its diurnal variability (not shown), suggesting that the assimilated low-level flow is largely driven by the physics of the ABL parameterization. The nocturnal LLJ is equally visible in simulated and assimilated profiles of mean wind speed over Ft. Worth, Texas (Fig. 1). Above the ABL, where the assimilated winds are driven by data, they are significantly weaker than the simulated winds. In the ABL region however, where there is no data to drive the assimilation, the assimilated winds are close to the simulated winds and only slightly weaker.

Fig. 2 uses mandatory and significant-level wind data to validate an assimilated time series of LLJ structure over Ft. Worth for July, 1993. (The significant-level data are not included in the assimilation process.) There is excellent agreement between the assimilated and observed series of LLJ structure, showing that, indeed, the information contributed to the assimilation system by the ABL parameterization is realistic and useful.

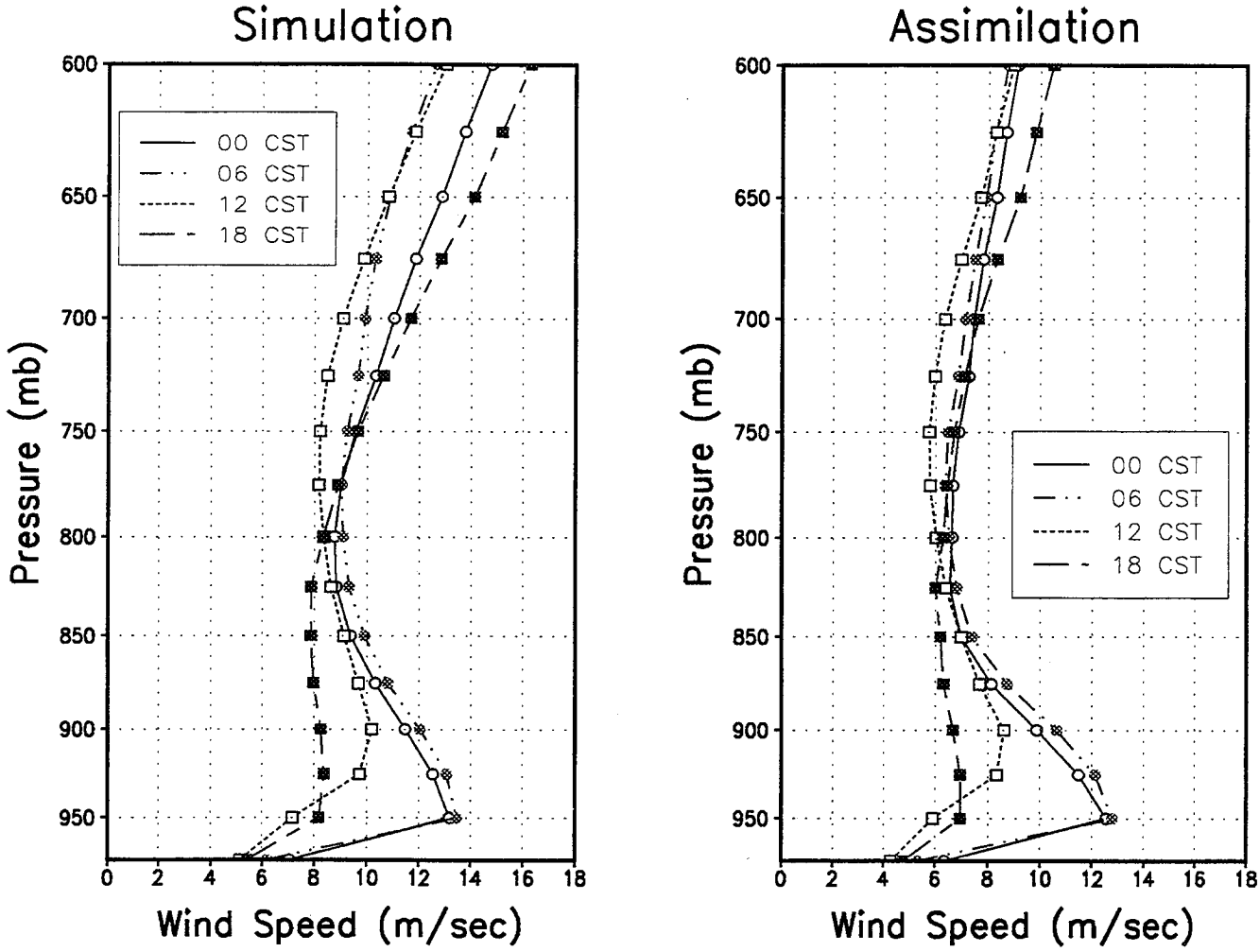

Figure 1: The mean wind speed (May 1-July 1,1989) at 97.5W and 32N from a simulation with the GEOS-1 GCM (lower panel), and from the GEOS-1 assimilation (upper panel).

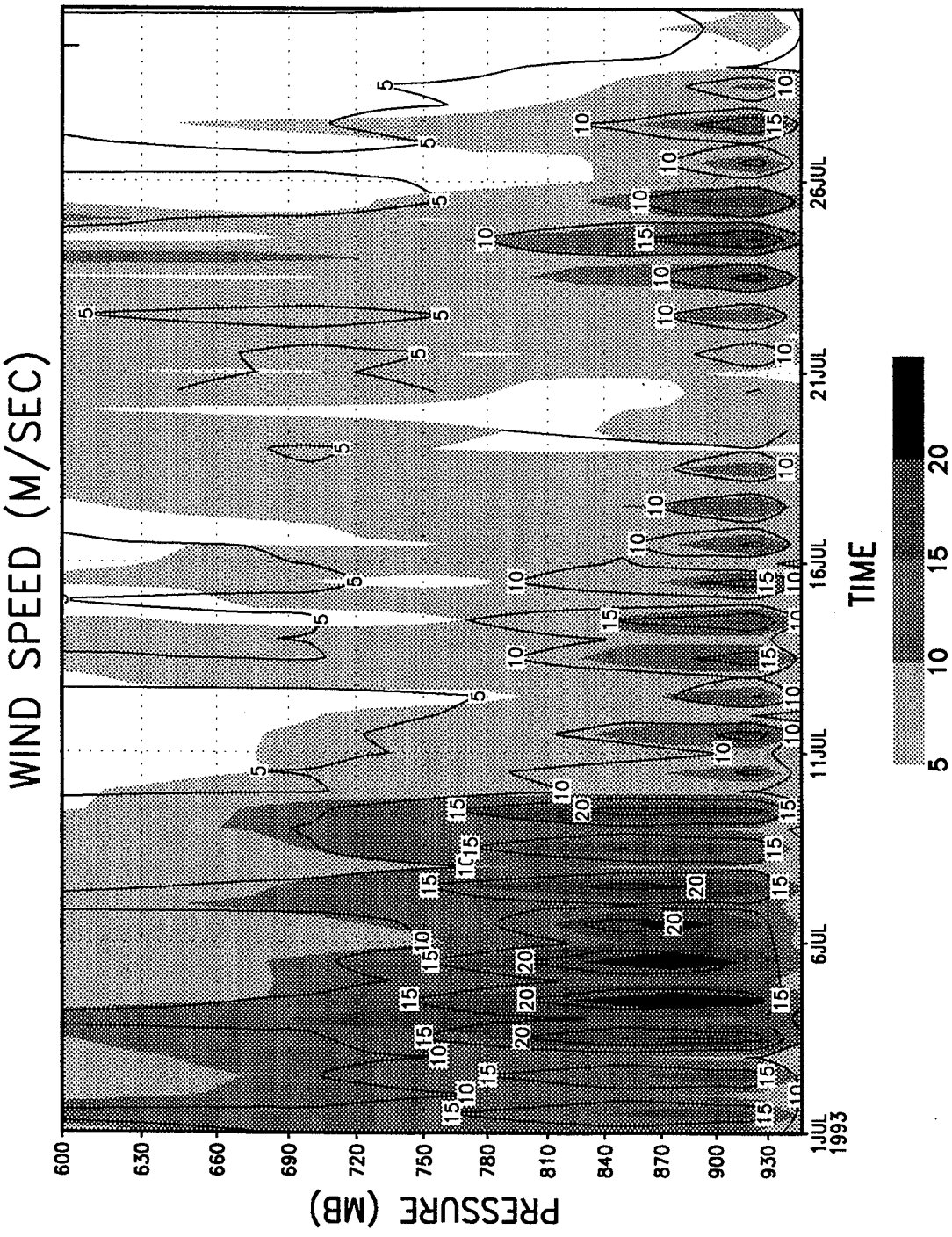

Figure 2: Time series of the wind speed for July 1993 at Ft. Worth, Texas. Shading corresponds to the assimilation. The contours are the verifying station values which include significant level winds and the 925mb mandatory pressure level (these were not assimilated).

The Moisture Budget of the Central United States in Spring as Evaluated in the NMC/NCAR and the NASA/DAO Reanalyses

R. W. Higgins[1], K. C. Mo[1] and S. D. Schubert[2]

1. Climate Analysis Center, NOAA/NWS/NMC
2. NASA/Goddard Laboratory for Atmospheres

1. Introduction

The moisture budget of the Central United States during May was examined using multi-year (1985-1989) gridded datasets produced by the NASA/DAO and the NMC/NCAR. Comparisons to each other and to station observations were used to evaluate their limitations for studies of the atmospheric component of the regional hydrologic cycle. Attempts were made to reconcile differences in terms of disparities in the analysis systems. Results from this study are presented in detail in Higgins et al. (1995).

2. Results

Both reanalyses overestimate daily mean precipitation rates by a factor of almost two over the southeastern United States (Fig. 1a-1c). Over the Great Plains the reanalyses generally capture observed synoptic-scale precipitation events but the variability of the daily mean precipitation (May 1985-89) is underestimated, particularly in the DAO (Fig. 1d-1f). Over the eastern half of the United States both reanalyses underestimate the number of days without precipitation and overestimate the number of days with precipitation, especially at slower rainfall rates (Fig. 2). The DAO also has trouble capturing observed fast precipitation rates. The partitioning of monthly mean total precipitation in terms of rainfall rate is handled quite well in the NMC reanalysis. The amplitude of the diurnal cycle of rainfall exceeds observations in both reanalyses with precipitation occurring mainly during the afternoon and with little evidence of the nocturnal maximum over the Great Plains (Fig. 3).

Examination of the fluxes of moisture (May 1985-89) onto the continent shows that the strongest influx occurs at low levels over the South Central U. S. and Northeastern Mexico in both reanalyses. This is also where the largest uncertainties in the moisture transport are found. Stronger inflow along the Gulf Coast in the NMC reanalysis is consistent with the ability of the NMC reanalysis to produce more extreme rainfall rates than the DAO in this region. While the net precipitation is similar in both budgets, the moisture source due to an excess of evaporation over precipitation is more than a factor of 7 larger in the DAO due to overestimates of net evaporation. There is a strong diurnal cycle in the moisture transport with the largest and most extensive anomalies being those associated with the nocturnal inland flow of the Great Plains low level jet (LLJ) over the south central United States. Composites of the nocturnal fluxes of moisture during LLJ events reveal a horizontally-confined region of strong excess southerly transport to the east of the Rocky Mountains sandwiched between well defined synoptic-scale cyclonic (anticyclonic) circulations to the northwest (southeast). Low level inflow from the Gulf of Mexico increases by more than 50% over mean values in both reanalyses, though the excess inflow is more than 30% stronger in the NMC. On LLJ days both reanalyses also show excess low-level convergence and precipitation over the Great Plains. Composite patterns of nocturnal precipitation during LLJ events compare favorably to observations though amplitudes are underestimated.

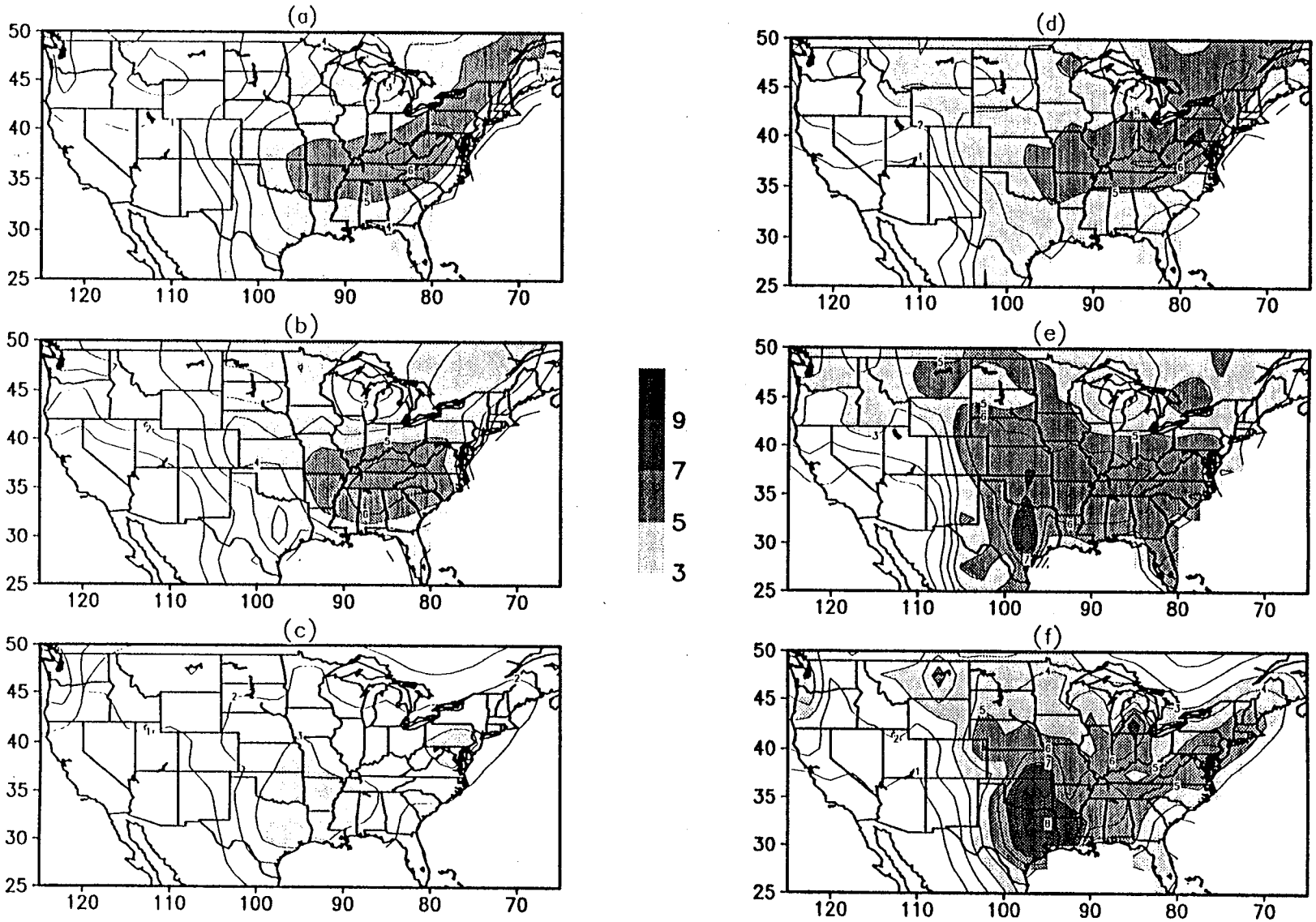

Figure 1. Daily mean precipitation rates (units: mm day^{-1}) for May 1985-89 over the United States in (a) the DAO reanalysis, (b) the NMC reanalysis and (c) the observations. Standard deviation of the daily mean precipitation rates (units: mm day^{-1}) within May 1985-89 over the United States in (d) the DAO reanalysis, (e) the NMC reanalysis and (f) the observations. In (a) - (f) the contour interval is 1 mm day^{-1} and rates greater than 3 mm day^{-1} are shaded.

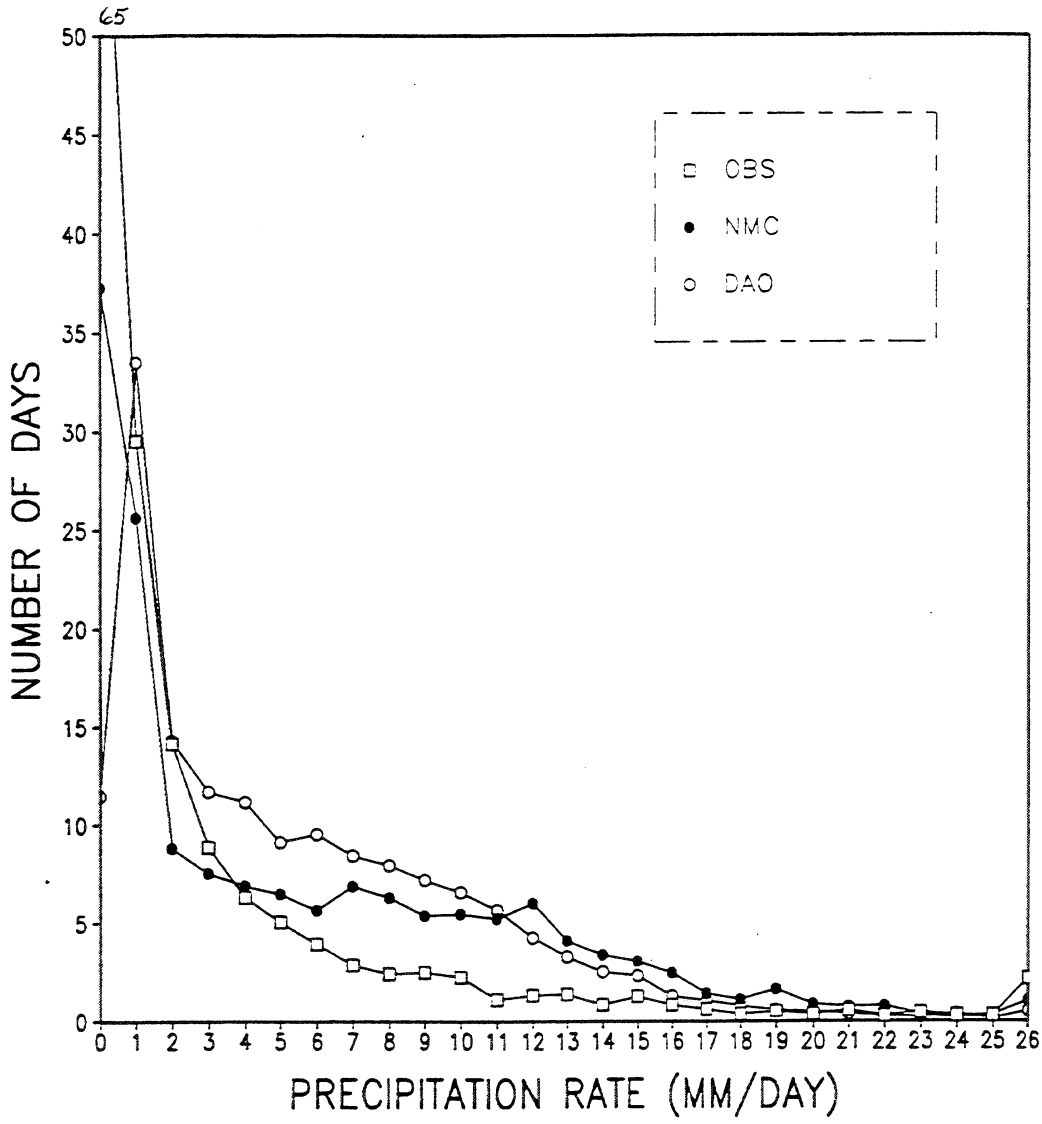

Figure 2. The average number of days with precipitation as a function of precipitation rate for a rectangular region over the southern Great Plains (100° W - 90° W, 30° N - 40° N) in the DAO reanalysis (open circles), the NMC reanalysis (closed circles) and the observations (open squares). A precipitation rate of zero includes all days without measurable precipitation. A precipitation rate of 1 mm day^{-1} indicates all rates greater than zero but less than or equal to 1 mm day^{-1}, etc. A precipitation rate of 26 mm day^{-1} includes all days with rates greater than 25 mm day^{-1}.

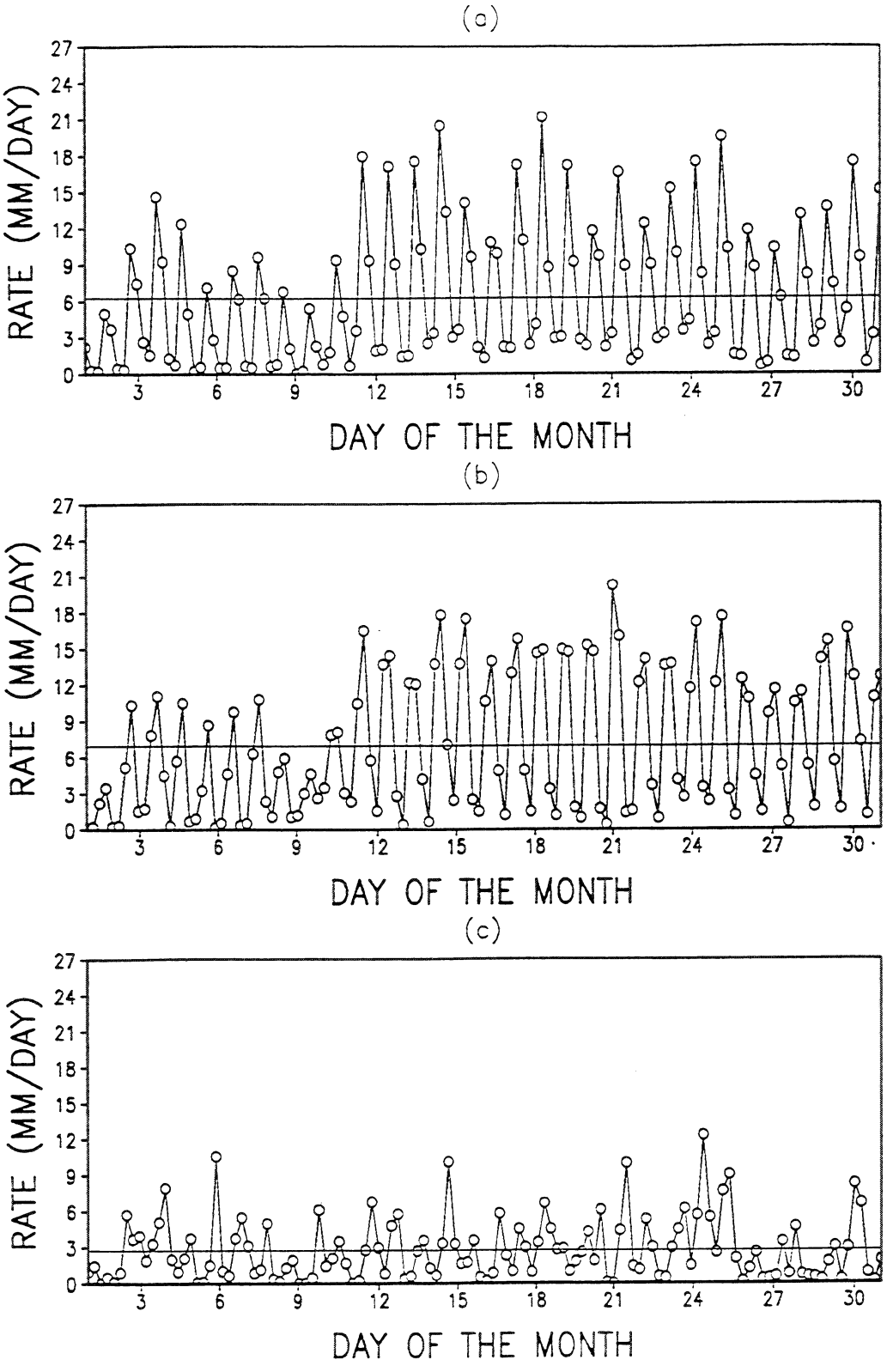

Figure. 3 The 6 h precipitation rates (units: mm day^{-1}) for May 1987 averaged over a rectangular region of the southern Great Plains (100° W - 90° W, 30° N - 40° N) in (a) the DAO reanalysis, (b) the NMC reanalysis and (c) the observations. Mean precipitation rates for May 1987 are indicated by a horizontal line on each panel.

SEASONAL AND INTERANNUAL VARIABILITY OF THE ATMOSPHERIC HYDROLOGIC CYCLE

Todd K. Schaack, Donald R. Johnson, Allen J. Lenzen

University of Wisconsin
Madison, Wisconsin

1. INTRODUCTION

An understanding of climate and climate change requires knowledge of the processes responsible for controlling the current climate. Atmospheric hydrologic processes assume a fundamental role in determining climate and climate variability. These processes regulate global and regional climate through surface evaporation, release of latent heat in moist convection and the attenuation of the radiative flux of energy by water vapor and clouds. The differential heating from these processes strongly interacts dynamically with the atmosphere's circulation at all scales. Within the past decade, the hydrologic cycle has become a central focus in the study of climate.

Diagnostics derived from 4-D data assimilation datasets have greatly enhanced our understanding of atmospheric circulation on global and regional scales. The primary objective of this research is to investigate the large scale atmospheric structure of hydrologic processes from assimilated data. Diagnostics derived from GEOS-1 data for January and July 1986-88 have been compared with observations and corresponding distributions diagnosed from ECMWF operational analyses. Similar comparisons have been made for August 1985 using assimilated data from the GEOS-1 system and the pilot version of the NMC climate reanalysis system. In data sparse regions, distributions of precipitation minus evaporation (P-E) and atmospheric heating are highly dependent on the assimilation model formulation and it is likely that the largest differences between assimilated datasets would appear through comparison of such fields. Although close agreement between estimates from different datasets does not guarantee accurate analysis, the level of agreement does provide a measure of the quality of a particular analysis.

The overall results indicate broad agreement for the spatial patterns of the vertically averaged heating, precipitable water and distributions of (P-E) diagnosed from GEOS-1 and ECMWF assimilated data for corresponding periods in 1986-88. Both datasets depict the salient features of the large scale circulation including the seasonal migration of the tropical regions of deep moist convection, the Northern Hemisphere wintertime extratropical storm tracks and the subtropical regions of evaporation and infrared cooling. Both datasets also capture the evolution of both the warm and cold phases of the ENSO cycle which occurred during 1986-88.

However, substantial differences occur between diagnostics from the assimilated dataset in several regions, particularly in the tropics where data are sparse and model formulation plays a critical role in determining the structure of the atmospheric component of the hydrologic cycle. The magnitude of these differences are similar in magnitude to the interannual variability of the large scale heating and (P-E) distributions for January and July 1986-88 diagnosed from either the ECMWF or GEOS-1 datasets and thus represent a substantial fraction of the estimates from either dataset.

Fig. 1 compares the area-averaged precipitation minus evaporation L(P-E) averaged over the tropical belt between 22.5 N and 22.5 S and the Northern Hemisphere and Southern Hemisphere extratropical regions poleward of these latitudes for January and July 1988 diagnosed from the GEOS-1 and ECMWF assimilated datasets. The results highlight the uncertainty involved in resolving the hydrologic cycle with the estimates from the two datasets sets having opposite signs over these regions. The magnitude of the differences between datasets suggest that only limited quantitative information with respect to climate variability can be determined. The reasons for such differences need to be resolved and similar diagnostics need to be performed with other climate reanalysis datasets in an effort to understand the capability of current datasets to discern climate change.

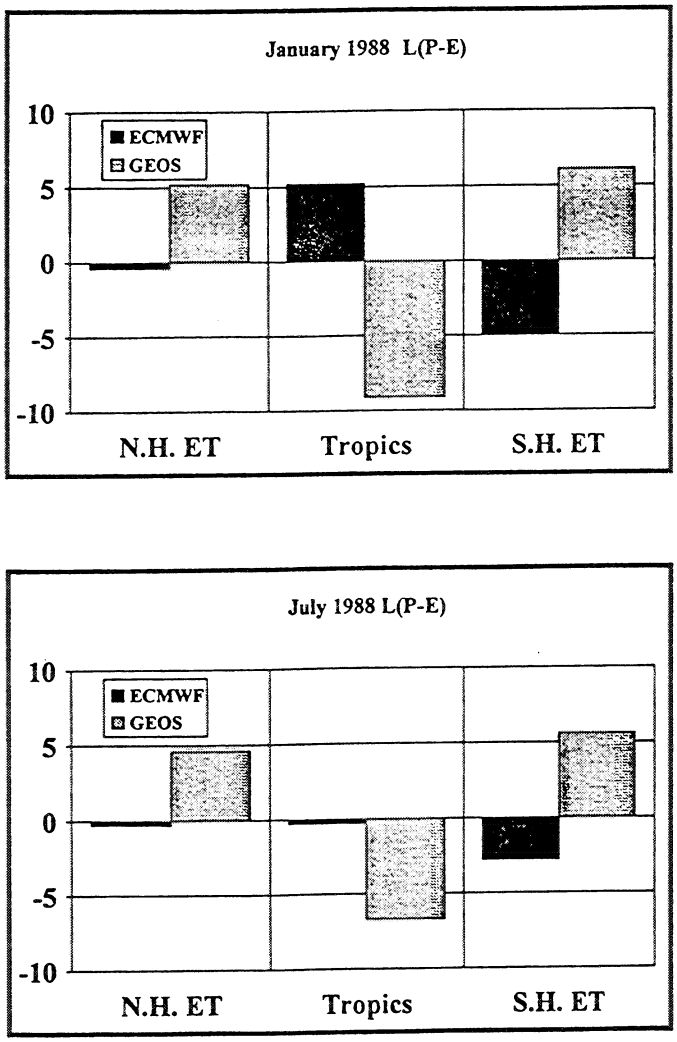

Fig. 1. Area-averaged precipition minus evaporation, L(P-E), averaged over the tropical belt between 22.5 N and 22.5 S and the Northern Hemisphere and Southern Hemisphere extratropical regions poleward of these latitudes for January and July 1988 diagnosed from the GEOS-1 and ECMWF assimilated datasets (W/m^2).

AN OBJECTIVE METHOD FOR ASSESSING SOURCES OF MODEL ERROR

Siegfried Schubert and Yehui Chang [1]
Data Assimilation Office
NASA/Goddard Laboratory for Atmospheres
Greenbelt, MD 20771

1. Introduction

Diagnostic analyses of model simulations and/or forecasts often provide little guidance for isolating model deficiencies since the analyzed errors are the end result of interactions between various scales and model components. Klinker and Sardeshmukh (1992) suggested a novel approach to isolating the local errors produced by the various parameterized terms. This involves examining the average of many one-time step model integrations and comparing the adiabatic and diabatic terms in the equations. For those quantities with little error in the analyzed fields, the systematic difference between the adiabatic and diabatic terms represents errors in the physical parameterizations. Their results for the ECMWF model showed considerable success in isolating possible problems in the momentum balance.

The results of data assimilation with GCMs provide a unique resource for understanding the sources of model error. During an assimilation, short term model forecasts are continually compared with observations and adjustments are made to keep the model forecast close to nature. We present here an application of a Restricted Statistical Correction (RSC) approach to inferring the sources of model error. This approach may be considered an extension of the Klinker and Sardeshmukh (1992) method in that it makes use of both the random and systematic components of the analysis increments (or more generally, short term forecast errors), and makes no *a priori* assumptions about the reliability of the terms in the equations. The general method is presented in Schubert and Chang (1995).

2. Results

This section employs RSC to assess the nature of the short term errors in the vertically-integrated moisture over the continental United States based on the GEOS-1 assimilation. The multi-year assimilation project is described in Schubert et al. (1993, 1995). The GEOS-1 data assimilation system (DAS) is described in Pfaendtner et. al. (1995). The assimilation covers the

[1]General Sciences Corporation, a subsidiary of Science Applications International Corporation

period March, 1985 - February, 1990. Results are presented for the spring season (March/April and May/June) during which both evaporation and precipitation contribute strongly to the moisture budget.

The vertically-integrated moisture equation in the GEOS-DAS may be written symbolically as

$$\frac{\partial Q}{\partial t} = dyn + precip + evap + filter + \Delta Q \equiv \sum_{r=1}^{4} \Phi_r + \Delta Q, \qquad (1)$$

where Q is the vertically-integrated specific humidity. The right hand side includes all the GCM forcing terms grouped into 1) the *dyn* term which is the convergence of the transport of Q, 2) *precip* which is (minus) the precipitation from convective and large-scale processes, 3) *evap* which is the evaportion, and 4) *filter* which includes both the Shapiro filter and filling (from below) due to the occurrence of negative moisture. The ΔQ are the vertically-integrated analysis increments in the specific humidity.

We consider linear transformations (B_r) of the GCM forcing terms (Φ_r) which produce a best (in a restricted least squares sense) estimate of the tendency. The systematic components of the vertically-integrated moisture equation over the United States are dominated by the time mean and diurnal cycle. Thus we consider the regression problem

$$\Delta Q' = \sum_{r=1}^{4} A_r \Phi_r' + \varepsilon', \qquad (2)$$

with constraints of the form

$$\overline{\Delta Q}^m = \sum_r A_r \overline{\Phi_r}^m, \qquad (3a)$$

and

$$\overline{\Delta Q}^d = \sum_r A_r \overline{\Phi_r}^d, \qquad (3b)$$

where $A_r = B_r - I$, and the primes denote deviations from the average diurnal cycle. Also, $\overline{x}^m \equiv \frac{1}{2}\left(\overline{x}^{\tau_1} + \overline{x}^{\tau_2}\right)$ and $\overline{x}^d \equiv \frac{1}{2}\left(\overline{x}^{\tau_1} - \overline{x}^{\tau_2}\right)$, where the τ_1 and τ_2 refer to two phases of the diurnal cycle separated by 12 hours. It should be noted that the incremental analysis update (IAU, Bloom et. al. 1991) approach was not designed to correct for model bias; the extent to which the bias is corrected depends on the frequency with which observations are available. Further information on the implementation of the incremental analysis update approach may be found in Pfaendtner et. al. (1995).

In general, the system (2) contains contains many more equations and coefficients than is feasible to estimate. Thus the application of this method must rely on *a priori* methods of reducing the number of degrees of freedom. Here this is be done by employing the eigenvectors of the covariance matrix of the analysis increments (Schubert and Chang 1995).

The following analysis will focus on the early spring period (March/April) and the systematic errors only. For comparison, selected results are also presented for May/June. Figure 1 shows the results of the restricted regression for the time mean fields. The quantities ($A_r \overline{\Phi_r}^m$) show how the mean error (analysis increment) is partioned among the various model forcing terms. The two top panels (1a-b) compare the original mean analysis increments to those reconstructed by the regression. These two fields should be identical except for smoothing associated the eigenvector truncation; the strong similarity between these two fields suggests that the 20 eigenvectors provide an adequate representation of the mean fields. Figs. 1c-f show that most of the error is associated with too much evaporation, especially over the central Great Plains (eastern slopes of the Rocky Mountains) and the southeast. The results also suggest that the GCM rains too much over the southeastern U.S., and rains too little to the north. Very little is contributed by the convergence and filter terms.

The identical analysis was carried out for May/June. The time mean corrections during these months (Fig. 2) are such that water is being removed throughout the west and northeast, while the analysis is adding water over the south central and south eastern part of the country. The results of the regression in this case suggest that the bias can be corrected primarily by reducing the both the mean precipitation and evaporation (Figs. 2e-f). The largest corrections occur near 100°W and 37°N. These results differ substantially from the March/April results where the error is dominated by the evaporation term.

We can get some idea of how well the RSC method has determined the true precipitation correction by comparing the GEOS-1 DAS precipitation with station observations (Fig. 3). The comparison for March/April (Fig. 3a and c) shows considerable differences in the two patterns; however, both estimates are consistent with the notion that the errors are primarily in the evaporation. This is further supported by a calculation in which the observed precipitation is used as a constraint in the regression: the results (not shown) are similar to those shown in Fig. 1. The comparison for May/June (Figs. 3b and d) shows the largest discrepancies at 100°W, where the RSC suggests rather large reductions in precipitation which are not supported by the observations. In this region, the corrections (Figs. 2e and f) in evaporation and precipitation are producing large but compensating changes in the moisture. This may be partly the result of problems with the analysis increments since this is a region (with sloping terrain) where the moisture field undergoes a rapid transition from the wet conditions of the southeast to the much drier conditions of the west. When the observed precipitation is included in the regression as a

constraint for May/June (not shown), the results are similar to Fig. 2, but with a reduced evaporation correction at 100°W.

The tendency for the precipitation and evaporation corrections to become large and of opposite sign is symptomatic of a problem that occurs to a greater degree during July-August. The failure of the RSC method in this case appears to be the result of a spurious feedback in the convective parameterization resulting from the forcing by the analysis increments. This problem was first documented for the tropical regions by Molod et. al. (1995), but appears to also be true for the continental United States during summer.

3. Conclusions

RSC models short term forecast error by considering linear transformations of the GCM's forcing terms which produce a "best" model in a restricted least squares sense. The results of RSC provide 1) a partitioning of the systematic error among the various GCM's forcing terms, and 2) a consistent partitioning of the non-systematic error among the GCM forcing terms which maximize the explained variance.

An example of RSC is presented for the Goddard Earth Observing (GEOS) GCM's vertically-integrated moisture equation over continental United States during spring. The results are based on the history of analysis increments ("errors") from a multi-year data assimilation experiment employing the GEOS model. The RSC analysis suggests that during early spring the short term *systematic forecast errors* in the vertically-integrated moisture are dominated by errors in the evaporation field, while during late spring the errors are large in both the precipitation and evaporation fields.

The RSC analysis appears to provide (in most regions) reasonable corrections as verified from station observations of precipitation. Details in the spatial patterns differ, however, and the RSC method fails (produces large unrealistic corrections) in regions and times of year where the moisture increments are likely to have the most problems. This is especially true during the middle of summer when the precipitation over much of the central and eastern United States is dominated by small-scale convective events. In this case the analysis increments appear to generate a feedback response in the convective precipitation (see Molod et al. 1995), and thus produce statistical relationships between the increments and GCM forcing terms which have little to do with the errors in the GCM.

REFERENCES

Bloom, S. C., L. L. Takacs and E. Brin, 1991: A scheme to incorporate analysis increments gradually in the GLA assimilation system. *Ninth Conference on Numerical Weather Prediction*, Denver, CO.

Klinker, E. and P.D. Sardeshmukh, 1992; The diagnosis of mechanical dissipation in the atmosphere from large-scale balance requirements. *J. Atmos. Sci.*, **49**, 608-627.

Molod, A., H.M. Helfand, and L.L. Takacs, 1995: The climate of the GEOS-1 GCM and its impact on the GEOS-1 data assimilation system (submitted).

Pfaendtner, J., S. Bloom, D. Lamich, M. Seablom, M. Sienkiewicz, J. Stobie, A. da Silva, 1995: *Documentation of the Goddard Earth Observing System (GEOS) Data Assimilation System-Version 1*. NASA Tech. Memo. No. 104606, volume 4, Goddard Space Flight Center, Greenbelt, MD 20771.

Schubert, S. D., R. B. Rood and J. Pfaendtner, 1993: An assimilated data set for Earth science applications. *Bull. Amer. Meteor. Soc.*, **74**, 2331-2342.

Schubert, S., C.-K, Park, C.-Y. Wu, W. Higgins, Y. Kondratyeva, A. Molod, L. Takacs, M. Seablom. R. Rood, 1993: *A multiyear assimilation with the GEOS-1 system: overview and results*. NASA Tech. Memo. No. 104606, volume 6, Goddard Space Flight Center, Greenbelt, MD 20771.

Schubert, S. D. and Y. Chang, 1995: An objective method for inferring sources of model error. Submitted to *Mon. Wea. Rev.*.

Suarez, M. J. and L. L. Takacs, 1995: *Documentation of the Aries-GEOS Dynamical Core:Version 2*. NASA Tech. Memo. No. 104606, volume 5, Goddard Space Flight Center, Greenbelt, MD 20771.

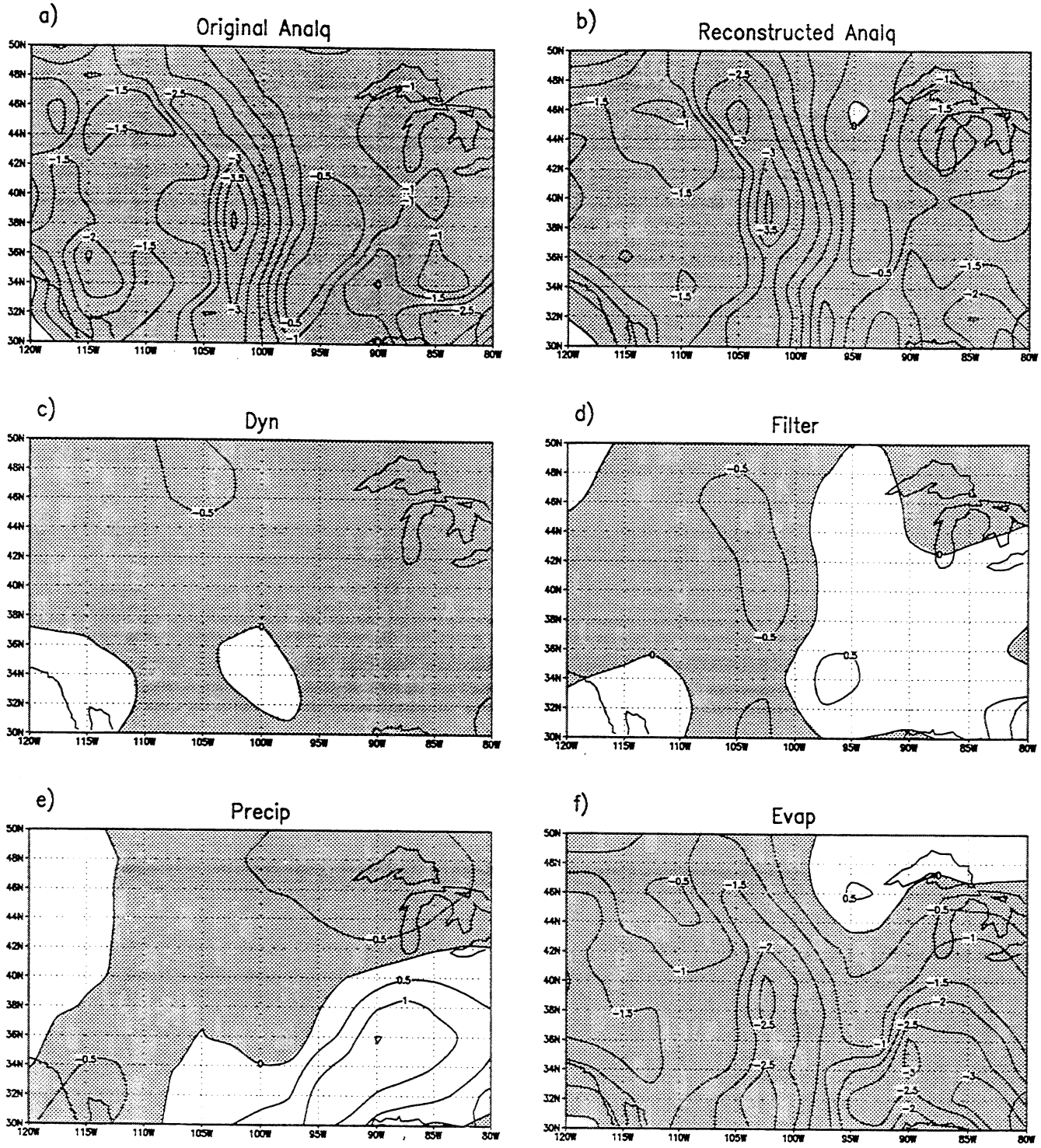

Fig.1: The results of the RSC for the mean correction ($A_r\overline{\Phi_r}^m$). a) The reconstructed time mean analysis increment, b) the original analysis increments, c) the correction to the convergence, d) the correction to the filter, e) the correction to the (minus) precipitation, and f) the correction to the evaporation. Units are mm/day.

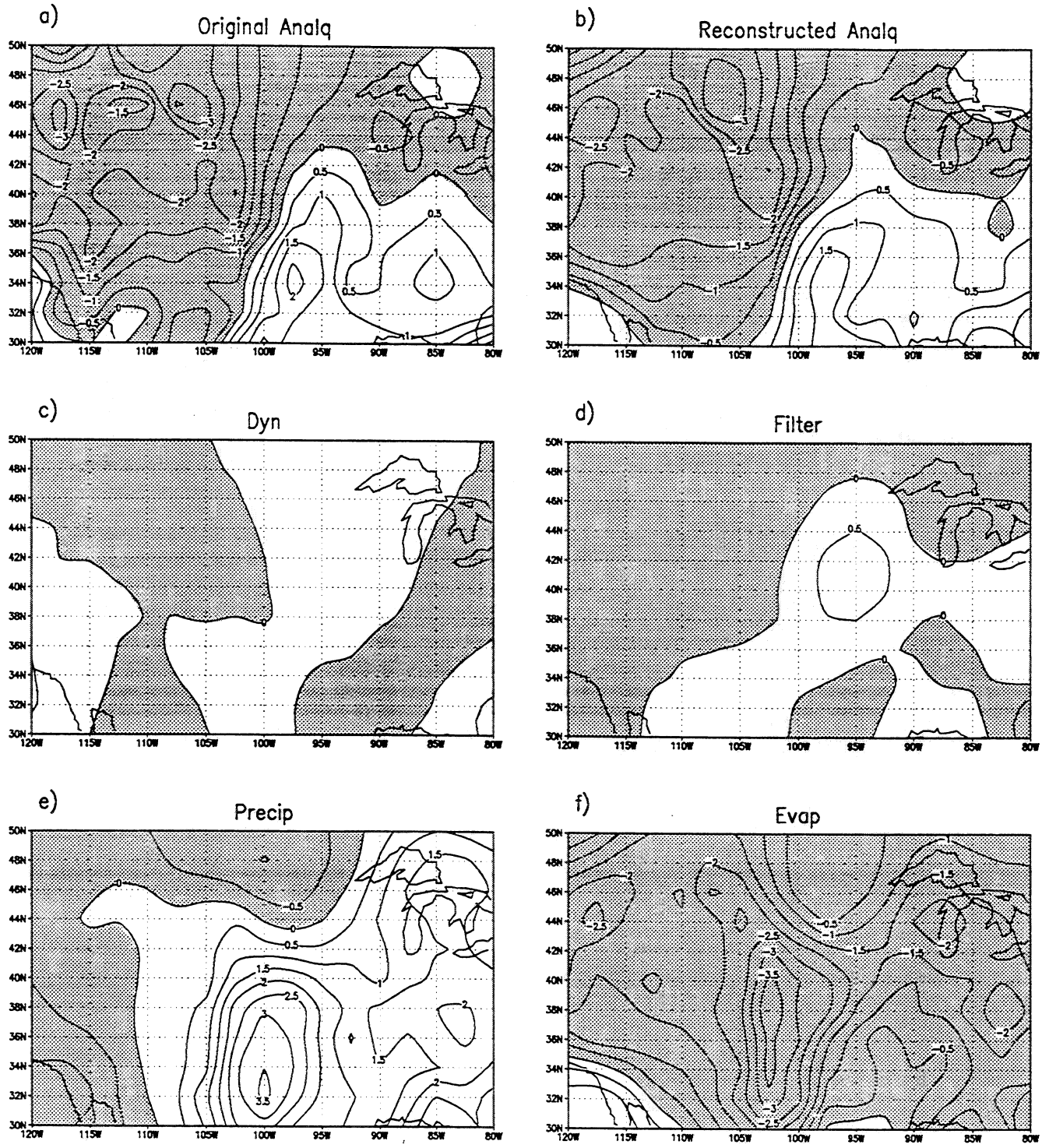

Fig.2: Same as Fig.1, except for May/June.

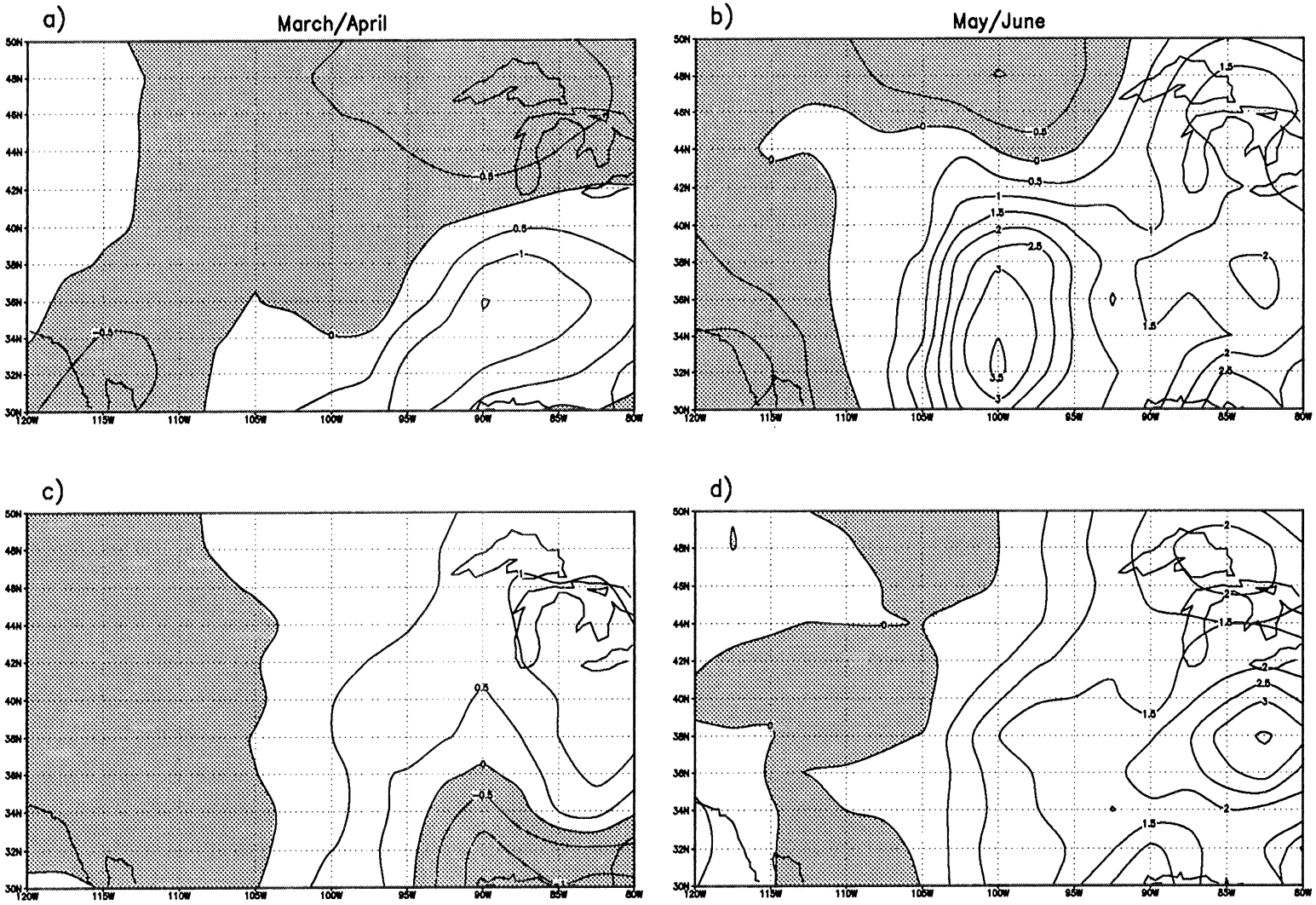

Fig.3: The precipitation corrections determined from the RSC (a and b) and from observations (c and d) for March/April and May/June.

2.4 Surface Characteristics

USING GEOS-1 WIND STRESS TO MODEL THE VARIATION OF TRANSPORT THROUGH THE STRAITS OF FLORIDA

by Richard J. Greatbatch(1) and Arlindo M. da Silva(2)

(1) Department of Physics, Memorial University of Newfoundland, St. John's, Newfoundland, Canada, A1B 3X7.

(2) Data Assimilation Office, NASA Goddard Space Flight Center, USA.

On average, about 30 Sv (1 Sv = 10^6 m^3 s^{-1}) of water is carried by the Florida Current through the Straits of Florida between Florida and the Bahamas. The Florida Current forms part of the Gulf Stream System (Stommel, 1965), and is an important source of heat for the North Atlantic climate system. Larsen(1992) describes the use of an abandoned submarine cable to monitor transport through the Straits. The cable extends from Jupiter Inlet, on the Florida side, to Settlement Point, in the Bahamas. Transport through the Straits is related to the voltage difference between the ends of the cable (the voltage difference is induced by the flow of the current through the earth's magnetic field). Larsen describes the calibration of the cable for estimating transport. It has been known for some time that the northward transport through the Straits on average peaks in the summer, and drops to a minimum in the fall (Niiler and Richardson, 1973). Anderson and Corry(1985) showed that a linear, barotropic model of the North Atlantic driven by seasonally-varying, climatological wind stress can reproduce the phase of the seasonal transport variation, but some uncertainty remained as to the amplitude. The seasonal variation of transport has also been studied by Boning et al.(1991), using the North Atlantic eddy-resolving model that forms the WOCE Community Modelling Effort (WOCE-CME). They found that the amplitude of the modelled seasonal cycle depends strongly on the wind stress climatology used to drive the model, a conclusion supported by Fanning, Greatbatch, da Silva and Levitus(1994). These authors used four different wind stress climatologies to drive a linear barotropic model, and obtained results that confirmed those of Boning et al..

With the advent of Larsen's data, we now have daily means of transport covering a ten year period from 1981-1991. It is no longer necessary to restrict attention to the seasonal cycle; rather we can attempt to model transport variability on time scales of days to years. Greatbatch et al.(1995) describe results using a barotropic model with the same resolution as the WOCE-CME; that is, 1/3^o in latitude, and 0.4^o in longitude, corresponding to a grid spacing of 37 km at 34^o N. The model equations are linearised about a state of rest (the only nonlinearity in the model is the use of a quadratic bottom friction parameterisation). Greatbatch et al. drove their model with wind stress calculated using the formula of Large and Pond(1981), applied to the 10 m wind product provided by the TOGA/WCRP ECMWF Level III Basic Data Set. A visual comparison between the model-computed transport and the cable derived transport estimates shows many similarities. Coherence squared between the two time series has peaks between 0.4 and 0.5, and is above the 95% confidence level in the period range 6 to 100 days.

Given the encouraging results obtained by Greatbatch et al.(1995), and the dependence we found previously on the wind stress product used to drive the model (Fanning, Greatbatch, da Silva and Levitus, 1994), it was clearly desirable to repeat Greatbatch et al.'s calculation using the surface wind stress produced by the GEOS-1 analysis. In addition, comparison between the model-computed transport and the cable data provides a valuable, independent check on the wind stress product produced by GEOS-1. Figure 1 compares the cable-estimated transport (solid line) with time series of transport computed

using the model driven by the GEOS-1 product. There are clearly many similarities between the two time series, together with some obvious discrepancies. In particular, the model shows a tendency to overestimate the amplitude of the observed signal. Also, although it does quite well at capturing the long period variability in most years, there is an event beginning in April 1986 and ending in December 1986, that is missed by the model. This event is also missed in the model run using ECMWF derived forcing. In general, the ECMWF-driven model does less well at capturing the long period variability (time scales greater than 2 months) than the GEOS-1 model run.

Figure 2 shows coherence squared and phase between the model-computed transport and the cable data, and compares the run using GEOS-1 forcing with the run using ECMWF forcing. The horizontal line shows the 95% significance level. The GEOS-1 case shows significant coherence at all time scales beyond 3 days, and, overall, performs marginally better than the ECMWF case. The phase difference at long periods in the GEOS-1 case has a significant contribution from the event in 1986, mentioned previously, and for which the model incorrectly predicts the phase. Figure 3 shows variance conserving spectra for the cable data and the two model runs. Clearly, the GEOS-1 model run has too much energy at periods beyond 10 days. Figure 4 shows the daily and monthly means of transport for the three cases, using cable data and model output from the years 1985-89. This shows the tendency for the GEOS-1 case to overestimate the seasonal cycle compared to the cable data. Both the GEOS-1 and ECMWF cases show stronger northward transport in summer than at other times of year, in keeping with the cable data.

In summary, using the GEOS-1 product to drive the model leads to more energetic model-computed transports than obtained using ECMWF data. GEOS-1 generally improves the comparison with the cable data, but appears to overestimate the amplitude at periods beyond 10 days, including the seasonal cycle.

Acknowledgements: We are grateful to Allan Goulding for his help in setting up the model code used in these experiments, and to Vembu Subramanian for producing the computer drawn plots.

References:

Anderson, D.L.T., and R.A. Corry, 1985: Seasonal transport variations in the Florida Straits: A model study. J. Phys. Oceanogr., 14, 7-40.

Boning, C.W., R. Doscher and R.G. Budich, 1991: Seasonal transport variation in the western subtropical North Atlantic: Experiments with an eddy-resolving model. J. Phys. Oceanogr., 21(9), 1271-1289.

Fanning, A.F., R.J. Greatbatch, A.M. da Silva and S. Levitus, 1994: Model-calculated A comparison using different wind stress climatologies. J. Phys. Oceanogr. 24(1), 30-45.

Greatbatch, R.J., Y. Lu, B. deYoung and J.C. Larsen, 1995: The variation of transport through the Straits of Florida: A barotropic model study. J. Phys. Oceanogr., ubmitted.

Large, W.G., and S. Pond, 1981: Open ocean momentum flux measurements in moderate to strong winds. J. Phys. Oceanogr., 11, 324-336.

Larsen, J.C., 1992: Transport and heat flux of the Florida Current at 27^o N derived from cross-stream voltages and profiling data: theory and observations. Phil. Trans. R. Soc. Lond. A, 338, 169-236.

Niiler, P.P., and W.S. Richardson, 1973: Seasonal transport variability of the Florida Current. J. Mar. Res., 31(3), 144-167.

Stommel, H.M., 1965: The Gulf Stream. University of California Press.

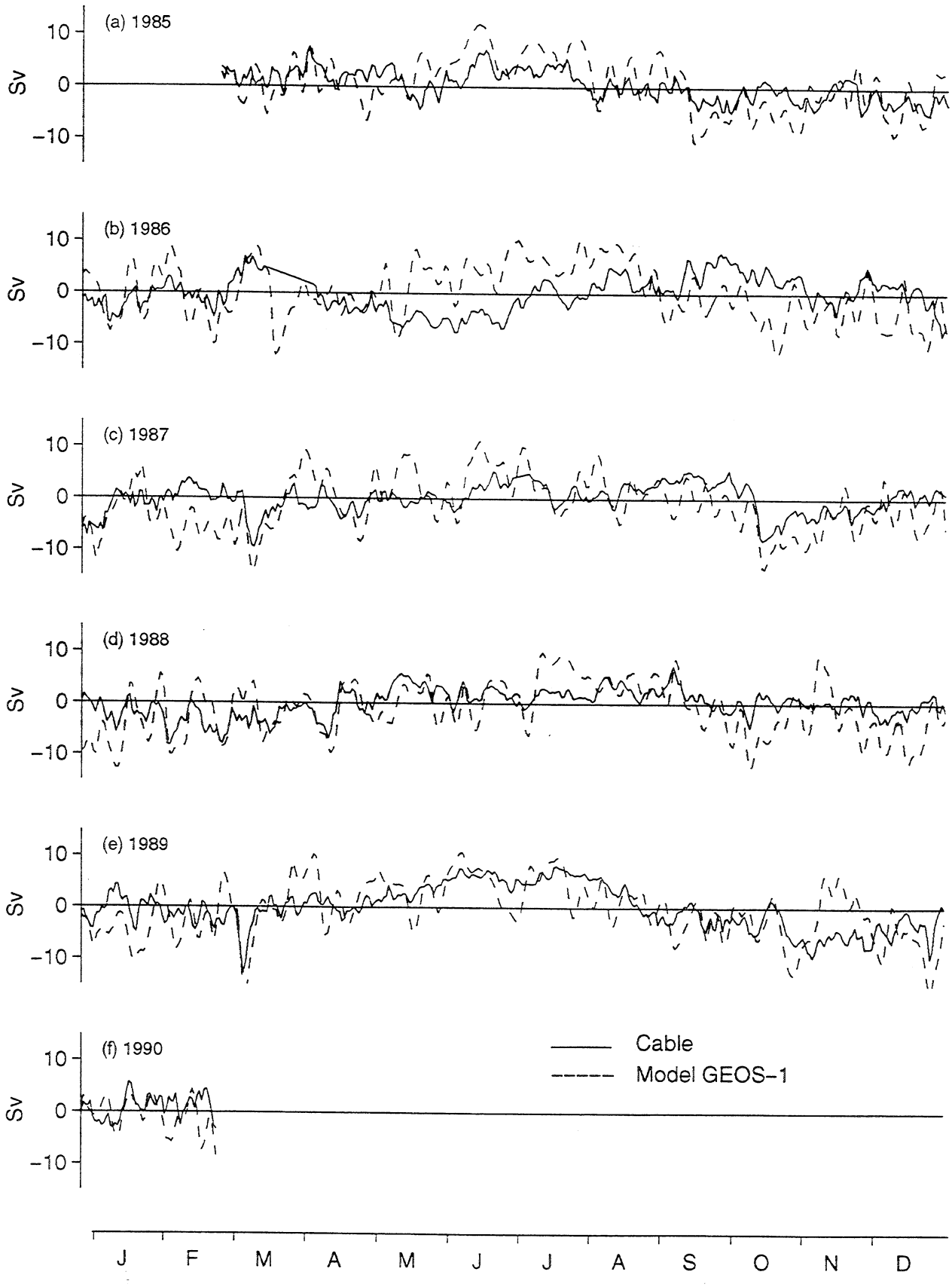
(a) 1985
(b) 1986
(c) 1987
(d) 1988
(e) 1989
(f) 1990
Sv
10
0
−10
Cable
Model GEOS−1
J
F
M
A
M
J
J
A
S
O
N
D

Figure 1

GEOS–1 versus Cable

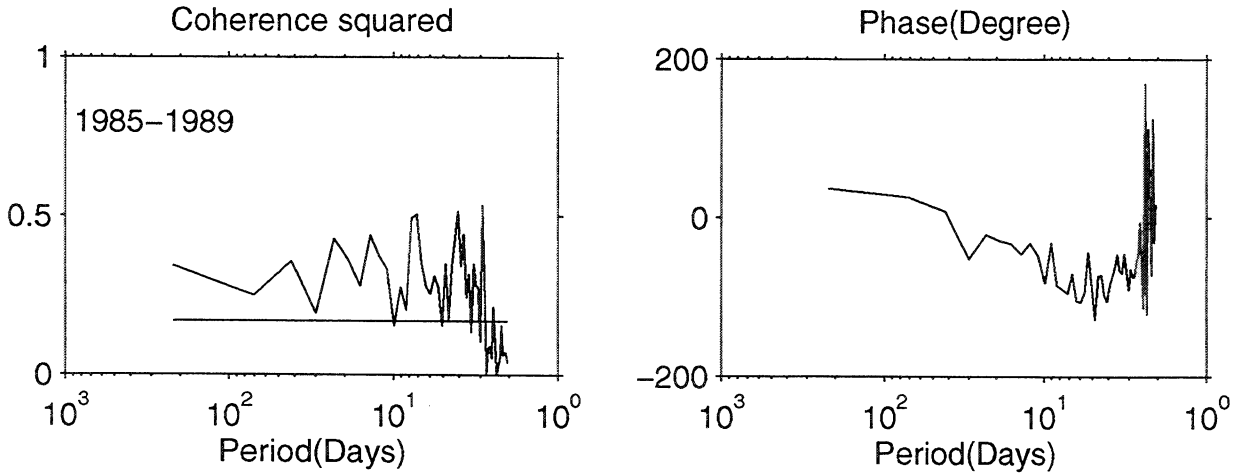

Positive phase means model leads cable

ECMWF versus Cable

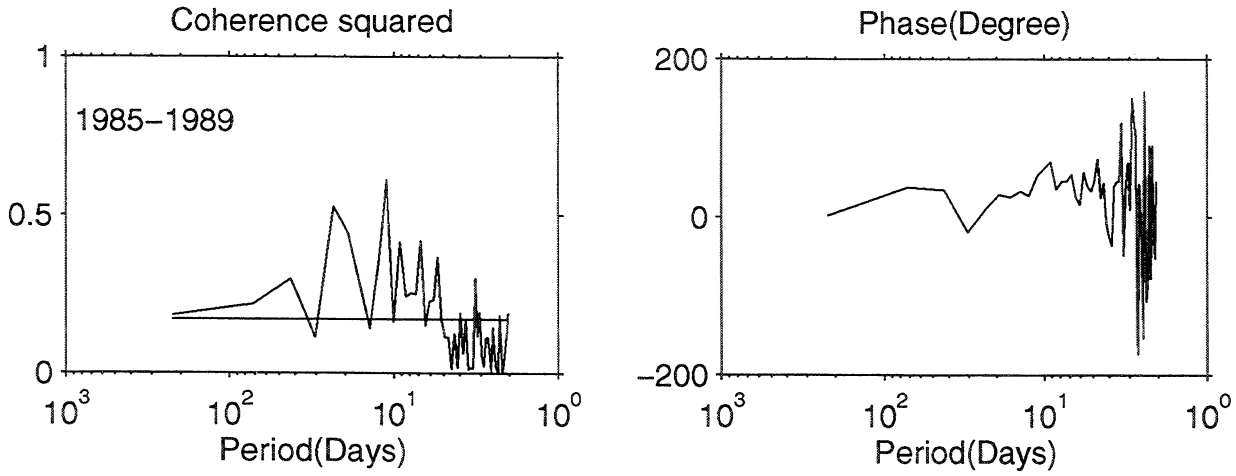

Figure 2

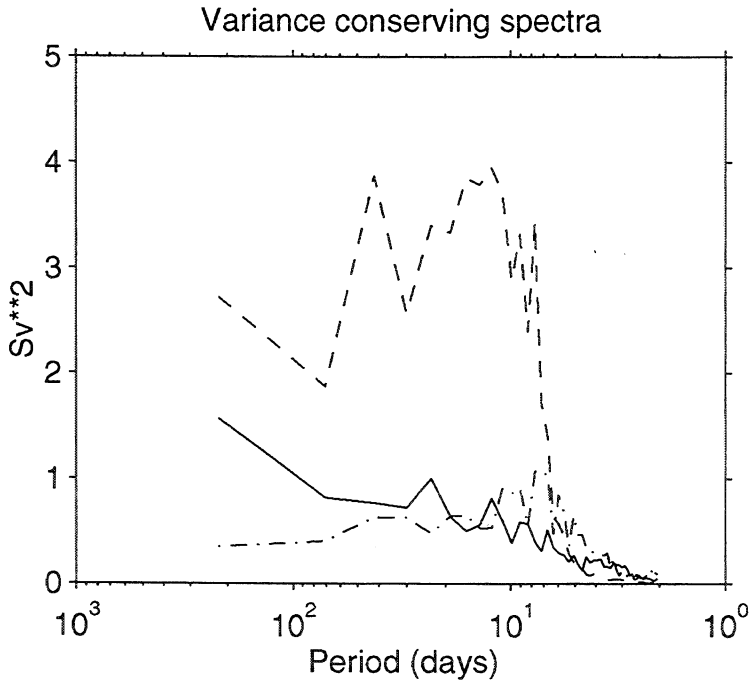

Cable – (Solid line)

GEOS–1 – (Dashed line)

ECMWF – (Dashed dot line)

Figure 3

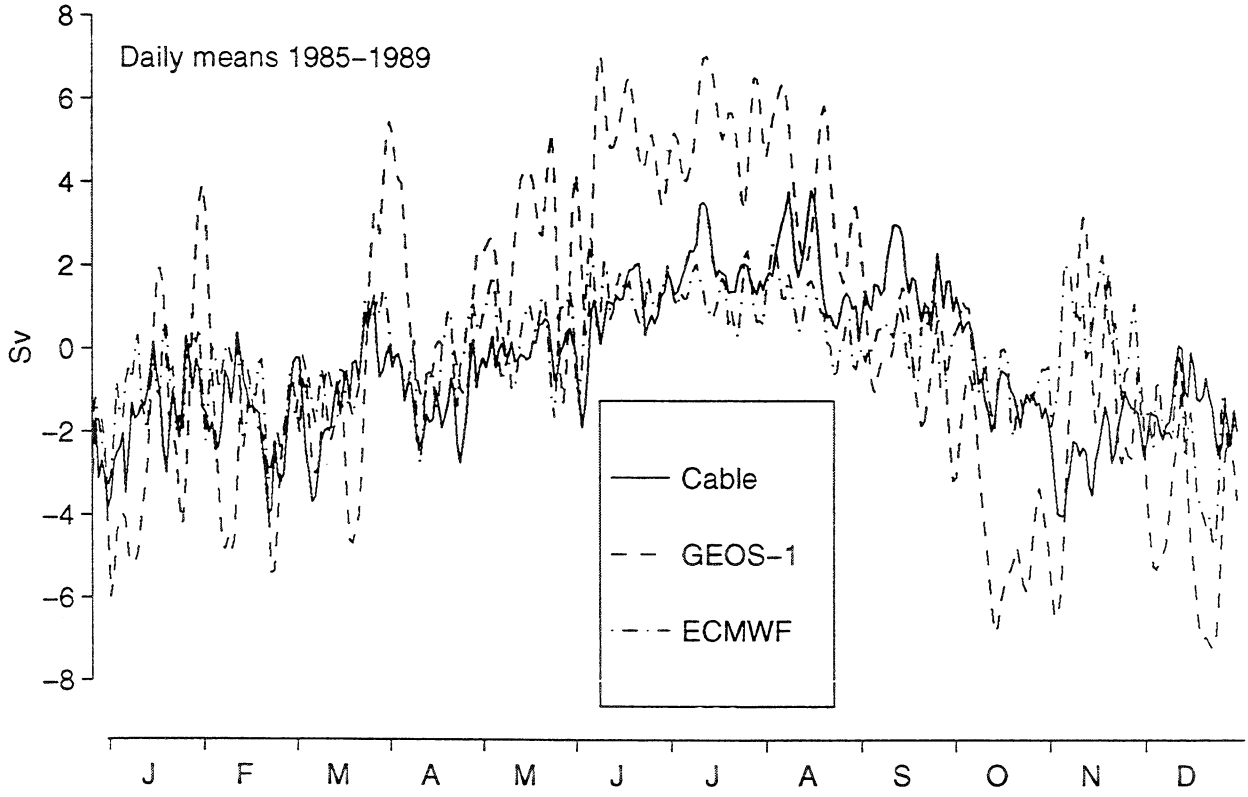
Daily means 1985–1989
Sv
8
6
4
2
0
−2
−4
−6
−8
Cable
GEOS−1
ECMWF
J
F
M
A
M
J
J
A
S
O
N
D

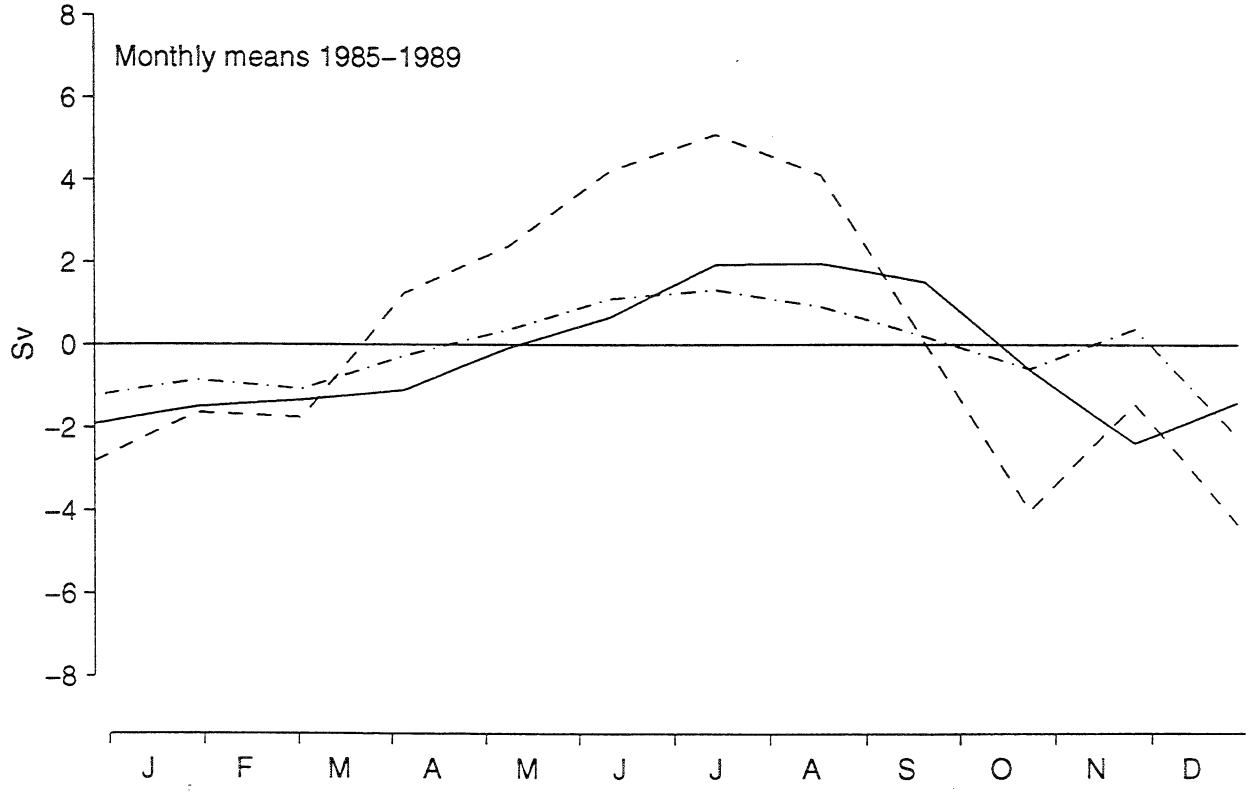
Monthly means 1985–1989
Sv
8
6
4
2
0
−2
−4
−6
−8
J
F
M
A
M
J
J
A
S
O
N
D

Figure 4

A comparison of Surface Marine Fluxes from GEOS-1/DAS and NMC Reanalyses

ARLINDO DA SILVA
Data Assimilation Office, NASA Goddard Space Flight Center, USA

AND

GLENN WHITE
Development Division, NMC/NWS/NOAA

Workshop on Results from the GEOS-1 Five Year Assimilation
Greenbelt, Maryland, March 1995

1 Introduction

A central problem in global ocean modeling is the specification of accurate fluxes of heat, momentum and fresh water at the air-sea interface. The sparseness of historical surface marine observations, especially in the tropics and southern oceans, introduces great uncertainties which are compounded by several instrument biases (e.g., Isemer and Hasse 1987, Kent and Taylor 1995, da Silva *et al.*1995) and limitations in the bulk parameterizations frequently used. Modern data assimilation systems, by virtue of using sophisticated physical parameterizations and a model forecast to fill in data void areas have in principle the potential to produce more reliable surface marine fluxes.

The purpose of this abstract is to discuss some of the difficulties associated with surface marine fluxes from data assimilation systems, and to compare estimates from the GEOS-1/DAS (Schubert *et al.* 1993) and NMC reanalyses (Kalnay et *et al.* 1995).

2 Surface Marine Flux Calculation

In current data assimilation systems, an *analysis* of the prognostic variables is produced using a statistical interpolation algorithm. A typical analysis equation reads

$$w_a = w_f + K\,(w_o - H w_f)$$

where

w_a	analysis state vector
w_f	forecast state vector (first guess)
w_o	observation vector
H	"interpolation" operator
K	weight matrix

In the Goddard EOS Data Assimilation System (GEOS-1/DAS) the analysis increments $w_a - w_f$ are introduced every 6 hours as time-independent forcing terms in a continuous model integration:

$$\frac{\partial w}{\partial t} = \mathcal{F}_{adv}(w) + \mathcal{F}_{phys}(w) + \frac{w_a - w_f}{6 \text{ hours}}$$

where w represents the state of the atmosphere, $\mathcal{F}_{adv}(w)$ and $\mathcal{F}_{phys}(w)$ represent advective and physical processes. Diagnostic quantites such as heat fluxes and precipitation produced by this data constrained model integration are saved as 6 hour averages. Details of the data assimilation system can be found in Pfaendtner *et al.* (1995).

NMC's Climate Data Assimilation System (CDAS) uses an intermittent data assimilation system in which the model state is updated with the analysis w_a every synoptic time. The analysis state w_a in CDAS is produced using the Statistical Spectral Interpolation (SSI) algorithm of Parrish and Derber (1992). Diagnostic quantities from the NMC/CDAS are derived as averages of 6 hour forecasts.

3 Impact of Data Assimilation on Fluxes

Because of the frequent correction of the model state by the observations, an additional complication arises

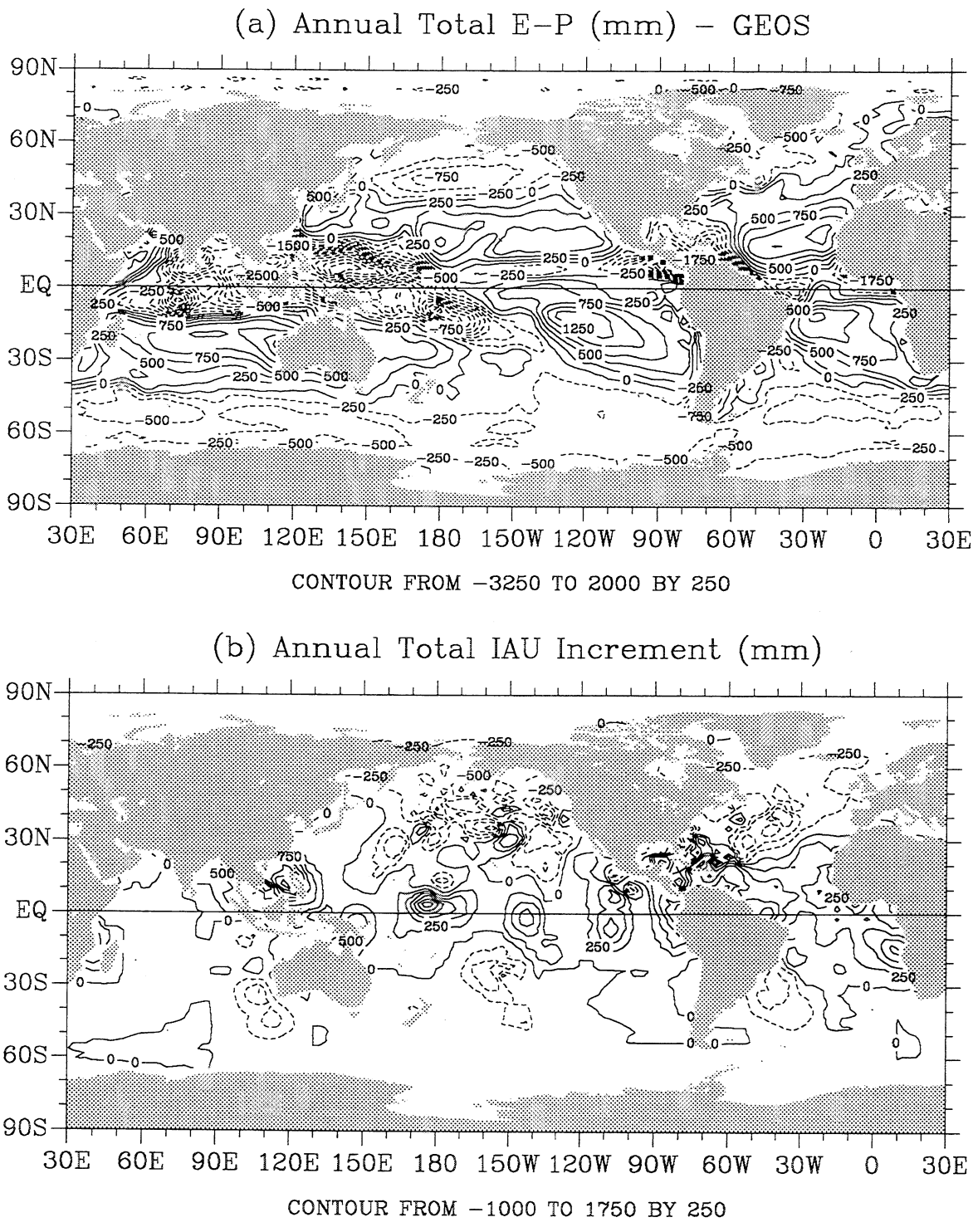

Figure 1: Annual total estimates of a) Evaporation minus precipitation and b) vertically integrated specific humidity analysis increments divided by 6 hours. Countour interval: 250 mm. Both estimates computed from the GEOS-1/DAS system using data from the period March/85 to February/90.

in budget calculations from data assimilation systems. As an example, consider time mean, vertically integrated moisture budget for a *climate model* with specified SST, but otherwise without any influence of observations:

$$\nabla \cdot \mathbf{Q} = E - P$$

Within numerical accuracy, the vertically averaged divergence of the moisure flux ($\nabla \cdot \mathbf{Q}$) is balanced by evaporation minus precipitation ($E - P$). However, in a data assimilation system, an aditional term due to the correction by the data must be included:

$$\nabla \cdot \mathbf{Q} = E - P + \Delta$$

The term Δ reflects uncertainties in $\mathbf{Q}$, E, and P. In principle there is no guarantee that the globally averaged $E - P$ will vanish (much less over the oceans). Figure 1 shows annual mean $E - P$ and Δ computed from the 5-year (March 85–February 90) GEOS-1/DAS reanalsyis. Despite the sparseness of moisture data over the oceans, a relatively large Δ is found in the tropics and northern oceans. Ideally one would like to improve model and analysis system so that $\Delta << E - P$. The extent to which Δ is non-neglible in the "observed" parts of the oceans is an indication of the confidence one should place on diagnostic fluxes produced by the data assimilation systems.

4 Results

For the sake of conciseness we focus on the annual means computed for the the period March/85 to February/90. This comparison is based on an earlier version of the NMC fluxes which was later found to contain an error in the SSM/I assimilation of wind speeds.

In addition to fluxes computed from GEOS-1/DAS and NMC's reanalysis, the following data sets are used for comparison:

UWM/COADS: Revised monthly mean fluxes (da Silva *et al.* 1995):

- Calculations from individual observations
- Large and Pond (1981,1982) transfer coefficients with stability dependence
- Revised Beaufort equivalent scale.
- Climatology for 1945-89.

SRB: Surface Radiation Budget (Pinker *et al.* 1995 estimates)

- Based on ERBE & ISCCP data
- Radiative transfer scheme
- Period: March/85 to December/88

Hellerman and Rosenstein Wind Stress: computed from individual ship reports, with wind speed dependent drag coefficient and stability correction. Reported winds assumed at 10 m.

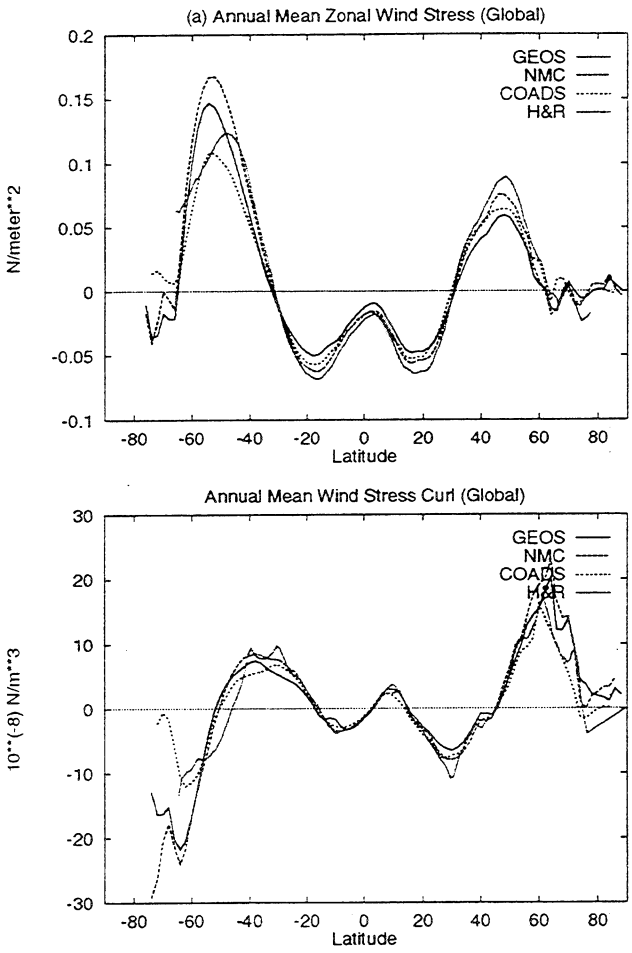

Figure 2: Zonal averages of annual mean a) zonal component of wind stress (τ_x), and b) curl of the wind stress. Estimates from GEOS-1/DAS, NMC/CDAS, COADS and Hellerman and Rosenstein.

4.1 Momentum fluxes

Figure 2 shows the zonal mean of the annual mean component of the surface wind stress over the oceans (τ_x), along with the curl of the wind stress. Overall, the NMC stress is stronger than GEOS in mid-latitudes; the curl of the stress is in general agreement. Notice that in the southern hemisphere, the zonal component of the stress estimated by Hellerman and Rosenstein (1981) peaks northwards of the

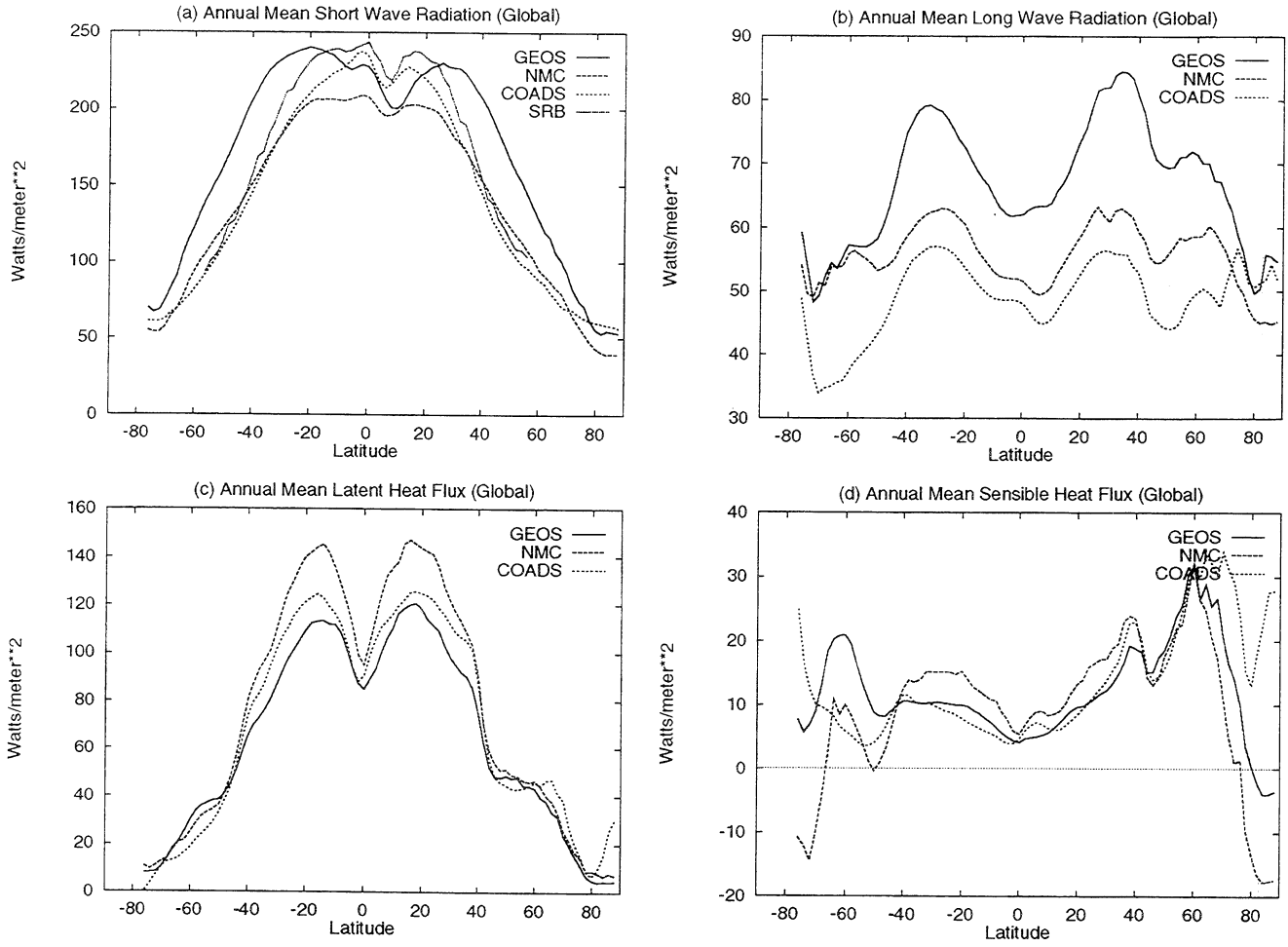

Figure 3: Zonal averages of annual mean a) surface net shortwave radiation, b) surface net longwave radiation, c) surface latent heat flux, and d) surface sensible heat flux. Estimates from GEOS-1/DAS, NMC/CDAS, COADS and SRB (shortwave radiation only).

other estimates. The time variability of the GEOS-1/DAS stress in the North Atlantic is examined in a companion talk (Greatbatch and da Silva 1995). Rienecker's (1995) compares the GEOS-1/DAS stress to other standard products in the North Pacific ocean.

4.2 Heat Fluxes

The net heat flux at ocean surface is denoted by

$$Q_{NET} = R_{SW} - (R_{LW} + Q_L + Q_S)$$

where

R_{SW}	net short wave radiation
R_{LW}	net longwave radiation
Q_L	latent heat flux
Q_S	sensible heat flux

The zonal mean of each annual mean heat flux component is presented in Figure 3. The main points can be summarized as follows:

Shortwave radiation: Compared to SRB and COADS, GEOS shortwave is under-estimated in the tropics and over-estimated in the extra-tropics. These short wave differences can be largely explained by deficiencies in the GEOS cloud cover (not shown). NMC's shortwave radiation is smaller than most estimates in the tropics, despite reduced cloud cover. Comparing the clear-sky incoming to outgoing shortwave from NMC one finds a ratio of about 15%, about twice the prescribed albedo without the zenith angle dependence. This large dependence of the albedo on zenith angle is being investigated at NMC.

Longwave radiation: GEOS' longwave appears too strong compared to NMC and COADS. This deficiency is likely due to the underprediction of marine stratus throughout the oceans (including the tropics).

Latent Heat Flux: In the tropics, NMC's latent heat flux estimate stronger by about 20 Watts/m^2 compared to both COADS and GEOS. This over-prediction of latent heat flux in the tropics by the NMC system is likely related to the problem with SSM/I wind speed assimilation mentioned earlier.

Sensible Heat Flux: NMC's sensible heat fluxes slightly stronger than GEOS.

4.3 Precipitation and Evaporation

The zonal averaged annual mean precipitation from both assimilations tends to agree in the tropics, with GEOS estimates generally lower in mid-latitudes (Figure 4). Annual mean evaporation minus precipitation fields from NMC tends to be larger than GEOS due to the enhanced evaporation in the NMC product.

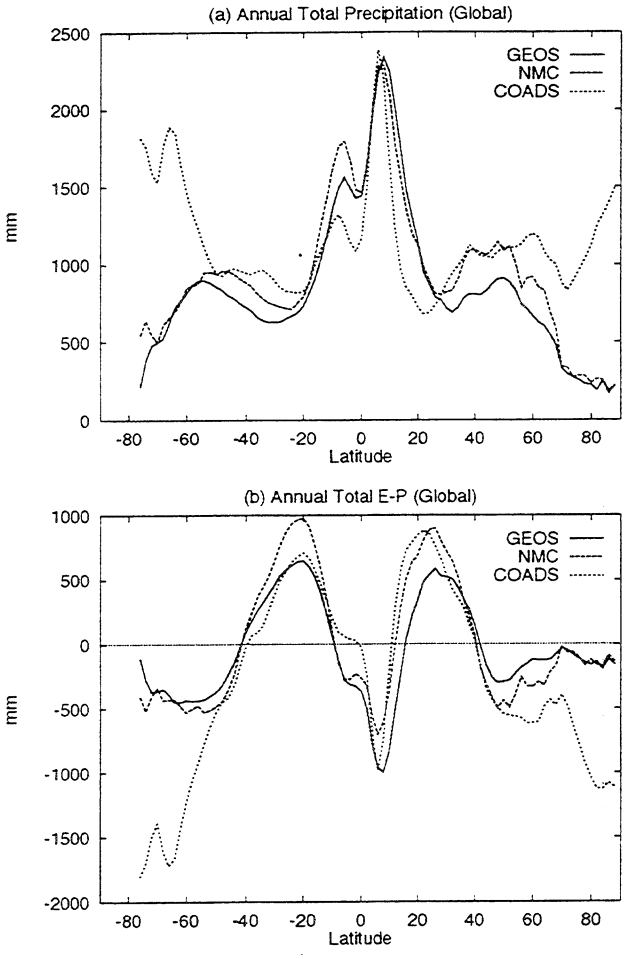

Figure 4: Zonal averages of annual total a) precipitation (mm) b) evaporation minus precipitation. Estimates from GEOS-1/DAS, NMC/CDAS and COADS.

5 Implied Oceanic Heat Transport

The vertically integrated heat budget equation for the oceans can be written as

$$\frac{\partial H}{\partial t} + \nabla \cdot \mathcal{H} = Q_{net}$$

where

H = Heat content

$\mathcal{H}$ = Heat transport

$$
\begin{aligned}
Q_{net} &= \text{Net heat flux at the surface} \\
&= Q_{SW} - (Q_{LW} + Q_L + Q_S)
\end{aligned}
$$

Integrating over many years and assuming the heat storage to vanish:

$$\nabla \cdot \overline{\mathcal{H}} = \overline{Q_{net}}$$

Assuming no transport at east/west boundaries, one can compute the zonally integrated meridional heat transport by the oceans,

$$\mathcal{H}_y(y) = \mathcal{H}_y(y_N) + \int_y^{y_N} dy \int_{x_W}^{x_E} \overline{Q_{net}}\, dx$$

Equilibrium considerations require that

$$\int \int_{Oceans} \overline{Q_{net}}\, dx, dy = 0$$

Since sea surface temperature is specified, and there is an external forcing by the data, the net heat fluxes derived from assimilation systems are not guaranteed to be in balance, and the condition above is not necessarily met. Figure 5 shows the annual net heat from GEOS and NMC. The GEOS estimate of the neat heat flux into the oceans is positive over most of the oceans and the derived implied heat transport by the oceans is unrealistically large. The NMC estimate of the neat heat flux has a higher degree of balance, with the implied oceanic transport having realistic magnitudes (Figure 6a). Notice, however, that the implied transport in the Indian ocean is primarily northward contrary to previous estimates from ship data which suggest a southward transport. It is interesting to note that the balance in NMC's neat heat flux is largely attained by reduced shortwave and enhanced evaporation in the tropics. However, enhanced evaporation in this version of the NMC fluxes is related to a problem with the SSM/I assimilation, and the reduced shortwave could be due to a problem with the zenith angle dependence of the albedo.

Using a simple version of linear inverse theory (e.g., Isemer et al. 1989), individual heat fluxes components can be adjusted under the constraint of global balance. In this calculation, each heat flux component have been multiplied by the non-dimensional factors given in Table 1. Constrained implied oceanic heat transport derived from both assimilations are more realistic when their shortwave field is replaced with the SRB estimate (Figure 6b,c).

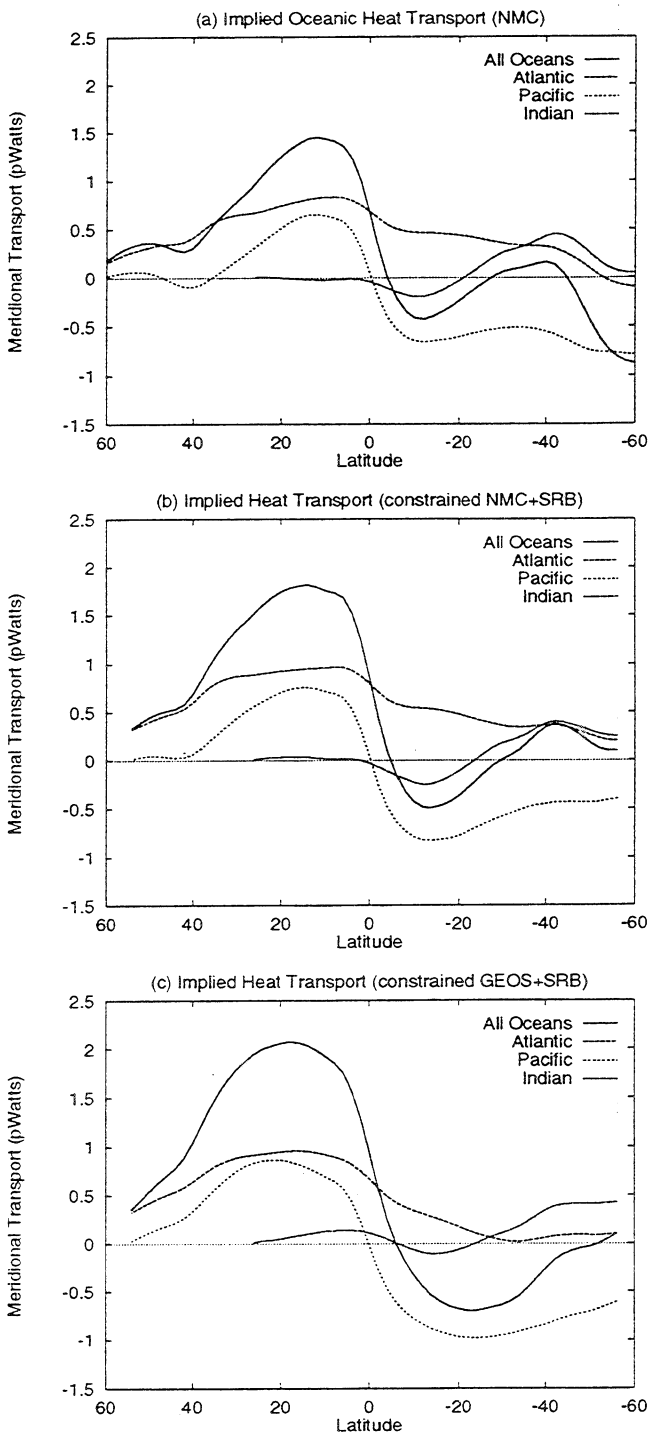

Figure 6: Implied zonally integrated meridional heat transport by oceans: a) estimated from original NMC/CDAS fluxes, b) estimated using longwave, sensible and latent heat fluxes from NMC/CDAS and net shortwave radiation from SRB, and c) estimated using longwave, sensible and latent heat fluxes from GEOS-1/DAS and net shortwave radiation from SRB. Annual means computed using data from the period March/85 to February/90. See text for details.

6 Summary

We have compared surface marine fluxes from both GEOS and NMC reanalysis. The results can be summarized as follows:

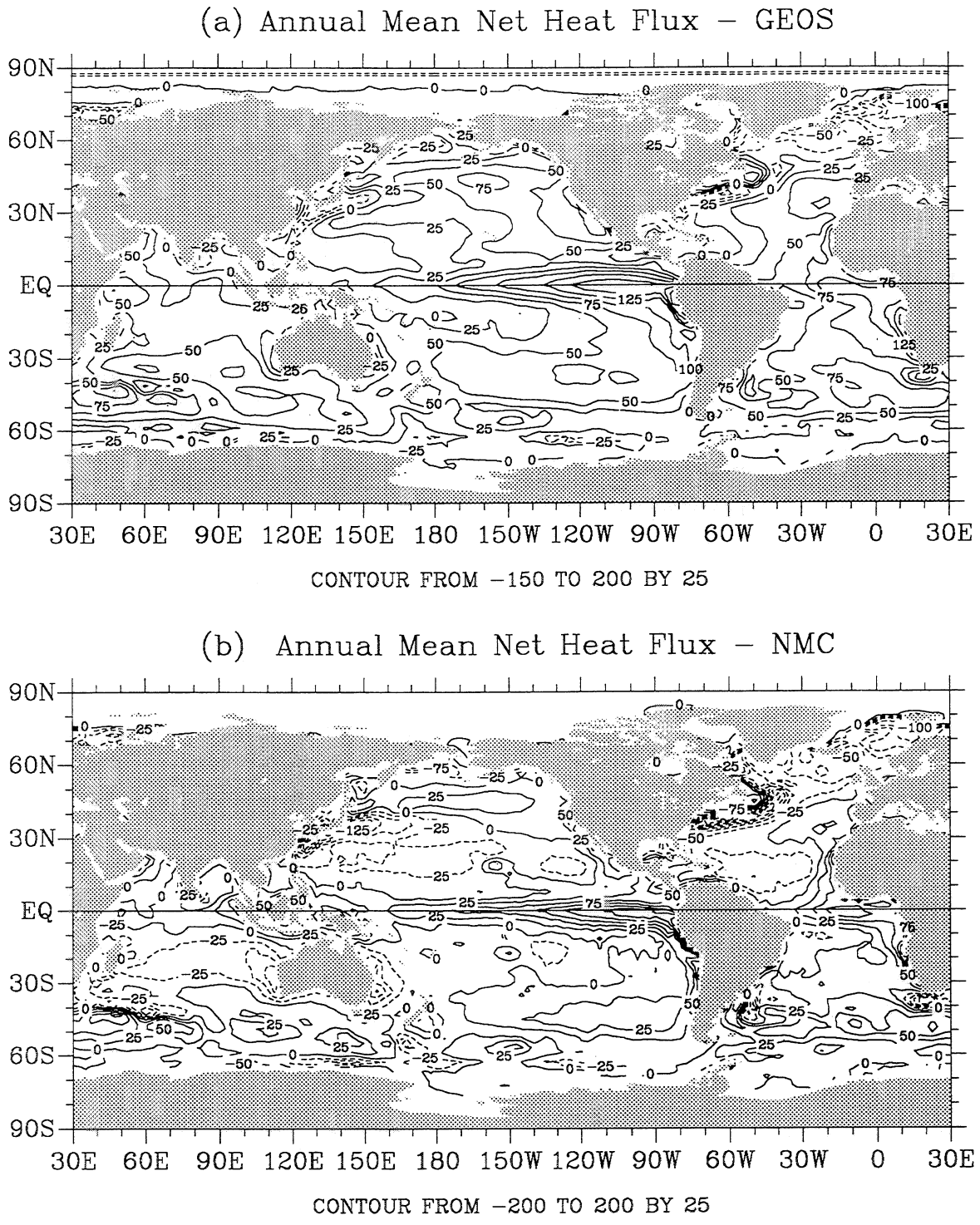

Figure 5: Annual mean estimates of net heat flux into the ocean from a) GEOS-1/DAS, b) NMC/CDAS. Countour interval 25 W/m^2. Both estimates computed using data from the period March/85 to February/90.

Table 1: Multiplicative factors used when computing the constrained implied heat transports shown in Figs. 6b,c. Each heat flux component has been scale by the factors below.

Flux component	NMC/CDAS	GEOS-1/DAS
R_{SW}	0.92	0.88
R_{LW}	1.02	1.05
Q_L	1.04	1.05
Q_S	1.01	1.01

- NMC's stress stronger than GEOS in mid-latitudes; curl of stress in general agreement.
- Shortwave radiation:
  - GEOS' shortwave differences from SRB largely explained by deficiencies in cloud cover.
  - NMC's shortwave smaller than most estimates in the tropics, despite reduced cloud cover.
- GEOS' longwave appears too strong compared to NMC and COADS.
- In the tropics, NMC's latent heat flux estimate stronger by about 20 Watts/m^2 compared to both COADS and GEOS.
- NMC's sensible heat fluxes slightly stronger than GEOS.
- Annual mean precipitation from both assimilations tends to agree in the tropics, with GEOS estimates generally lower in mid-latitudes.
- NMC's annual mean net heat flux has the best global balance.
- Constrained implied oceanic heat transport derived from both assimilations are more realistic when the shortwave field is replaced with the SRB estimate.

7 References

Greatbatch, R. J. and A. M. da Silva, 1995: Using GEOS-1 Wind Stress to Model the Variation of Transport Through the Straits of Florida. *Workshop on Results from the GEOS-1 Five Year Assimilation*, Greenbelt, Maryland, March 1995.

Hellerman, S. and M. Rosenstein, 1983: Normal monthly wind stress over the World Ocean with error estimates. *J. Phys. Oceanogr.*, **13**, 1093–1104.

Isemer, H.-J. and L. Hasse, 1987: *The Bunker Atlas of the North Atlantic Ocean. Vol. 2: Air-sea interactions.* Springer Verlag, 252 pp.

Isemer, H.-J., J. Willebrand and L. Hasse, 1989: Fine adjustment of large air-sea energy flux parameterizations by direct estimates of ocean heat transport. *J. Climate*, **2**, 1173–1184.

Kalnay, E., M. Kanamitsu, R. Kistler, W. Collins, D. Deaven, L. Gandin, M. Iredell, S. Saha, G. White, J. Woollen, Y. Zhu, M. Chelliah, W. Ebisuzaki, W. Higgins, J. Janowiak, K. C. Mo, A. Leetma, R. Reynolds, R. Jenne and Dennis Joseph, 1995: The NMC/NCAR 40-Year Reanalysis Project. Submitted to *Bull. Amer. Met. Soc.*.

Kent, E. C. and P. K. Taylor, 1995: A comparison of heat flux estimates for the North Atlantic ocean. *J. Phys. Oceanogr.*. In press.

Large, W., and S. Pond, 1981: Open ocean momentum flux measurements in moderate to strong winds. *J. Phys. Oceanogr.*, **11**, 324–336.

Large, W., and S. Pond, 1982: Sensible and latent heat flux measurements over the ocean. *J. Phys. Oceanogr.*, **12**, 464–482.

Parrish, D.F. and J.C. Derber, 1992: The National Meteorological Center's statistical spectral interpolation analysis system. *Mon. Wea. Rev.*, **109**, 1747-1763.

Pfaendtner, J., S. Bloom, D. Lamich, M. Seablom, M. Sienkiewicz, J. Stobie, A. da Silva, 1995: Documentation of the Goddard Earth Observing System (GEOS) Data Assimilation System-Version 1. NASA Tech. Memo. No. 104606, volume 4, Goddard Space Flight Center, Greenbelt, MD 20771.

Pinker, R.T., I. Laszlo, C.H. Whitlock and T. P. Charlock, 1995: Radiative Flux Opens New Window on Climate Research. *EOS Trans. Amer. Geophys. Union*, **76**, 145–158.

Rienecker, M., 1995: A comparison of surface wind products over the North Pacific Ocean. *Workshop on Results from the GEOS-1 Five Year Assimilation*, Greenbelt, Maryland, March 1995.

Schubert, S. D., J. Pfaendtner and R. Rood, 1993: An assimilated data set for Earth Science applications, *Bull. Am Met. Soc.*, **74**, 2331–2342.

da Silva, A. M., C. C. Young and S. Levitus, 1995: Atlas of Surface Marine Data 1994, Volume 1: Algorithms and Procedures. NOAA Atlas NESDIS 6, U.S. Department of Commerce, NOAA, NESDIS. In press.

NMC'S GLOBAL PRESSURE ANALYSIS VERSUS NCDC'S U.S. OBSERVATIONS

J.O. Roads and S.-C. Chen

Climate Research Division
Scripps Institution of Oceanography
University of California, San Diego, 0224
La Jolla, CA 92093-0224
Phone: (619)534-2099
Fax:: (619)534-8561
e-mail: jroads@ucsd.edu

Many times a day, at thousands of locations around the world, disparate meteorological observations are made and forwarded to meteorological forecast centers. Objective analysis schemes have been developed to merge these observations with short-range numerical weather predictions on a regular grid. The purpose of this merge is to produce a consistent initial state for a forecast model. From this initial state, short, extended, and medium-range forecasts are then produced. The analyzed initial state, or analysis, is almost always used to verify these large-scale forecasts. These weather prediction analyses are also used to verify large-scale general circulation models. The analyses are becoming an almost de facto data set for describing large-scale variations in the present weather and climate.

Just how accurate are these large-scale analyses? They are certainly getting better as the prediction models get better and new observation systems begin to come on line. Unfortunately, this constant improvement can be detrimental for studying long term climate variations, especially if consistency rather than physical verisimilitude is required. To develop this consistency, various re-analysis projects are underway; although data inputs will vary, these projects will at least use a consistent model to re-analyze long periods of time in the recent past. However, since these re-analysis projects are utilizing the present large-scale numerical weather prediction models, any biases and inaccuracies in the present analysis system will continue. We should certainly know as we begin these re-analysis efforts just what the ultimate error is likely to be.

There are a number of potential errors in the analyses. The large-scale analysis only coarsely resolves the vertical structure of the boundary layer. In fact, it is much more common to use the analysis to study the 500 mb height than the near-surface features. However, as large-scale models improve and achieve higher vertical resolution, especially in the planetary boundary level, it would seem reasonable that the near surface analysis as well as near-surface forecasts are also improving and are providing more useful near-surface information. Another potential error is that in the past, analyses were developed and archived on constant pressure surfaces. Near the surface, the constant pressure surfaces interesect the land surface and extrapolation procedures have been developed to provide a constant pressure analysis underneath the land surface. More recently, since about 1990, NMC has begun to make available the original model sigma analysis from which the pressure analysis is derived. The sigma analysis certainly has the potential of providing more accurate near-surface analyses.

Similarly, as the large-scale models achieve higher horizontal resolution, it would seem reasonable that the models could begin to topographic features. Achieving sufficiently high global resolution is not possible though within the near term. An interim solution, for

particular regions, is to use a mesoscale model, with mesoscale topography, forced at the boundary and initialized with the large scale analysis as well as individual station observations.

As we begin these new studies, we really need to establish just how accurate the past large-scale pressure analysis has been. We will then better understand what corrections may need to be made in the in order to utilize the large-scale analyses for climatological studies. We will better understand what improvements the sigma analysis provides. We will be able to assess systematic errors in NMC's global reanalysis. We will be better able to assess what kinds of improvements regional models forced at the boundary and initialized by large-scale analyses provide.

The National Meteorological Center's (NMC's) twice-daily, global 2.5 degree pressure analyses of temperature, relative humidity and wind speed are compared, over the coterminous U.S., to the National Climatic Data Center's (NCDC's) twice daily upper-air rawinsonde observations and hourly, first-order, surface observations for the period Jan. 1, 1988-Dec. 31, 1992.

As can be seen in Fig. 1, NMC's analyses have clearly improved during this time period. Still, there are some noticeable differences, especially near the surface and especially at 12 UTC. During the nighttime there is a cold bias, relative humidity is too low, and the surface wind speed is too strong. Weaker systematic errors occur during the daytime; there is a cold bias; relative humidity is too high and the surface wind speed is still too strong. Above the surface, the bias is noticeably reduced, except for the wind speed which is somewhat too weak. The analysis wind speed also has too strong a temporal variation near the surface and too weak a variation aloft.

We can correct for the analysis climatology at each station simply by removing the bias. We can further correct daily events simply by multiplying the anomalies by the ratio of the station standard deviation to the analysis standard deviation. Correcting for the biases and variances and spatially interpolating the station corrections to a .5 degree grid provides a useful guess for local conditions, especially if there is not a surface or rawinsonde station within about 200 kms.

Further details are found in Roads et al. (1995). We will be performing similar comparisons this year with the NMC and NASA reanalysis, which we have just started to receive.

Reference:

Roads, J. O., Chen, S.-C., K. Ueyoshi, 1994: NMC's Global Pressure Analysis versus NCDC's U.S. observations. (to appear, J. Climat, 1995)

Intercomparison of basic atmospheric fields on monthly and seasonal time scales from the NASA and NMC/NCAR Reanalysis Projects for the 1985-89 period.

Muthuvel Chelliah, Wesley Ebisuzaki, and Wayne Higgins
Climate Analysis Center, NMC, NWS/NOAA, Washington D.C.

Introduction:

Reanalysis of past atmospheric flow fields, devoid of artificial changes in the climate record introduced by changes in the model and analysis method, is a new venture being pursued at several meteorological and research centers around the world. In this preliminary study for the 1985-89 period, we make a zeroth order intercomparison of basic atmospheric flow fields produced at the Data Assimilation Office (DAO) at NASA and the NMC/NCAR Reanalysis Project. Except for a large overlap in the observational data base used, there are major differences between the two reanalysis systems such as the atmospheric model, data assimilation approach, physical parameterizations and so on. We extracted gridded monthly mean zonal & meridional wind (u & v), temperature (T) and geopotential height (H) fields at fifteen common pressure levels (1000, 850, 700, 600, 500, 400, 300, 250, 200, 150, 100, 70, 50, 30, and 20 mb) on a 2 degree latitude by 2.5 degree longitude grid.

Analysis and Results:

No attempt has been made in this preliminary study to remove the monthly climatology from the fields considered, or to conduct regional analyses, even though such calculations will be pursued later. We computed very basic spatial (global) and temporal correlations of the fundamental total flow fields. The pressure-time cross sections of spatial correlations, computed over the entire globe, between the respective variables at all pressure levels for U, V, T, and H showed, not surprisingly, good agreement between the two reanalyses with correlations exceeding 0.95 in the middle and lower troposphere. However lower correlations were noted in the lower troposphere and upper stratosphere, where the coarser vertical resolution of the DAO model could be a contributing factor. Moreover, strange "bulls-eyes" of lower correlations were found around Feb-Mar-Apr-May-Jun of every year in the temperature field at 200 mb, where larger than usual differences were noted in the analyses south of 60^0S.

Spatial maps of temporal correlations (March 1985 - December 1989, 58 months) at each grid point revealed that the lower and middle latitudes of either hemisphere are well correlated (Corr. >0.95) at all levels. However, correlations are generally lower in the tropics and near the poles. NMC's spectral model has the advantage of handling the flow near/over the poles much better than DAO's grid point model. Figure 1 shows the temporal correlation map for the meridional component of wind (V) at 850, 500, 200 and 50 mb. It is interesting to note that the correlation is negative at many regions in the data-poor tropics at even 500 mb. Examination of time series over the equatorial east Pacific/south American region reveal that even the annual cycle is out of phase. Aircraft reports at 200 mb make the analyses and hence the correlations relatively better.

Figure 2 shows the pressure-time section of spatially averaged U near Canton Island in the tropics. This figure shows the march of the QBO signal in both reanalyses in the stratosphere, a region long ignored in NMC operational analyses due to lack of sufficient vertical resolution.

The monthly time series of geopotential height field at 180E and 50N, near the region of the Aleutian low is shown in Fig. 3 at 1000 and 850 mb. Since a time series plot of 850 or 1000 mb temperature at the same location (not shown) reveals acceptable differences, there apparently is a post processing error in DAO's 1000 mb height field.

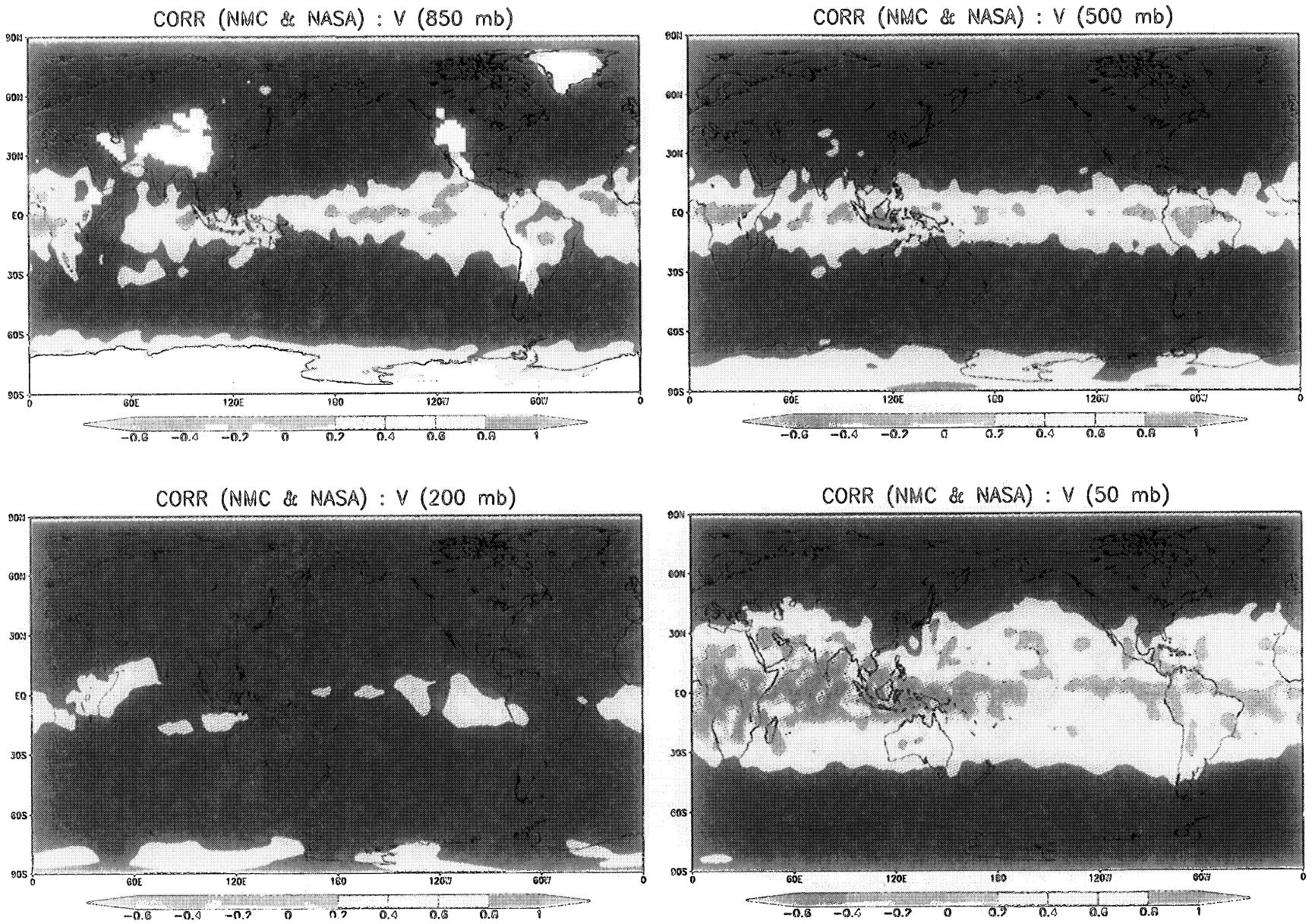

Fig. 1 Spatial map of the temporal correlation (based on 58 months of monthly mean data from March 1985 through December 1989) at each grid point between NMC and NASA reanalyses of the V-component of wind at the indicated levels.

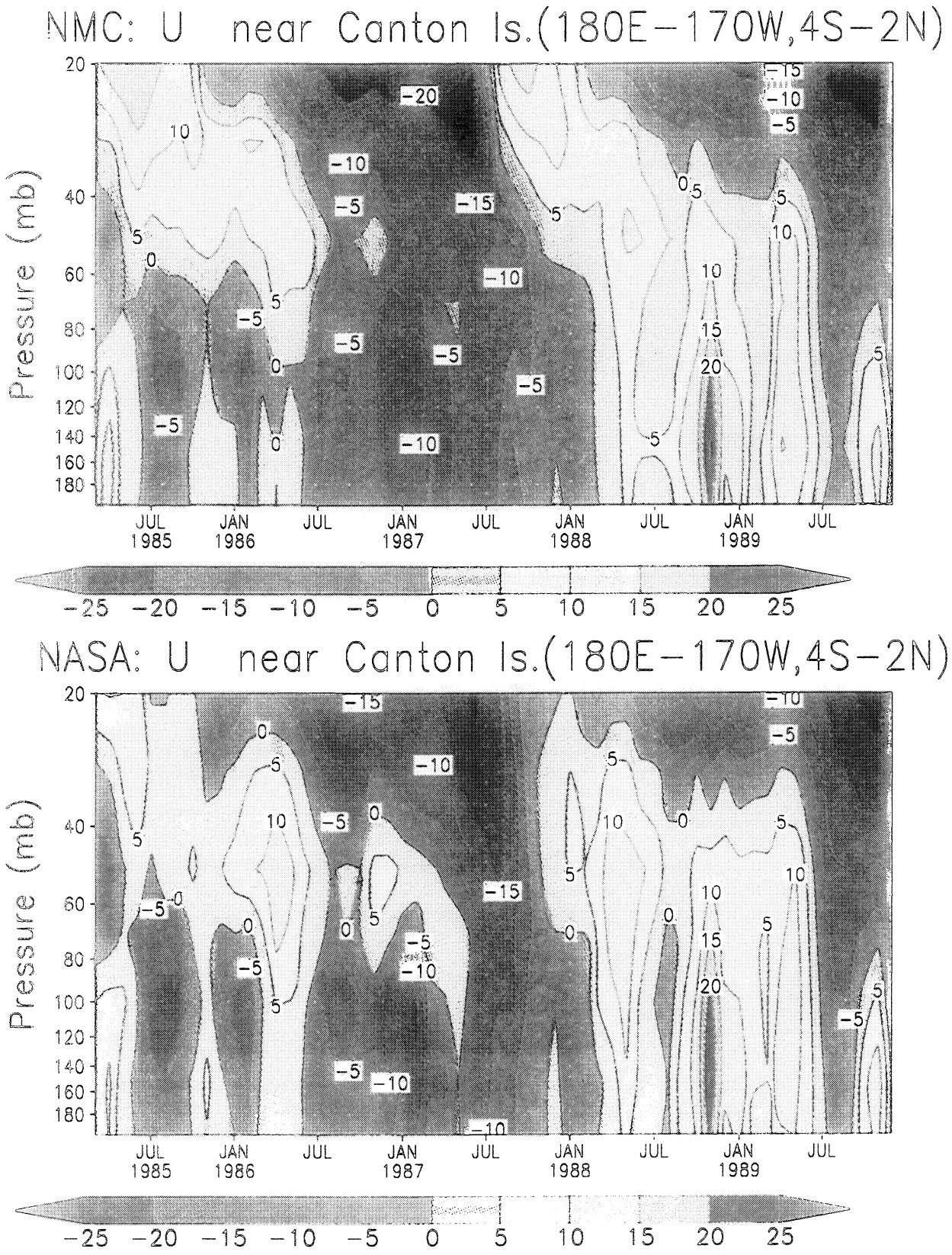

Fig. 2 Pressure-Time section of monthly mean area (180E-170W, 4S-2N) averaged zonal component of wind U near Canton Island for the NMC (top) and NASA (bottom) reanalyses.

PAGE 142 INTENTIONALLY BLANK

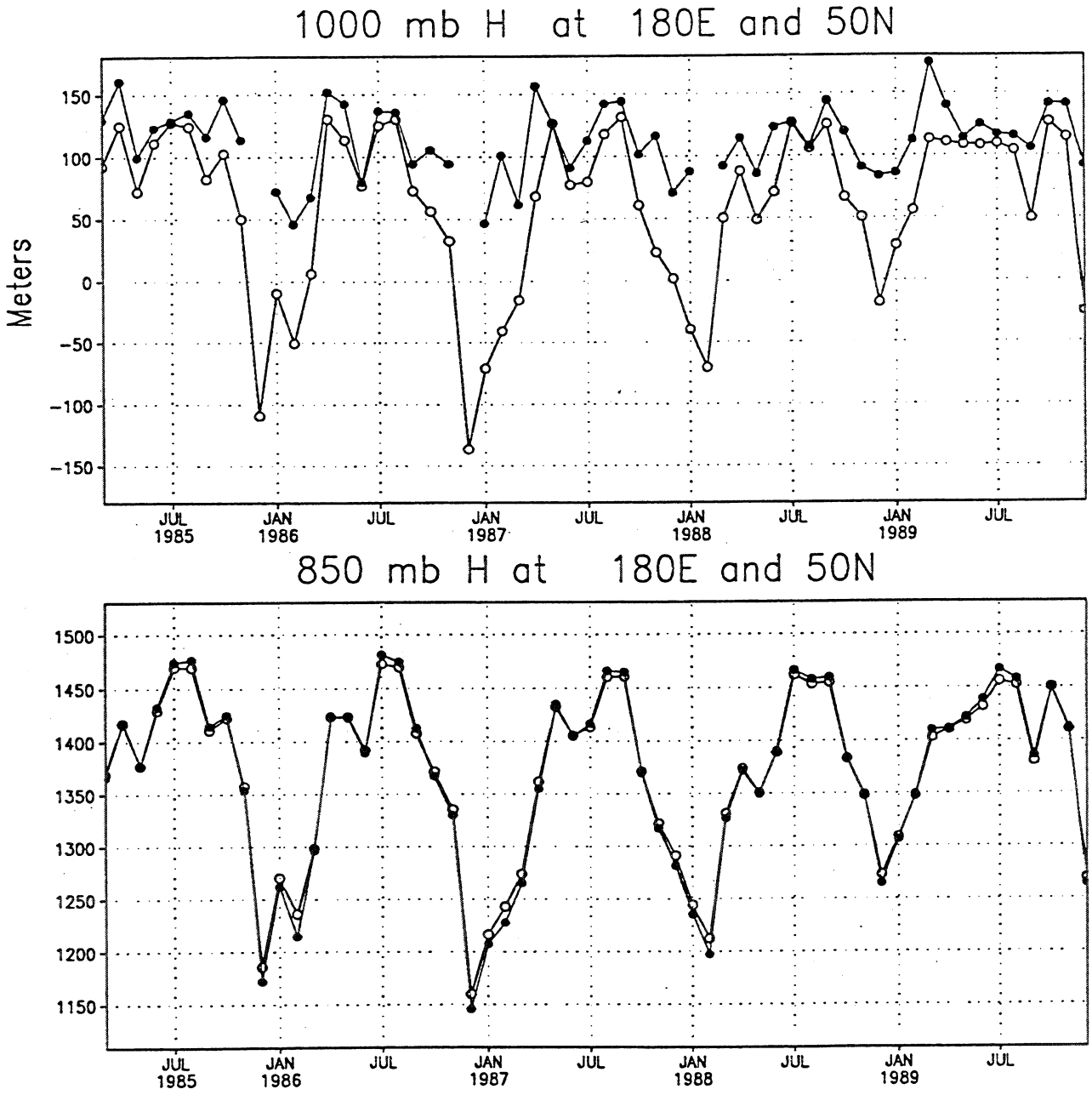

Fig. 3 Time series of monthly mean geopotential height (in meters) at 1000 mb (top) and 850 mb (bottom) at 180E and 50N. NMC is open circles and NASA is closed circles.

A COMPARISON OF SURFACE WIND PRODUCTS OVER THE NORTH PACIFIC OCEAN

Michele Rienecker
Oceans and Ice Branch
NASA/Goddard Space Flight Center

Four surface wind products which may be used to force ocean circulation models of the North Pacific are compared: wind stress derived from the the Atlas SSM/I based surface wind analyses (July 1987–June 1991), the Goddard Earth Observing System (GEOS) wind assimilation product at 10 m (March 1985–February 1990) and, at the appropriate overlapping times, the ECMWF wind analyses and the Comprehensive Ocean-Atmosphere Data Set (COADS). The COADS product used in this study, based on monthly-averaged winds, underestimates the monthly-averaged stresses in the higher latitudes where the submonthly variance is high. The largest differences between the model-based analyses tend to occur during winter in the northernmost region of the North Pacific basin where the spatial and temporal variability is largest. The seasonal mean Atlas SSM/I wind stress curl is consistently stronger (by up to 5 $\times 10^{-8}$ N m^{-3}) than the other products in both subpolar and subtropical regions, with larges differences occuring near the local curl maxima. In the zonal average, the GEOS and ECMWF curl are very close, and the Atlas zonal average curl is larger by up to 3 $\times 10^{-8}$ N m^{-3} in the high latitudes during Winter (Figure 1). The COADS curl based on monthly mean winds is too weak in the subpolar regions. The GEOS wintertime curl pattern is closer to COADS than ECMWF or Atlas SSM/I north of 40N but its magnitude is weaker than the other model products. Whereas the temporal rms variability of the GEOS curl is not as high as that of the Atlas SSM/I curl in the higher latitudes, the two are in good agreement in the tropics–subtropics. Of the four curl products, the Atlas SSM/I and GEOS are closest in pattern and intensity in the tropics in both summer and winter.

A quasi-geostrophic model of the North Pacific circulation has been forced with the COADS curl (with curl artificially increased by a factor of 1.3 to compensate for the use of monthly winds), with the GEOS curl and with the Atlas SSM/I curl. Although the overall mean streamfunction patterns are in generally good agreement, the Kuroshio Extension in both the GEOS and COADS is broad and diffuse (Figure 2), with maximum mean surface speeds of about 22 cm/s. The mean streamfunction from the Atlas curl, in contrast, shows a strong, coherent Kuroshio Extension out to 170E, with maximum surface speeds of about 40 cm/s. All simulations show a bifurcation of the Kuroshio Extension much farther to the east than normal — probably a consequence of the continued forcing of the basin by winds from a short time span. The maximum speeds in the Kuroshio south of Japan are 45 cm/s in the COADS simulation and 40 cm/s in both the GEOS and Atlas simulations.

The average subpolar circulation in the GEOS simulation is better organized than in the Atlas simulation, with a distinct gyre in the western half of the basin, in keeping with recent observations. There is also a more distinct, though small scale, recirculation in the Gulf of Alaska, in keeping with most observations. The southward penetration of the Oyashio in the western basin is better in both GEOS and Atlas simulations and highlights the negative impact of the weak subpolar curl in the COADS fields. The maximum speed in the Alaskan Stream is found off Kodiak Island in all three simulations and is 20 cm/s for COADS, 25 cm/s for GEOS and 35 cm/s for Atlas.

The distribution of surface eddy kinetic energy (not shown) is more realistic from the Atlas simulation, with penetration of high levels of energy out to 180E, at about half the energy level estimated

from GEOSAT altimeter data. In contrast, most of the eddy energy in both GEOS and COADS simulations is confined west of Shatsky Rise.

Data access experiences:

The GEOS surface time series (DIAG4 files) were accessed through the UniTree mass storage system on the NCCS Convex with no problems.

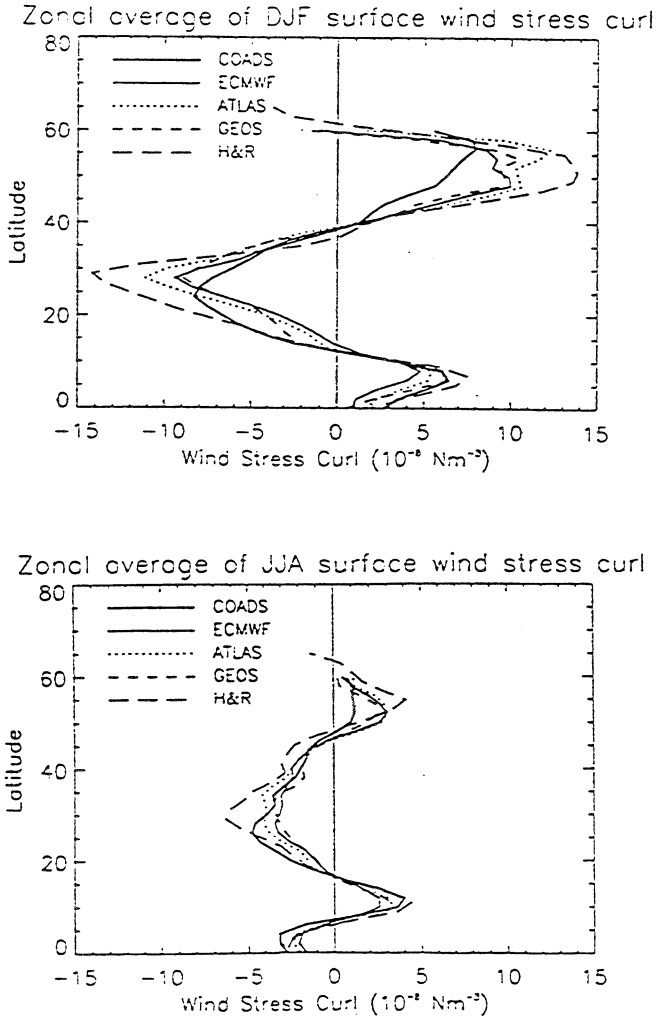

Figure 1: Zonal average profiles of seasonal mean surface wind stress curl from data products for 1987 to 1989 (December 87 excluded). The model-based curls are based on 12-hourly wind stress analyses; the COADS curl is based on monthly mean winds and have been scaled by 1.3 .

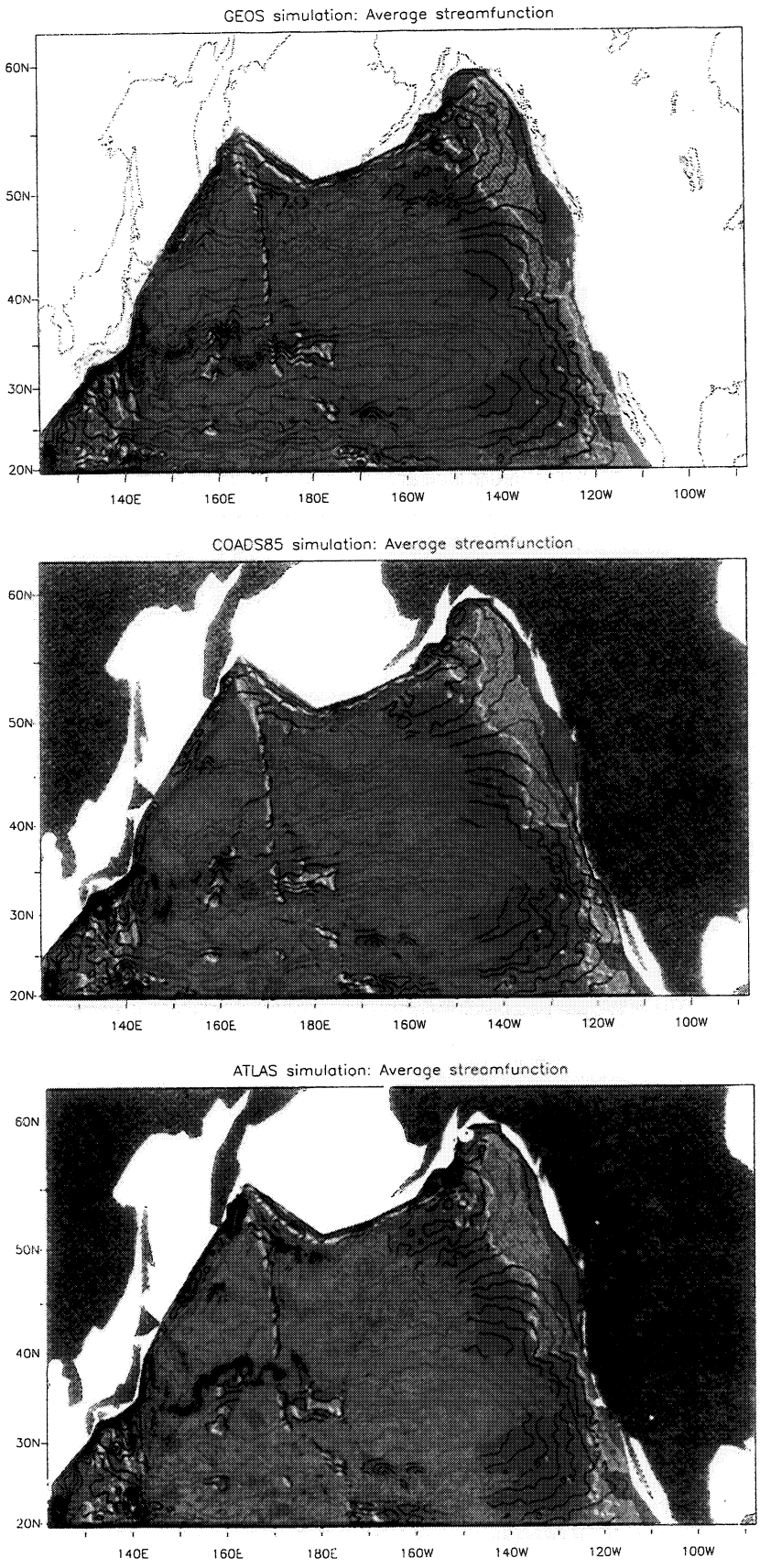

Figure 2: Mean surface streamfn from QG model simulations for 10 years, sampled every 5 days.

2.5 Related Projects and Collaboration

Reanalysis-related Studies at COLA

J. Shukla

Center for Ocean-Land-Atmosphere Studies
Institute of Global Environment & Society
Calverton, MD 20705-3106

1. INTRODUCTION

When the idea of reanalysis was originally suggested (Fein, personal communication; Bengtsson & Shukla, 1988), it was difficult to find a NWP group that was willing to undertake the massive task of assembling the data sets and conducting the reanalysis with a "frozen" analysis-forecast system. The operational centers, which have the primary mission to improve forecasts for the future, found little justification for reanalyzing the data for the past. The research centers considered the task to be routine, tedious and boring. It is in this context that COLA proposed to carry out a pilot project to reanalyze 18 months of data during 1982-83 to establish the feasibility of reanalysis (Kinter and Shukla, 1989; Paolino et al, 1995). Subsequently, several groups (NMC, GSFC, ECMWF, NRL) have started a massive effort to reanalyze past meteorological observations (Kalnay and Jenne, 1991; Schubert et al, 1994).

The original idea of reanalysis was dominated by the problem of spurious variability introduced by frequent changes in models and data assimilation systems at the NWP centers. For brevity, we consider data quality control procedures to be part of data assimilation system. However, with so many groups conducting reanalysis for the same period, we are now faced with new questions. For example, how do we interpret the differences among various reanalysis products? Are they simply due to differences in models and data assimilation systems of various groups, or are they due to different input data used by different groups? In this respect, we are faced once again with the same problem we had before reanalysis was started in that we have to compare results from quite different models and data assimilation systems. Furthermore, due to special field experiments and the introduction of space-borne observing systems, there are large changes in the amount and type of input data for reanalysis.

2. PROPOSED STUDIES AT COLA

COLA has no plans to conduct reanalysis to produce data sets. However, COLA plans to conduct several reanalysis-related investigations which are summarized below.

2.1 Quantification of "Irreducible" Uncertainty in the Description of the General Circulation of the Atmosphere

As mentioned in the introduction, there are substantial differences in the models and data

assimilation systems used by different groups for reanalysis. We would like to propose that several (if not all) groups re-reanalyze certain periods (1-5 years) using identical input data. Assuming that all analysis-forecast systems had comparable skill in short range (0-3 days) weather forecasting, the differences among re-reanalyzed fields will be considered as the inherent uncertainty in defining the general circulation of the atmosphere. COLA will obtain the re-reanalyzed fields from each group and carry out a comprehensive analysis of the annual mean, annual cycle, and intraseasonal variability of general circulation including heat, momentum, and water fluxes, energy and water cycle and spectral energetics.

It is expected that as different groups improve short range predictions by improving their models, quality control procedures and assimilation systems, the reanalyzed fields using identical input data will converge and reduce the uncertainty of the general circulation of the atmosphere.

2.2 Feasibility of Reanalysis for the Period 1900-1960

The absence of upper air data in the first part of the twentieth century makes it difficult to conduct reanalysis. However, global SST fields can be used to force realistic atmospheric GCMs to produce tropical heating fields and global circulation fields. Additional research will be necessary to develop relationships between surface pressure tendency and the vertical structure of the divergence. Variational methods need to be developed to determine three dimensional circulation fields that are consistent with surface observations of rainfall, pressure and pressure change.

Observing system simulation experiments need to be carried out by artificially degrading the observing system for the current period to investigate the feasibility of reanalysis for the early periods.

2.3 Reanalysis for Climate Change

It has already been noted that the introduction of new observing systems can produce spurious climate variability. Therefore, for the purpose of investigating climate change using reanalysis data, it is not sufficient that the model, the quality control and the assimilation system be frozen for the entire period. It is also necessary that there are no large changes in the input observations.

Based on the observing system simulation experiments for the current data-rich period, a minimal observing system needs to be determined which can be used to reanalyze past data to study climate change.

In summary, there are several research questions related to reanalysis that need to be investigated, including the techniques for combining insitu and space observations. Addressing these questions is no less important and urgent than carrying out large volumes of reanalysis with different models.

3. REFERENCES

Bengtsson, L. and J. Shukla, 1988: Integration of space and in situ observations to study climate change. *Bull. Amer. Met. Soc.*, **69**, 1130-1143.

Kalnay, E. and R. Jenne, 1991: Summary of the NMC/NCAR reanalysis workshop of April 1991. *Bull. Amer. Soc.*, **72**, 1897-1904.

Kinter, J. L. and J. Shukla, 1989: Meeting Review: Reanalysis for TOGA (Tropical Oceans Global Atmosphere). *Bull. Amer. Meteor. Soc.*, **70**, 1422-1427.

Paoline, D. A., Q. Yang, B. Doty, J. Kinter, J. Shukla, D. Straus, 1995: Results of a pilot reanalysis project at COLA. *Bulletin of the American Meteorological Society*, **76**, 1-10.

Schubert, S. D., R. B. Rood, and J. Pfaendtner, 1994: An assimilated dataset for earth science Applications. *Bull. Amer. Met. Soc.*, **74**, 2331-2342.

Re-Analysis Problems - Some Experiences gained with the ECMWF Re-Analysis (ERA) Project

J. K. Gibson

Project Manager, ERA Project, ECMWF

1. Introduction

Re-analysis is a complex and costly process. Building a re-analysis system requires careful choices to be made with respect to the scientific validity of the components to be used, and the technical integration of those components into a reliable and robust system. The resulting system must contain sufficient checks to ensure the elimination of gross errors, but must be sufficiently optimised to enable re-analysis to proceed at a fast pace. Data must be processed which are many years old, may have undergone several transformations, and which may require further transformation before being compatible with the re-analysis system. Each transformation is a potential source of data error or data loss. Problems also occur because of changes to the hardware and systems software which provide the environment in which the re-analysis system is run.

2. Choice of System

The choice of the various components of a re-analysis system is inevitably a compromise between:

- the current scientific "state of the art"
- the desire to generate a well proven system
- the resources available.

Experience at ECMWF has been that these choices benefit from an iterative process. The generation and optimisation of the re-analysis system provides the means for rapid analysis. This results in an excellent tool for the advancement of research. This in turn leads to the possibility of generating a better re-analysis system. Thus there is the major problem of when to call a halt.

There are two solutions. First, a pragmatic approach is necessary. Potential components must be assessed both as candidates for inclusion, and on performance after inclusion. Eventually, when after consultation with appropriate experts it is agreed that the best system in the circumstances has been identified, full production must be attempted. For the ERA Project various Validation Projects have been set up. The Validation Partners have proved invaluable in the process of checking and validating the components which were eventually incorporated into the ERA system.

The second solution is to regard re-analysis as an ongoing process which must be repeated at appropriate intervals. The first solution is still relevant, but in this case during the production phase the assessment process can continue, with the objective of generating a better system for the next re-analysis. A consequence of this approach is that the production phase should generate as much in terms of helpful metadata as possible to enable subsequent re-analyses to benefit from production experience.

3. System Generation

The main source of problems in this area are:

- the complexity of the system required
- incorporating resilience
- scheduling the component processes
- making best use of the computer resources
- generating the required results
- making the archive of results usable

The ERA system is based on the concept of many small computer tasks, each typically one job step. These are linked using a programmable scheduler which can control processes across the available computer environment. Since each process is simple, processes may be re-run usually without side effects. A failed process usually indicates the precise area which is problematic - simply because it performs a single task. Production processes are run over and over again. Thus, once they are developed and debugged they can be expected to be reliable. The scheduler has a graphical interface, which enables relationships between processes to be visualised. It also has a command line interface enabling maintenance to be performed using dial-up services from home.

The scheduling system in use enables complex task dependencies to be resolved. Thus it is possible to analyze the data flow, run data processing tasks as far ahead as is reasonable, and generate many applications which can run in parallel. The computational resources have been chosen such that the forecast model, objective analysis and 1 dimensional variational satellite retrieval run on the Cray C90. Two two Silicon Graphics (SGI) Crimson servers handle the bulk data and data management. SGI Indigo workstations are used for graphical display. Relational data bases obtained from Empress Software Inc. are used for observations, analysis feedback statistics, and global fields of analysis and forecast results. Metadata are stored as relational entities, while whole observations and whole products are stored as binary bulk data. This enables the relational aspect of the data bases to be used for duplicate identification, data identification, and for access to selected sub-sets of data - essential in dealing with data problems.

The ECMWF Meteorological Archive and Retrieval System (MARS) has the ability to check the data base attributes of the data bases on the C90, the SGI servers, and the main archive. Thus results are accessed via a common interface, irrespective of residence. MARS also contains features which enable sub-area extraction, interpolation, access to sub-sets of fields, etc. The interface to MARS is well known to users within the ECMWF and its Member States, thus enabling access to the data by Validation Partners immediately they are produced.

4. Data Related Problems

These may be categorised as problems related to:

- data selection;
- data conversion;
- duplicate elimination;
- data quality.

4.1 Data Selection

In the ideal world there would be a surfeit of data such that, for re-analysis purposes, it would be

possible to identify a subset of data which would be constantly available for each analysis cycle throughout the re-analysis period. Since this is far from the case, and since observations, to some extent may be regarded as "forcing parameters" with respect to the forecast model, it is believed that the variability of their availability is somewhat less important than the use of a consistent data assimilation system with respect to analysis and forecast model components.

One problem regarded as very important with respect to ERA is that of the gradual improvement over the years of satellite sounding data. The solution adopted has been to use the cloud cleared radiance data directly with a 1 dimensional variational system. Since the instrumental responses have been reasonably similar over the ERA period (1979 through 1993) this approach should limit the variability of the satellite data used.

With respect to other data it was decided to use all data which could be reasonably collected within the available resources. The ECMWF archive, supplemented by selected data from the archive of the Japan Meteorological Agency (JMA), FGGE 2b, COADS, ALPEX, and 250 km Cloud Cleared Radiance data form the main data sources. Australian PAOB surface data are used with a low weighting to supplement the analyses in data sparse areas of the Southern Hemisphere.

4.2 Data Conversion

The interface to ECMWF applications which use observational data is the WMO FM94 BUFR. However, BUFR has evolved over the years, and some applications are less tolerant of these changes than others. Rather than go through each application and add the appropriate flexibility it was decided to convert old data to modern standards. This has proved a major undertaking, and has occasionally resulted in somewhat unexpected problems.

One such problem relates to TEMP data. BUFR requires TEMP data to use geopotential as a vertical co-ordinate. Character code TEMP data contain heights in geopotential metres. The Meteorological Community has only slowly caught up with the rest of the scientific community with respect to their interpretation of the conversion required. Originally the conversion factor was defined as 9.8. This was later amended to 9.80665. Not everybody introduced this change at the same time - in fact ECMWF only introduced it into some of their applications very recently. This illustrates the type of problem that can arise every time units are converted. On the other hand, if parameters are always retained as reported the full information with respect to the then reporting practice must be preserved.

When data are converted mistakes can be made. Early ECMWF BUOY reports contain identification numbers which are missing the first two digits, and padded with two zero digits at the end. Thus they are no longer unique, making a tracking check difficult.

A further problem related to data conversion results from minor differences in data representation and data storage accuracy between different computers. Thus minor differences of positional parameters such as latitude and longitude can be introduced simply because the same observation has been converted to the desired form, but using different computers.

4.3 Duplicate Elimination

The positional data conversion problem listed above initially caused problems with respect to the identification of duplicate ships which occur both in the MARS observations and in COADS. It was solved by introducing a deliberate rounding of the positional attribute used within the Empress data base. This solution is rather elegant, as it leaves the observational data unchanged.

Identification of duplicate ship data is made more difficult because of two problematic occurrences:

- some ships are received both with, and without their correct identification characters;
- some ships reports are received twice as two separate data types (eg both as a ship, and as an abbreviated ship)

Since, for re-analysis purposes, only that sub-set of ship information included in the abbreviated ship message is actually used, both of the above problems were solved by omission of the data type and the identification from the duplicate check. Thus any ship report having the same date/time and location (within epsilon) as one already encountered is regarded as a duplicate and ignored.

4.4 Data Quality

Pre-analysis quality control at ECMWF is based on:

- consistency checks with observations, normally carried out during decoding;
- blacklisting, based on analysis of the feed-back statistics from the data assimilation system;
- bias correction of TEMP data, using a scheme dependent on sonde type, solar angle, and previous history;
- ship and buoy tracking;
- running the OI analysis in check mode to assess likely observation errors prior to the analysis proper.

For ERA a reasonably comprehensive blacklisting is carried out, and the operational bias correction scheme for TEMP data has been implemented for a limited sub-set of well known radiosonde types. A major problem in this area is that, with the speed of re-analysis production, it is impossible to be as thorough as is the case for the operational system. A bye-product of the re-analysis is that tools are being developed to enable a better assessment of contamination from observational errors.

Where there has been a known loss of quality, such as is the case with the ECMWF archive of BUOY data, the strategy followed is to select the best source and insert data from that source first. Thus it has been identified that the best source for the BUOY data is COADS, which are added first to the data base. Buoy data from the ECMWF archive are added later, and only get added if the corresponding data was not in the COADS set.

There are other aspects of data quality about which little can be done. There was one occasion where the results of an analysis made the subsequent forecast unstable. Data type were removed one by one, until the removal of one data type from one source made the difference between a stable and an unstable solution. The source of this error is still not known, but even the investigation carried out so far resulted in a delay which put back production by a couple of months.

Other aspect of data quality have important repercussions for re-analysis. One such aspect is the apparent improvement in the TEMP quality over the period since 1979. Initial investigations using the ERA system indicate a significant improvement in the fit to radiosonde data even when results from 1979 and from 1985 are compared. A further breakdown by known radiosonde types supports the finding that this improvement is real, and is associated with sub-sets of the system known to have changed to better instruments.

4.5 Satellite Data

There are a number of problems specific to satellite data processing. These include:

- variable quality with respect to the derived soundings;
- operational problems concerning specific channels on specific satellites for specific periods;
- miss-located data;
- missing data.

The ERA assimilation system uses the cloud cleared radiance data directly, avoiding the problems related to the variability of the derived soundings.

NESDIS have been extremely helpful in providing lists of known operational problems. These have been useful, enabling the strategy for satellite data inclusion to be defined in advance. Additionally, all CCR data have been scanned in advance, analyzed with respect to individual brightness temperatures, and information derived to help decide which satellite(s) to use when. This information has also been effective in supplementing the NESDIS lists with respect to dates which require caution, and additional dates which require re-processing of the 1b data have also been identified.

Calibration of the radiance data is made for the ERA system on a monthly basis, using the previous month's accumulated statistics. On dates where there is a significant change in instrument characteristics production is interrupted so that re-calibration can be based on a reasonable period of analysis, and that period re-run with the corrected calibration.

Algorithms have been derived to check the satellite location information in the CCR data, and to make corrections where data are miss-located.

A system to generate 250 km CCR data from the 1b data has been prepared, and will be used to supplement gaps of more than 3 days in the 250 km CCR data.

Overview of the NMC Reanalysis Project

R. Kistler, J. Woollen, M. Kanamitsu, S. Saha and E. Kalnay
National Meteorological Center
Washington DC 20233

In this project a 40-year reanalysis of past atmospheric and oceanic data will be performed over a period of 3 years using a state-of-the-art but frozen data assimilation system (Kalnay et al., 1995). The observations (including many data sets that were not available in real time) have been gathered at NCAR. The old data will be reassimilated within an analysis cycle with the statistical analysis and model modules are kept unchanged throughout the Reanalysis. In addition, starting in January 1995, the same system of data assimilation will be continued into the future as a "Climate Data Assimilation System" (CDAS), so that the climate researchers can compare the present climate anomalies with a very long climatology obtained with the same frozen reanalysis system. The project should be completed by 1997. At that time there will be 40 years of reanalysis/CDAS available to the research community (1957-1996).

In order to perform this huge task within a reasonable time, we have to carry out the reanalysis at a much faster rate than the operations (which go at a rate of just one day of analysis per clock day). This has required the development of a new system able to perform one month of reanalysis per clock day, and for which humans can monitor the quality of the input data and of the output products at a much faster rate than is possible in operations. The Reanalysis system was developed over three years, and the execution phase started in June 1994. In the next section we describe the main computer system characteristics of the reanalysis system, and a new way to process the data, and in the last section we review results from the 1985-1990 reanalysis already completed.

System Configuration

The CDAS/Reanalysis is executed at the the NOAA Central Computer Facility in Suitland, Maryland. Unlike the operational NMC system, which currently is based on both IBM-MVS type and Cray-UNIX computers, in the CDAS/Reanalysis system all processing is done in the Cray-UNIX environment. This new system eliminates the transmission of large amounts of data across different systems, has many new advanced features, and will be also adopted in the NMC normal operations. The Reanalysis will be performed using the present Cray YMP 8 processors, 128 MW supercomputer and the smaller Cray EL2. Other hardware includes a Robotic Silo, upgraded to 4490 STK, with storage capacity of 0.6GB per tape. 2200 Silo slots have been reserved for this project. Since the Cray YMP was saturated, the start of the Reanalysis had to wait for the new Cray C90 acquired by NMC to be installed (early 1994) and the operational systems migrated out of the Cray YMP (April 1994). Software used includes the Unicos 8 operating system, workstation NFS mount of Cray complex files, POSIX (Korn) shell UNIX scripts, Fortran, some C, some X Windows, the Data Migration Facility, the Cray Reel Librarian, and the graphics system GrADS (COLA). We expect that the Cray YMP and Cray EL2 will be replaced in 1995 by two Cray J916's.

The Reanalysis System

The NMC/NCAR Reanalysis System has three major components:

a) Data preparation module:

In this module, observations from many different sources and different formats are decoded, sorted and checked for duplicates. They are encoded into BUFR (Binary Universal Format Representation). This BUFR representation has been extended, so that it includes not only the data itself, but also its history as it is processed and quality controlled in the Reanalysis System. For example, each datum will include the climatological average for that variable at its space and time location, as well as the first guess and the final analysis value. The complex quality control system at NMC frequently corrects the observations when communication problems result in simple errors such as digit transposition. The BUFR data will contain the original value, the corrected value, and the results of other quality control decisions. The logistics involved in automatically recording and reviewing quality control "events" are quite challenging. The flexibility of the BUFR format makes the methodology described above feasible. Manipulation of the BUFR reanalysis datasets has been simplified by the development of BUFR interface program library routines, which separate application programmers, or Reanalysis users, from many of the technical aspects of the BUFR format, allowing read/write access to information by means of mnemonic references and queries similar to databases. The machine independent FORTRAN programs and documentation will be available to investigators who can, for the first time, easily obtain useful information about the quality of the observations.

This module preprocesses data for sequences of a year or longer, and the results are presented to human monitors. If major problems are encountered, such as missing data, data mislocated, etc., specialists have a few days to correct them before the execution of the data assimilation module, which is the most computer costly.

b) Data assimilation module:

This is the core of the system, and includes a model and analysis system as in Fig. 3. The model has horizontal resolution of about 210 Km and 28 vertical levels. The model is identical to the NMC global model operationally implemented in January 1995, except for the horizontal resolution, which is double for the operational model (Kanamitsu, 1989). The analysis is performed with the Spectral Statistical Interpolation (SSI or 3-D variational) analysis, (Parrish and Derber, 1992). The quality control includes complex QC of rawinsonde data, with confident corrections of heights and temperatures (Collins and Gandin, 1992) and Optimal Interpolation based complex QC of all other data (Woollen, 1991, 1994).

c) Reanalysis output and data distribution:

The reanalysis archive has been designed to satisfy two major users' requirements: the output should be comprehensive, allowing, for example, the performance of detailed

water budget studies, and it should be easily accessible to the user interested in a long time series of data. It is not possible to satisfy both requirements with a single archival format. For this reason the output module includes several different archives, including level-2 BUFR data archive with QC metadata, comprehensive sigma and time series files, and 8-day forecasts. A "quick look" archive on CD-Roms, one per year, has been developed including most widely used fields: daily values of variables at selected pressure levels, surface and top of the atmosphere fluxes, precipitation, monthly and zonal averages of most quantities, covariances, isentropic level variables, etc.

Part of the output is posted in the NMC public server NIC, and is available through anonymous FTP. NCAR, the National Climatic Data Center and the Environmental Reasearch Laboratories/Climate Diagnostic Center will distribute the bulk of the reanalysis data.

Execution

The execution phase of the reanalysis started in June 1994, on the Cray YMP-8 supercomputer provided by NMC for this project. About 24 hours of the CRAY YMP (2-7 processors) are needed in order to perform one month of reanalysis and forecasts per day. By April 1995, ten years (1985-1994) should be completed (in addition to several years of reruns performed to assess the impact of changes in observing systems, etc.). Next the period 1979-1985 will be reanalyzed, and completed around October 1995, followed by the 1957-1978 decades. We expect to complete the 40 years of reanalysis (1957-1996) by early 1997. The extension into 1948-1957, if feasible, would be done during 1997.

This first phase of reanalysis will be followed by a second phase in which a 1998 state-of-the art system will be used for reanalysis. NMC plans currently call for an updated reanalysis every five years or so.

Results

Results and "lessons learned" will be presented at the workshop.

Reference

Kalnay, E., M. Kanamitsu, R. Kistler, W. Collins, D. Deaven, L. Gandin, M. Iredell, S. Saha, G. White, J. Woollen, Y. Zhu, M. Chelliah, W. Ebisuzaki, J. Janowiak, K. C. Mo, C. Ropelewski, J. Wang, A. Leetmaa, R. Reynolds, and Roy Jenne, 1995: The NMC/NCAR Reanalysis Project. Submitted to Bull. Amer. Meteor. Soc.

Roy Jenne
18 Apr 1994
Rev 23 Mar 1995

Observations for Global Reanalyses

The task to assemble the world's daily observations that are needed to reanalyze the atmosphere each 6 hours for many years will be described. This is a huge number of observations. The data include surface data (for land and oceans) and upper air data, including remotely sensed data. We will briefly describe the work to assemble the data (NCAR's role). The work at NMC to ingest the data and prepare it for reanalysis is described elsewhere. The data include data from real-time global telecom, and delayed data from the archives of a number of countries.

The data needed to reanalyze the atmosphere are extensive. We want to prepare most of the world's surface and upper air observations from about 1948-on. In this present work we are focusing on daily data over both land and ocean areas from 1957-on, but a considerable amount of the earlier data has also been prepared. The data are from ships, buoys, and land stations. They include upper air data from rawinsonde balloons (usually twice daily) and from aircraft. The global satellite sounders start in 1969, and satellite cloud drift winds start in 1967. This is a lot of data. We owe special thanks to all of the observers of the world.

NCAR has the data tapes of observations from the NMC processing of upper air data from global telecom (GTS) for 1962-on; these are still in the original NMC file structures so that it is possible to detect and correct problems. The first step of data preparation is to take these major existing datasets and fix some time and location problems. Then many other datasets are added to increase the data coverage and extend the data back in time. Many diagnostics are required to find the problems that exist in the data so that they can be fixed. NMC has been obtaining data for 1979-93 from NCAR. The older data will be sent in time to keep ahead of the reanalysis schedule. The status of the projects at NCAR to prepare major types of data follows:

- Global rawinsondes and upper winds (e.g., pibals), with data starting 1946 to 1950.

- Aircraft and reconnaissance data start 1947. GTS sources start Mar 1962. Some constant level balloon data are included. Data from projects like GATE are included.

- Satellite sounding data starts Apr 1969. VTPR started in Nov 1972. The NOAA TOVS started in Nov 1978. The 2.5° TOVS cloud-cleared data will be used in reanalysis. Most of the data are ready.

- Satellite cloud winds. Data exists on the original NMC tapes from about 1967. Delayed archives start 1974 for GOES and 1978 for GMS.

- COADS: Global surface marine (ships and buoys) and pack ice buoys. Data for 1980-93 is done. We are developing a new, more complete version of COADS for 1947-79.

- Global land surface synoptic data. Coverage is good for Eurasia and Australia by 1948. GTS sources start mostly in 1967. These data are almost all ready at NCAR.

- Projects to prepare station library data. There are location and elevation errors on the operational tapes. There are also errors in the station catalog tapes that exist. NCAR has run many diagnostics to detect problems, and has corrected the serious errors.

A text is available from NCAR that gives a feeling for data coverage versus time: "Data for Reanalysis, Inventories," Jenne, Nov 1992. NCAR also has a series of texts that describe the component datasets used to prepare the major datasets above.

The staff on this project at NCAR is rather small (3 FTE), but we can draw on many years of work already done. Also, other nations and centers have provided data.

Figure 1 shows the global coverage of rawinsonde data in 1958. In general, the coverage is quite good. The stations on the west coast of S. America and most of Antarctica started July 1957. Prior to that time there will be poor coverage for the southern part of the southern hemisphere.

NMC/NCAR Reanalysis Summary

1. Resolution
   - — T62, 28 levels (208 km)
   - — Output each 6 hours

2. Seven years done (1985-91), in Mar 1995; will rerun some to fix problems with SSMI data.

3. Data for each 6 hours
   - Sigma (on Gaussian) (28 levels)
   - Pressure (2.5°) (17 levels)
   - Isentropic (2.5°) (11 levels)
   - Flux fields (on Gaussian)

4. Data formats used
   - — The International WMO GRIB and BUFR formats
   - — Data are compact, speed is fast
   - — User learning time is very small for GRIB

5. Data access
   - On-line at NCAR
   - Master Exabyte tapes for bulk access
   - One CD-ROM each year has subset (prepared by NMC)

6. Period for reanalysis
   - 1957-96 (40 years)
   - Maybe also do 1948-56

7. For more information:
   - — Paper in Bull. AMS (Dec 1991)
   - — New paper for Bull. AMS
   - — Obtain list of papers at NCAR
   - — wd23ek@sunl.wwb.noaa.gov (E. Kalnay)
   - — jenne@ncar.ucar.edu

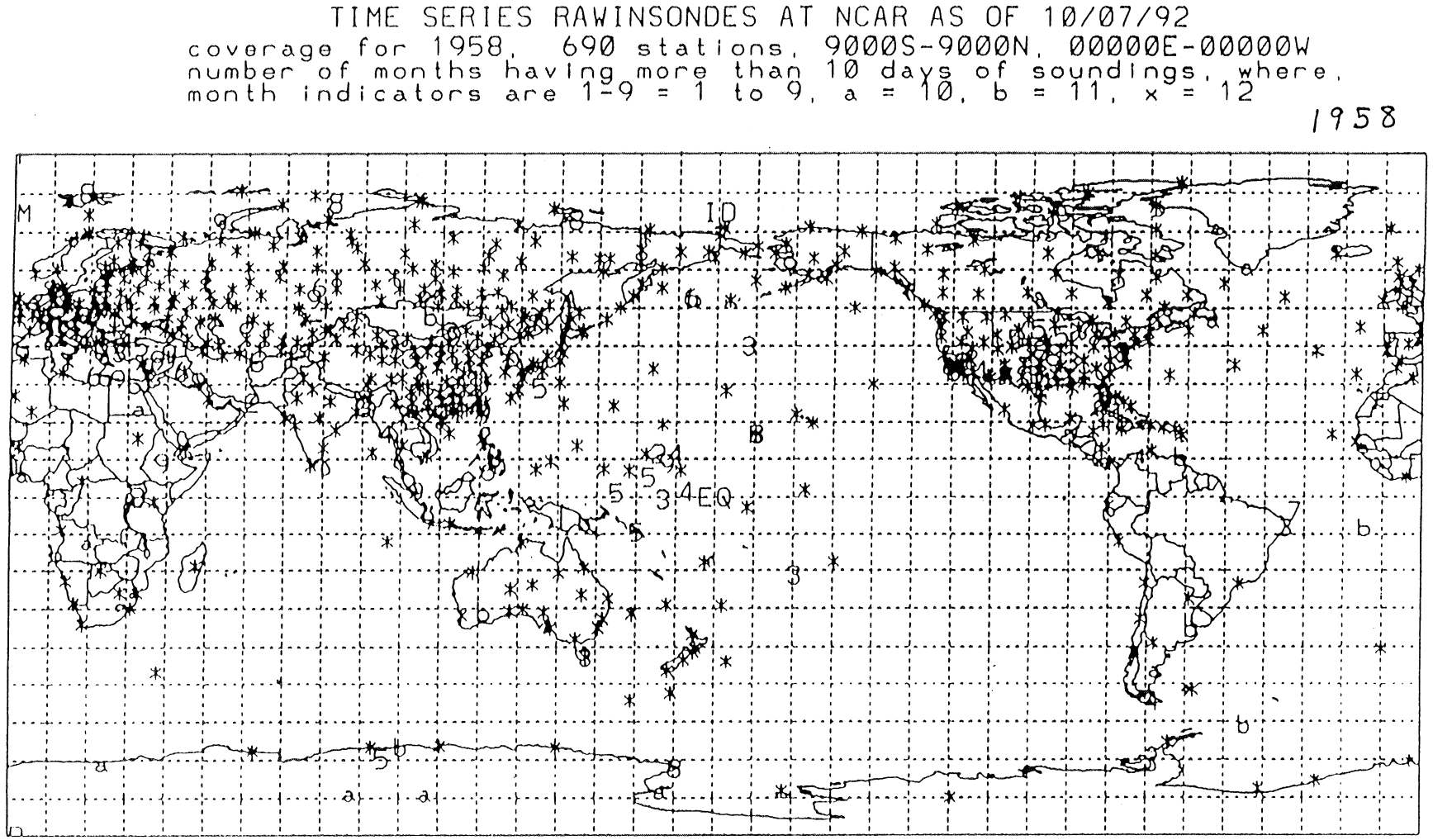

Figure 1. Coverage of daily rawinsonde data in 1958. A '*' means that daily data is available for all 12 months (a 'b' means 11 months, '5' means 5 months, etc.). Most stations take two observations each day.

2.6 Current and Future Development

On the Use of Coordinate Rotation in the Goddard Earth Observing System Data Assimilation System

by

Lawrence L. Takacs
Laboratory for Atmospheres, Data Assimilation Office
NASA/Goddard Space Flight Center
Greenbelt, Maryland 20771, USA

In this report we examine the impact of using coordinate rotations in the Goddard Earth Observing System (GEOS) Data Assimilation System (DAS). The GEOS-DAS is currently being used at NASA/GSFC's Data Assimilation Office (DAO) to produce multi-year global assimilated datasets for atmospheric and climate research. In addition, the GEOS-DAS is being used in field missions such as the Airborne Southern Hemisphere Ozone Experiment / Measurements for Assessing the Effects of Stratospheric Aircraft (ASHOE/MAESA) for the planning of flights by the high-altitude ER-2 aircraft.

The Eulerian grid-point dynamics module used in the GEOS-DAS is the Aries/GEOS Dynamical Core (Suarez and Takacs, 1995). This module discritizes the momentum equations, written in vector-invariant form, using a fourth-order energy and potential enstrophy conserving scheme on the Arakawa C-grid. Inherent in many schemes of this type is the computational instability discussed by Hollingsworth et al. (1983) which arises from the non-cancellation in finite-difference form of the underlined terms illustrated in the following shallow water example:

$$\frac{\partial v}{\partial t} + \left(fu + u\frac{\partial v}{\partial x} - \underline{u\frac{\partial u}{\partial y}} \right) = -\underline{\frac{\partial}{\partial y}\left(\frac{1}{2}u^2\right)} - \frac{\partial}{\partial y}\left(\frac{1}{2}v^2 + gh\right) \qquad (1)$$

An analysis of the linearized system shows that the instability is proportional to the mean zonal wind speed, U, and the coriolis parameter f. While this instability is easily controlled away from the poles by using a slightly modified kinetic energy formulation, variations of the scheme near the poles required from conservation constraints still result in polar noise when confronted with strong cross-polar flow. By rotating the computational grid to the geographic equator, however, the instability near the computational pole is removed due to the vanishing coriolis term. In addition, the geographic pole now using the transformed grid is also free of noise.

The accompanying figure shows instantanious results at 1 mb of wind speed, vorticity, and temperature from the GEOS-DAS assimilation, using both the rotated and non-rotated systems. The plots are of the northern hemisphere from 50° N to 90° N.

References

Hollingsworth, A., P. Kållberg,, V. Renner, and D.M. Burridge, 1983: An internal symmetric computational instability, *Quart. J.R. Met. Soc.*, **109**, 417-428.

Suarez, M. J., and L. L. Takacs, 1995: Documentation of the Aries/GEOS Dynamical Core Version 2, NASA Technical Memorandum 104606 Volume 5, Goddard Space Flight Center, Greenbelt, MD 20771.

Rotated (Top) vs Non-Rotated (Bottom) GEOS Assimilation at 1 mb

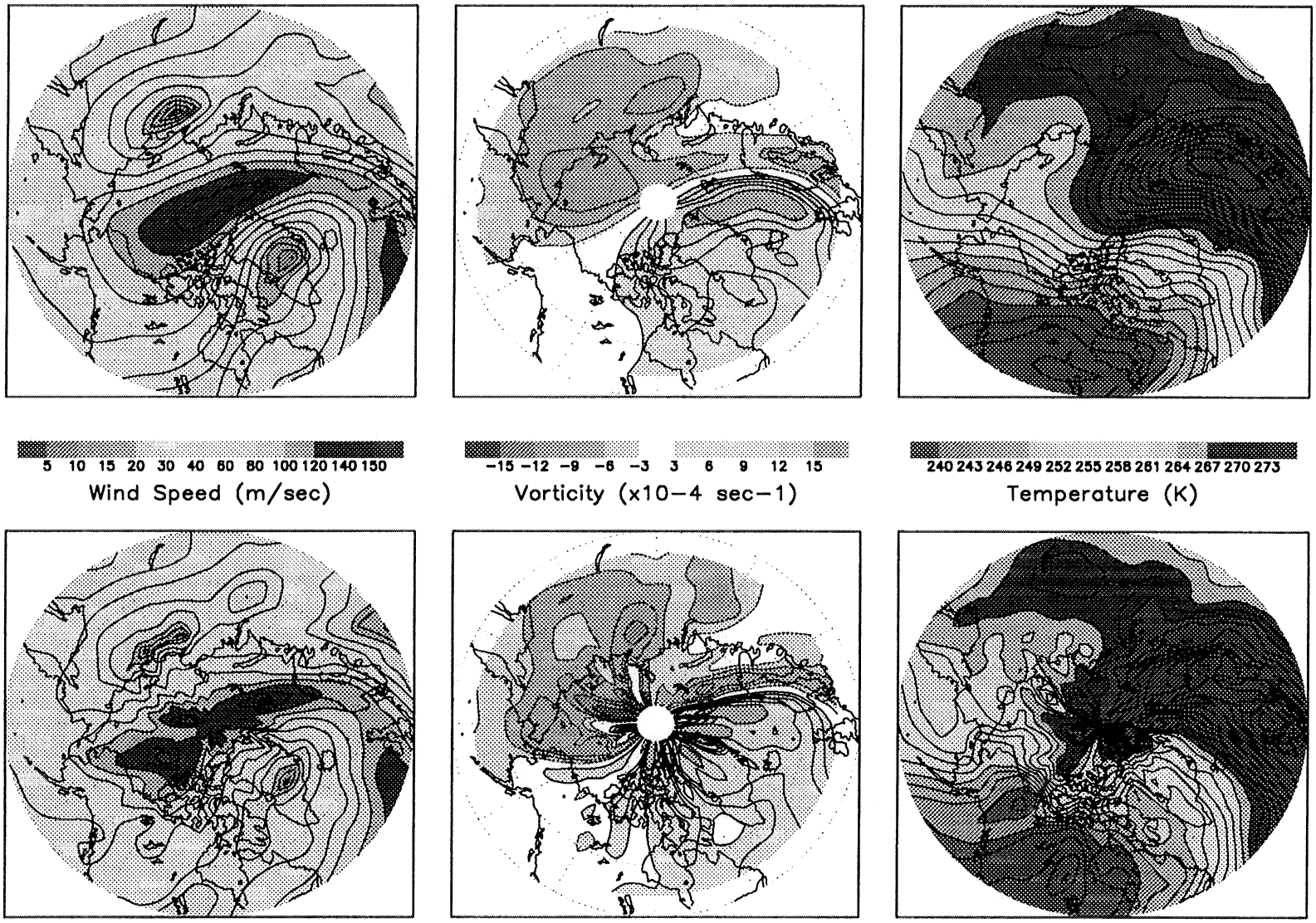

ON THE STRUCTURE OF WATER VAPOR AND CLOUDS AND THEIR TRANSPORT WITHIN BAROCLINIC WAVE REGIMES

Donald R. Johnson
1225 W. Dayton Street
Space Science and Engineering Center
University of Wisconsin
Madison, WI 53706

1. INTRODUCTION

Global distributions of precipitable water reveal large variability seasonally and regionally. In the Northern Hemisphere extratropics, the atmospheric water vapor between January and July increases by a factor of three over continental regions and by a factor of two over oceans. A global time scale basic to hydrologic interaction is a period of nine to ten days, commonly called the residence time. If replenishment by evaporation were lacking, this is the period required to deplete the global tropospheric reservoir provided precipitation were to continue falling at its time averaged rate. However, this global time scale results from markedly different time scales in extratropical and tropical regimes (Johnson et al. 1994). From the condition that the temporally, vertically, and zonally averaged meridional water vapor transport vanishes near 23°N in January, NH extratropical and polar latitudes enjoy a residence time of five days. This natural constraint imposed by the systematic differences in the equatorial transport of water vapor by the trades and poleward transport by baroclinic waves leads to the condition that, in the mean, the precipitation poleward of 23°N ultimately stems from evaporation of water vapor from the portion of ocean basins poleward of 23°N. During the wintertime, baroclinic waves in extratropical latitudes are the dominant circulation features that in effect transport water vapor from oceanic source regions to the continental regions. Moreover, accurate modeling of the water vapor balance in baroclinic cyclones and the cloud radiative interactive energy exchange of extratropical latitudes is absolutely essential to understand the climate system and advance earth system science modeling.

2. SOME PROBLEMS ENCOUNTERED IN ANALYSIS AND MODELING OF WATER VAPOR AND CLOUDS AND THEIR TRANSPORTS

Baroclinic amplification of waves in conjunction with vorticity advection, deformation and vertical wind shear creates "lens-like" filamentary and comma shaped structures of water vapor and clouds within extratropical latitudes. By virtue of the dominance of isentropic processes over much of the domain of baroclinic waves, these structures tend to lie along isentropic surfaces. The exceptions to such structures occur within the planetary boundary layer where mechanical mixing and diurnal heating dominate and in regions of precipitation where latent heat and moist convective instabilities lead to vertically extended distributions of either water vapor and/or cloud.

A series of experiments have been conducted comparing the ability of the UW θ-σ model and other σ models to simulate cloud generation and the transport of water vapor and trace constituents (Zapotocny et al. 1991; Johnson et al. 1993; Zapotocny et al. 1993; Zapotocny et al. 1994). Extensive analyses have revealed the following:

1.) The backing and veering of the wind with height as part of the vertical wind shear of baroclinic systems is the primary mechanism which creates the extreme vertical gradients of water vapor as evident in radiosonde observations.

2.) The regions within which vertical wind shear creates the extreme vertical gradients of water vapor are common with the regions of most intense vertical motion, either as subsidence in regions of cold air advection or ascent in regions of warm air advection.

3.) Filamentary structures are maximized along regions of deformation.

4.) These features and processes pose difficulties in both numerical analysis and simulations.

5.) Weighting functions used in the merging of first guess and observational data either isobarically or in sigma coordinates are not optimized in that the maximum correlations of the distribution of water vapor are along isentropic surfaces not sigma surfaces (Benjamin 1989).

6.) The structure of frontogenesis with strong vertical wind shear as a first order process creates constituent fields which are essentially discontinuous in the vertical such as is observed in radiosonde data. The numerics of simulating the intense vertical advection of water vapor in these regions of deformation and vorticity advection induces spurious vertical dispersion in σ models throughout the time-space scales of baroclinic waves. Increased vertical resolution in sigma models does not necessarily ameliorate the spurious vertical dispersion since higher resolution inherently creates stronger gradients of water vapor and intensifies vertical motion.

7.) The vertical dispersion of trace constituents modeled in isentropic coordinates as a first order process does not occur across isentropic surfaces by virtue of the dominance of isentropic processes in baroclinic waves.

8.) In regions of latent heat release, the dynamics of diabatic vertical advection in isentropic coordinates differ in that a change in entropy due to latent heat release only induces vertical advection in the local region of the condensation process. Therefore, any spurious dispersion remains isolated from the large scale environment of isentropic exchange. Even if it occurs, its temporal scale is limited in that latent heat release and precipitation quickly induce saturated conditions over vertically extended regions of a baroclinic atmosphere, a condition which alleviates spurious dispersion (Johnson et al. 1993). In sigma models the divergence/convergence structure which accompanies the propagation of baroclinic waves excites vertical advection throughout the atmospheric column in association with Dines compensation and thus the potential for spurious dispersion exists throughout the entire vertical and horizontal extent of the extratropical atmosphere.

3. REFERENCES

Benjamin, S. G., 1989: An isentropic Mesoα-Scale analysis system and its sensitivity to aircraft and surface observations. *Mon. Wea. Rev., 117*, 1586-1603.

Johnson, D. R., T. H. Zapotocny, F. M. Reames, B. J. Wolf, and R. Bradley Pierce, 1993: A comparison of simulated precipitation by hybrid isentropic-sigma and sigma models. *Mon. Wea. Rev., 121*, 2088-2114.

Johnson, D. R., T. H. Zapotocny, F. M. Reames, A. J. Lenzen, and T. K. Schaack, 1994: The dynamical structure of atmospheric transport processes within extratropical cyclones viewed through isentropic analysis. Preprint Volume II for the Life Cycles of Extratropical Cyclones, June 27-July 1, 1994, Bergen, Norway, 233-238.

Zapotocny, T. H., D. R. Johnson, F. M. Reames, R. B. Pierce, and B. J. Wolf, 1991: Numerical investigations with a hybrid isentropic-sigma model, Part II: The inclusion of moist processes. *J. Atmos. Sci. 48*, 2025-2043.

Zapotocny, T. H., D. R. Johnson, and F. M. Reames, 1993: A comparison of regional isentropic-sigma and sigma model simulations of the January 1979 Chicago blizzard. *Mon. Wea. Rev., 121*, 2115-2135.

Zapotocny, T. H., D. R. Johnson, and F. M. Reames, 1994: Development and initial test of the University of Wisconsin global hybrid isentropic-sigma model. *Mon. Wea. Rev. 122*, 2160-2178.

ON THE USE OF SATELLITE SURFACE WIND DATA

Robert Atlas
Satellite Data Utilization Office
NASA/Goddard Space Flight Center

Stephen Bloom
Satellite Data Utilization Office
General Sciences Corporation

A number of scientific issues can be addressed with the use of remotely-sensed wind data:

(1) How can satellite data be used most effectively to improve global surface wind analyses?
(2) What is the impact of satellite surface wind data on ocean surface wind analyses and air-sea fluxes?
(3) What is the role of wind forcing in the formation and decay of sea surface temperature anomalies?
(4) How does air-sea interaction contribute to the development of storms over the oceans and to the existence of persistent climatic anomalies over land?

Previous sources of oceanic surface winds (ships, buoys) have been too irregularly distributed in space and time to provide adequate data for global surface climate studies. We describe two currently available sources of remotely-sensed information about wind near the ocean surface: SSM/I wind speeds and ERS-1 scatterometer winds.

SSM/I WIND SPEEDS

SSM/I (Special Sensor Microwave / Imager) is a PASSIVE sounder on DMSP satellites, sensing 4 frequencies with dual polarizations (19 GHz horz/vert, 22 GHz vert, 37 GHz horz/vert, and 85 GHz). The basic mechanism underlying the measurement is that the "sea state" (ensemble of waves and swell) will mix the horizontal and vertical polarizations of the emitted radiation. The surface wind speed is retrieved using a set of regression equations which also account for the effects sea level temperature, total column water vapor and rainfall. Note that this is a double inference:

V&H mix --> sea state --> wind speed.

Although the SSM/I data very good global coverage, they need to be converted into wind VECTORS to be used in GEOS-DAS; i.e. we need to invoke a direction assignment mechanism. We have investigated a number of approaches, the two best being:

(1) CONVENTIONAL ANALYSIS ASSIGNMENT - uses interpolated directions from non-SSM/I surface analyses.
Used at GSFC, NMC and NOARL

(2) VARIATIONAL DIRECTION ASSIGNMENT - uses a descendant of Hoffman's SEASAT dealiasing algorithm.
Variational schemes are being pursued actively at a number of centers.

ERS-1 SCATTEROMETER WINDS

The ERS-1 (European Remote Sensing Satellite) scatterometer is an ACTIVE sensing instrument; it senses the backscatter of radar from small (few centimeter) wavelength capillary waves on the ocean surface. The first scatterometer flew on the SEASAT platform in 1978; NASA will have NSCAT available in 1996 on the Japanese ADEOS satellite. The radar backscatter is picked up by multiple antennae having different

orientations; these multiple measures of backscatter lead to estimates of the amplitude and phase of the surface capillary waves, which are then used to estimate the surface wind velocity. Unfortunately, the relation between backscatter and wind velocity is given by a highly nonlinear MODEL FUNCTION:

sigma(I) = F (speed, direction, angle(I))

where (speed,direction) defines the surface wind, and angle(I) is the incidence angle for the Ith antenna. Inverting the model function generally leads to multiple solutions for the surface wind, usually referred to as ALIASES. There are two kinds of approaches for dealing with aliases (both used at GSFC):

(1) RETRIEVAL/DEALIASING - original approach, used for SEASAT data and now by ESA. Use some background field to choose "most likely" alias, tends to be extremely sensitive to errors in the background.

(2) VARIATIONAL ASSIMILATION OF BACKSCATTER - combine all information (background, other data, backscatter) simultaneously in one penalty function. Our experiments with such an approach have been promising, the sensitivity to errors in the background appears to be reduced.

CURRENT STATUS OF SURFACE WIND DATA USAGE

SSM/I

* SSM/I wind speeds can be assimilated effectively using directional assignment methods.
* Preliminary results show a generally positive impact of SSM/I winds in data assimilation.
* Care must be taken with simple assignment methods, especially where background fields have large errors.

ERS-1 SCATTEROMETER

* Variational approach appears quite promising; not as sensitive to an inaccurate background as the retrieval/dealiasing approach.
* Current research efforts on: Combining SSM/I and ERS-1 Scatterometer data.

  Combining surface variational algorithms with GEOS-DAS, to make the best use of surface wind data.

Near Term and Future Development Plans for the GEOS Analysis System

ARLINDO DA SILVA AND STEPHEN E. COHN
Data Assimilation Office, NASA Goddard Space Flight Center, USA

Workshop on Results from the GEOS-1 Five Year Assimilation
Greenbelt, Maryland, March 1995

Contents

1 Introduction

The ultimate goal of data assimilation is to obtain best estimate of the atmospheric state by optimally combining forecast from a dynamical model with observations. A successful data assimilation system (DAS) requires a *good* dynamical model, *reliable* observations and a good representation both model and observation error characteristics. The conceptual framework of estimation theory provides the foundation for combining data and model first guess in a statistical analysis system. In the remaining of this abstract we highlight the major improvements made to the operational analysis system since GEOS-1 and briefly describe some future development plans.

2 PSAS: DAO's Physical-space Statistical Analysis System

The *Optimal Interpolation* (OI) analysis system implemented in GEOS-1 includes the following simplifying assumptions: a) homogeneous and isotropic horizontal correlation functions, b) separable vertical and horizontal correlation structures, c) multivariate wind and height analysis with some sort of "geostrophic" constraint built in the covariance model, d) *local approximation:* each grid point analysis incorporates data only in the neighborhood of that grid point, e) *data selection:* only a relatively small portion of the observations in the neighborhood of the grid point is actually included in the analysis. As of this writing, many Numerical Weather Prediction (NWP) centers have replaced (or will soon replace) OI with global analysis systems which relax the local approximation and avoid data selection altogether. Simultaneously, most of these new systems also include changes in error covariance modeling and imposed balance constraints, so that assessing the impact of each factor on the overall improvement of the system is not always immediate.

The Physical-space Statistical Analysis System (PSAS) being developed at the Data Assimilation Office (DAO) of NASA's Goddard Space Flight Center is designed as an incremental improvement over the current OI-based system. In particular, the error covariance statistics are the same as currently used in the OI system, as is the simple geostrophic balance constraint used to relate height and wind statistics. PSAS only differs from OI in the numerical method used to solve for the analysis increments: a global conjugate gradient solver includes all available observations to produce the analyzed field. Before improved error covariance statistics are developed we assess the impact of global analysis with no data selection on our assimilation system. Preliminary results of this study are presented next.

In this section we discuss the spectral characteristics of 500 hPa analysis increments $w_a - w_f$ obtained with the OI and PSAS systems. Analysis increments are expanded in terms of spherical harmonics and the power spectra are displayed as functions of total wavenumber in Figs. 1–3. The general spectral char-

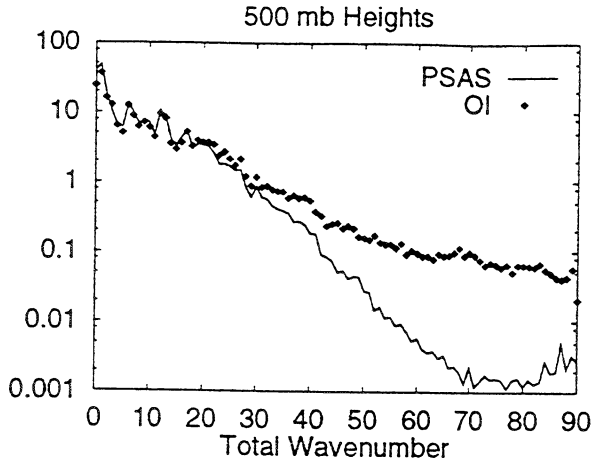

Figure 1: Power spectra as a function of spherical harmonic total wavenumber for PSAS (solid) and OI (points) analysis increments of geopotential height at 500 hPa (January 1, 1989, 12 GMT). Units: m^2.

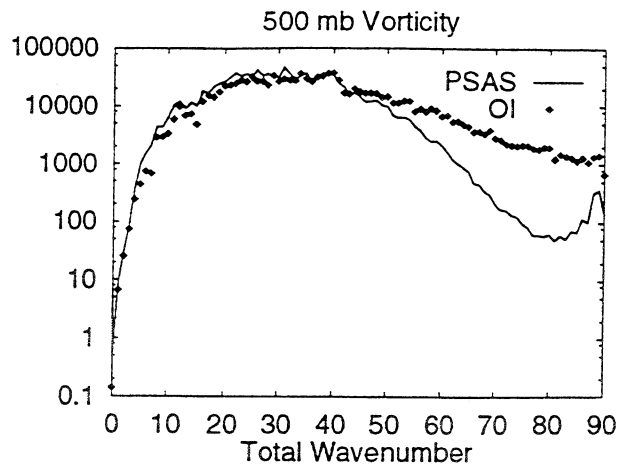

Figure 2: As in fig. 1, but for 500 hPa relative vorticity. Units: $10^{-16}s^{-2}$.

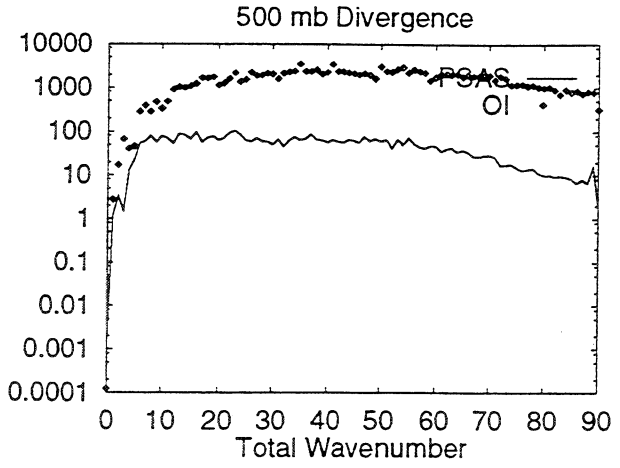

Figure 3: As in fig. 1, but for 500 hPa divergence. Units: $10^{-16}s^{-2}$.

acteristics of the analysis increments showed very little case-to-case variability in the 5 member ensemble considered. Therefore we discuss here only the results for a particular day (January 1, 1989, 12 GMT).

Fig. 1 depicts the power spectra of 500 hPa analysis increments obtained with PSAS (solid) and OI (points) systems. Overall, there is very little difference between the spectra for wavenumbers up to around 15. For higher wavenumbers the OI analysis increments have considerably more power than the PSAS increments. This is related to the relatively flat spectral slope of the OI increments, a shortcoming related to the local approximation and data selection. Notice that the PSAS increment also shows signs of saturation at around wavenumber 70. However, there is a negligible amount of power at these wavenumbers.

The impact of OI's data selection on the wind field are presented in Figs. 2–3 in terms of the power spectra of divergence and vorticity. There is a good agreement between the OI and PSAS analysis increments of relative vorticity (Fig. 2) up to about wavenumber 40. At higher wavenumbers the OI increments again show more power than the PSAS increments. For the divergence field (Fig. 3), both OI and PSAS increments show a rather flat spectrum for wavenumbers greater than about 20. For wavenumbers beyond 20 the OI increments have 1 to 2 orders of magnitude more power than the PSAS increments. The upshot is that the ratio of divergence to vorticity in the OI increments is much larger than in PSAS. This large amount of divergence in the OI increments is likely to contribute to an unbalanced analyzed state contaminated by gravity waves. Therefore, the imbalances often found in OI analyses are not entirely due to the crude geostrophic balance used to relate wind forecast error statistics to height error statistics. A great deal of spurious divergence is due to the local approximation and data selection.

Similar analysis has been carried out for the power spectra of mixing ratio analysis increments (figure not shown). Again, the OI increments show a greater amount of noise reflected by the additional power in higher wavenumbers. Although similar to the increments of geopotential heights, the discrepancies between OI and PSAS are not as accentuated in this case. This fact is consistent with the smaller correlation lengths assigned to the mixing ratio forecast error covariance. The tighter correlation function for

the mixing ratio is more amenable to the local approximation of the OI system. However, at large scales the OI increments have considerably less power than the PSAS increments.

3 Tuning of Error Statistics

The multi-year assimilation data set produced with GEOS-1 can be used to assess the consistency of the assumed error statistics, as well as to better formulate the statistical description of these errors. Within the framework of stationary and horizontally homogeneous/isotropic statistics, the following improvements are scheduled for the near future:

1. Implementation of non-separable forecast error correlations with improved balance wind-mass balance constraints.

2. Generalization of satellite error covariances to include the uncorrelated portion of error.

3. Use maximum-likelihood principle to estimate model parameters.

4 Consistent Assimilation of Retrieved Data

The satellite error covariance currently implemented in GEOS-1/DAS is based on the following approximations: a) separable horizontal/vertical correlation structures; b) horizontally homogeneous/isotropic correlations; c) stationary, and d) state-independent. Theoretical error analysis development by C. Rodgers (1990) provides systematic methodology to estimate state dependent error statistics from knowledge of retrieval operators (e.g., forward model, contribution function). The Consistent Assimilation of Retrieved Data (CARD) methodology developed by R. Ménard combines Rodgers' error analysis with Kalman filtering theory leading to a consistent treatment of retrievals errors in the analysis equation. The main advantages of CARD are:

1. Less expensive than direct assimilation of radiances (3D-VAR), yet based on possibly fewer assumption than 3D-VAR.

2. Assimilates retrieved data produced by instrument teams; simplifies logistics.

Work is under way to compare CARD with the direct assimilation of radiances methodology currently used at NMC and ECMWF.

5 Retrospective Analysis

Since the DAO does not have the operational constraints of NWP centers, it can rely on data past the analysis time to improve its estimate of the atmospheric state. The lag-1 smoother, uses data up to one synoptic time beyond the analysis time to update the conventional analysis $w^a_{k-1|k-1}$ which uses data up to the current synoptic time. The corresponding analysis equation can be written as

$$w^a_{k-1|k} = w^a_{k-1|k-1} + P^a_{k-1|k-1} A'^T H_k^T x_k$$

where

$w^a_{k-1\|k}$	$\rightarrow$	analysis using data up to next synoptic time k
$w^a_{k-1\|k-1}$	$\rightarrow$	analysis using data up to current synoptic time $k-1$
$P^a_{k-1\|k-1}$	$\rightarrow$	analysis error covariance matrix associated with $w^a_{k-1\|k-1}$
A'^T	$\rightarrow$	adjoint of linear tangent model
x_k	$\rightarrow$	available from the current PSAS analysis

$$\left(H_k P^f_k H_k^T + R_k\right) x_k = w^o_k - H_k w^f_{k|k} \qquad (1)$$

Notice that there is no perfect model assumption as in four dimensional variational data assimilation schemes (4D–VAR). The current implementation of PSAS has most of the building blocks necessary to implement the lag-1 smoother. The adjoint of the (adiabatic) linear tangent model developed at the Florida State University is currently undergoing tests. Overall, the cost of the lag-1 smoothers is equivalent to an additional analysis cycle.

6 Approximate Forecast Error Evolution

According to estimation theory the time evolution of the forecast error covariance is also governed by the dynamics of the system. A common approximation is the extended Kalman filter which prescribes the following prognostic equation for the forecast error covariance:

$$P^f_{k+1} = A' P^a_k A'^T + Q_k(\alpha) \qquad (2)$$

where P^f_{k+1} is the forecast error covariance at time $k+1$ and $Q(\alpha)$ is the *model error covariance* which may depend on some tunable parameters α. The computational cost of directly evaluating this expression is prohibitive for operational data assimilation and approximate methods must be sought. Two practical approximations to this equation is currently under development at DAO (Cohn and Todling 1995):

Partial Singular Value Decomposition: analysis error covariance is explicitly evolved in the subspace of the leading "optimal" modes of tangent linear model A':

$$\begin{aligned} A' &= USV^T, \qquad U = (U_L|U_T) \\ P^f_{k+1} &= U_L S_L \left(V_L^T P^a_k V_L\right) S_L U_L^T \\ &\quad + Q_k(\alpha + \delta\alpha) \end{aligned}$$

Partial Eigenvalue Decomposition: analysis error covariance is explicitly evolved in the subspace of the leading eigenvectors of $A' P^a A'^T$:

$$\begin{aligned} A' P^a_k A'^T &= XDX^T, \qquad X = (X_L|X_T) \\ P^f_{k+1} &= X_L D_L X_L^T + Q_k(\alpha + \delta\alpha) \end{aligned}$$

In both decompositions the change $\delta\alpha$ in parameter α can be estimated with a maximum-likelihood method using recent innovation vectors (Dee 1995).

7 New Data Types

Several new data types are currently being implemented in GEOS/DAS or are scheduled for the near feature. A partial list follows.

- Thickness analysis
- Total precipitable water
- Precipitation assimilation
- Analysis of surface marine data (moisture, temperature)
- SSM/I and ERS-1 surface winds

In addition, consistent with its mission, DAO is developing a comprehensive plan for assimilation of data from several EOS platforms. A preliminary list of these data types is discussed in another talk by Dr. R. Rood.

8 References

Cohn, S. E. and R. Todling, 1995: Approximate Kalman Filters for Unstable Dynamics. *Proceedings of the International Symposium on Assimilation of Observations in Meteorology and Oceanography*, Tokyo, Japan, 241–246.

Dee, D. P, 1995: On-line estimation of error covariance parameters for atmospheric data assimilation. *Mon. Wea. Rev.*, in press.

Rodgers, C. D., 1990: Characterization and Error Analysis of Profiles Retrieved from Remote Sounding Measurements. *J. Geophys. Res.*, **95**, 5587–5595.

Improving the Hydrological Cycle in the GEOS-DAS using Satellite Data

Arthur Y. Hou and David V. Ledvina*
Data Assimilation Office, Laboratory for Atmospheres
NASA Goddard Space Flight Center
Greenbelt, Maryland, 20771 USA

**General Sciences Corporation*
Laurel, Maryland

1. Introduction

The TOGA-COARE Intensive Observing Period (November 1992 through February 1993) provides an unique opportunity to validate and test atmospheric models and data assimilation systems in a normally data sparse region. The Data Assimilation Office has produced a series of global reanalyses for this period to study how well the hydrological processes are represented in the GEOS-DAS analysis and investigate the impact of assimilating remotely sensed total precipitable water (TPW) and surface wind estimates provided by the Special Sensor Microwave/Imager (SSM/I) instruments aboard the Defense Meteorological Satellite Program (DMSP) satellites.

2. Results

The CONTROL in these experiments is the analysis produced by the standard GEOS-1 DAS (Schubert et al. 1993). Results show that compared with COARE sounding, the GEOS-DAS does a very good job in capturing the westerly wind burst events in the Intensive Flux Array (IFA) region (150E-160E, 0-5S), despite a slight westerly bias at the upper levels. Hovmoller diagrams show that the episodic eastward moving intraseasonal convective events seen in the OLR data are well correlated with signals in the time-longitude plots of the 200 mb divergence, the total precipitable water, and the vertically integrated moisture convergence. While the analysis does a credible job in depicting winds and transport, these intraseasonal signals are not as evident in the precipitation field and are poorly captured in the OLR, due to the poor representation of clouds in the tropics in the GEOS-DAS.

Preliminary results show that assimilation of SSM/I TPW estimates significantly reduces a known dry bias in the tropics in the operational GEOS-1 DAS, which currently assimilates only rawinsonde moisture data. The reduction of the dry bias in the lower troposphere noticeably improves the intensity and spatial structure of rainfall in the COARE Large-scale Sounding Array (140E-180, 10S-10N), as compared with the retrieved GPI and SSM/I rainfall estimates. It also has a tendency to intensify precipitation along the ITCZ in the eastern Pacific. This result is encouraging for it demonstrates that assimilation of a given type of data can transfer information through model physics to improve the related fields.

Assimilation of the SSM/I surface wind speed estimates appears to have a direct impact on the evaporation field in the GEOS-DAS analysis, with a direct correspondence between the anomaly patterns (analysis with SSM/I winds minus CONTROL) in these two fields. The incorporation of surface wind data can alter the local surface evaporation rate by as much as 30%. During the IOP surface wind data tend to increase the convergence of low-level moisture in the ITCZ region and in the western Indian Ocean. The enhanced convergence, in turn, leads to increased precipitation in these regions, where the rainfall rates are typically underrepresented in the GEOS-1 DAS.

3. Concluding Remarks

Assimilation of SSM/I total precipitable water and surface wind speed estimates has a positive impact on the assimilated fields of the GEOS-1 DAS. Utilization of the SSM/I TPW reduces a known dry bias in the tropics and improves the global distribution of precipitation. F or the COARE IOP, assimilation of SSM/I surface wind speed estimates enhances the low level convergence along the ITCZ and western Indian Ocean, and improves rainfall in these areas. It is noteworthy that the incorporation of these data not only improves the moisture and wind fields, but also related fields such as precipitation and evaporation.

Work is underway to produce a reanalysis assimilating both SSM/I TPW and surface wind estimates simultaneously to investigate the extent to which there may be a positive feedback between the two data types. Our future plans include using the COARE IOP level 2b data for validation of these reanalyses and producing a final GEOS-DAS reanalysis incorporating all COARE data and assess the their impact on the reanalysis.

DIABATIC DYNAMIC INITIALIZATION WITH AN ITERATIVE FILTER

Michael Fox-Rabinovitz
JCESS, Department of Meteorology
University of Maryland

Acknowledgments:

J. Pfaendtner, R. Govindaraju, D. Lamich, L. Takacs, V. Rathod

CONTENTS

ABSTRACT

The new diabatic dynamic initialization technique with an iterative time integration scheme as a filter has been developed and tested for an intermittent global data assimilation system. The method employs only the forward full diabatic model integration as a balancing procedure. The initial balancing is accomplished efficiently by using the new iterative Euler scheme as a filter. The iterative Euler scheme converges rapidly, employing only a few iterations. It provides an effective selective filtration mostly for high frequency and small scale modes. The initial spin-up effect is practically eliminated, and balancing of initially disturbed external and internal modes is achieved by the initialization procedure during only a few initial time steps of model integration with the iterative Euler scheme, or a total of 1/2 to 1 hour. After this short initialization period is completed the standard model integration is continued with the resulting noise-and-spin-up free initialized fields.

The diabatic dynamic initialization procedure has been implemented within the Goddard Earth Observing System (GEOS) Data Assimilation System (DAS) employing the GEOS Global Climate Model (GCM). Both instantaneous and monthly mean analysis and diagnostic fields calculated for January and February 1989, show a positive impact due to applying the initialization procedure. Most importantly, the rms height errors calculated against the radiosonde data at station locations over the globe, are significantly reduced. Moreover, five 10 day forecasts show scores that are marginally improved when using initialized initial conditions.

The initialization procedure is computationally efficient, and can be easily applied to various large-scale and mesoscale model systems.

CONCLUSIONS

1. The new version of diabatic dynamic initialization (DDII) that employs the new iterative time integration scheme (IES) as a highly selective filter, has been developed and tested.

2. DDII is free of any irreversibility effects because it includes only a forward full diabatic model integration.

3. DDII provides a very fast balancing. Only 1 h of model integration is enough for suppressing noise and eliminating a spin-up effect.

4. The comparative experiments performed with the GEOS DAS have shown that when using DDII the following major improvements are achieved.

    - The Hadley circulation (usually underestimated) becomes stronger.
    - Precipitation (P) is increased whereas the spin-up, or P-E is decreased.
    - The polar, and upper boundary noise is reduced.
    - Most importantly, the analysis errors are significantly reduced.
    - 10 day forecast scores are improved.

5. DDII is computationally efficient.

6. DDII can be easily applied to various large-scale and mesoscale models/systems.

FUTURE PLANS

1. Continue assessing the BIAU impact on stratospheric assimilation

2. Implement BIAU into the new production version of GEOS DAS

3 Summary

We attempt here to summarize some of the salient results concerning the quality of the GEOS–DAS products. We discuss also the relevant development efforts which address the deficiencies, and some concerns about accessing the data from the Goddard Distributed Active Archive Center (DAAC), the NASA Center for Computational Sciences (NCCS) Unitree system and the local DAO server. This summary is not meant to be comprehensive: the reader is referred to the individual reports in section 2 for missing details and other aspects of the GEOS assimilation not covered here.

The primary strength of the GEOS–1 assimilation system lies in its ability to capture many of the key climate variations associated with El Nino and La Nina events, monsoons, droughts and other low frequency variations. This appears to be, in part, due to the incorporation of an incremental analysis update procedure (Bloom et al. 1995), which virtually eliminates the shocks associated with data insertion, and allows the model to respond gradually to the observations. Also, the GCM's physical parameterizations appear to respond quite realistically to the variations in boundary forcing. The results on low frequency variability include the following:

The global signature of low frequency variations in the atmospheric moisture field compare favorably with SSM/I data. This signal appears to be captured better in the GEOS–1 assimilation than either the NMC or the ECMWF operational products.

The tropical zonal winds and pressure fields have been successfully used to describe and analyze various aspects of the large–scale circulation such as the Madden–Julian Oscillation and westerly wind bursts. The large scale tropical divergent wind field also captures the evolution of the Madden–Julian Oscillation quite well.

Various El Nino signals are successfully captured in the GEOS assimilation. These include a large cloud forcing anomaly in the central equatorial Pacific associated with 1986/87 El Nino which compares favorably with ERBE data. Also, the tropical Pacific precipitation anomalies associated with the 1987/88 El Nino/La Nina event compare favorably with OLR observations. The monsoon precipitation anomalies associated with the 1987/88 El Nino/La Nina event are consistent with the outgoing longwave radiation (OLR) observations.

The reduced precipitation during the 1988 drought and the much enhanced precipitation during the 1993 wet conditions over the United States compare favorably with surface observations. In general, the monthly precipitation anomalies compare favorably with station observations, though there are cases where this is not true.

GEOS–1 captures the seasonal placement of upper tropospheric moisture patterns quite well. The spatial correlations between GEOS–1 fields with observations (TOVS brightness temperatures) are similar to those found with ECMWF analyses.

A number of shorter term fluctuations are also well represented in the assimilation. These are primarily associated with fluctuations in the zonal wind and/or the boundary layer winds and surface stresses. Over land, these results indicate that the performance of the GCM's planetary boundary layer (PBL) parameterization generates very realistic wind fields, since the GEOS–DAS assimilates few wind observations below 850mb. Over the oceans, the results suggest that both the surface wind/pressure analysis and the PBL parameterization are performing well. The relevant results are:

The GEOS–1 equatorial winds appear to successfully capture the subdaily atmospheric tidal variations.

GEOS–1 winds compared with length of day measurements suggest that the momentum variations are well captured for periods as short as 8–9 days. Comparisons between NMC and GEOS–1 reanalyses shows coherence on all time scales longer than 3 days, which is shorter (better) than has been typically obtained from operational analyses. This suggests the reanalyses are in closer agreement than operational series have been in the past for this quantity.

The horizontal winds, convective cloud mass flux, detrainment, and PBL depth are of sufficient quality to be used with significant success as input to tropospheric chemistry transport models for Freon–11, Rn–222, and CO. Middle latitude synoptic variability is well captured; however, interhemispheric gradients are not well simulated. Convective transport suggests that the cloud mass fluxes are of the right magnitude; however, the mixing connects the PBL and the upper troposphere too directly, underestimating middle tropospheric entrainment and detrainment. The need for a downdraft parameterization is seen clearly in the CO simulations.

GEOS–1 wind stress provides good estimates of ocean transport through the Florida Straits. The GEOS wind stress generally provides improvements over the operational ECMWF results, but tends to overestimate amplitudes beyond about 10 days.

Variations in the low level winds over the Great Plains are quite realistic despite the lack of observations going into the GEOS–1 DAS below 850mb.

The following climate mean quantities are generally consistent with available verifying observations, and/or are consistent or better than found in other analyses:

The climate mean and seasonal evolution of the basic prognostic fields appear to be well captured in the GEOS analysis. Differences with ECMWF analyses over the Northern Hemisphere land masses are small. The largest differences occur over the tropics, and the Southern Hemisphere oceans, where observations are sparse and model bias is apparently playing a role (more on this below).

The clear sky longwave flux and albedo are in good agreement with ERBE measurements.

The general patterns of tropical convection and their seasonal evolution are consistent with available observations, but details of local maxima and amplitudes are not.

GEOS–1 wind stress fields have been employed to force an ocean model in the North Pacific with some success, particularly in producing the subpolar circulation.

The greatest deficiencies in the GEOS–1 products are tied to biases in the humidity and cloud fields. There are several reasons for this. Moisture biases of the GCM are clearly playing a role, as well as, deficiencies in how the available moisture observations (currently only radiosonde) are being assimilated. One of the most disturbing aspects of the results is the manner in which the observations and model first guess appear to generate spurious feedbacks (Molod et al. 1995). A number of development activities are geared to addressing these deficiencies. For example, substantial improvements in the moisture field have been obtained with the assimilation of SSM/I observations. The introduction of downdrafts, a cloud water/ice scheme, improvements to the PBL (moist turbulence scheme, an improved mixed layer), further tuning of the convective parameterization, and the assimilation of relative humidity (instead of mixing ratio) should alleviate many of these problems. Some of the key moisture and cloud–related problems are:

A much too wet upper troposphere (300 mb) over the Pacific Ocean compared with available observations. The horizontal moisture gradients between very moist and very dry regions of the upper troposphere are too weak.

The tropics and subtropics over the oceans are too dry compared with the vertically integrated moisture from SSM/I.

Longwave and shortwave cloud radiative forcing (LCRF, SCRF) are overestimated over regions of deep convection in the ITCZ especially during Northern summer.

Middle–latitude LCRF and SCRF are weaker than ERBE especially over the storm tracks of both hemispheres. The vertical distribution of diabatic heating and vertical heat transport may also be too shallow in these regions (especially the North Atlantic).

Low level coastal stratiform clouds are underestimated.

There are various problems with the precipitation, and near surface temperature and humidity fields. Over land, these include substantial errors in the diurnal cycle. Some of these appear to be tied to the convective parameterization and should be remedied with the introduction of the changes outlined above. Improvements to the diurnal cycle and longer term impacts of soil moisture variations must await the introduction of a land surface model (currently being implemented). The known problems are as follows:

Summertime precipitation over eastern North America is overestimated.

The amplitude of the diurnal cycle of the precipitation over the southeast US is too large with little evidence of a nocturnal maximum over the Great Plains.

Wintertime precipitation is too low over the Northern Rockies and along the southern coast of the United States.

Over India, the gap between the western Ghats and the Bay of Bengal is missing.

Too much rain over continental Europe and northern Asia in July and too little over the Mediterranean during January.

The assimilation produces too many days with small rain amounts and not enough days with no rain. The most intense rain amounts also appear to be underestimated. However, it was shown that this may not be the most meaningful comparison, since the observations represent point measurements while the values from the assimilation represent a grid square.

The 1988 drought over the United States appears to extend too long into the summer with warmer and drier conditions than were observed in July.

The near surface temperature is too cold over the northern United States and Canada during winter.

Subtropical deserts are less reflective than in ERBE. The diurnal cycle of out–going longwave radiation over land shows significant phase shifts with respect to ERBE.

A number of other problems have been identified (listed below). For example, the model's zonal wind bias introduces a bias in the assimilation in data sparse regions. Current model experiments suggest that much of the westerly bias (and the related cooling at high latitudes) can be eliminated with the introduction of gravity wave drag. Problems associated with noise at the poles have been addressed in the latest version of the model with the generalization of the dynamics module to allow rotation of the poles.

The Hadley cell during Northern winter is weaker than that obtained in either the ECMWF or NMC analyses.

There is a zonal mean bias at 40°–50°S in sea level pressure and in the zonal wind.

The northward component of the summertime low level wind over the Great Plains appears to be underestimated. The northward transport of moisture appears to be about right; this occurs because the low level moisture field is overestimated in this region.

Various quantities including the temperature and sea level pressure show evidence of noise near the poles.

In general, the magnitude of the wind stress appears to be underestimated over the North Pacific.

Results from several applications of a special configuration of GEOS to resolve the stratosphere were reported. There are now more than four years of GEOS analyses from the ground to 0.4 mb, starting in January 1991. Douglass et al. (1995) and the references therein give a status of the current transport capabilities.

Forecasts from the GEOS system have been used with general success in planning and directing flights of the high-altitude NASA ER–2 aircraft to potential vorticity, and hence chemical, targets in middle and high latitudes. Tropical forecasts have been poor in GEOS and all other available products.

Lagrangian tracking techniques have been successful in mapping tracer structures that are much finer than the resolution of the assimilating model. Tracking of the Pinatubo eruption cloud with GEOS winds has been more successful than similar experiments with NMC winds.

GEOS winds have been successfully used to model ozone chemistry and transport for integrations longer than one year. Prior experiments that did not use the IAU were not useful for more than a three month integration. Synoptic and planetary–scale variability are well simulated. The background residual (i.e. Hadley and Brewer–Dobson) circulation is much improved in the IAU product. However, tropical upward motion remains too strong and wintertime polar descent too weak, leading to systematic biases in the ozone field in the year–long integrations.

The barrier between tropical and middle latitudes is too weak in the lower stratosphere. The GEOS analysis, as well as other assimilation products, show more mixing between tropical and middle latitudes than is observed in tracer measurements from the upper stratospheric research satellite. The tropics in the stratosphere are much too noisy as revealed by comparisons with high resolution ozone data.

The rotated pole model effectively eliminates spurious noise that was noted at the pole in earlier versions of the GEOS analysis. The location of the computational pole at low latitudes does not appear to cause a problem; this is likely because the coriolis term is small.

There remains a warm bias at the wintertime pole for the most extreme cold events. This is a problem common to all assimilation analyses and is related to both the data not being representative, and the inability of the model to simulate the most extreme events.

The tropical quasi–biennial wind oscillation is present in the analyses; however, a self–consistent indirect circulation is not evident. Tropical Kelvin waves are not well represented.

The GEOS winds have been transferred to Lawrence Livermore National Laboratory for use in 3–D chemical assessments of the environmental impact of civil aviation.

Feedback on experience with data access and retrieval was rather limited. One of the major findings was that most users were accessing the data directly from the NCCS Unitree system, instead of from the Goddard DAAC. A large number of users have also obtained the monthly means from the local DAO server. Most users were satisfied with the access from the NCCS Unitree system which is geared to high speed near–online (robotically–controlled) data access. Complaints were generally associated with data organization and occasional glitches with the retrieval system. Those accessing the monthly means from the DAO server were also generally happy with the access, and especially the online documentation; however, the large sizes of the files gave some users problems due to their limited local storage capabilities. For those people obtaining the data from the Goddard DAAC, the experiences were somewhat mixed. Some of the early users had difficulties obtaining the data in a timely manner. The problems were primarily associated with "growing pains" of the DAAC, and the more recent users appear to be satisfied with DAAC performance. The Goddard DAAC received very high marks for responsiveness to user concerns and suggestions. From a more general perspective, there is a concern that the mode of access provided by the DAACs (search and order) is not satisfactory for many users accustomed to high speed interactive access.

The major complaints centered on the large file sizes of the DAO output and the lack of a subsetting capability. This is a major issue which the DAACs and data providers must address. The options range from providing a more efficient organization of the files (including smaller file sizes), to providing several popular versions (organizations) of the data, to providing an on–demand subsetting capability. The first option may not satisfy enough of the users, while the last option would very likely quickly overwhelm the current resources of the DAACs.

Acknowledgements Funding for the workshop was provided by NASA headquarters through the support of Ken Bergman. Jean Rosenberg (workshop coordinator) provided excellent logistical and technical support, and helped collect and organize the reports. The high quality and consistency of this very heterogeneous collection of reports is largely the result of the careful drafting and proofreading performed by Laura Rumburg. Travel arrangements for the workshop were made by Denise Dunn of the Universities Space Research Association. The assimilation was carried out employing the NASA Center for Computational Sciences (NCCS) computing facilities. The experiment was supported by the EOS Interdisciplinary Science Program and by the NASA Research and Applications Program. Computing resources and funding were provided by the EOS Project through the Scientific Computational Facility of the Data Assimilation Office.

Appendix: The GEOS–1 DAS

The two primary components of the GEOS–1 DAS are the GEOS–1 GCM and an optimal interpolation (OI) analysis scheme. The GEOS–1 GCM is described in Takacs et al. (1994), Suarez and Takacs (1995) and Molod et al. (1995). The analysis scheme is described in Pfaendtner et al. (1995). For convenience, the GEOS–1 DAS is summarized below.

The OI Scheme

The GEOS–1 DAS employs an optimal interpolation (OI) analysis scheme, which for the multiyear assimilation described here, was carried out at a horizontal resolution of 2° latitude by 2.5° longitude at 14 upper–air pressure levels (20, 30, 50, 70, 100, 150, 200, 250, 300, 400, 500, 700, 850, 1000 mb) and at sea–level. The analysis increments are computed every 6 hours using observations from a +/− 3 hour data window centered on the analysis times (00, 06, 12, and 18 UTC). The innovation vector (observation minus background forecast) used as input to the OI is computed using a single forecast valid at the analysis time.

The upper–air analyses of height, wind, and moisture incorporate the data from rawinsondes, dropwindsondes, rocketsondes, aircraft winds, cloud tracked winds, and thicknesses from the historical TOVS soundings produced by NOAA NESDIS. The satellite heights are computed using a reference level that depends on the analyzed sea–level pressure. The only bogus data used are 1000 mb height observations, which are generated above pressure reports from ships. These serve to further couple the surface and upper–air analyses.

The OI scheme is multivariate in geopotential height and winds and employs a damped cosine function for the horizontal correlation of model prediction error. The height–wind cross–correlation model is geostrophic and scaled to zero at the equator. The multivariate surface analysis scheme over the oceans adopts an Ekman balance for the pressure–wind analysis. The moisture analysis for mixing ratio employs only rawinsonde moisture data. All grid point analyses are done using up to 75 nearby observations from within a circular data–selection cylinder of 1600 km radius.

The assimilation system does not include an initialization scheme and relies on the damping properties of a Matsuno time differencing scheme to control initial imbalances generated by the insertion of observations. However, the initial imbalances and spinup have been greatly reduced over earlier versions by the introduction of an Incremental Analysis Update (IAU) procedure (Bloom et al., 1991, 1995). In the IAU procedure, standard OI analysis increments are computed at the analysis times; the increments are then inserted gradually into the AGCM by rerunning the forecast and adding a fraction of the increment at each model time step over the 6 hour period centered on the analysis time (see Pfaendtner et al. 1995 and Bloom et al. 1995 for details of the implementation and the statistical properties

of the IAU approach). The assimilation thus effectively consists of a continuous AGCM forecast with additional heat, momentum, moisture and mass source terms updated every 6 hours from observations.

The GEOS–1 Model

The tropospheric version of the GEOS–1 GCM uses the potential enstrophy and energy–conserving horizontal differencing scheme on a C–grid developed by Sadourny (1975), and further described by Burridge and Haseler (1977). An explicit leapfrog scheme is used for the time differencing, applying an Asselin (1972) time filter to damp out the computational mode. An 8th–order Shapiro filter (Shapiro, 1970) is applied to the wind, potential temperature, and specific humidity to avoid non–linear computational instability. The filter is applied at every step in such a way that the amplitude of the two–grid interval wave would be reduced by half in two hours. Applying the filter weakly at each time step eliminates the shock that occurred in earlier assimilations by intermittent application of filter. The model also uses a polar Fourier filter to avoid linear instability due to violation of the CFL condition for the Lamb wave and internal gravity waves. This polar filter, however, is applied only to the tendencies of the winds, potential temperature, specific humidity, and surface pressure. The model's vertical finite differencing scheme is that of Arakawa and Suarez (1983). The above dynamics routines are organized into a plug–compatible module called the ARIES/GEOS "dynamical core" (Suarez and Takacs 1995).

The infrared and solar radiation parameterizations follow closely those described by Harshvardhan et al. (1987). In the longwave, water vapor absorption is parameterized as in Chou (1984), the 15 micron band of CO_2 as in Chou et al. (1983), and ozone absorption as in Rodgers (1968) with the modifications suggested by Rosenfield et al. (1987). The shortwave follows Davies (1982), as described in Harshvardhan et al. (1987). Shortwave absorption by water vapor uses a k–distribution approach as in Lacis and Hansen (1974). Cloud albedo and transmissivity for the model layers are obtained from specified single–scattering albedo and cloud optical thickness by using the delta–Eddington approximation (Joseph et al., 1976; King and Harshvardhan, 1986).

The penetrative convection originating in the boundary layer is parameterized using the Relaxed Arakawa–Schubert (RAS) scheme (Moorthi and Suarez, 1992), which is a simple and efficient implementation of the Arakawa–Schubert (1974) scheme. Unlike the Arakawa–Schubert scheme, which solves an adjustment problem by considering simultaneous interaction among all possible cloud types, RAS considers only one cloud at a time, and rather than adjusting fully every hour or two, it does a series of partial adjustments that tend to relax the state toward equilibrium. The AGCM also includes a parameterization that models the evaporation of falling convective rain as described in Sud and Molod (1988). Negative values of specific humidity produced by the finite–differenced advection are filled by borrowing from below.

The planetary boundary layer (PBL) is explicitly resolved in a 2 to 4 layer region. Wind, temperature, and humidity profiles in an "extended" surface layer (which can be up to 150 m thick), and the turbulent fluxes of heat, moisture, and momentum at the surface are obtained from Monin–Obukov similarity theory by selecting similarity functions that approach the convective limit for unstable profiles and that agree with observations for very stable profiles. Surface roughness lengths are taken as functions of vegetation type over land and as a function of surface stress over water. Turbulent fluxes above the "extended" surfaced layer are computed using the second order closure model of Helfand and Labraga (1988). In this scheme, the turbulent kinetic energy is a prognostic variable and the remaining second order moments are diagnosed from it and from the atmospheric sounding.

For the multiyear assimilation, GEOS–1 was integrated on a 2° latitude by 2.5° longitude grid with 20 sigma levels. The sigma levels are distributed to provide enhanced resolution in the planetary boundary layer and at upper levels. The topography used in GEOS–1 was prepared from the 10 minute topography obtained from the Navy Fleet Numerical Oceanography Center in Monterey. The 2° latitude by 2.5° elevation values were obtained by averaging the high resolution values (areas with more than 60% water were considered water points), and then applying a Lanczos (1966) filter. The Lanczos filter was designed to remove small scale structure (it completely removes $2\Delta X$ waves) while minimizing the Gibbs phenomena.

This version of the AGCM is run without a land surface model (note that current development efforts include the incorporation of a land surface model). For the assimilation described here, soil moisture is computed off–line, based on a simple bucket model that used monthly mean observed surface air temperature and precipitation (Schemm et al., 1992). The snow line and surface albedo are prescribed and vary with the season (see Takacs et al. 1994). The sea–surface temperature is updated according to the observed monthly mean values provided by the Climate Analysis Center at NMC and the Center for Ocean-Land-Atmosphere Studies (COLA).

References

Arakawa, A. and W. Schubert, 1974: Interaction of a cumulus ensemble with the large–scale environment. Part I, *J. Atmos. Sci.*, **31**, 674–701.

Arakawa, A. and M.J. Suarez, 1983: Vertical differencing of the primitive equations in sigma coordinates. *Mon. Wea. Rev.*, **111**, 34–45.

Arpe, K. 1990: Impact of changes in the ECMWF analysis–forecasting scheme on the systematic error of the model. Ten years of medium–range weather forecasting. Volume 1, 4–8 September 1989, June 1990, ECMWF, Shinfield Park, Reading RG2 9AX, U.K.

Asselin, R., 1972: Frequency filter for time integrations. *Mon. Wea. Rev.*, **100**, 487–490.

Barnes, S. L., 1964: A technique for maximizing details in numerical weather map analysis. *J. Appl. Meteor.*, **3**, 396–409.

Bengtsson, L. and J. Shukla, 1988: Integration of space and in situ observations to study global climate change. *Bull. Amer. Meteor. Soc.*, **69**, 1130–1143.

Bloom, S.C., L.L. Takacs, and E. Brin, 1991: A scheme to incorporate analysis increments gradually in the GLA assimilation system. *Ninth Conf. on Numerical Weather Prediction*, Denver, CO, Amer. Meteor. Soc., 110–112.

Bloom, S.C., L.L. Takacs, A.M. da Silva, and D. Ledvina, 1995: Data assimilation using incremental analysis updates. *To be submitted to Mon. Wea. Rev.*

Burridge, D.M. and J. Haseler, 1977: A model for medium range weather forecasting–adiabatic formulation, *Tech. Report. No. 4, European Center for Medium Range Weather Forecasts*, Brachnell, Berkshire, UK.

Cayan, D.R., C.F. Ropelewski, and T.R. Karl, 1986: An atlas of United States Monthly and Seasonal Temperature Anomalies, December 1930–November 1984. *NOAA US Climate Program Office*, 244pp.

Chou, M.–D., 1984: Broadband water vapor transmission functions for atmospheric IR flux computation. *J. Atmos. Sci.*, **41**, 1775–1778.

Chou, M.–D., and L. Peng, 1983: A parameterization of the absorption in 15–micron CO_2 spectral region with application to climate sensitivity studies. *J. Atmos. Sci.*, **40**, 2183–2192.

Cressman, G. P., 1959: An operational objective analysis scheme. *Mon. Wea. Rev.*, **87**, 329–340.

Daley, R., 1991: *Atmospheric Data Analysis.* Cambridge University Press, Cambridge, 457pp.

Da Silva, A., C.C. Young and S. Levitus, 1995: Atlas of Surface Marine Data 1994 Vol. 1: Algorithms and Procedures, In preparation.

Davies, R., 1982: Documentation of the solar radiation parameterization in the GLAS climate model. NASA Tech. Memo. 83961, 57 pp. [Available from the U.S. Department of Commerce, National Technical Information Service, 5285 Port Royal Road, Springfield, VA 22161]

Douglass, A. R., C. J. Weaver, R. B. Rood, and L. Coy, 1995: A three dimensional simulation of the ozone annual cycle using winds from a data assimilation system. *J. Geophys. Res.*, to appear.

ECMWF, 1989: The description of the ECMWF/WCRP Level III–A global atmospheric data archive. European Center for Medium-Range Weather Forecasts, Shinfield Park, Reading/Berks., RG2 9AX, England. 5285 Port Royal Road, Springfield, VA 22161]

Gruber, A. and A.F. Krueger, 1984: The status of the NOAA outgoing longwave radiation data set. *Bull. Amer. Meteor. Soc.*, **65**, 958-962.

Hamming, R. W., 1989: *Digital Filters*, Prentice–Hall, Englewood Cliffs, N. J., 284pp.

Harshvardhan, R. Davies, D. A. Randall, and T. G. Corsetti, 1987: A fast radiation parameterization for atmospheric circulation models. *J. Geophys. Res.*, **92**, 1009–1016.

Helfand, H. M., and J. C. Labraga, 1988: Design of a non–singular level 2.5 second–order closure model for the prediction of atmospheric turbulence. *J. Atmos. Sci.*, **45**, 113–132.

Helfand, H. M., M. and S. D. Schubert, 1995: Climatology of the simulated Great Plains low–level jet and its contribution to the continental moisture budget of the United States. *J. Climate*, **April**.

Hurrel, J.W. and G.G. Campbell, 1992: Monthly mean global satellite data sets available in CCM history tape formats. NCAR Technical Note, NCAR/TN–371+STR, Boulder, CO.

Joseph, J.H., W.J. Wiscombe, and J.E. Weinman, 1976: The delta–Eddington approximation for radiative flux transfer. *J. Atmos. Sci.*, **33**, 2452–2459.

Kalnay, E. and R. Jenne, 1991: Summary of the NMC/NCAR reanalysis workshop of April 1991. *Bull. Amer. Meteor. Soc.*, **72**, 1897–1904.

King, M.D., and R. Harshvardhan,1986: Comparative accuracy of selected multiple scattering approximations. *J. Atmos. Sci.*, **43**, 784–801.

Lacis, A. A., and J. E. Hansen, 1974: A parameterization for the absorption of solar radiation in the Earth's atmosphere. *J. Atmos. Sci.*, **31**, 118–133.

Lanczos, C., 1966: *Discourse on Fourier Series.* Hafner Publishing, 255 pp.

Large, W. G. and S. Pond, 1981: Open ocean momentum flux measurements in moderate to strong winds. *J. Phys. Oceanogr.*, **11**, 324–336.

Levitus, S., 1982: Climatological Atlas of the World Ocean, NOAA Prof. Paper No. 13, U. S. Government Printing Office, Washington DC, 17 fiches, 173 pp.

Molod, A, H.M. Helfand, and L.L. Takacs, 1995: The climate of the GEOS–1 GCM and its impact on the GEOS–1 data assimilation System. (submitted)

Moorthi, S., and M. J. Suarez, 1992: Relaxed Arakawa Schubert: A parameterization of moist convection for general circulation models. *Mon. Wea. Rev.*, **120**, 978–1002.

Pfaendtner, J., S. Bloom, D. Lamich, M. Seablom, M. Sienkiewicz, J. Stobie, and A. da Silva, 1995: Documentation of the Goddard Earth Observing System (GEOS) Data Assimilation System–Version 1. NASA Tech. Memo. No. 104606, Volume 4, Goddard Space Flight Center, Greenbelt, MD 20771.*

Rienecker, M. M., R. Atlas, S. D. Schubert, and C. A. Scholz, 1995: A comparison of surface wind products over the North Pacific Ocean. *Submitted to J. Geophysical Research–Oceans.*

Rodgers, C. D., 1968: Some extension and applications of the new random model for molecular band transmission. *Quart. J. Roy. Meteor. Soc.*, **94**, 99–102.

Rosenfield, J. E., M. R. Schoeberl, and M. A. Geller, 1987: A computation of the stratospheric diabatic circulation using an accurate radiative transfer model. *J. Atmos. Sci.*, **44**, 859–876.

Sadourny, R., 1975: The dynamics of finite difference models of the shallow water equations, *J. Atmos. Sci.*, **32**, 680–689.

Schemm, J., S. Schubert, J. Terry, and S. Bloom, 1992: Estimates of monthly mean soil moisture for 1979–1989. NASA Tech. Memo. No. 104571, Goddard Space Flight Center, Greenbelt, MD 20771.

Schubert, S. D., C.–Y. Wu, J. Zero and J.–K. Schemm, 1991: Quality control of the consolidated ECMWF/TOGA analyses. Goddard Space Flight Center, Greenbelt, MD. [Report avaliable from S. Schubert, e–mail schubert@dao.gsfc.nasa.gov]

Schubert, S. D., J. Pfaendtner and R. Rood, 1993: An assimilated data set for Earth Science applications, *Bull. Am Met. Soc.*, 74, 2331–2342.*

Schubert, S., C.-K. Park, C.-Y. Wu, W. Higgins, Y. Kondratyeva, A. Molod, L. Takacs, M. Seablom, and R. Rood 1995: A multiyear assimilation with the GEOS-1 system: overview and results. NASA Tech. Memo. No. 104606, Volume 6, Goddard Space Flight Center, Greenbelt, MD 20771.*

Schubert, S. D. and Y. Chang, 1995: An objective method for assessing sources of model error, *To be submitted to Mon. Wea. Rev.*.

Shapiro, R., 1970: Smoothing, filtering and boundary effects. *Rev. Geophys. Space Phys.*, **8**, 359–387.

Spangler, W.M.L. and R. L. Jenne, 1990: World monthly surface station climatology. National Center for Atmospheric Research, Boulder, CO.

Suarez, M.J. and Takacs, L.L., 1995: Documentation of the ARIES/GEOS Dynamical Core: Version 2. NASA Tech. Memo. No. 104606, Volume 5, Goddard Space Flight Center, Greenbelt, MD 20771.*

Sud, Y. C., and A. Molod, 1988: The roles of dry convection, cloud–radiation feedback processes and the influence of recent improvements in the parameterization of convection in the GLA GCM. *Mon. Wea. Rev.*, **116**, 2366–2387.

Takacs, L.L., A. Molod, and T. Wang, 1994: Documentation of the Goddard Earth Observing System (GEOS) General Circulation Model–Version 1. NASA Tech. Memo. No. 104606, Volume 1, Goddard Space Flight Center, Greenbelt, MD 20771.*

Takacs, L.L., and, M.J. Suarez, 1995: Evaluation of the climate of the GEOS–1 GCM: Dynamical processes. (in progress)

Trenberth, K.E., and J.G. Olson, 1988: ECMWF global analyses 1979–1986: Circulation statistics and data evaluation. NCAR Technical Note, NCAR/TN–300+STR, Boulder, CO.

Wentz, F.J., 1992: Revision–1 Update for SSM/I Geophysical Tapes User's Manual. Remote Sensing Systems Techical Memorandum 040792.

* Available from DAO MOSAIC home page (http://hera.gsfc.nasa.gov/dao.home_page.html)

Previous Volumes in This Series

Volume 1 *September 1994*	Documentation of the Goddard Earth Observing System (GEOS) General Circulation Model - Version 1 **L.L. Takacs, A. Molod, and T. Wang**
Volume 2 *October 1994*	Direct Solution of the Implicit Formulation of Fourth Order Horizontal Diffusion for Gridpoint Models on the Sphere **Y. Li, S. Moorthi, and J.R. Bates**
Volume 3 *December 1994*	An Efficient Thermal Infrared Radiation Parameterization for Use in General Circulation Models **M.-D. Chou and M.J. Suarez**
Volume 4 *January 1995*	Documentation of the Goddard Earth Observing System (GEOS) Data Assimilation System - Version 1 **James Pfaendtner, Stephen Bloom, David Lamich, Michael Seablom, Meta Sienkiewicz, James Stobie, and Arlindo da Silva**
Volume 5 *April 1995*	Documentation of the Aries-GEOS Dynamical Core: Version 2 **Max J. Suarez and Lawrence L. Takacs**
Volume 6 *April 1995*	A Multiyear Assimilation with the GEOS-1 System: Overview and Results **Siegfried Schubert, Chung-Kyu Park, Chung-Yu Wu, Wayne Higgins, Yelena Kondratyeva, Andrea Molod, Lawrence Takacs, Michael Seablom, and Richard Rood**